Evaluation of Methane Hydrate Technology for the Utilization of Stranded Natural Gas

Chukwuma M. Anyigor

Chemical Engineering in the School of Engineering

A thesis submitted for the degree of Doctor of Philosophy

Newcastle University

November 2019

Abstract

Natural gas (NG) is a promising solution to reducing CO_2 emissions from energy plants because it is the cleanest fossil fuel and an abundant energy resource, but it is largely under-utilized. About 40 – 60 % of NG is considered stranded because of low volume capacity fields, along with high transport and infrastructure cost for small and large size reserves' utilization. The utilization of NG is further constrained with having relatively low energy density compared to other fossil energy resources. In addition, NG utilization technologies require stringent safety and environmental considerations being in gaseous form, which results in cost intensive operations. Among the various technologies for utilizing stranded NG, methane hydrates technology (MHT) could offer advantage for NG transportation.

In this research, qualitative evaluation and comparison of typical technologies for stranded NG utilization was first carried out using focus indicators of; technology development stage, process complexity, gas volume capacity and storage, economic feasibility, environmental and safety merits. The observations revealed the key role of NG utilization as a low CO_2 emission fuel and a prime contributor to the widely increasing global energy demand. Among the examined technologies; liquefied natural gas (LNG), compressed natural gas (CNG), gas to liquid (GTL), gas to wire (GTW), and pipeline technologies, the prospects of MHT were primly underlined with also its limitations on level of technology development in terms of research and commercialization. The need for further investigations on the feasibility of MHT aggregately for stranded small and large capacity NG reserves' utilization was indicated.

Commercial scale methane hydrate (MH) production simulation in a reactor from pure methane gas (pre-processed NG) and pure water at high-pressure condition was carried out and further processed to pellets for transportation of NG in three main project units; MH pellet production, transportation and regasification of the MH pellets. In this work, the MHT chain was studied with the focus on enhancing it for stranded natural gas utilization from small and large commercial reserves.

For the production unit, a methane hydrate pellet production (MHPP) model was developed which comprised the reactor, hydrate slurry dewatering and pelletization, and pellet storage units based on pilot-scale system data in literature. The MHPP reactor model implemented in Aspen HYSYS® was used to simulate steady state operation of a jacketed continuous stirred tank reactor (CSTR) for MH production process with an adapted gas consumption rate correlation based on experimental study in literature. In various case scenarios, the developed MHPP model was used to size and investigate MH reactor and downstream combined filtration-pelletization machine with a base simulation of 9.16×10^{-3} m^3 volume at 5.40 MPa and 285.15K

for 10 kg hr^{-1} methane hydrate pellet production. On this basis, scale-up considerations were assumed in eight case scenarios for plant capacities employed for the evaluation of commercial gas reserve capacities. Therefore, from this study detailed commercial cost estimation protocol and data were obtained for the MHT chain based on developed MHPP model, sea transportation, and regasification framework for 0.3 - 566.0 bcm per year capacity reserves. This is applicable for the utilization of stranded NG from Nigerian Niger-Delta offshore region to the end-users' market of Europe and Asian continents (10,000 km).

Furthermore, a sensitivity analysis summary of the key parameters of MHPP reactor simulation was implemented in MATLAB with the HYSYS simulation data and revealed the significant effect of superficial gas velocity (gas injection rate) on the methane gas consumption rate, about double the effect each of stirring rate, pressure or subcooling.

For the transportation unit, equations were developed based on consideration of sea transport leading to computation of the required number of ship bulker-carrier trips as well as round trip transport time associated with the MH production capacity and market distance. On this basis, the detailed costing of the MHT offshore/sea transportation was implemented.

For the regasification unit including dehydrating system and compressor, a framework for the assumptions made relating to the main equipment and utilities required are presented.

Finally, cost estimation and analysis of the MHT chain for stranded gas utilization was carried out, the results indicating that it is an economical option for stranded gas utilization for 2.8 – 566.0 bcm per year commercial reserve capacities (for 20 years project life) over 10,000 km market distances.

In addition, the small-scale reserve category evaluation revealed that MHT shows the best economic viability for utilizing stranded gas compared to CNG for 2.8 – 25.5 bcm per year reserve capacities but does not seem viable for reserve capacities below that for 10,000 km market distance. CNG was observed to be the best alternative for small market distances of 2000 km for 0.3 – 2.8 bcm per year reserve capacity. For 28.3 – 566.0 bcm per year reserve capacity over 10,000 km market distance, MHT showed economic viability but LNG and CNG showed clear advantage over MHT below 7000 km and 5000 km respectively. As a result, LNG and CNG seem to be the best options for utilizing stranded gas of 28.3 – 339.8 bcm per year reserve capacities from Nigeria to European continent (less than 7000 km and 5000 km respectively).

Table of Content

Abstract iii

Table of Content v

List of Tables x

List of Figures xii

Nomenclature xiv

Acknowledgments xvi

Chapter 1 Introduction 1

1.1 Research background and rationale 1

1.2 Natural gas reserves 3

1.3 Stranded natural gas reserves 4

1.3.1 Pre-processing of stranded natural gas 6

1.3.2 Nigerian natural gas resource for stranded gas utilization 8

1.4 Stranded gas utilization technologies 9

1.4.1 Pipeline 10

1.4.2 Liquefied natural gas (LNG) technology 11

1.4.3 Compressed natural gas technology 13

1.4.4 Gas to Liquid GTL technology 14

1.4.5 Gas to Wire (electricity power generation) technology 16

1.4.6 Gas to hydrate (methane gas hydrate) technology 17

1.5 Comparison of technologies considered for stranded gas utilization 19

1.6 Concluding remarks 23

Chapter 2 Literature survey on gas hydrates 25

2.1 Introduction 25

2.2 Gas hydrate structures 25

2.3 Physical and chemical properties of gas hydrates 29

2.4 Gas hydrate phase equilibrium 31

2.4.1 Enthalpy of hydrate formation....35
2.4.2 Hydration number....36
2.5 Gas hydrate formation and dissociation kinetics....37
2.5.1 Gas hydrate nucleation and formation driving force....38
2.5.2 Gas hydrate growth and driving force....38
2.5.3 Gas hydrate dissociation....43
2.6 Applications of gas hydrates technology....44
2.7 Concluding remarks....45
Chapter 3 Review of process simulation and economic assessment studies on NGH (methane) production for stranded gas utilization....47
3.1 Introduction....47
3.2 Methane gas hydrate production....48
3.2.1 Production concept of gas hydrate in stirred tank reactors....49
3.2.2 Scale up....54
3.3 MH hydrate dewatering, pelletization and storage....55
3.4 Methane hydrate pellet regasification....58
3.4.1: Self-preservation phenomena....58
3.4.2 Methane hydrate pellet regasification and produced methane gas dehydration....59
3.5 Review of economic assessment of natural gas hydrate for transporting natural gas....61
3.6 Concluding remarks and research objectives....63
3.6.1 Motivation....63
3.6.2 Objectives....64
Chapter 4 Evaluation Methodology: Methane hydrate pellet production (MHPP) model....65
4.1 Introduction....65
4.2 MHPP model framework and process description....65
4.3 Reactor unit development and implementation using Aspen HYSYS....66
4.3.1 Reactor Design....66
4.3.2 Application of hydrate formation rate correlation....67

4.3.3 Implementation in Aspen HYSYS and key process simulation specification 69

4.3.4 Evaluation of the HYSYS base case reactor simulation using energy balance calculations 71

4.3.4.3 E 73

4.3.5 Evaluation and sensitivity analysis of the parameters used in the simulation 75

4.3.6 Reactor scale up and specification of considered natural gas reserve capacities 76

4.4 Dewatering and pelletization units 78

4.4.1 Modelling and simulation of MH slurry dewatering unit (constant rate filtration) . 79

4.4.2 Modelling and simulation of MH secondary operation and compression 81

4.5 Specification of MHPP storage unit at 253 K 83

4.6 Concluding remarks 84

Chapter 5 Simulation results and discussion of the methane hydrate pellet production (MHPP) model 85

5.1 Introduction 85

5.2 HYSYS simulation results and discussions of the MHPP reactor unit 85

5.2.1 Base case reactor design and simulation results 85

5.2.2 Hydrate equilibrium estimation for methane gas using HYSYS (version 8.8) 87

5.3 Analysis and evaluation of the HYSYS base case reactor simulation using energy balance calculations 89

5.3.1 The simulation results of MHPP reactor model design with cooling characteristics 89

5.4 Results and discussion of the key process parameters for MHPP 91

5.4.1 Simulation conditions for the critical evaluation of the MHPP reactor model 91

5.4.2 Effects of superficial gas velocity and methane gas injection rate on methane gas consumption rate using MHPP simulation 91

5.4.3 Effects of stirring rate and methane gas injection rate on gas consumption rate using MHPP simulation 93

5.4.4 Effects of subcooling and methane gas injection rate on methane gas consumption rate using MHPP simulation 94

5.4.5 Effects of water – gas ratio (hydration number) and enthalpy of methane hydrate formation (dissociation) using MHPP simulation 95
5.4.6 Result of the sensitivity analysis.....98
5.5 Result and discussion of the dewatering and pelletizing simulations 105
5.5.1 MHPP base case hydrate pellet processing machine (HPPM) simulation results ..105
5.6 Simulation result of scale-up case scenarios of MHPP reactor simulation.....108
5.6.1 Stranded gas utilization simulation specifications.....108
5.6.2 MHPP reactor model scale-up simulation case results.....110
5.7 MHPP storage unit 113
5.8 Concluding remarks 113
Chapter 6 The transportation and regasification Units and Economic Evaluation of Methane Hydrate Technology Chain 115
6.1 Methane hydrate pellet transportation unit.....115
6.2 Methane hydrate regasification unit 115
6.3 Economic estimation of methane hydrate technology (MHT) Chain 117
6.3.1 Total capital investment estimation for MHT chain.....120
6.3.1.1 MH pellets production CAPEX estimate.....120
6.3.1.2 Estimate of MH pellet transportation CAPEX 121
6.3.1.3 MH pellets Regasification CAPEX Estimate 122
6.3.2 MHT total operating cost estimation 123
6.3.2.1 MH pellet production system operating cost estimate.....124
6.3.2.2 MH pellets transportation OPEX estimate 124
6.3.2.3 MH pellets regasification unit OPEX estimate.....124
6.3.3 Revenue estimation.....125
6.4 Economic evaluation of methane hydrate technology (MHT) chain: case scenarios for natural gas utilization 125
6.4.1 Estimation results of MHT production and regasification CAPEX and OPEX based on the small capacity reserve scenarios 126

6.4.2 Estimated cost of MHT transportation CAPEX and OPEX for the small capacity reserve scenarios technology over 10,000 km 126
6.4.3 Summary of economic analysis of MHT chain based on small capacity stranded gas 129
6.4.5 Summary of economic analysis of MHT chain based on large capacity stranded gas 130
6.5 Economic comparison of stranded gas utilization technologies for large and small-scale capacities: MHT, LNG and CNG case as well as MHT and CNG case 132
6.5.1 Comparison of small reserve stranded gas utilization scenario for MHT and CNG 133
6.5.2 Comparison of the large reserve capacity scenarios using MHT, LNG and CNG 135
6.6 Concluding remarks 137
Chapter 7 Conclusions and recommendations for future work 138
7.1 Comprehensive conclusion 138
7.2 Future research recommendations 140
Reference 142
Appendix A1: MHPP base case reactor simulation in HYSYS 156
Appendix A2: Production CAPEX and OPEX of MHT chain for 0.3 bcm/yr capacity reserves 158

List of Tables

Table 1.1: Fossil fuel resource outlook 3

Table 1.2: Required gas specifications based on considered gas transport technologies 7

Table 1.3: Typical pipeline sales gas (product) specification 8

Table 1.4: Summary of advantages and disadvantages of stranded gas utilization technologies 21

Table 2.1: Cavity size ratio (molecular diameter/cavity diameter) for natural gas hydrates 28

Table 2.2: Densities of some hydrates, ice, and water at 273 K 29

Table 2.3: Enthalpies of dissociation of hydrates of some single gas components at 273.15 K 36

Table 4.1: Simulation specification for small and large capacity stranded gas utilization 78

Table 5.1: Parameters and values in the base case of MHPP reactor unit in HYSYS 86

Table 5.2: HYSYS simulation properties specification for methane hydrate at 285.15 K 88

Table 5.3: The MHPP reactor model design with coolant 90

Table 5.4: Cooling characteristics of the MHPP jacketed reactor simulation 91

Table 5.5: Simulation conditions of the critical evaluation of the MHPP reactor model 91

Table 5.6: Methane hydrate enthalpy of formation ΔH_f and hydration number at pressure range 5.40 – 9.0 MPa and 285.15 K using Clausius-Clapeyron method and HYSYS estimated equilibrium temperatures 96

Table 5.7: Enthalpy of dissociation and hydration number measurements 98

Table 5.8: Parameter for the sensitivity analysis of the MHPP reactor model 99

Table 5.9: Summary of the sensitivity analysis of gas consumption rate MHPP correlation 104

Table 5.10: Design parameters, slurry and cake properties and operational conditions for the constant rate filtration, constant pressure, and compression simulation 106

Table 5.11: Simulation specification for small and large capacity stranded gas utilization 109

Table 5.12: MHPP reactor HYSYS model scale-up simulation result 112

Table 5.13: Methane hydrate pellet storage vessel capacity 113
Table 6.1: Typical factors for CAPEX estimation 121
Table 6.2: MHT production and regasification CAPEX and OPEX small capacity scenarios 126
Table 6.3: Transportation CAPEX and OPEX for the transport of 25.5 bcm/yr of NG 128
Table 6.4: Cost estimation details for Transportation CAPEX and OPEX 128
Table 6.5: Process parameters and considerations for the comparison study 133

List of Figures

Figure 1.1: Proven natural gas reserves 2
Figure 1.2: Range of gas reserve capacities against number of gas reserves globally 5
Figure 1.3: Technologies for moving gas to market 10
Figure 1.4: Breakdown of LNG Process Chain Cost 12
Figure 1.5: LNG Supply Chain Distribution 12
Figure 1.6: GTL block flow diagram 15
Figure 1.7**:** GTW technological distribution network 17
Figure 1.8: Qualitative illustration of the stranded gas technologies based on volume capacity and market distance constraint 20
Figure 2.1: Common natural gas hydrate structure 26
Figure 2.2: P-T of binary system methane-water at 260-310 K 34
Figure 3.1: Typical stirred tank reactor configuration 51
Figure 3.2:Power number and Reynold number correlation for Rushton turbines 52
Figure 3.3: Flooding (a) – loading (b) – complete dispersion (c) for Rushton turbine 53
Figure 3.4: Hydrate pellet production scheme of BSU with the four major steps 56
Figure 4.1: Summary framework of the MHPP model 66
Figure 4.2: Process flow diagram for MH production 67
Figure 4.3: HYSYS process flowsheet for methane hydrate process 70
Figure 4.4: CSTR reactor with jacketed cooling showing an open system 72
Figure 4.5: Constant rate filtration operation of MHPP model 80
Figure 4.6: Constant pressure filtration operation of the MHPP model 82
Figure 4.7: Compression operation of the MHPP model 83
Figure 5.1: Methane hydrate equilibrium curve using HYSYS (version 8.8) 88
Figure 5.2: Methane gas consumption rate against superficial gas velocity at 5.4 MPa, stirring rate of 6.7 s^{-1}, and 276.09 K 92
Figure 5.3: Methane consumption rate against gas injection rate at stirring rate 6.7−13.3 s^{-1}, pressure 5.4 MPa, and 276.09 K subcooling 93
Figure 5.4: Methane consumption rate against methane gas injection rate at subcooling 276.09 K (2.94 ℃) – 281.09 K (7.5℃), 5.4 MPa pressure, and 6.7 s^{-1} stirring rate 95
Figure 5.5: Clausius-Clapeyron plot of logarithm of pressure against inverse of temperature for methane hydrate equilibrium from 5.40 – 9.0 MPa. Hydrate equilibrium data obtained from HYSYS 96

Figure 5.6: Clausius-Clapeyron plot of logarithm of pressure against inverse of temperature for methane hydrate equilibrium from 5.40 – 9.0 MPa. Hydrate equilibrium data obtained from CSMhyd 97
Figure 5.7: Sensitivity analysis - effect of superficial gas velocity on the methane gas consumption rate 100
Figure 5.8: Sensitivity analysis - effect of stirring rate on the methane gas consumption rate 101
Figure 5.9: Sensitivity analysis - effect of subcooling on the methane gas consumption 101
Figure 5.10: Sensitivity analysis - effect of pressure on the methane gas consumption 102
Figure 5.11: 3D plot of the effects of both superficial gas velocity and stirring rate on gas consumption rate 103
Figure 5.12: Simulation of pressure drop increment with filtrate volume at constant rate filtration 107
Figure 5.13: Filtrate volume discharge per time at constant pressure filtration 108
Figure 6.1: Summary framework of methane hydrate regasification 116
Figure 6.2: Implemented glycol dehydrating unit in HYSYS after MH regasification 117
Figure 6.3: Summary of MHT estimate cost components 118
Figure 6.4: MHT transportation (a) CAPEX and (b) OPEX 127
Figure 6.5: MHT NPV for the utilization of small-scale capacity reserve over 10,000 km distance 129
Figure 6.6: CAPEX and OPEX for 28.3 bcm (1.0 Tcf) stranded gas (large capacity reserve) 130
Figure 6.7: MHT NPV for large capacity reserve scenarios 131
Figure 6.8: Comparison of the NPV of MHT and CNG for 0.3 – 25.6 bcm (0.01-0.9 Tcf) reserve capacities (Small-capacity reserve scenarios) 134
Figure 6.9: Comparison of the NPV of MHT, LNG, and CNG for 28.3 – 566.0 bcm (scenario 5−8) reserve capacities 136

Nomenclature

A	Cross section area, (m^2)
a, b	correlation coefficient $(-)$
C_w	Dry cake weight, $(kg\ m^{-2})$
c_m	Average dry cake per unit filtrate volume, $(kg\ m^{-3})$
D	Reactor diameter, (m)
D_i	Impeller diameter, (m)
d	One-way trip distance from the plant to the receiving terminal, (km)
F	Gas feed stream, $(mol.\ s^{-1})$
Fr	Froude number $(\frac{N^2 D_i}{g})$
FI	Gas flow number $(\frac{Q_g}{ND_i^3})$
g	Gravitational acceleration, $(m^2 s^{-1})$
N_p	Power number $(\frac{P}{\rho N^3 D_i^5})$
N	Stirring rate, (s^{-1})
N_t	Number of bulk-carriers, $(-)$
p	Pressure, (MPa)
P_{ug}	Power consumption, (W)
P_g	Power consumption at gassed conditions, (W)
q	Methane hydrate formation rate, $(m^3 s^{-1})$
q	Methane hydrate formation rate/water dispersion volume, $(mol\ m^{-3} s^{-1})$
q_f	Filtrate flowrate, $(m^3 s^{-1})$
Q_g	Feed gas flowrate, $(m^3 s^{-1})$
Q_s	Feed slurry flowrate, $(m^3 s^{-1})$
Re	Reynold number $(\frac{\rho N D_i^2}{\mu})$
R_m	Filter medium resistance (m^{-1})
s_0	Average speed, $(km\ hr^{-1})$
t	Time (s)
v_{sg}	Superficial gas velocity, (ms^{-1})
V	Volume, (m^3)
V_M	Vessel capacity, (m^3)
V_w	Water dispersion volume, (m^3)

V_{tr} Filtrate volume (m^3)

V_f Cumulative filtrate volume (m^3)

X Conversion, (%)

Z Compressibility factor

Greek Symbols

ρ Mass density ($kg\ m^{-3}$)

ρ_m Molar density ($mol\ m^{-3}$)

α_{av} Average cake Resistance ($m\ kg^{-1}$)

Abbreviations

bcm Billion cubic metres

bcf Billion cubic feet

CNG Compressed natural gas

CSTR Continuous stirred tank reactor

EIA Energy Information Administration

GTL Gas-to-liquid

GTW Gas-to-wire

GTH Gas-to-hydrate

LNG Liquefied natural gas

Mcf Thousand cubic feet

MMBtu Million British thermal unit

MMscf Million standard cubic feet

MHT Methane hydrate technology

MHPP Methane hydrate pellet production

MTPA Million tonnes per annum

NNPC Nigerian National Petroleum Cooperation

NLNG Nigerian liquefied natural gas

Tcf Trillion cubic feet

UNCTAD United Nations Conference on Trade and Development

Acknowledgments

My appreciation goes to my supervisors, Dr Jonathan Lee and Professor David Reay, for their support and guidance.

I wish to thank the Ebonyi State Scholarship Board, Nigeria and Ebonyi State University Abakaliki, Nigeria for their sponsorship covering until the second year of this programme.

I am most grateful to my dear wife, Sophia and my family for their consistent understanding and support. I also wish to acknowledge my siblings and my parents for their financial support and prayers. Special thanks to Dr Adejo and Dr Suleiman for their friendship and support.

Special thanks to authors, Dr David Wood and Dr Rajab Khalilpour and Gaurav Bhattacharjee for their useful comments by email communication.

I am also grateful to my friends and my colleagues who provided encouragement and love.

I would like to thank the Chemical Engineering, School of Engineering Newcastle University.

In addition, I thank the staff of the Philip Robinson Library, Newcastle University.

I would also like to thank my church, City of God Christian Centre for their love and prayers.

In all, I thank God Almighty for keeping me.

Chapter 1 Introduction

1.1 Research background and rationale

Natural gas, crude oil and coal are the most dominant world fossil energy resources (Ritchie and Roser, 2018). Natural gas is the second most consumed power sector fuel globally after crude oil and is estimated to remain the most used fuel after crude oil with a steady decline for coal by 2050 (EIA, 2018). More so, natural gas is considered the cleanest fossil fuel because of the lower carbon emissions associated with it. It accounts for half the emissions of carbon dioxide per unit of electricity compared to the emissions from existing coal power stations. Oil and Gas UK reported a 16% reduction of annual emissions of carbon dioxide from electricity and 40% increase in electricity from 1990 to 2008 achieved by replacement of coal-fired power plants by gas-fired combined cycle gas turbines (Sarsfield-Hall and Gareth, 2010). Additionally, power generation using coal costs more compared to using natural gas. In the US, gas cost of $16 per megawatts hour used in utility plants was less compared to about $22 using coal for generating 1 megawatts continuously over an hour in 2016, which as earlier mentioned implies that natural gas is a cheaper energy resource compared to coal (Light, 2017).

Furthermore, the BP plc estimates a proven large global reserves volume of 193,452 billion cubic meters (bcm) of natural gas at the end of 2017, of which about 40 - 60 % of the reserves are considered stranded due to distribution infrastructure and uneconomical gas transportation issues (BP, 2018b). Stranded gas utilization has become more attractive in recent years because of the significant global natural gas consumption growth which increased by 3 % (96 bcm) in 2017, being the fastest growth rate since 2010 (BP, 2018a). Figure 1.1 shows the location of the top 20 proven gas reserves in the world.

The World Bank's Global Gas Flaring Reduction (GGFR) Partnership reported that 141 bcm of natural gas were flared globally in 2017 at various oil reserves with severe effects on global warming (World Bank Report, 2018), despite the almost 5% decline in global gas flaring (Smedley, 2018). In addition, when natural gas is vented directly to the environment, this has an even more harmful effect on global warming because methane has about 21 times greater effect than CO_2 as a greenhouse gas (Khalilpour and Karimi, 2009).

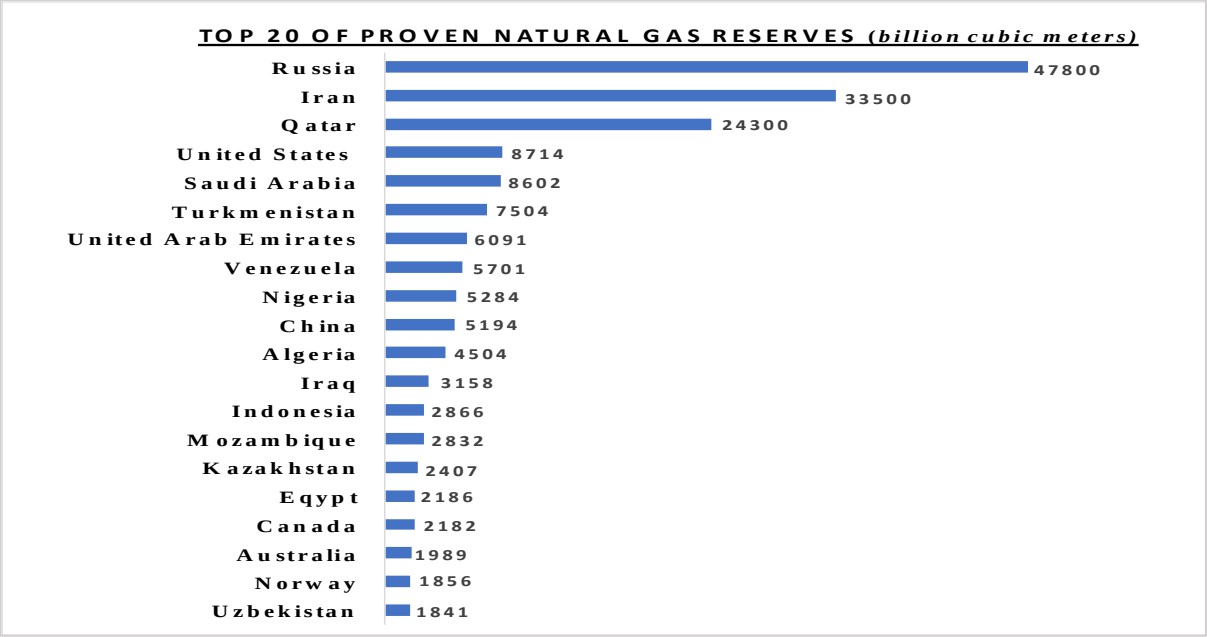

Figure 1.1: Proven natural gas reserves Source: (CIA, 2017)

Furthermore, fossil fuel is estimated to supply over 80 % energy until 2050 (EIA, 2018) to satisfy the world energy demands particularly for electricity and industrial sectors together projected to account for 71 % natural gas consumption by 2050 (BP, 2018a). This implies that fossil fuel will continue to dominate as the primary global energy source with natural gas accounting for the largest increase in global primary energy consumption after renewables. According to World Economic Forum report, it is expected that governments will begin implementing national and regional natural gas utilization plans with insightful explorations of natural gas as a low emission fossil fuel for the reduction carbon dioxide emissions (Jezard, 2017).

In the past, natural gas (associated gas) was an unwanted by-product from oil exploration due to the challenges of storage. As a result, the gas produced with oil often flared or even released directly to the environment with detrimental climate and health effects. However, with increasingly global interventions on gas flaring, constant decline in global gas flaring gas has been reported in recent years (Smedley, 2018). Natural gas is considerably a low CO_2 emitting gas compared to coal and crude oil because of its low carbon-to-hydrogen ratio. As a result, there is a continuous rising growth in the demand of gas especially with the global aim to keep atmospheric temperature rise below 2 degrees Celsius (King et al., 2017).

BP (2018a) suggests global coal demand is likely to be displaced by gas consumption in the next two decades. Conversely, the main demerit of natural gas is its considerably low energy density compared to other fossil fuel resources. This contributes majorly to the required complex infrastructure and challenges of high cost of NG transportation, added to the

difficulties associated with gas transportation in the gaseous phase such as greenhouse gas emissions. Table 1.1 shows the disparity in energy density of natural gas, oil, and coal together with their approximate heating values. Although NG is the cleanest fossil fuel, it is believed to be one of the lowest utilized energy resources globally.

Table 1.1: Fossil fuel resource outlook Adapted from BP (2018a)

Fossil Fuel Resource	Proven Reserves (Quads)	Approximate Heating value (Btu/scf)	Carbon-to-Hydrogen Ratio (molar)
Natural Gas	6.6×10^3	1.0×10^3	0.25
Crude Oil	9.6×10^3	1.0×10^5	$7 - 10$
Coal	3.2×10^4	5.0×10^5	$20 - 40$

Quads equivalent to 1.055×10^{18} Joules, Btu equivalent to 1055 Joules, scf equivalent to $0.0283 m^3$

1.2 Natural gas reserves

Raw natural gas (NG) is explored from conventional geographical formation of earth's crust usually trapped beneath impermeable rock caps in deep reservoirs. It is either associated with crude oil commonly known as associated gas or in reservoirs with insignificant composition of crude oil called non-associated gas.

The other raw natural gas sources commonly known as unconventional such as that associated with shale oil production, coal-bed methane gas, and gas hydrates (which form in permafrost areas) come from non-traditional sources. For the purpose of this study, the focus is on the conventional natural gas reservoirs largely applicable to established oil and gas industries. However, the increasing demand for primary energy has resulted in natural gas exploration towards more challenging remote locations (Azarinezhad et al., 2008), such as the north slope of Alaska, Siberia and deep under the oceans floor or complex geologic formations . Additionally, more than 50 % of such reserve locations including the Russian Yamal Peninsula, northern Australia, Indonesia, offshore eastern Canada, and Vietnam are considered stranded with economic limitations for gas and associated gas utilization (Institutional Analyst Inc, 2018). Natural gas compositions vary significantly from well to well and locations and countries which makes it difficult to discuss a typical gas composition generically (Kidnay et al., 2011). Natural gas consists predominantly methane gas but can also have composition of variety of elements and compounds. Non-hydrocarbon components such as water, hydrogen sulphide, carbon dioxide, water vapour as well as higher hydrocarbons: ethane, butane, propane, butane and natural gas liquids (NGL) and occasionally nitrogen, mercury and helium may be present in a typical natural gas reserves (Kidnay et al., 2011). For instance most NG wells in Nigeria

are reported to have insignificant hydrogen sulphide and sulphur compounds and are commonly referred to as sweet gas (Ekejiuba, 2017). Whereas in most other locations or countries, that is not the case, as relatively substantial amount these non-hydrocarbon contaminants may be contained, commonly known as sour gas. Raw natural gas, which comes with little or no crude oil from gas or condensate wells, is the non-associated gas.

Raw natural gas (weather sour or sweet) are generally produced from gas wells while condensate wells produce natural gas condensates as a highly dense, high-pressure fluid. Furthermore, non-associated natural gas could be classified into different types based on the proportion of hydrocarbons heavier than methane as dry or wet raw natural gas. Natural gas with 95 % compositions of methane gas is considered as dry or lean gas whereas natural gas with more than 5 % of heavier hydrocarbons (ethane, propane, butane) are classified as wet gas (Chandra, 2006a). Lean gas is practical for some natural gas reservoirs or for gas stream having had, the heavier hydrocarbons removed.

1.3 Stranded natural gas reserves

Stranded gas can be defined as natural gas discovered in a field with no economic value because of the inability to utilize it (Dickson et al., 2015). A lack of infrastructure (pipeline network or viable gas transport technology) and cost limitations mean that the reservoirs, especially small capacity reserves in remote locations are not explored (Kang et al., 2016). Many gas reserves are too remote from large populations or are too small to justify investment economically. So natural gas in reserves that cannot be used due to transportation and economic limitations is referred to as stranded natural gas which can account for more than 50 % of proven natural gas globally (Institutional Analyst Inc, 2018). An example is a gas field with volume capacity too small to justify the utilization of expensive technologies such as LNG for gas transportation. Although natural gas is the cheapest fossil fuel which provide alternative to the use of coal and oil, most stranded gas reserves are under-utilized or unused.

Stranded gas reserves can be classified as large or small (which may include marginal reserves) based on the field volume capacities. Further classification of stranded gas reserves are remote gas and associated gas reserves. Although, large gas reserves have proven volume capacity that can sustain development for long-term gas production, it becomes stranded for instance, with limitations either of economically unreasonable distances or in locations (countries) with high terror occurrence and risk. Excess gas reserves are sometimes also classified in this category of stranded reserves as it can result in oversupply of the market (Shah and Durr, 2009). It is claimed that less than 1000 number of large capacity reserves exist globally in different sizes and locations (Mitsui Engneering and Shipping, 2016) as shown in Figure 1.2.

Therefore, gas reserves with volume capacity of above 28.3 bcm (1 Tcf) can be said to be a large capacity gas reserve. Likewise, Moulijn et al. (2013) suggests the number of gas reserves in this category are relatively just about 30 % of the number of natural gas reserves globally which appear to agree with Figure 1.2.

On the other hand, marginal gas reserves are reserves with depleting or diffident volume capacity, which cannot justify an economic development, for instance, a gas pipeline or expensive LNG development for long-term production. Although, there are proven gas reserves but cannot be exploited due to poor economic viability. Marginal gas reserves can be classified alongside small gas reserves in terms of volume capacity range (Kojima, 1999) and it is claimed to account for about 70 % of the number of natural gas reserves globally (Mitsui Engneering and Shipping, 2016).

Utilization of stranded gas especially the marginal and small gas reserves' challenges are identified needful for evaluation, which aligns with the motivation for this research. Additionally, majority of conventional gas utilization technologies require large gas capacity reserves to be viable for development. Therefore, the need for a comprehensive evaluation of technologies for the utilization of stranded natural gas cannot be over-emphasized. Nevertheless, the limitations of under-utilization of natural gas due to technological and economic gaps effect end-users, examples are small gas users and independent power producers which may not access natural gas at reasonable prices (Tamsilian et al., 2013).

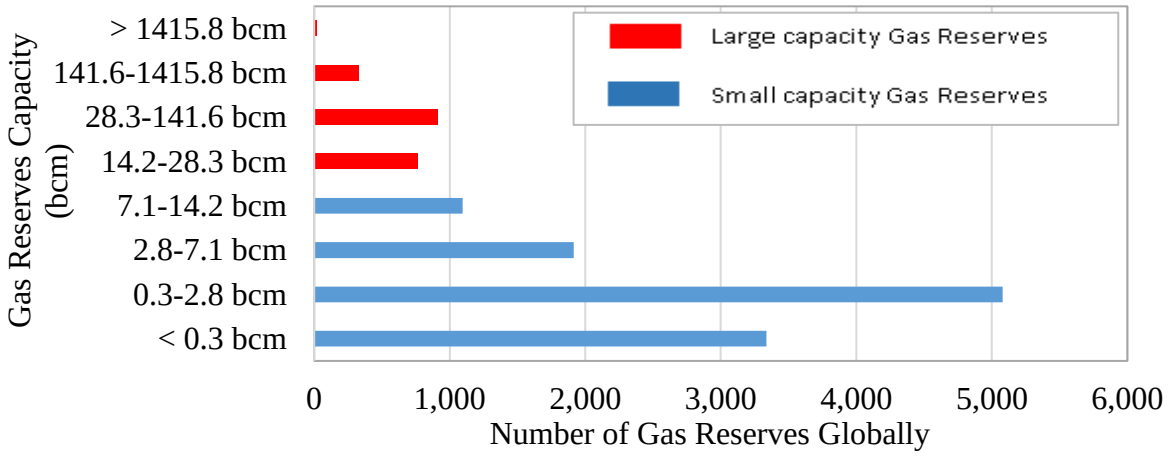

Figure 1.2: Range of gas reserve capacities against number of gas reserves globally **(1.0 trillion cubic feet (Tcf) equivalent to 28.3 billion cubic meters (bcm)**) (Mitsui Engneering and Shipping, 2016).

Associated gas can also be classified to be within the same category of small gas volume capacity range (Khalilpour and Karimi, 2009), as for instance pipelines may not be available for utilizing associated gas due to volume uncertainty. About 141 bcm of natural gas was

reported to have been flared from various oil reserves in 2017 resulting in roughly 400 metric tonnes of CO_2 emission to the environment (World Bank Report, 2018). The majority of associated gas resources are too small to justify high capital investment and were commonly flared in the past by oil and gas companies. However, with stringent international environmental laws and pressures, an aroused attention in utilization of associated gas resources has been observed in recent years.

It is the belief of the author that more research efforts is required to effectively reduce the barriers to stranded and associated gas utilisation and channel this cheaper energy resource to useful purposes such as cleaner fuel for power generation and production of chemicals. Natural gas is fast becoming a premier fuel resource in the world economy, as such adequate transportation, and infrastructures for processing and moving gas from stranded gas locations to market is a key research consideration. As mentioned earlier, It is estimated that more than 50 % of the world proven natural gas are considered stranded, and more than half of these stranded gas resources are of small gas reserve range of about 0.3 – 28.3 bcm (0.01 – 1.00 Tcf) (Moulijn et al., 2013, Mitsui Engneering and Shipping, 2016).

1.3.1 Pre-processing of stranded natural gas

In view of the increasingly growth in demand for natural gas, the discussion of the pre-processing of raw natural gas is necessary. Raw natural gas processing typically involves separation of non-hydrocarbon contaminants, non- methane hydrocarbons (depending on end-use) and no heating value components. The required pre-processing route or steps for raw stranded natural gas reserves depend on the raw natural gas stream composition, associated contaminants, and the required gas quality specifications, which therefore define the technological requirement for the processing. In most cases, the objective of pre-processing of raw natural gas are essentially for meeting gas pipeline quality and specifications of the technology employed for gas transport. Usually C_{4+} (NGL) are limited due to dew point reasons and hydrogen sulphide, carbon dioxide and water are removed for corrosion reasons as well as nitrogen is limited due to combustion or emission reasons. Dust or solid particulates are also not acceptable for mechanical reasons and the required heating values are satisfied. Generally, gas reserves from different regions and geographical areas are of different compositions as such, pre-processing requirements differ based on peculiar reservoir raw natural gas composition.

For instance, if a typical scenario involving associated gas stream of raw natural gas composition (% mole) of: CH_4 91.01; C_2H_4 4.35; C_3H_8 1.61; iC_4H_{12} 0.34; nC_4H_{12} 0.42; iC_5H_{10} 0.15; nC_5H_{10} 0.09; nC_6H_{14} 0.24; N_2 0.13; CO_2 1.67 (Agip Port Harcourt, Nigeria Gas Well) is considered. Then, using gas hydrate technology for gas transportation will require pre-processing route, which involves CO_2 removal, and N_2 rejection processes as well as the NGL

removal. The natural gas liquid (C_{2+}) removal is also indicated for expected downstream lean natural gas predominantly methane gas. Natural gas liquids (NGLs) are hydrocarbons that are in the same family of molecules as natural gas and crude oil composing only hydrogen and carbon. Examples of NGLs include ethane, propane, butane, and natural gasoline liquefied at surface of the reservoir facilities or pre-processing plant. Natural gasoline is usually pentane and heavier hydrocarbon mixtures extracted usually from natural gas processing plants (Kidnay et al., 2011). Therefore, for hydrate technology in which sI hydrate (methane) is the focus, the NGL will involve refining or pre-processing for pure methane gas feed downstream the hydrate-forming reactor. Similarly, for a Fischer-Tropsch GTL process which also requires just the C_1 feed for syngas generation. For CNG and LNG end users' requirements typically plays a role as to the extent of pre-processing depending on the C_{1+} gas compositions.

Typically, for a specified raw natural gas stream, different pre-processing requirements and stringent equipment requirements are required for any considered stranded gas utilization technology. Table 1.2 indicates specification limits for natural gas based on stranded gas utilization technologies. Further discussions on the stranded gas utilization technologies are presented in Section 1.4.

Table 1.2: Required gas specifications based on considered gas transport technologies

Gas Constituents	Pipeline	LNG	CNG	NGH (CH_4 hydrate)	GTL (FT)	GTW
H_2O	84 ppm	0				< 10 ppmv
H_2S	4 ppm	0				
CO_2	2 %mol	< 50 ppmv				
C_1	> 75 %mol			Pure CH_4		85−100 %mol
C_2	> 10 %mol			0	0	15 %mol
C_3	> 5 %mol			0	0	15 %mol
NGL, C_{4+}				0	0	5 %mol

Data obtained from (Kidnay et al., 2011)

Although natural gas is sometimes used as petrochemical feedstock, it is primarily used for the production of sales gas (pipeline quality gas) for industrial and residential end-users for fuel. This is considered as the product basis for this study. Hence, one of the reasons for pre-processing of raw natural gas is to ensure removal of contaminants, which may inhibit its utilization as industrial and residential fuel, or damage equipment used for its production, transportation, or regasification as may be required.

Table 1.3 shows the typical pipeline sales gas (product) specifications that ensure gas qualities and pre-processing requirements and environmental targets are met. This ensures standard

pipeline gas quality for provision of safe and clean fuel gas to end-users. Furthermore, the sales gas must also have the heating values specifications to ensure the required operation of combustion equipment and gas turbines so as to reduce emissions (Chandra, 2006b). In addition, the standard pipeline gas quality is also satisfied for regasification at the receiving terminal for technologies such LNG and gas to hydrate.

Table 1.3: Typical pipeline sales gas (product) specification (Kidnay et al., 2011)

Major Components	Specification	
	Minimum (mol %)	Maximum (mol %)
Methane	75	None
Ethane	0	10
Propane	0	5
Butane	0	2
Pentane and heavier	0	0.5
Nitrogen	< 1	2
Carbon dioxide	0	3
Trace components		
Hydrogen sulphide	6 – 24 mg/Nm^3	
Total sulphur	100 – 400 ppm	
Oxygen	10 ppmv – 1.0 %	
Water vapour	68 – 120 mg/Nm^3	
Mercury	0.01 μg/Nm^3	
Other characteristics		
Heating value (Wobbe number)	37.4 – 45.3 MJ/Nm^3	
Liquids	Free of liquid hydrocarbon (at delivery pressure and temperature)	
Solid particulates	Totally free of particulates at quantity harmful to equipment	

1.3.2 Nigerian natural gas resource for stranded gas utilization

Nigeria is the most populous country in West Africa with a geographical area of 923,768 km^2 and proven abundant natural gas reserve of 5094 bcm (180 Tcf) and is the largest natural gas reserves in Africa (EIA, 2016). Nigerian National Petroleum Cooperation (NNPC) report shows a potentially 16980 bcm (600 Tcf) more gas to be found if oil and gas companies intentionally explore gas rather than oil (NNPC, 2010). Nigeria has been one of the leading exporters of LNG globally to Europe and Asia.

Furthermore Nigerian natural gas is also considered a lucrative resource to Europe and Asia because of its high quality and quantity as well as efficacy of the natural gas composition, which has no sulphur (popularly known as sweet gas) (NNPC, 2016). 30 bcf/d Trans-Sahara pipeline was also proposed and still under construction to Europe via Algeria, which is expected to be a major sales gas utilization for natural gas when completed (EIA, 2016). However, gas resources

usually can only be developed when it can be economical produced and transported to demand market. Furthermore, there are complexities associated such as varying gas prices and demands as well as gas contracts, which requires necessary flexibility and economic tenacity. More so especially for the small gas reserves categories natural gas to the global market from Nigeria could be considered stranded due to high cost and complexity of technology accessible for transportation of natural gas. Therefore, there is a need for feasible and better economic technologies such as is expected with methane hydrate technology for exporting and utilization of natural gas globally. This forms part of the motivations for this study.

1.4 Stranded gas utilization technologies

Storage and transportation of gas presents graver environmental concerns and challenges compared to solid and liquid fuel. This could result in high transportation costs of natural gas from reservoir locations to demand market or end-users. However, although natural gas is a cheap energy resource, it is of little or no value unless it can be economically moved from gas wellhead to the demand market. In recent years, large attention is drawn to the exploration of stranded gas reservoirs that were previously considered too remote, too small or technically too challenging to develop and commercially unreachable by pipelines (Attanasi and Freeman, 2012). The fundamental factor that must be considered aside from the limitations due to non-pipeline and market distance is the stranded gas volume size (reserve capacity). Reserve capacity is a crucial consideration to the choice and economic viability of utilization method (Khalilpour and Karimi, 2012). For instance, the LNG process is reported to require up to 5000 MW power capacity infrastructure if utilized for electricity in a 20 years production life (Economides et al., 2006), implying it will require over 2830 bcm reservoir capacity. The traditional liquefied natural gas (LNG) technology has commercialized many large capacity remote reservoirs, playing a key role in large capacity stranded gas utilization but is conversely highly expensive technology. However, for a small gas field of about 14.2 bcm will yield up to 17 MW of electricity which is economically viable for small and medium gas producers or stranded gas utilisation case (White and Morgan, 2012).

In this section, an evaluation of stranded gas utilization methods explored based on published literature. Two reserve capacity scenarios formed the basis of the evaluations; large, and small (which includes marginal and associated gas reserves) stranded gas sources.

Wood et al. (2008) suggested six technologies for the utilization of stranded gas, which has attracted enormous research attention both industrially and academically: pipeline, compressed natural gas (CNG), liquefied natural gas (LNG), gas to liquids (GTL), gas to solid (GTH), and gas to wire (GTW). These technologies or methods are at various stages of technological development and commercialization (Saavedra and Fales, 2012, Dickson et al., 2015).

The criteria that define limitations of stranded gas utilization include production, transportation, economic viability, market distance, environmental consideration, and social-political consideration such as terrorism. Moreover, emphasis on the process supply chain as well as technical performance analysis of each method defined the evaluation with a conceptual outcome of the technology with most significant potential for the utilization of stranded natural gas. Figure 1.3 indicates the considered technologies for stranded gas utilization from remote gas sources to end-users' gas market

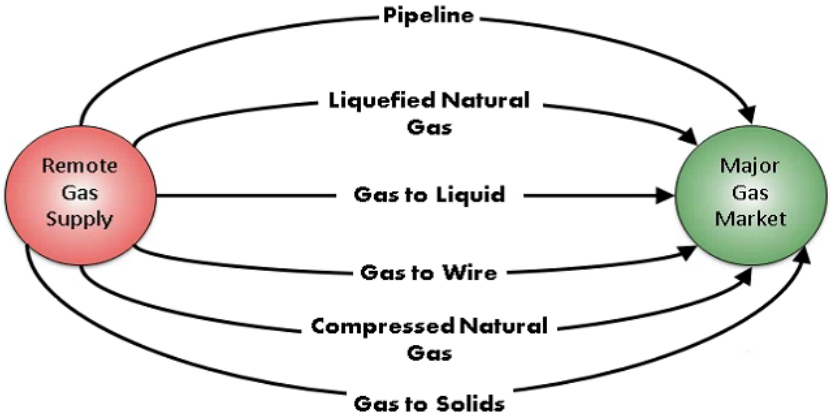

Figure 1.3: Technologies for moving gas to market. (Wood et al., 2008)

1.4.1 Pipeline

Pipeline is one of the most fully established technologies used for moving processed natural gas to demand market. It is a fully commercial technology, which can be used onshore and underwater for offshore gas transportation. It is a commonly used technology but is not flexible. Therefore, it requires significant established reserves, high-value proven market, and market distance considerations for it to be economical. Pipeline is generally considered economical for near onshore gas transportation of natural gas. However, when it involves longer transport distances particularly in deep water offshore reserves, its development becomes expensive and technically challenging, which requires long-distant large diameter pipeline network (Wang and Economides, 2009). Therefore, key factors such as market distance, pipeline dimensions, throughput, reserve volume capacity, and compression-station cost requirements are economically evaluated before pipeline is considered. Some hazards are associated with pipeline such as pipeline plugging by hydrates, political shutdown and terrorism particularly for intercontinental pipeline network crossing countries which may increase the propensity of supply interruptions (Mokhatab et al., 2015).

Large capital cost investment is usually required in pipeline development comprising the pipeline system and compressor stations. Gas pipeline project in the last decade cost as much

as $3.38 million per mile (Smith, 2008). However, “largest untapped energy resources in the world are "stranded" gas in offshore reserves, which fall beyond the reach of pipeline systems” or not economical using pipeline (Davies and Stenning, 2015).

1.4.2 Liquefied natural gas (LNG) technology

LNG technology is the most commercialized and long-established methods for transporting natural gas to market after pipelines. LNG is condensed as a liquid produced when natural gas is cooled to about $111\ \mathrm{K}$ ($-162\ ℃$) at close to atmospheric pressure. A volume reduction factor of about 600 is achieved comparative to volume of the natural gas. This volume reduction makes it easier to transport LNG economically by ships over long distance rather than pipelines and its onshore local distribution to market.

According to the International Gas Union 2018 report, the LNG industry continues to be the most vibrant segment of the world’s natural gas value chain with a 12 % (45.8 bcm) growth at the end of 2017 (IGU, 2018). Furthermore, LNG technology still dominates in offshore sea transportation because of its technological maturity and viability for utilization of large gas reserves. However, due to the complexity of LNG supply chain, it is highly capital intensive and is not viable for utilization of stranded natural gas in locations with small and marginal capacity gas reserves (Mokhatab et al., 2015). As a result, the leading exporters of LNG are traced to locations in the world with proven large reserves such as Qatar, Australia, Malaysia Nigeria, Indonesia, United States and Russia etc (IGU, 2018).

Natural gas transportation using LNG technology is associated with challenges of process chain complexity and high cost of investment of LNG plant. These challenges are due to requirements, including stringent design and safety standards, the cryogenic materials used and strict raw natural gas processing. The LNG process chain comprises of three primary components: liquefaction, shipping, and regasification. Liquefaction plant accounts for the largest cost and energy component of LNG supply chain because of quantity of cryogenic materials required and strict safety and design standard requirements (Kidnay et al., 2011). Figure 1.4 shows a breakdown of cost components of LNG process chain. Additionally, LNG investment typically require long term contracts such as $20 - 25$ years to guaranteed economic security (DOE, 2017). However, the growing floating LNG (FLNG) technology, which incorporates the LNG processing, and storage facilities on an offshore moored vessel could minimize cost, making small remote gas reserves feasible. It is projected that the cost reduction with the FLNG due to exclusion of pipelines and offshore platforms as well as port facilities could overcome some technical and economic limitations (Mokhatab et al., 2015).

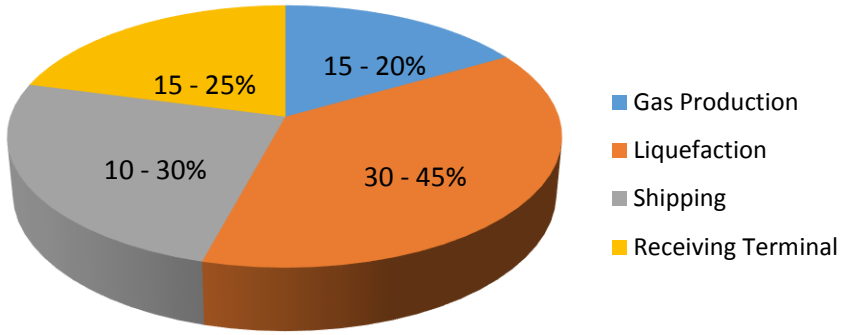

Figure 1.4: Breakdown of LNG Process Chain Cost Adapted from: (Kidnay et al., 2011)

In the liquefaction stage, natural gas after processing is moved via pipeline to liquefaction plant. Liquefaction plants are categorized as peak shaving or baseload based on their use. For the peak-shaving LNG liquefaction facility, it is designed for production of LNG for storage and regasification in times of peak demand. Conversely, baseload plants are designed for liquefaction facilities for conversion of processed natural gas from reservoir or field to LNG primarily for transit. Figure 1.5 shows a typical LNG chain distribution. LNG at receiving terminal is regasified and sent to the storage or distributed after treating to pipeline quality via pipeline network to demand market usually for sales gas and power generation.

Although LNG has a high efficiency of about 85 % (Khalilpour and Karimi, 2012), boil-off gas (usually about 10%) are inevitable on LNG transportation vessels or ships (Hasan et al., 2009). Boil-off gas can be flared for security reasons if the quantity of boil-off gas exceeds capacity but boil-off gas are usually utilized; burned in the boiler as added power input to the ship or in some cases re-liquefied back to LNG (Zakaria et al., 2013).

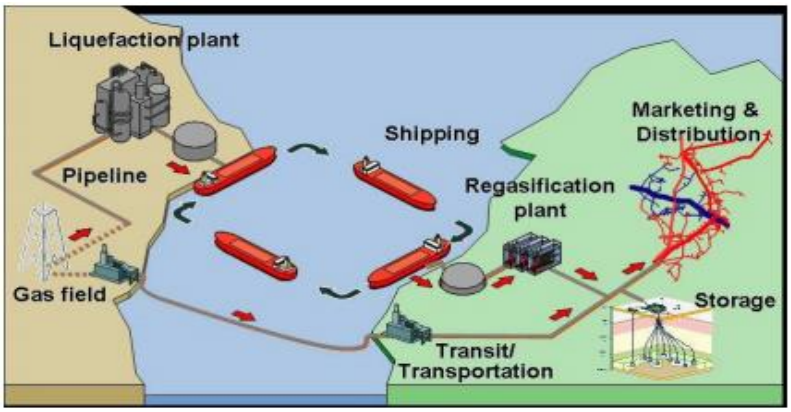

Figure 1.5: LNG Supply Chain Distribution Source: (Nous et al., 2010)

1.4.3 Compressed natural gas technology

In compressed natural gas (CNG) technology, gas transportation involves the compression of gas in specially designed containers stacked in ships at 12.4 MPa for rich gas (with substantial amount of higher hydrocarbons of propane, butane etc) to about 24.8 MPa for lean gas having mainly methane (Mokhatab et al., 2015). CNG gas is compressed to a gas ratio of about 200 m^3 to 1 m^3 of natural gas at ambient temperature, the reduction in volume of the gas making it more economical (Wang and Economides, 2009). The complete CNG supply chain involves compression, transportation and decompression of gas to meet sales gas quality and pressure specifications on receiving terminal (Saavedra and Fales, 2012).

The key merit of CNG is the potential of offering economic stranded gas utilization for small and remote offshore reserves as well as associated gas reserves (Davies and Stenning, 2015). It also provides solution for projects requiring long-distant subsea pipelines, which are not economically feasible, or markets with diffident demand and reserves uneconomical with high cost of liquefaction and regasification facilities using LNG. In addition, it can be a cost-effective solution to intercontinental and regional gas projects rather than pipelines and proffers better economic flexibility as well as less risk compared to the LNG technology (Mokhatab et al., 2015).

CNG production require gas pre-processing but the pre-processing is simpler compared to that for LNG liquefaction plant. The end users' requirements typically set the extent of pre-processing depending on the C_{1+} gas compositions. However, the core pre-processing requirements which also apply to other alternatives for stranded gas utilization are removal of contaminates such as hydrogen sulphide and carbon dioxide, removal of heavier hydrocarbons to prevent condensation when storing as CNG, and dehydration.

CNG ships account for over 85 % of total investment of CNG project (Wood et al., 2008), which implies it is highly sensitive to market distance and suggests a more beneficial project decommissioning on event of diminished reserve. Furthermore, CNG transportation system can be onshore with truck having loading facility with gas compression and offloading, with heating, let-down and metering at end-user site (World Bank, 2015). According to World Bank (2015) study on small capacity stranded gas utilization (using CNG), for production capacity more than 141,261 m^3/d (5 MMscf/d at 288 K) viability of CNG truck delivery becomes uncertain because of the resultant substantial number of vehicles that will be required. Additionally to a significant degree of loading and offloading facilities especially for longer distances becomes a limitation.

For offshore gas transport (marine transport), the volume capacity of gas, and the market distance are the significant factors, which define the transportation cost of the CNG chain. CNG

is typically considered economical moving stranded gas over shorter distances, where no pipeline infrastructure exists (Wood et al., 2008). The current CNG development projects are based on conventional bulk carriers with different containment designs (World Bank, 2015): Sea NG Coselle^{TM} (Canada) of coiled X70 line high-strength steel pipe forming a cylindrical container and the EnerSea (US) Votrans^{TM} of X80 carbon steel cylinder, which are in advanced development status. The others still in concept stage development are: TransCanada CNG Technologies of reinforced steel gas transport modules; Trans Ocean Gas of composite HDPE and fibreglass cylinders; CETech of composite or X80 pipe or steel. EnerSea volume optimized transport and storage (Votrans^{TM}) containment system in terms of delivery and system efficiency is the most cost efficient containment system with transport capacity ship of up to 28 million cubic meters (1000 MMscf at 288 K) (Mokhatab et al., 2015).

Although CNG is believed to be a potentially economical viable alternative to LNG and has gained attention in several companies, CNG for large-scale gas utilization is yet to be fully established commercially.

1.4.4 Gas to Liquid GTL technology

GTL is a process where natural gas predominantly methane gas is chemically converted to liquid fuels prior to transport. Unlike LNG, GTH, and CNG, GTL involves a chemical transformation. Fischer-Tropsch (FT) synthesis via reforming process is commonly used for the production of GTL fuel, which is one of the most commercially sanctioned (Wood et al., 2012). In the reforming process, methane gas mixed with steam is used to produce synthesis gas (mixture of carbon monoxide and hydrogen). The reforming process is an energy intensive process that produces synthesis gas used as feed for the FT process. The Fischer-Tropsch reaction is highly exothermic process that chemically converts synthesis gas to higher hydrocarbon fuels and a variety of chemical products over a metal catalyst, usually cobalt and iron (Spath and Dayton, 2003)..

The possible GTL end products are jet fuel, naphtha, diesel and gasoline, waxes and other chemicals, which are determined by catalyst selectivity and the reaction conditions as well as the length of hydrocarbon chain. Figure 1.6 shows the FT GTL process configuration, which is essentially in three stages of synthesis gas production, FT conversion, and product upgrade.

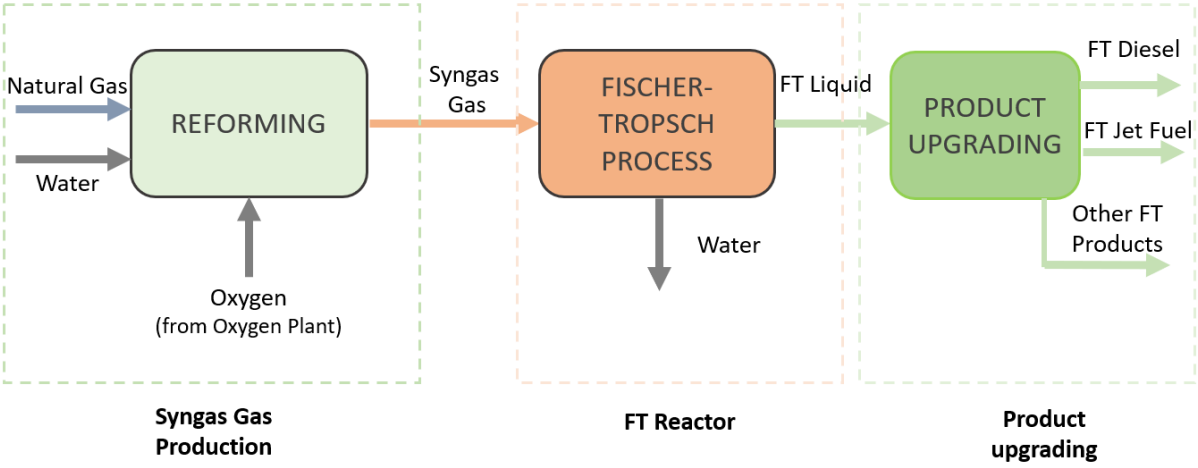

Figure 1.6: GTL block flow diagram. Adapted from (Dry, 1996)

Increasing interest has been observed in the Fischer-Tropsch technology because its potentials for large stranded gas utilization and the environmental benefits of GTL products with improved air quality compared with conventional transportation fuel emissions (Mokhatab et al., 2015). In addition, the fact that GTL fuel can be transported to market using the conventional crude oil marine vessels suggests reduced transportation cost (Khalilpour and Karimi, 2012). GTL technology has emerged as a technology with vast product opportunities and market diversification. This option is also believed to have advantage because it can utilise small scale stranded gas, related to natural gas especially regarding exploration in off-shore platforms with the emerging exploits in microchannel GTL technology (Farias et al., 2007).

However, GTL technology present challenges which centre on high capital cost, efficiency, competitive crude oil and petroleum market and reliability of complex process sequences (Wood et al., 2012).

Furthermore, FT synthesis occurs at high process conditions of temperatures about 463 – 553 K and pressure 1.5 – 2.5 MPa (Koortzen et al., 2013). In addition, in conventional FT process the rapid removal of heat forms a major consideration of design of suitable FT reactors. Insufficient removal of heat in a FT reactor leads to carbon deposition and higher selectivity for undesired methane at the expense of desired FT products (Dry, 1996). GTL fuel and products are in direct competition with crude oil refined fuel. As a result, the economic viability of a GTL plant is highly dependent on crude oil and gas price (Economides, 2005a).

Typically, the factors that determine the economic viability of a GTL plant are capital and operating cost, product premiums, shipping cost, location of plant, and environmental considerations (SPE International, 2013, Shah and Durr, 2009, Wang and Economides, 2009). Although, recent developments in intensification of GTL processes by companies like Compact

GTL and Velocys may improve the economics of GTL technology, cost and complexity of supply chain remains a hurdle.

1.4.5 Gas to Wire (electricity power generation) technology

The gas-to-wire (GTW) technology involves the conversion of natural gas to electric power and its transmission and distribution to the consumers. Typically, major proportion of transported gas is utilized as fuel for electricity using installed gas turbine generators either in simple or combined cycle configuration. The combined-cycle configuration gas turbines are integrated with heat recovery systems. Although the combined-cycle turbines are capital intensive, it offers an effective power throughput compared to the simple-cycle turbines (SPE, 2013).

Electric power generating plants can be constructed onshore or offshore with marine cabling on either stationary platform or floating power generating plants (FPGP) (Angays et al., 2013). For the FPGP option, power-generating plant is constructed on-board a floating vessel that uses treated gas resource from nearby gas reservoirs and then power generated is transmitted to shore via submarine electrical cables. According to Angays et al. (2013), this is only practicable for a gas feed that can produce 1 gigawatts (GW) electricity located 300 km from shore. Hence, FPGP is limited by distance and economic viability compared to other gas utilization options for remote locations.

Equally, platform offshore gas turbine generator construction with submarine high voltage direct current cables transmission to onshore grid offers route for remote gas utilization. This extends to submarine HVDC transmission distance of up to 1500 km (Mokhatab et al., 2008, Mokhatab and Poe, 2012). High voltage direct current (HVDC) compared with the high voltage alternative current HVAC transmission offers the most viable technical option for moving large quantity of electric energy with minimal 10% energy loss over 1500 km distance (Mokhatab and Poe, 2012, Mokhatab et al., 2015). However, the need for end-to-end installation of transformers and converter stations make HVDC solution very capital intensive. This is because HVDC transmission lines (cables) require transformers for voltage step up/down and converters for alternative current (AC) to direct current (DC) as well as from DC to AC at local distribution point to consumers. As a result, this option appears to be almost as cost intensive as constructing pipelines (Mokhatab and Poe, 2012). Furthermore, Shah and Durr (2009) approximated the thermal efficiency of GTW option (excluding transmission) to about 30 – 60 % which makes it seem less viable to other options.

GTW is viable for stranded gas reserves in locations with onsite electrical grid or close shoreline grid. For example, in Indonesia with several islands where gas volume reserves as low as 20,000 m^3 per day (equivalent to 0.7 MMscf/d at 288 K) can fire a 3 MW generator for electric power generation for 7500 homes (Vitucci, 2010).

Oil and Gas Authority (2018) reported a recent development due to the installation of large offshore windfarms (offshore electrical infrastructure consisting sub-stations platforms and subsea cables) exporting power to shore. This implies an extension of the UK's national grid to the East Irish Sea and UK Southern North Sea production fields (Oil and Gas Authority, 2018). Figure 1.7 shows a schematic illustration of a GTW option with HVDC transmission line installations. For an associated gas field, generator operational shut down may require total shut down of the entire gas production process or the gas channelled to flare (Mokhatab et al., 2008). This could cause economic waste and bridge of gas demand contracts. The relative location of the gas resource, the end market and transmission techniques, as well as cost is the core challenges associated with this option.

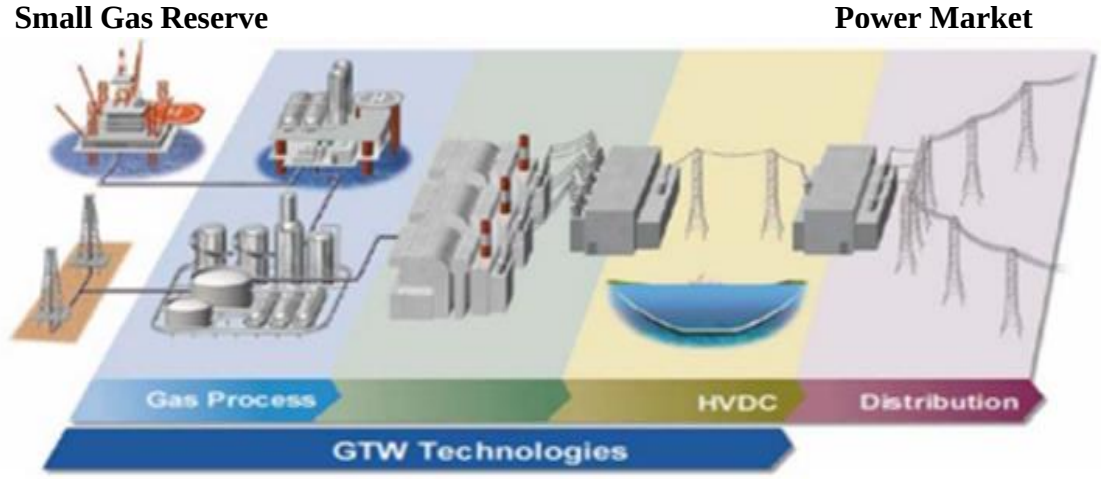

Figure 1.7**:** GTW technological distribution Network. Source: (Anosike, 2013)

1.4.6 Gas to hydrate (methane gas hydrate) technology

Gas hydrate technology involves transport of natural gas in the form of solids called gas hydrates. Natural gas hydrates are formed by mixing water and processed natural gas at low temperature, high pressure conditions and can be employed as a gas transport technology (Gudmundsson, 1996a). Gas hydrates are crystalline compounds of water molecules of hydrogen bonded cage-like structures enclosing suitably sized guest molecules within the clathrate lattice formed at low temperature and high pressure (Masoudi and Tohidi, 2005). When the feed stream is pure methane gas, it is referred to as methane hydrate, which is the single (sI) crystalline structure of guest methane gas surrounded in lattice of water molecules called clathrate. Methane gas forms sI hydrates while natural gas (sII) hydrate usually predominantly methane gas and other guest gas molecules of low-molecular diameter gases include methane, ethane, propane, carbon dioxide, tetrahydrofuran (surfactants) etc (Prasad and Chari, 2015).

Gas hydrate technology comprises of three major stages: production, transportation and regasification (Nakai, 2012a). Several research studies show that gas hydrate production is technically feasible and have potentials for transportation of gas in frozen form in insulated vessels (Gudmundsson and Borrehaug, 1996b) or refrigerated slurry mixed with refrigerated crude oil for transport in crude oil trucks (Gudmundsson et al., 1999) or pellet form at atmospheric pressure and 253 K (Kanda, 2006). At the receiving terminal, the gas hydrate is regasified by the supply of heat externally for the gas hydrate dissociation into water and gas. The regasification is followed by gas treatment and compression of the gas to market gas quality specifications. This technology could be a viable and safe alternative for storage and transportation of stranded gas due to the less severe operating conditions and energy inventory (Gudmundsson, 1996b, Tamsilian et al., 2013). Gas hydrate technology for transportation of natural gas can be via sea transportation and land according to demonstrations by MES Ltd with an established pilot plant (Nogami et al., 2011). Conceptual studies on offshore/sea transport are also reported for gas hydrate pellets (Rehder et al., 2012, Gudmundsson, 1996b), which is considered a safer form of transport.

Furthermore, Sloan and Koh (2008) highlighted the self-preservation phenomenon of methane gas hydrates which essentially reduces the amount of refrigeration requirement for prolonged stability during storage and transportation of the hydrate. Self-preservation is a phenomenon which has been observed experimentally by several researchers where gas hydrate display a prolonged stability for extended time away from the hydrate stable region (Prasad and Chari, 2015, Rehder et al., 2012). As such, the transportation of stranded gas is believed to be relatively of lower cost and a safer operation with insignificant gas emissions due to the self-preservation phenomenon for the methane hydrate pellets, which are stable at 253 K compared to 111 K. In addition, some conceptual evaluation studies of gas hydrate as a gas utilization or transportation technology suggest it to be a viable alternative to LNG for large capacity gas reserves over long distances (Gudmundsson, 1996b, Nakai, 2012a). Conversely, in terms of energy density, 1 m^3 of natural gas hydrate contains about 180 m^3 of natural gas while 1 m^3 of LNG equals 600 m^3 of natural gas limiting amount of gas transported using the hydrate technology compared to LNG. Furthermore, the application of gas hydrate technology is still not established commercially. However, it is conceptually proven to be technically feasible by laboratory, pilot and research studies such as British Gas Group (now BP plc)/Advantica, UK (Fitzgerald and Taylor, 2001), Norwegian University of Science and Technology (NTNU) (Gudmundsson et al., 2000), MES Engineering and Shipping Company (Nakai, 2012a)and German integrated Submarine Gas Hydrate Resources SUGAR project (Rehder et al., 2012). Some of the setbacks for the gas hydrate technology are complexities relating to slow kinetics and cost (Mokhatab et

al., 2015). Rajnauth and Barrufet (2008) emphasized in his study that formation of large volumes of gas hydrates will be a long process due to low formation rate of hydrate. However, several research advances have been reported with the production of gas hydrates. The use of thermodynamic promoters (like Tetrahydrofuran, THF and Tetra-n-butyl ammonium bromide, TBAB) and surfactants such as sodium dodecyl sulphate (SDS) that enhance rate of hydrate formation (Tohidi Kalorazi et al., 1996, Prasad and Chari, 2015, Rehder et al., 2012, Lin et al., 2004). In addition, advances in reactor configurations such as stirred-tank reactors in continuous mode operations and scale-up studies, which could apply industrially (Mork and Gudmundsson, 2002, Mork et al., 2001, Mori, 2015). The use of other reactor configurations such as packed-bed and flow reactors for hydrate process are presented in review by (Yin et al., 2018)

1.5 Comparison of technologies considered for stranded gas utilization

The fundamentals of each of the technologies for transportation or utilization of stranded natural gas are discussed in Section 1.4. The two major factors that influence the choice of stranded natural gas utilization technologies are reserve volume capacity (reservoir production volume) and market distance (Wood et al., 2008). The key element of addressing the stranded gas utilization problem is the ability of project decision makers and developers to access a framework of technologies evaluated case by case. The range of stranded gas utilization technologies which are available to project decision makers, operators and developers are typically illustrated using a qualitative model of reserve volume capacity against market distance as shown in Figure 1.8, adapted from Wood et al. (2008). The qualitative illustration intends to show the boundaries of the alternatives indicating where the application of different technologies might be best suited based on the potential production volume and market distance.

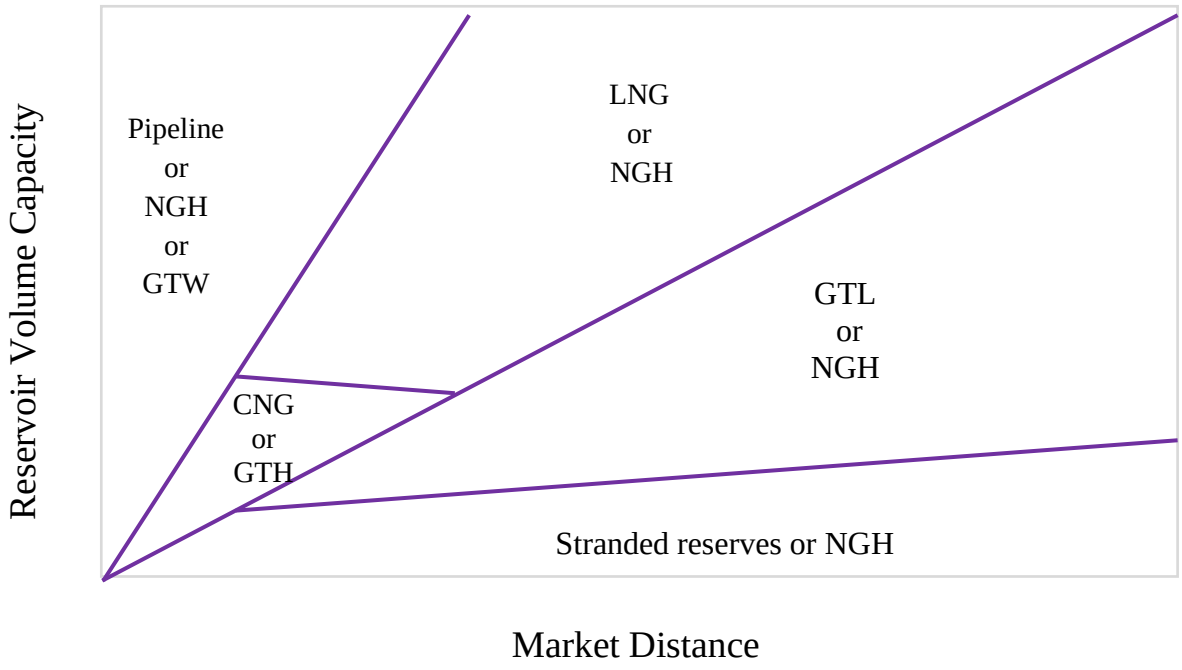

Figure 1.8: Qualitative illustration of the stranded gas technologies based on volume capacity and market distance constraint. Adapted from (Wood et al., 2008)

Pipelines and liquefied natural gas are the most commercial established technologies for the utilization of stranded gas. However, the limitations of scenarios of low volume capacity or depleting reservoirs as well as consideration of remote locations without existing pipeline network affect the decision. As discussed in Section 1.4, these two technologies, although high capital cost investments, are established viable options for large capacity stranded gas utilization but are limited by market distance and small volume capacity reserves. In addition, the GTL (Fischer Tropsch) technology although commercialized, requires technological advancement to improve efficiency.

However, the question whether the NGH technology can be feasible alternative for large and small volume capacity reservoirs over long distance market distance for stranded gas utilization will be addressed qualitatively as well as quantitatively in subsequent chapters in this study. In Table 1.4 below, a comparison of the major highlights of each of the discussed six technologies is compared, comprising the advantages and disadvantages respectively. Other factors aside from volume capacity and market distance may also include the energy density of fuel transported; commercialization stage of the technologies; economic reality of technologies; investment cost of technologies; revenue security.

Table 1.4: Summary of advantages and disadvantages of stranded gas utilization technologies based on section 1.4.1 – 1.4.6

Technology		Developmental stages	Process Complexity	Volume capacity and storage	Economic feasibility	Environmental and safety merit
Pipeline technology	**Advantages**	Fully commercialized.	Pipe network and compression stations.	Suitable for large volume capacity reserves depending on pipe dimensions and capacity.	For large gas capacity reserves and proven gas market over short distances. Long term supply contracts.	Required pre-processing depending on gas composition.
	Disadvantages	Risk of political shutdown and terrorism especially for intercontinental pipe networks. Pipeline technology is not flexible.	Challenges of hydrate formation especially for underwater pipelines.	Unsuitable for stranded NG including small and marginal gas reserves.	Non-viable for stranded gas reserves. Require high capital investment with compression stations relative to distance and size.	Risk of vandalism of pipeline network due to cross-countries or inter-border disputes.
Liquefied natural gas (LNG) technology	**Advantages**	Mature technology for NG transport over far distances like cross-countries where pipeline network does not exist.	Provide storage of LNG at receiving centres used at peak demand periods	High energy density due to volume reduction 600 v/v	Viable to transport large gas instead of pipelines over long distances	Requires stringent gas processing compared to other discussed technologies. Cannot be considered for modest demand market
	Disadvantages	Long-term contracts 20-25 years, not accessible for small gas users and independent power producers.	High-energy inventory for Liquefaction. Technological complexities using cryogenic materials and strict designs and safety protocol.	It requires large gas reserves to substantiate high capital investment.	High supply chain capital investment including cryogenic vessels.	Boil-off
Compressed natural gas (CNG) technology	**Advantages**	Solution for projects requiring long-distant subsea pipelines which is not economically feasible or markets with diffident demand and reserves.	Multistage compression, simpler compared to LNG. No distinct gas recovery in chain.	Volume reduction to about 200 v/v	Suitable for modest transport from small gas reserves Movable asset investment on field decommissioning.	
	Disadvantages	Technology not yet of full commercialization.	High capital investment multistage compression.	The use of CNG for large capacity scale is not yet commercially sanctioned.	High capital investment pressure storage vessels.	High safety risk.

Gas to liquid (GTL) technology (Fischer-Tropsch Synthesis)	**Advantages**	Commercialized Technology. Variety of product options (diesel, gasoline, naphtha etc).	High-energy combustion process. GTL fuel can be transported standard crude oil vessels Easy of transport compared to other technologies .	GTL fuel can be blended with crude oil, offering solution for associated gas utilization from oil and gas reservoirs.		GTL products are clean burning fuel with potentials of reducing transportation fuel emissions.
	Disadvantages	Technology require technological advancement to improve efficiency.	High cost of catalysts and process complexities.	Associated low energy efficiency of production of syngas.	Market competition with petroleum fuel and crude oil prices for its economic viability.	Low safety risk in liquid form.
Gas to hydrate (NGH) technology	**Advantages**	Gas hydrates can be transported in solid form (pellets) at 253 K and atmospheric pressure with cooling energy inventory to LNG.	Production, transport, and regasification. NGH slurry form can be transported using crude oil marine vessels which could be a viable solution for associated gas reservoirs.	Offers compact energy storage in pellet form with 180 v/v nearly similar energy density with CNG.	Less estimated capital investment cost compared to LNG.	Insignificant emission due to self-preservation (for sI, pure methane hydrate) and low safety risk in solid form. Safer gas transportation solution in event of disasters compared to LNG or CNG, it is non-explosive.
	Disadvantages	Technology not commercialized yet. NGH shipping vessel still on research development stage. Processing of gas hydrate slurry to pellets is still in research and development stage.	Low kinetics of NGH and not still evolving. Low kinetics may imply challenges at large scale production.	Low energy density fuel compared to conventional LNG and pipeline technologies.	Self-preservation effects of NGH not clearly recognised yet for sII hydrates, which implies further gas pre-treatment may be required to pure methane with cost consideration.	
Gas to Wire (GTW) technology	**Advantages**	Technology advanced which offers suitable alternative for gas reserves with proximity electricity grid.	Technology provides adequate solution for on-site grid supply of electric power from gas turbines. Gas from offshore reservoir can be used to fuel power plant.	GTW via high voltage direct current (HVDC) transmission lines is technological viable solution for transport large capacity electric power over more 1000 km about 10 % energy loss.	Viable for reserves close enough to electricity grid such as Indonesia with several islands	
	Disadvantages	Limited market supply, that is, electric power market.	Associated high installation cost of converters and facilities.	Offers limited electric power transmission distance to 1500 km.	High capital investment due to end-to-end need for operating converters and transformers.	

Table 1.4 shows that LNG appears to dominate over other technologies for large capacity utilization over long market distances. 1 m^3 of LNG equals 600 m^3 of natural gas while 1 m^3 CNG and NGH contain 200 m^3 and 180 m^3 of natural gas respectively. This indicates that with LNG technology maximum energy density fuel is achieved compared to CNG and NGH. Similarly, in terms of developmental stage of technologies, LNG and pipeline technologies clearly show dominance over other options as the most established technologies commercially. However, with the consideration of other factors such as technology complexity, better economic viability, and environmental merit, a drawback from LNG technology is observed. Likewise, in specific scenarios where there is no pipeline network and need for onsite electric power supply or a power market proximate offshore reservoir, GTW would be considered as best option.

Nakai (2012a) reported a 20 – 30 % cost advantage of NGH technology chain over LNG for large volume capacity production (Large volume reserves). He argued that, the lower investment cost of NGH development compared to the liquefaction process requiring temperature of 111 K with expensive cryogenic materials as well as the less transport energy inventory (253 K and at atmospheric pressure) of gas hydrate pellets offsets the large energy density merit of LNG making it economically more viable.

However, a major disadvantage associated with NGH technology is its development stage. NGH as stated previously is not yet commercialized as the existing projects of NGH chain are still in laboratory, research development, and pilot plant stage. Companies like Mitsui Engineering and Shipping Ltd, Mitsubishi Heavy Industries and JFE Engineering Corporation are leading in the research and development of NGH technology for stranded gas utilization. However, there is need for further research into these challenges to enable the commercialization of the NGH technology.

As a comprehensive survey of previous economic assessments on NGH for gas transportation is presented in Chapter 3. Furthermore, in Chapters 4, 5 and 6, NGH technology using sI hydrates with a pure methane gas and water feed is explored using process simulation of the reactor with Aspen HYSYS software including the downstream processing units, transportation, and regasification units. This is employed for the NGH chain detailed costing and economic evaluation covering small and large volume capacities over long-distant market and further compared with alternative technologies.

1.6 Concluding remarks

This chapter presented the background and rationale for the utilization of natural gas as a low-carbon fossil fuel compared to coal and crude oil and the essential role it plays in the global energy supply. The clear perspective of stranded natural gas reserves as having low capacity or

being too far from demand market in addition to the technologies for its utilization were discussed.

The advantages and disadvantages of the technologies for NG utilization were also compared using the criteria of developmental stages, process complexity, volume capacity and storage, economic feasibility, and environmental and safety merits. Methane hydrate technology was highlighted as a promising alternative although still evolving method for utilizing stranded small capacity NG reserves. In addition, the composition of raw stranded natural gas was discussed which, highlighted the pre-processing requirements in addition to its variability for different gas reserves.

Chapter 2 Literature survey on gas hydrates

2.1 Introduction

The purpose of this chapter is to provide a review of gas hydrate process and their properties and structures with emphasis on methane hydrate production and its applications for gas storage and transportation. Natural gas hydrates composing of beyond methane are also discussed as well as highlights of the discovery of gas hydrates and development in research over the years. The discovery of gas hydrates is credited to the first introduction in research at the Birmingham laboratory by Joseph Priestley in 1778. On performing cold experiments in which he left his windows open in winter evening, Priestley discovered gas hydrates with vitriolic air (SO_2) impregnating water at the freezing condition (Sloan and Koh, 2008). Then in 1810, Sir Humphrey Davy also reported chlorine hydrate formation. He noted the formation of ice-like solid at temperature above freezing point of water and that the solid was composed of not just water. The chlorine hydrate when melted released chlorine gas. Michael Faraday further confirmed the discovery of chlorine hydrates in 1823. Over the eighteen to nineteen centuries, gas hydrate research activities were largely considered academic explorations with focus on determination of substances forming hydrates and at what temperature and pressure conditions the formation would occur (Englezos, 1993). Among the researchers, Villard and de Forcrand were prolific with measurements of hydrate conditions over wide range of substances including N_2 and H_2S. The existence of methane, ethane, and propane hydrates was also first determined by Villard in 1888 (Sloan and Koh, 2008). Among other discoveries, was that of gas hydrate formation in gas pipelines with water at high pressure and above water freezing point temperature (Hammerschmidt, 1934). This discovery of hydrate plugging of natural gas pipelines marked the onset of intense research advances on natural gas hydrates by the government, industry and academia (Englezos, 1993). Forthwith and in recent years, overwhelming number of research papers, reviews, conference proceedings on gas hydrates have been published including experimental studies and pilot plants covering gas hydrate properties, structures, thermodynamics, kinetics, promoters, and attainable technological and energy applications etc.

Gas hydrate also called clathrate hydrate is an inclusion compound in which the ‘host’ cavities of polyhedra of hydrogen bonded water molecules accommodates the ‘guest’ gas molecules forming solid crystalline cages at high-pressure low temperature conditions (Koh et al., 2011).

2.2 Gas hydrate structures

Gas hydrate crystals are three-dimensional structures in which hydrogen-bonded water molecules (host) form cavities that entraps the guest molecules within it. The guest molecules

inside the cavities or cages interact with water molecules by weak van der Waals forces as gas hydrates are not chemical compounds. This implies the guest molecules maintain their inherent properties stored inside hydrates and the gas molecules released by disturbing the van der Waals forces (Carroll, 2014). The gas hydrate structure formed depends on the guest molecule size, as well as the pressure and temperature conditions (Koh et al., 2011). Several studies have been reported relating to the structures of hydrates which is presented in review paper by (Sloan, 1998). This includes studies on gas hydrate structures measurement and characterization using diffraction (neutron diffraction and X-ray diffraction) and spectroscopic (nuclear magnetic resonance, NMR and roman spectroscopy) measurement techniques. The extensive X-ray diffraction studies by (v. Stackelberg and Müller, 1954) led to the determination of the sI and sII hydrate structures as well as sH hydrate discovered with NMR spectroscopy and x-ray and neutron powder diffraction evidence provided by Ripmeester and co-workers (Ripmeester et al., 1987).

The three common gas hydrate structures in which natural gas hydrates normally forms are cubic structure I (sI), cubic structure II (sII) and Hexagonal structure (sH). These structures have characteristic cavity size, shape, and water molecules forming a unit crystal cell. The common hydrate cavity or the basic building block is the pentagonal dodecahedron (5^{12} – 12 pentagonal faces). The cavities in which the hydrated guest molecule is situated are formed by framework of water molecules.

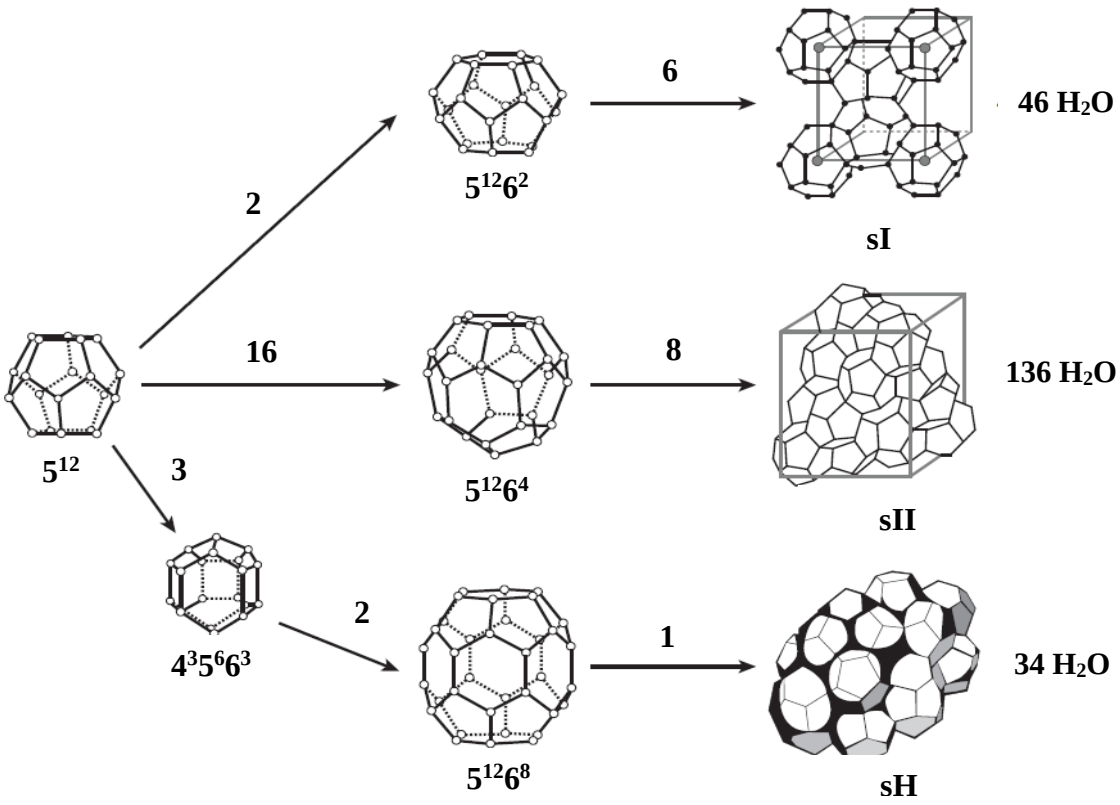

Figure 2.1: Common natural gas hydrate structure (Sloan and Koh, 2008)

The sI is the least complex gas hydrate structure composed of two cavities of small pentagonal dodecahedron 5^{12} and six large cavities of tetrakaidecahedron $5^{12}6^2$ (14-sided polyhedron with 12 pentagonal and 2 hexagonal faces) which are the small and large cavities respectively. sI contains 46 water molecules in its unit cell as illustrated in Figure 2.1 below. The molecular size of the guest and the conditions of hydrate formation determine the type of hydrate structure formed. Typically guest molecules with diameters between 0.4−0.6 nm (nanometre) form sI such as methane, ethane, and non-hydrocarbon like carbon dioxide, and hydrogen sulphide (Sloan, 1998). The theoretical formula for the sI and sII if both cages are filled with guest molecules is $X.5.75H_2O$ and $X.5.67H_2O$ respectively (that is the ideal hydration number) where X denotes the 'guest' molecule, that is, one mole of X for every 5.75 and 5.67 moles of water respectively. However, actual hydrate composition depends on amount of X molecules that fit into the various cage structures of the water lattice as well as temperature, pressure and associated fluid phases' composition. It is also important to note that because hydrates are nonstoichiometric, which indicates that even without a guest molecule filling all the cages, a stable hydrate can still form with the degree of saturation depending on the temperature and pressure conditions. Therefore, the earlier stated composition is theoretical not the actual composition of the hydrate (Sloan and Koh, 2008).

The sII hydrates are made up of larger guest molecules of diameters 0.6 – 0.7 nm such as ethane, propane, and iso-butane. Molecules less than 0.35 nm are too small to stabilize any cavity while molecules above 7.5 nm becomes too large to fit into any sI or sII cavity (Sloan and Koh, 2008). However, exceptions for sII are small guest molecules such as nitrogen, argon, and hydrogen which with diameters less than 0.4 nm but also form sII hydrate (Sloan and Koh, 2008). It contains 136 water molecules in a unit cell. The theoretical composition of the sII hydrate if each of the cages is filled with guest molecule is $X.5.67H_2O$ (where X is the 'guest' molecule and 5.67 is the hydration number). The sII hydrates are composed of sixteen small cavities of pentagonal dodecahedron 5^{12} and eight large cavities of the hexakaidecahedron $5^{12}6^4$ (6-sided polyhedron with 12 pentagonal and 4 hexagonal faces). However, as often is the case, if only the large cages are occupied by the guest molecules, then the theoretical composition is $X.17H_2O$ (Carroll, 2014).

The sH hydrates are formed by guest molecules greater than 0.7 nm and are less common hydrates which are binary hydrates because two sizes of molecules are necessary to stabilize the structure. sH require a small molecule such as methane and large molecule greater than 0.7 nm like benzene, 2,2-dimethyl butane, cyclopentane as such contain two different hydrate formers unlike the sI and sII which typically form hydrates by single occupants having small

and/or large cavity (Ye, 2013, Sloan and Koh, 2008). A unit crystal cell of sH which consists of 34 water molecules has three size cavities which are three small dodecahedron 5^{12}, two medium irregular dodecahedron $4^3 5^6 6^3$ (with three square, six pentagonal and 3 hexagonal faces), and eight large irregular icosahedron $5^{12}6^8$ (20-sided polyhedron with twelve polyhedron and 8 hexagonal faces). A theoretical formula for the sH structure is difficult because two hydrate formers are required to form the hydrate (Sloan and Koh, 2008).

To describe the cavity size ratio of hydrates, Table 2.1 is used with size ratios of natural gas components for sI and sII. A lower bound size ratio of below 0.76 indicates less molecular attractive forces for stability. When the size ratio exceeds unity, the guest molecules will not fit within the cavity and a hydrate will not form. The guest molecules size and the occupancy in lattice cage or cavity determine the hydrate structure type formed. In such case as pure methane, stability can be achieved for the 5^{12} as well as the $5^{12}6^2$ or $5^{12}6^4$ cavities of either sI or sII respectively, although with preference for sI. This is because slightly higher stability to the $5^{12}6^2$ cavity is usually achieved than the $5^{12}6^4$ cavity in sII (Sloan, 1998, Sloan and Koh, 2008).

Table 2.1: Cavity size ratio (molecular diameter/cavity diameter) for natural gas hydrates (Sloan and Koh, 2008)

Guest molecules		**Cavity size ratio (Saturation)**			
Molecule	**Diameter (nm)**	**Structure I**		**Structure II**	
		5^{12}	$5^{12}6^2$	5^{12}	$5^{12}6^4$
CH_4	0.44	0.86	0.74	0.87	0.66
C_2H_6	0.55	1.08	0.94	1.10	0.83
C_3H_8	0.63	1.23	1.07	1.25	0.94
i-C_4H_{10}	0.65	1.27	1.11	1.29	0.98
n-C_4H_{10}	0.71	1.39	1.21	1.41	1.07

Guest molecules like propane or iso-butane can only stabilize the large cavity, $5^{12}6^4$ of sII as shown in Table 2.1. Usually for gas mixtures, the largest constituent guest molecule determines hydrate structure formed. An example is natural gas comprising propane ($C_1 - C_3$), will form sII because propane is too large to fit into the $5^{12}6^2$ cavity of sI as shown in Table 2.1. It is interesting to note also that, methane usually stabilizes preferentially the sI small cavity 5^{12} (size ratio of 0.86), although the size ratio of the sII 5^{12} cavity is slightly higher (size ratio of 0.87).

This is attributed to the extra stability added by the guest molecule occupying the $5^{12}6^2$ cavity (Sloan, 1998).

2.3 Physical and chemical properties of gas hydrates

The common hydrates contain approximately 85 % (mol) water and 15 % (mol) gas if the cages of each structure are filled. This suggests that the gas hydrate properties are similar to that of ice (Davidson et al., 1987, Sloan, 1998). The heat capacity, mechanical, and electrical properties of hydrates are comparable to those of ice. However, the main difference being that hydrates form with gas components (guest gas) of suitable sizes whereas ice forms as a pure component. The comparison of the properties of sI and sII hydrates with the ice Ih crystal is comprehensively reported in (Sloan and Koh, 2008). For the thermal conductivity, that of ice is 2.2 $Wm^{-1}K^{-1}$, which is higher than sI, and sII hydrates (~0.5 $Wm^{-1}K^{-1}$). The relatively low value explains why hydrates require more time to melt compared to ice. Durham et al. (2003) suggested higher mechanical strength for hydrates, in their compression deformation experiments for sI hydrates (methane) at 260−273 K. They reported that hydrate is about 20 times stronger than ice with equally applied stress, which is attributed to the fact that the rate of water diffusion in hydrates is much slower than in ice. sI hydrates (methane) also have slightly higher heat capacity (~2250 J $kg^{-1}K^{-1}$) than that of ice (2060 $Jkg^{-1}K^{-1}$) (Carroll, 2014). On the similar properties, the densities of sI, sII hydrates and ice are less than that of water and the same volume expansion occur in both hydrates and ice upon freezing of water. However, although hydrates have ice-like properties, they can be formed above water freezing temperature at elevated pressures. Table 2.2 show the densities of some sI, sII hydrates, water, and ice at 273 K, indicating proximate values of densities.

Table 2.2: Densities of some hydrates, Ice, and water at 273 K

Component	Structure Type	Density (kg m^{-3})
Methane	sI	913
Ethane	sI	967
Propane	sII	899
Isobutane	sII	934
Ice	1h	917
Water	H−O−H	1000

Hydrate densities calculated based on (Carroll, 2014) using saturation values obtained with CSMHYD

As earlier mentioned, gas hydrates are not chemical compounds. Water molecule consists of an atom of oxygen covalently bonded to two hydrogen atoms and a hydrogen bond due to the attraction of the positive on one molecule to the negative pole on adjacent water molecule. The covalent bond energy (426.8 $kJmol^{-1}$) which exists in water molecules is far higher than that of hydrogen-bond energy (20.9 $kJmol^{-1}$) which applies for ice and gas hydrate. When hydrates form or dissociates, just the hydrogen bond between neighbouring molecules is considered alongside the weak bonding by van der Waals forces (1.3 $kJmol^{-1}$), that stabilize guest molecules in water cages (Sloan and Koh, 2008).

The solubility of guest gas in liquid water, which is a chemical property, is a vital element in hydrate formation system. Solubility is measured in terms of the maximum guest gas (solute) dissolution in liquid phase at equilibrium resulting in saturation. However, the gas available in the liquid phase exceeding the solubility (that is the maximum gas content in equilibrium) results in supersaturation or the metastable state. This surplus, which is the degree of supersaturation, induces the transition to the solid hydrate from the liquid/gas phase, which describes the driving force for hydrate formation (Kashchiev and Firoozabadi, 2002). In other words, a supersaturated regime is obtained for a given temperature when methane gas dissolves in liquid water at a higher pressure than the equilibrium formation pressure. The supersaturation phenomenon has been experimentally demonstrated in several experimental studies in which the gas is in contact with liquid water under isobaric and isothermal conditions (Englezos et al., 1990, Englezos et al., 1987b, Englezos et al., 1987a, Vysniauskas and Bishnoi, 1983). Further discussion on the rate of gas hydrates formation is presented in Section 2.5.

Another vital component of gas hydrates is the flow properties of hydrate-water slurries (hydrate in water slurry), as hydrates are known to block high-pressure pipelines in deep-water offshore fields. Typically, as gas hydrates form in a gas hydrate forming system, the viscosity, as well as the density of the hydrate-slurry changes with hydrates concentration (Meindinyo and Svartaas, 2016). Therefore, at increasing hydrate concentration, as slurry viscosity shows increasing non-Newtonian behavior based on laminar flow experiments (Andersson and Gudmundsson, 1999).

Andersson and Gudmundsson (2000) in their study considered hydrate-water slurries based on visual observations to behave homogeneously attributed to the fact that the slurries are non-settling due to having small particles sizes as well as the small difference between the fluid and solid densities. The apparent viscosities of the hydrate-water slurries were investigated using the Bingham viscosity model which considered the flow behaviours at 6.0−9.0 MPa and 275−283 K comprising hydrates sI (pure methane) and sII hydrates (93 % methane, 5 % ethane and 3% propane) in tube viscometer connected to the experimental hydrate-forming rig. The

results showed that hydrates flow as homogeneous slurries, also indicating increase in the viscosities of hydrate-water slurries with increasing concentration with no difference between the sI and sII hydrate slurries relating to viscosity. These typically apply to laminar flow regime (Andersson and Gudmundsson, 2000). However, effective viscosities similar to water viscosity were obtained for the turbulent regime experiments with different concentrations (0−21 vol %) of the hydrate-water slurries using the slurry hydraulic gradient equation verses water Reynolds number plot. This concludes that the carrier water phase alone determines the frictional pressure drops of the hydrate-water slurries when in turbulent region (Andersson and Gudmundsson, 2000). Therefore, in this study with water-hydrate slurry within the hydrate concentration of approximately 11 vol % in turbulent flow regime (in hydrate forming reactor), the viscosity of water was assumed in Chapter 4.

Furthermore, a modified equation for determining hydrate-water viscosity based on the derivation of Meindinyo and Svartaas (2016) which uses the energy input, P per unit volume, V of fluid in a stirred reactor (P/V) is as follows:

$$\mu_{slurry} = \left(\frac{P}{V}\right).\left(\sqrt{(\frac{P}{V})/\mu_w)}\right)^{-2} \qquad 2.1$$

The viscosity of water is denoted as μ_w and μ_{slurry} the hydrate-water slurry. The equation was also used to verify estimate of hydrate-water slurry viscosity in this study.

On the other hand, some other experimental studies reported in literature align with the fact that the use of anti-agglomerants contributes to hydrates transportation by ensuring dispersion of formed hydrates into slurries (Moradpour et al., 2011, Bbosa et al., 2018). This also ensures prevention of flow line blockages especially with high concentration hydrate slurries and high subcooling systems. Moradpour et al. (2011) in their study on the use of anti-agglomerant using 60−80 % water-cut system reported transport of hydrate slurries of up to 30 % solid fraction with no blockages. The study suggested that the hydrate slurries transportability is determined by the amount of hydrates in the system and not on the water-cut contrary to what is largely believed. The study also established the use of very low anti-agglomerant concentration (0.15−2 %w/w of aqueous phase) in forming transportable hydrate slurries in high water-cut systems where the gas is the control reactant (Moradpour et al., 2011). This has economic and environmental potentials industrially.

2.4 Gas hydrate phase equilibrium

Hydrate formers or guest molecules in water form hydrates at thermodynamic conditions, as earlier mentioned. Since the discovery of gas hydrates research, finding suitable hydrate formers as well as their respective incipient hydrate formation conditions have been embarked including both theoretical and experimental investigations (Bishnoi et al., 1989, H. van der

Waals and C. Platteeuw, 1959, Khan et al., 2016). Several studies on gas hydrates equilibrium have concentrated on gathering of emerging equilibrium hydrate formation data as well as developing predictive approaches for determining phase equilibria (Khan et al., 2016).

The formation conditions refer to the situations that an infinitesimal amount of hydrate phase is in equilibrium with liquid water and gas (Englezos et al., 1990). Thermodynamic equilibrium is said to be established in a system when the chemical, thermal and mechanical equilibrium coexist, in which context the temperature, pressure and chemical potentials of the system ceases to vary with time (Keszei, 2012). Gas hydrate equilibrium can therefore be defined as a system having gas hydrates in thermodynamic equilibrium. In other words, the three-phase equilibrium of hydrate, liquid water, and vapour ($L_w - H - V$) or ice phase ($I - H - V$) which typically exist in a common hydrate formation system which are subject to thermodynamic conditions.

Prior to the widespread availability of software, the K-factor method, and gas gravity method are two common approaches for estimating the gas hydrate formation conditions attributed to Katz and co-workers. These methods involve the use of charts and hand calculations. Although, there are still popular methods, the methods are considered not highly accurate (Carroll, 2014). The K-factor method employs the distribution of the component between hydrate and the gas ($K = {}^{y_i}/_{s_i}$) on a water-free basis, where y_i and s_i are mole fractions of component i in vapour and hydrate respectively. While for the gas gravity method, appropriate correlation expression of the Katz gravity chart can be employed in estimating the hydrate formation condition (Towler and Mokhatab, 2005).

Further hydrate research development stimulated studies on advances in statistical thermodynamic prediction of phase equilibrium properties (D. Sloan, 1990). Largely reported being the model developed by van der Waal and Platteewu, with which prediction of the three-phase pressure or temperature of hydrate formation can be achieved by defined gas composition of the system (H. van der Waals and C. Platteeuw, 1959). The van der Waal and Platteewu model provides industrially useful statistical thermodynamics prediction of phase equilibria. This and many other models have been reported in several studies (Bishnoi et al., 1989, Gupta et al., 1991, Ng and Robinson, 1976).

Khan et al. (2016) reported a detailed review of hydrate and vapour-liquid equilibria prediction studies and data, which are essential in tuning hydrate phase equilibrium predictions as well as for gas hydrate systems process design (Khan et al., 2016, Khan et al., 2018). In which the liquid and gas phase can be described by cubic equations of state (EOS) such as van der Waals, Trebble-Bishnoi, Peng-Robinson, Redlich-Kwong etc. Several of these EOS are imbedded in chemical engineering computer programs and software such as Aspen HYSYS. Davarnejada et

al. (2014) in their study applied HYSYS software using Peng-Robinson EOS in hydrate formation simulation of Lavan-3 and Salman gas fields. Comparing the predicted data with experimental one, they concluded that HYSYS has capability to predict hydrate formation with < 1 % average absolute error. Applications of HYSYS seem to be dominated in literature for prediction of gas hydrate formation relating to natural pipelines.

This study is intended to explore a robust chemical engineering flow sheeting software such as HYSYS for simulation of gas hydrate production in CSTR for gas transportation and storage, which as far as investigation has been rarely seen in literature for methane hydrate production. Furthermore, the Colorado School of Mines Centre for Hydrate Research also developed two hydrate phase equilibrium predictive models implemented in computer program application, CSMGem and CSMhyd (Ballard and Sloan, 2002, Ballard and Sloan, 2004). These provide prediction of hydrate formation conditions at defined pressure, temperature, and compositions. Other popular commercial software packages for hydrate prediction are Multiflash, EQUI-Phase Hydrate, and PVTSim. Some authors have compared the accuracy of prediction of hydrates with experimental data using some of these commercial softwares (Carroll, 2014, Ballard and Sloan, 2002). Carroll (2014) attributed an acceptable accuracy of hydrate condition prediction using HYSYS software. The hydrate temperature predictions of natural gas mixtures at given pressure were compared to an experimental data and its accuracy reported to be within an absolute error of 273.76 K (0.52 ℃), 273.77 K (0.53 ℃), and 273.20 K (0.05 ℃) for HYSYS, EQUI-Phase and CSMhyd respectively (Carroll, 2014). Similarly, (Ballard and Sloan, 2002) indicated smallest prediction error from measured data using CSMGem compared to CSMhyd, Multiflash, and PVTSim for pure methane component with over 1600 data points.

Furthermore, for experimental measurements of hydrate phase equilibrium, Khan et al. (2016) highlighted among several techniques, the isochoric high pressure rig by Tohidi et al. (2000) and high pressure differential scanning calorimetry, DSC as two commonly used methods. However, it should be noted that the choice of the technique usually depends on the required data, desired pressure and temperature range, and also cost considerations.

Phase diagram as shown in Figure 2.2 can be achieved using compiled data whether obtained experimentally or/and by prediction. This describes the equilibrium line between phases and thermodynamic regions associated with a hydrate formation system at P-T conditions, indicating regions where hydrates form and where hydrate formation cannot be achieved (Sloan and Koh, 2008). An illustration using a phase diagram for a single gas component (methane) hydrate in water system with typical phases as hydrate (H), liquid water (L_w), vapour (V) and Ice (I) is shown in Figure 2.2.

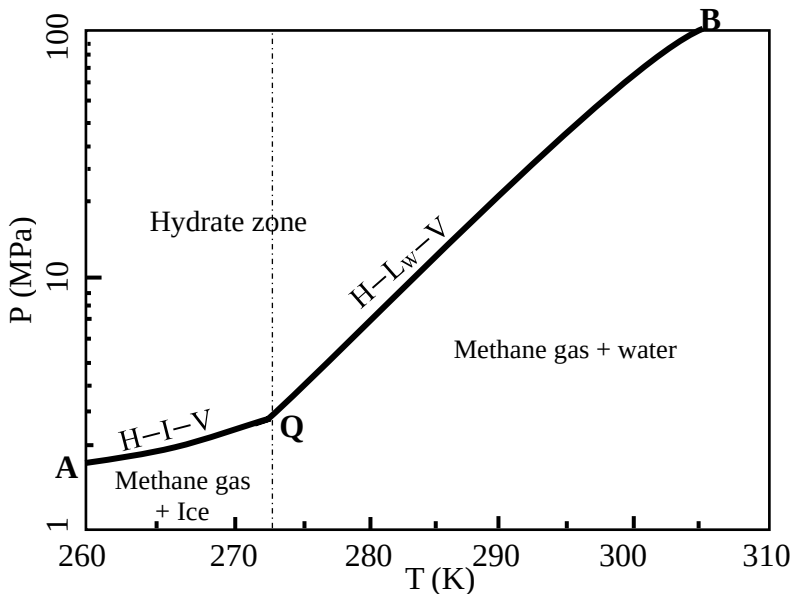

Figure 2.2: P-T of binary system methane-water at 260-310 K (Duan et al., 2011)

At typically 273 K as indicated, the vital equilibrium line past quadruple point (Q) describes the H−L$_w$−V three-phase equilibrium. Quadruple point indicates where the four phases are present. However, depending on critical properties of the guest gas molecule, a second quadruple may be present such as with ethane with higher supercritical temperature.

Since the formation of gas hydrate involves a phase change of a non-reactive process system, the Gibbs phase rule applies in defining the degrees of freedom of the system. The degree of freedom (F) is commonly used to describe the number of intensive independent variables with the number of phases and components of the system defined based on the Gibbs phase rule given as:

$$F = C - P + 2 \qquad 2.2$$

where, C and P are the number of components and number of phases in the system respectively. Consequently, for methane hydrate in water system at three-phase equilibrium will have one degree of freedom, which can be defined using pressure or temperature in a P−T diagram due to the easy of determining these properties directly. On the other hand, a binary gas hydrate such as methane + ethane hydrate in water will have two degrees of freedom, in which case the temperature or pressure as well as the guest molecules composition can be specified.

As earlier mentioned, the type of hydrate formed by hydrocarbons in contact with water is determined by the guest molecule size involved and the hydrate formation conditions. In other words, the structure and the guest to cavity size ratio of gas hydrates (hydrate stability) relate to the phase equilibrium properties. To illustrate, at 278.2 K the equilibrium pressure for methane hydrate (sI) is 7.28 MPa while that for ethane hydrate (sI) is just 0.87 MPa and that of

propane hydrate (sII) is further less 0.49 MPa. This shows a significantly lower hydrate formation conditions with ethane hydrates compared to methane hydrate and a much lower conditions when the hydrate structure changes to sII (propane hydrates) with larger size guest molecule at 278.2 K (Veluswamy et al., 2018). Sloan and Koh (2008) also illustrated the significant effect of gas composition on hydrate stability. Using (sI) hydrate formed from pure methane in water at 5.35 MPa and 280 k compared to (sII) hydrate formed with 1 % propane and 99 % methane components in water. About 42 % decrease in the equilibrium pressure to 3.12 MPa was observed due to large molecular size of propane in just a percent composition. This shows a significant difference in equilibrium conditions required for hydrate stability due to a transition in hydrate structure (Sloan and Koh, 2008).

2.4.1 Enthalpy of hydrate formation

Enthalpy of hydrate formation or dissociation is another important property that defines the amount of heat dissipated or required for hydrate to dissociate respectively. The hydrate formation of hydrate using liquid water and methane gas component is an exothermic process while hydrate dissociation back into liquid water and gas is endothermic. The enthalpy of methane hydrates ranges from $54.2-56.9$ KJmol^{-1} according to measured and correlated reports in literature (Holder et al., 1988b, Sloan and Fleyfel, 1992, Handa, 1986a, Handa, 1986b). Holder et al. (1988a) reported a correlation for determining enthalpy of dissociation for hydrates of some pure components using literature data of calculated dissociation pressures, which for methane given as:

$$\Delta H_d = 4.18\ (c + dT) \qquad 2.3$$

where c and d are correlation constants with values 13500.0 and 4.0 respectively for methane gas and water at temperature range of $0 - 25$ ℃ (273.15 – 298.15 K) while ΔH_d is the enthalpy of dissociation obtained at hydrate equilibrium. In consideration of a hydrate formation from a pure component as is the case in this study, correlation (Equation 2.3) can be used. According to Sloan and Fleyfel (1992), heat of dissociation, ΔH_d is commonly calculated using the Clausius-Clapeyron equation given as:

$$\left[\frac{d(\ln P)}{d(^1/_T)} = -\frac{\Delta H_d}{zR}\right] \qquad 2.4$$

where P and T are the pressures and temperatures of hydrate equilibrium. The formation pressure plot (logarithmic) against inverse of temperature produces a straight line for hydrate formation (either ice or liquid water). Equation 2.4, therefore indicates relatively constant values of the parameters including enthalpy of dissociation, ΔH_d, and the compressibility factor, z as well as the hydration number (stoichiometry ratios of water to guest gas) within range of conditions. It was researcher de Forcrand in early 1900s who originally proposed use

of Clapeyron equation for obtaining the heat of dissociation from 3-phase pressure-temperature data (Sloan and Koh, 2008).

A calorimetric measurement is another approach often used for experimentally determining ΔH_d of gas hydrates (Handa, 1986a, Handa, 1986c) but such measurement is painstaking although suggested as the most accurate method (Sloan and Fleyfel, 1992). The (Handa, 1986a, Handa, 1986c) values are quite comparable to those obtained using the Clausius-Clapeyron equation as shown in Table 2.3 but valid only for univariant systems.

Table 2.3: Enthalpies of dissociation of hydrates of some single gas components at 273.15 K

Gas Component	Estimated ΔH_d (kJmol^{-1}) Clausius-Clapeyron method	ΔH_d (kJmol^{-1}) Calorimetric method
Methane	56.90	54.19
Ethane	71.08	71.80
Propane	126.00	129.20
i-butane	130.40	133.00

Data based from (Sloan and Fleyfel, 1992)

Measurement usually carried for hydrate dissociation rather than during hydrate formation because of uncertainties that are associated with the metastable regime during hydrate formation. Conversely, hydrate dissociation is associated with defined pattern determined by the equilibrium conditions as long as a slow-rate heating is applied and the dissociation conditions are not within the self-preservation range when methane hydrate is considered (242−271 K) at 0.1 MPa (Khan et al., 2016).

2.4.2 Hydration number

Hydration number is the ratio of water molecules to gas molecules in gas hydrate. (Sloan and Koh, 2008), gave an account of the advances of various methods of determination of hydration number following the discovery of hydrates. Originally, direct determination of hydration number applied in which the amount of hydrated water and guest-gas molecules were each measured using different methods. The drawback with the direct measurement was that, the hydration numbers obtained differed widely for each substance nonetheless this reduced as the methods became refined. This drawback was because of the inability of water phase to be completely converted to hydrate without some occlusion and the irreproducible measurement of guest-gas molecules due to hydrate metastability hindrance (Sloan and Koh, 2008).

The Villard's rule ($X + 6H_2O$) was proposed after a review of experiments reported in that period by French researcher Villard. The X is the guest gas molecule and a hydration number of 6 considered good approximation for methane hydrates as it allows possibility of some empty

cages with respect to sI and sII (with hydration numbers 5.75 and 5.67 respectively, if both cavities are filled with guest gas molecules).

In early 1900s, an indirect method was applied which was attributed to researcher de Forcrand who used Clapeyron equation in determining ΔH_d from three phase, pressure-temperature data. The indirect method which is still used today is based on calculation of the enthalpies of formation of hydrate from gas and liquid water, alongside gas and ice (L_w-H-V and $I-H-V$). This method also excludes the drawbacks of occlusion and metastability as with the direct method since the pressure-temperature measurements are at equilibrium, and they are not a function of the amount of each phase present.

However, simple hydrates of sI hydration number, n can be determined using the fractional cage occupancy of the large, θ_L and small, θ_S cavities as (Cady, 1983a, Cady, 1983b):

$$n = \frac{46}{6\theta_L + 2\theta_S} \qquad 2.5$$

This was demonstrated with Equation 2.5, which he used to determine hydration number for simple hydrates with results agreeing with literature data. The value 46 represents the number of water molecules per unit cell of the sI hydrate structure that is made up of 6 large and 2 small cages.

2.5 Gas hydrate formation and dissociation kinetics

The kinetics of gas hydrate formation is described as crystallization process characterised by two distinct steps that are the most studied, nucleation and growth processes (Englezos et al., 1987b, Sloan and Koh, 2008, Ke et al., 2019). The nucleation and subsequent crystal growth usually occurs at the interface of the guest component (such hydrocarbon) and liquid water, being the location of very high concentration in the systems at high pressure and low temperature conditions (Kashchiev and Firoozabadi, 2002). In a stirred system gas hydrate formation may commence at any location depending on the dissolved gas concentration at the location and the system configuration (Bishnoi and Natarajan, 1996). Unlike the gas hydrate thermodynamics, which is substantially researched, the gas hydrate formation and dissociation phenomenon is complex, and the kinetics has not been sufficiently clarified (Englezos et al., 1990, Bishnoi and Natarajan, 1996). Two important aspects usually considered when time is a factor in hydrate formation studies are; the induction period, which is time taken for stable crystal to form and the rate at which the hydrate crystals grow (Englezos, 1993). On the other hand, for the kinetics of gas hydrate dissociation, it is characterized by sequence of hydrate crystal decomposition to gas and subcooled water.

2.5.1 Gas hydrate nucleation and formation driving force

Nucleation is an inherently stochastic process involving the formation, dissociation and growing of crystal clusters or nuclei at the gas−water interface until the achievement of critical nuclei size (stable hydrate nuclei) often indicated macroscopically by turbidity point. The nucleation process occurs when the solution is in supersaturated or subcooled regime and the stochastic nature due to the local concentration fluctuations following dissolution of the gas molecule in water (Natarajan et al., 1994). A spontaneous crystal growth follows with nuclei size increase beyond the critical value, indicating end of the nucleation phase. The associated time duration for nucleation starting from the onset of gas−water contact to the turbidity point is the induction period (Natarajan et al., 1994). Induction period is an essential characteristic of the kinetics of gas hydrate process.

Vysniauskas and Bishnoi (1983) reported the effect of water structure on the induction period in their experiments that measured the mean induction period using water of different qualities. The study suggested reduced induction period for ice and water from decomposed hydrate (memory water or subcooled) compared with water without history because of their higher tendency for more orderly structural arrangement due to the less molecular activity compared to preheated water (Vysniauskas and Bishnoi, 1983, Natarajan et al., 1994, Sloan and Koh, 2008). Apart from the water (memory water, gas composition, presence of foreign particles) effect on the induction period, the reactor type and configuration involving agitation rates, mass and heat transfer rates also effect the induction period (Sloan and Koh, 2008, Mork and Gudmundsson, 2002, Mork et al., 2001). These factors are important considerations as they affect the kinetics of hydrate formation. Studies on gas hydrate process have been reported with several reactor configurations such as stirred-tank, plug flow, packed-bed reactors (Yin et al., 2018, Veluswamy et al., 2018). This study however focuses on gas hydrate production using continuous stirred-tank reactors commonly used commercially as further discussed in Chapter 3.

2.5.2 Gas hydrate growth and driving force

In order to form an expression for the hydrate growth kinetics, the hydrate formation driving force should be first established. Thermodynamic considerations as well as the fact that gas hydrate formation is a crystallization process identify the driving force for hydrate formation (Englezos et al., 1990). The hydrate growth follows nucleation with spontaneous build-up once stable hydrate nuclei forms resulting in phase transition to solid phase with increase in temperature as it is an exothermic reaction. For methane gas, which is nonpolar with low solubility in water, a significant gas composition is typical, considering transitions via bulk of the solution, the V−L_w and L_w−H interfaces to attain the methane hydrate phase. This amounts

to usually hydrates of about 10-15 mol% solid concentration (Sloan and Koh, 2008). As such, the interfacial area including the mass and heat transfer processes are vital parameters that influence hydrate growth kinetics. This explains the fact that majority of the reported gas hydrate kinetics studies make use of agitator vessel experimental set-up (Vlasov, 2013, Bergeron et al., 2010, Skovborg and Rasmussen, 1994, Natarajan et al., 1994, Vysniauskas and Bishnoi, 1983).

Bishnoi and Natarajan (1996) further noted that the average hydrate crystal sizes obtained due to growth is a function of the degree of subcooling. Bishnoi and his group have largely studied natural gas and methane hydrate (MH) formation kinetics using the gas consumption rate with time in stirred-reactors operated in semi-batch mode at constant temperature and pressure (Vysniauskas and Bishnoi, 1983, Englezos et al., 1987a, Englezos et al., 1987b, Natarajan et al., 1994). Vysniauskas and Bishnoi (1983) reported subcooling as the driving force for methane hydrate nucleation and growth. They measured MH formation kinetics as gas consumption rate in a semi-batch stirred tank at isothermal and isobaric conditions. The experimental results indicated that formation kinetics were dependent on the interfacial area, temperature, pressure and degree of subcooling. The difference between the hydrate equilibrium temperature at equilibrium pressure and the experimental temperature defines subcooling. They observed an increase in the hydrate formation rate (gas consumption rate) at increase in the degree of subcooling. An increase in pressure and temperature decrease resulted in increase in growth rate respectively. A growth rate semi-empirical model was proposed using the critical parameters based on the experimental data generated:

$$r_{Vys} = Aa_s \exp\left(-\frac{\Delta E_a}{RT}\right)\exp\left(\frac{a}{\Delta T^{\beta}}\right)p^{\gamma} \qquad 2.6$$

where A is the lumped pre-exponential constant, ΔE_a is the activation energy for hydrate formation, p is total system pressure, ΔT is the degree of subcooling, a and b represent the empirical parameters and the γ indicates the overall order of the reaction.

The interface was also investigated between 5 – 10 s^{-1}, which indicated increase in gas consumption rate attributed to the increased interfacial area of gas-water contact due to increased stirring rate.

Englezos and his co-workers in their study of kinetics of natural gas hydrate formation also in a semi-batch reactor suggested a fugacity-based model (Englezos et al., 1987a, Englezos et al., 1987b, Englezos et al., 1990). They ascribed the driving force to the difference between the fugacity of the dissolved gas (f) at experimental temperature and pressure and that of the fugacity (f_{eq}) of dissolved gas at the experimental temperature, corresponding to the three-phase equilibrium pressure ($\Delta f = f - f_{eq}$). They reported the fundamental basis for hydrate

formation kinetics using crystallisation theory and two-film theory to demonstrate the crystal growth kinetics. The hydrate nuclei growth was described in two consecutive steps: the dissolved gas diffusion from the bulk of the solution via the laminar diffusion layer around the particle to the L_w-H interface, and the reaction at the interface (adsorption of gas molecules into clustered water molecules which subsequently stabilize as structured water). The rates of the above two-step processes are equal, as no accumulation is allowed in the diffusion layer around the particle. Therefore, for pure natural gas hydrate components, the growth rate per particle (assuming a spherical particle) considering overall driving force given as:

$$\left(\frac{dn}{dt}\right)_p = K^* A_p (f - f_{eq}) \tag{2.7}$$

where

$$\frac{1}{K^*} = \frac{1}{k_r} + \frac{1}{k_d} \tag{2.8}$$

where n is the moles of gas consumed during hydrate formation, A_p is the surface area of the particles, the combined rate parameter is K^*, k_r is the reaction rate constant, k_d is the mass transfer coefficient around the particle and Δf is the driving force of fugacity. However, observed that hydrate formation is not restricted to the gas-liquid interface but also occurs in the liquid bulk provided supersaturation exists.

However, while some researchers agree, several other studies have indicated contrasting views regarding the kinetics and driving forces of hydrate formation. Knox et al. (1961) attributed degree of subcooling as the driving force for the rate of gas hydrate formation as subscribed by Vysniauskas and Bishnoi (1983). Skovborg and Rasmussen (1994) reported that the driving force is the difference between the mole fraction of the gas at the gas-liquid water interface and the gas mole fraction in the liquid bulk at the pressure and temperature conditions of the system. Hence proposed a simplified model based on analysis that suggests that hydrate formation rate (expressed as gas consumption rate, $^{dn}/_{dt}$) as a function of mass transfer rate that depend on gas transport from the gas phase to the liquid bulk phase and given as:

$$\frac{dn}{dt} = k_L A_{(g-l)} c_{w0} (x_{int} - x_b) \tag{2.9}$$

where k_L is the mass transfer coefficient in the liquid film, $A_{(g-l)}$ is the gas-liquid interfacial area, c_{w0} the initial concentration of water molecules and $(x_{int} - x_b)$ the mole fraction driving force which is the mole fraction of gas in the water phase at the gas-liquid water interface in equilibrium with the gas phase at experimental temperature and pressure.

Herri et al. (1999) highlighted the importance of gas-liquid mass transfer in their study. They defined the driving force of methane hydrate formation in two stages, the difference in methane concentration at the gas-liquid interface and that of the liquid bulk as the driving force, $(C_{g-l} - C_b)$ for gas dissolution in water as shown in Equation 2.10:

$$r = k_l a(C_{g-l} - C_b) \quad 2.10$$

Then the difference between the concentration of the liquid bulk, C_b and the gas concentration in hydrate phase, C_{eq} for the growth rate, G as shown in Equation 2.11:

$$G = k_g(C_b - C_{eq}) \quad 2.11$$

In addition, they indicated that the gas dissolution in water follows a first order relationship. Furthermore, they included an agglomeration term although literature is largely focused on the two dominant crystallization processes, nucleation, and crystal growth kinetics. In contrast, Kashchiev and Firoozabadi (2002) attributed the driving force of nucleation and growth of methane gas hydrate, to supersaturation. This signifies the difference in the chemical potentials of the hydrate formation component in the solution and in hydrate crystal at isothermal and isobaric conditions.

A study was reported by Happel in 1994 on methane and nitrogen hydrate formation using 1.0 $\times 10^{-3}$ m^3 (1 L) continuous stirred tank reactor (Happel et al., 1994). The obtained methane hydrate formation rate from their study indicated much higher rates compared to the reported batch reactor studies by Vysniauskas and Bishnoi (1983) and Englezos et al. (1987a). While Navab et al. (2008) attributed the difference in the measured rates to the reactor design configuration. Additionally, using continuous stirred tank reactor (CSTR), Mork et al. (2001) and Mork (2002) studied methane and natural gas formation kinetics at steady state conditions indicating a dominance of the transport processes over kinetic processes which aligns with the views by Skovborg and Rasmussen (1994). Furthermore, the obtained CSTR gas hydrate formation rates results were compared with hydrate formation experimental data obtained from batch reactors. This indicated up to three orders of magnitude increase in rates compared to the batch reactors operated at similar temperature and pressure conditions. The study also proposed an empirical model for methane hydrate formation rate based on experimental results using a 9.5 $\times 10^{-3}$ m^3 CSTR, in which the gas consumption rate, r was suggested to be dependent in descending order, on the gas injection rate (superficial gas velocity,v_{sg}), pressure, p and gassed power consumption, P_g while subcooling, ΔT showed the least effect as shown in Equation 2.12.

$$r = kpv_{sg}^{a}(P_g + P_0)^{b}\,\Delta T^{b} \quad 2.12$$

In their methane hydrate experiments, continuous gas bubbled into the reactor, with the Rushton turbine, is dispersed in the liquid phase resulting in different flow regimes determined on the gas flowrate and agitation rate. They observed with nearly all the experimental runs, that the impeller at 6.7 s^{-1} and 13.3 s^{-1} stirring rates with up to a maximum superficial gas velocity of 2.4 $\times 10^{-3}$ ms^{-1} could at least completely dispersed or probably recirculate gas in water in the

reactor. This aligns to the reason earlier highlighted that the hydrodynamic effects of superficial gas velocity and power consumption to the hydrate formation rate was proportional to the superficial gas velocity while is less dependent on the power consumption. The experimental results further depicts that increase in superficial gas velocity, which implies more gas bubbles in the reactor and hence, increase in gas−liquid interfacial area is proportional to mass transfer rate (Mork, 2002).

In addition, the flow regimes as mentioned above indicate whether the process is impeller-controlled or gas-controlled in order to make conjectures relating to empirical correlation and scale up of the system.

Their observation indicated indifference in the gas consumption rate using more than one composition and thus argued that gas consumption rate was dominated by the gas−liquid mass transfer (rate of gas dissolution) rather than the rate of the inclusion into the hydrate structure. Hence, kinetics of sI and sII hydrates formation rate is gas mass transfer limited. In agreement, Skovborg and Rasmussen (1994) based on investigation of the Englezos et al. (1987a) experimental study results, which affirms that hydrate formation rate is not affected by the hydrate crystal surface area and suggested it as gas-liquid mass transfer process with no resort to the particle size distribution (Mork and Gudmundsson, 2002, Mork, 2002).

Freer et al. (2001) investigated kinetic parameters of methane hydrate formation using a high-pressure visual cell for film growth measurements at the methane-water interface. A continuous growth mechanism of crystallization due to the degree of subcooling was used to describe the growth rate. This indicated that growth rate was proportional to subcooling. The study proposed a model that accounts for interfacial hydrate growth kinetics and convective heat transfer. The model based on energy balance at the moving boundary, which indicates that the convective heat transfer cannot surpass heat generated at the moving interface. As such, a growth kinetics sluggish relative to heat transport is obtainable. The kinetic dependence was considered based on Arrhenius expression (Equation 2.15) and the heat transfer coefficient was assumed constant. The overall rate constant, K accounts for both the methane hydrate kinetic rate constant, k and heat transfer resistance, h and given as:

$$\lambda_H \rho_H \frac{dX}{dt} = K(T_{eq} - T_{bulk}) \quad 2.13$$

$$\frac{1}{K} = \frac{1}{k} + \frac{1}{h} \quad 2.14$$

$$k = k_0 \exp\left(\frac{-E_a}{R}\frac{1}{T_{eq}}\right) \quad 2.15$$

where $\frac{dX}{dt}$ is the velocity of the moving boundary, λ_H is the heat of dissociation, k_0 is the pre-exponential factor, E_a is the activation energy and T_{eq} and T_{bulk} are both the bulk and

equilibrium temperatures which must be definite to adequately define molecular attachment at the hydrate interface.

In a more recent study, using semi batch reactor Bergeron et al. (2010) studied the kinetics of methane hydrate formation based on their developed model independent of dissolution rate at the V-L_w interface. The reaction rate constant was obtained experimentally to increase as a function of temperature dependence following an Arrhenius-type constant. Similar to the studies like Englezos et al. (1987a) and Englezos et al. (1987b), the driving force for hydrate growth is based on the hydrate intrinsic kinetics, while others such as Skovborg and Rasmussen (1994) and (Mork and Gudmundsson, 2002) suggested models on the basis of mass transfer, neglecting the reaction rate constant. This further highlights the earlier mentioned controversy in literature regarding the driving force and hydrate formation kinetics. However, in this study, the author aligns with the Mork model because it was developed for the purpose of design of large-scale hydrate reactors corresponding to focus analysis in this study.

2.5.3 Gas hydrate dissociation

Similar to the divergent views as with the hydrate formation process, the transport phenomena and kinetic rate constant approaches govern the majority of reported studies on the dissociation of solid hydrates (D. Sloan, 1990). It is important to note that the discussions in this section on dissociation kinetics focused on gas hydrates in slurry form, which usually comprises of about 10 wt% hydrate and 90 wt% water (Rehder et al., 2012). The illustrations relating to other forms of gas hydrate (such as hydrate pellet) are discussed in Chapter 3.

The concept of hydrate dissociation process is believed to follow two steps, the hydrate host lattice destruction at the surface particle and desorption of the hydrate former gas or guest gas molecule from the solid surface entering into the bulk gas phase as dissociation progresses (Kim et al., 1987, Englezos et al., 1990, Bishnoi and Natarajan, 1996).

Using a semi-batch reactor stirred-tank reactor, Kim et al. (1987) studied methane hydrate slurry dissociation in water at temperatures range of about 273−283 K by reducing the pressure below the three-phase equilibrium pressure at the experimental temperature and thus suggested a fugacity-based model. The rate of hydrate particle dissociation or rate at which methane gas is released from the methane hydrate particle ($-{}^{dn_H}/_{dt}$) is therefore given as:

$$\left(-{}^{dn_H}/_{dt}\right)_p = K_d A_d (f_{eq} - f) \qquad 2.16$$

where n_H is the moles of methane in the hydrate, A_p is the surface area of the particles, and hydrate dissociation constant is K_d which has Arrhenius-type temperature dependence. The driving force (Δf) of the dissociation as proposed is the difference between the fugacity (f_{eq}) of

methane at the H-L_w-V equilibrium conditions and the fugacity (f) of methane at the solid surface. The fugacity of methane at the solid surface was assumed equivalent to the fugacity of methane in the bulk gas phase, since the stirring rates used in the experiment were high enough to eliminate influence of mass transfer. Furthermore, with the high stirring rates in the reactor, the hydrate particle temperature was assumed same as that of the water, since the heat transfer resistance from the bulk water to the hydrate particle surface was considered insignificant. Hence, suggesting that the hydrate dissociation kinetics is independent of mass and heat transfer effects (Kim et al., 1987, Englezos et al., 1990, Bishnoi and Natarajan, 1996).

Conversely, some authors hold the view that transport phenomena determines the phase transition across the interface as hydrate mass is in equilibrium with the fluid at its interface and thus proposed models identifying hydrate dissociation is heat transfer controlled (Ullerich et al., 1987, Kamath et al., 1984, Kamath and Holder, 1987). Kamath et al. (1984) developed a heat transfer correlation in their study on propane hydrate dissociation. They demonstrated that heat transfer rate is a power function of temperature difference (ΔT) between the bulk heating fluid and the hydrate surface subjected to dissociation. In a unified correlation applied to methane hydrate dissociation and in agreement with (Kamath et al., 1984), the dissociation rate as a function of interfacial temperature drop is given as (Kamath and Holder, 1987):

$$\frac{\dot{m}_H}{\emptyset_H A} = 6.464 \times 10^{-4} (\Delta T)^{2.05} \qquad 2.17$$

where $\dot{m}_H$ is the hydrate dissociation rate, $\emptyset_H A$ is the surface area of the hydrate and ΔT the interfacial temperature drop. The study concluded that methane hydrate as well as propane hydrate dissociation is a heat-transfer controlled process (Kamath and Holder, 1987). Ullerich et al. (1987) also modelled the rate of hydrate dissociation in their study, based on heat transfer considerations.

Furthermore, Gupta et al. (2007) reported a study on the methane hydrate (sI) dissociation mechanism on microscopic scale using nuclear magnetic resonance (NMR) spectroscopy. They highlighted a similar hydrate dissociation rate for the large and small cages in methane hydrate, indicating that the unit cell of structure I hydrate dissociates without preferential dissociation of the cages. This is contrary to the methane hydrate formation in which formation rate for large cages ($5^{12}6^2$) is slower than the small cages (5^{12}) (Gupta et al., 2007).

2.6 Applications of gas hydrates technology

Remarkable progress has been recorded by researchers on gas hydrate, starting as an academic curiosity, then to active relevance for flow assurance in the oil and gas industries. In the past, hydrates was only perceived as a nuisance relating to disrupting of facilities and blocking of pipelines in offshore oil and gas operations (Hammerschmidt, 1934).

The global environmental issues relating to mitigating gas flaring and under-utilization of natural gas especially regarding stranded gas field which presents less economic viability using conventional gas transport technologies (such as LNG), has also created considerable research interest (Call et al., 2008, Pallipurath, 2008, Khalilpour and Karimi, 2010). This has led to many studies on the potentials of gas hydrate as a produced energy resource, gas storage, and transportation medium for natural gas. For instances the Mitsui Engineering and shipping (MES) has established studies and designed supply chain on methane hydrate as compact pellets which explored feasible transport and storage conditions of the technology (Takaoki et al., 2011). Hydrate supply chain technology is further explored in this study in Chapter 3.

The discovery of naturally occurring hydrates deposits as potential long-term energy solution to depleting natural gas reserves stimulated immerse research interest in technological development, estimated scale of deposits and exploration of natural gas as well as environmental impacts of these hydrates deposits (Sloan and Koh, 2008). In recent years, researches on natural gas hydrate exploitation for different technologies spans into three aspects, experimental studies and simulations, numerical simulations and analysis, and field trial exploitations (Chong et al., 2016). The issues of natural release of methane from these methane hydrate deposits in permafrost and deep ocean sediments and the effects to global warming of these deposits has also generated research attention (Koh, 2002).

In the last two decades, several other research prospects of gas hydrates have been reported relating to laboratory studies and novel technological applications. These include in pre-combustion and post-combustion CO_2 capture (Linga et al., 2007, Linga et al., 2010, Babu et al., 2015), CO_2 sequestration (Goel, 2006, Lee Huen et al., 2008), (Jadhawar et al., 2005), H_2 storage (Veluswamy et al., 2014), gas separation (Eslamimanesh et al., 2012), and seawater desalination (Knox et al., 1961, Kang et al., 2014). For instance, Tohidi and his co-workers at the Centre for Gas Hydrate Research, Herriot-Watt University, UK explored the combined methane production and CO_2 sequestration by exchange of methane with CO_2 in methane hydrate reservoirs (Masoudi and Tohidi, 2005) and have credit for several other publications relating to gas hydrate research and development.

2.7 Concluding remarks

In Chapter 2, the fundamental gas hydrate structures and properties were discussed with emphasis on the sI and sII gas hydrates. The hydrate formation and dissociation kinetics were also discussed with inclination to the crystallization theory based on two most largely researched stages of hydrate nucleation and crystal growth (post-nucleation). The important notes taken are that the onset of gas hydrate nucleation or formation often occurs at the gas-liquid interface and that the hydrate crystal growth does not only occur at the interface but can

take place in the bulk, in addition, driving force for hydrate formation and hydrodynamic conditions significantly affect gas hydrate formation rate. Therefore, kinetics of hydrates formation has been considered by a couple of studies be to be mass transfer limited (Skovborg and Rasmussen, 1994, Mork, 2002).

The diversity of interpretations by researchers based on experimental and analytical studies, using different selected experimental variables and equilibrium conditions relating to the hydrate nucleation and crystal growth kinetics were also discussed with considerations of the controlling mechanisms as intrinsic kinetic reaction, mass transfer, and heat transfer or a coupled of the controlling factors. Among the discussed nucleation driving force theories (applied to one-component gases) the adopted subcooling by the Vysniauskas and Bishnoi (1983) kinetic model can be considered a good approximation. In terms of thermodynamics, Gibbs free energy, ΔG with the system entropy ($dG = Vdp - SdT$) indicating maximum possible work output by the process for isobaric condition (dp = 0) relates to subcooling, ΔT. In addition, Arjmandi et al. (2005) reported that the driving force for methane-water system over wide range of pressure as proportional to subcooling.

Furthermore, in the perspective of this study, reactor type, configuration and operation have significant effect on the hydrate formation kinetics. This implies that system specific experimental data according to Mork (2002) relating to reactor geometry and operation is required.

In this chapter, equilibrium conditions for gas hydrate stability were discussed and reported methods employed for determining enthalpy of gas hydrate process. Furthermore, the several applications of gas hydrate technology were also highlighted as well as the other developing research areas of gas hydrate technology.

Chapter 3 Review of process simulation and economic assessment studies on NGH (methane) production for stranded gas utilization

3.1 Introduction

Natural gas as the cleanest fossil fuel is an essential energy resource in meeting energy demand globally. There is therefore, the need for effective and efficient technology for NG transportation especially from remote locations as have been reiterated. In this chapter, the NGH (methane) technology chain is presented and reviewed comprising, methane pellet production in stirred-tank reactors, processing steps and regasification for storage and transportation of NG. The consideration of methane (sI hydrate) in this study is further explained. NG comprises of methane as a major component. In addition, hydrates that form in nature are mainly methane hydrates. Therefore, many of the reported studies explored hydrate formation using pure methane even though methane hydrates form at rigorous condition of high pressure. Methane hydrates are associated with the self-preservation phenomena of hydrates, which a discussion section is included to explain its advantages relating to process operation and economics for utilization of stranded gas. Furthermore, a review of previous studies on process simulation and economic studies of NGH is also presented.

Methane hydrate (MH) technology chain for utilization of stranded gas comprises of production, transportation, and storage/regasification units. The production unit has generated large research attention in recent years due to the intricacies relating to hydrate kinetics and reactor configuration for enhanced rate implementable for large-scale production (Rajnauth and Barrufet, 2012). Typically, mixing water and methane gas at high pressure and low temperature conditions form methane hydrate slurry, which is further processed into MH pellet. The produced hydrate pellet is then regasified into methane gas of market specification at the receiving terminal. With the transportation unit, the MH pellet is moved to the receiving terminals. These have been demonstrated using ships or cargos for offshore facilities (Takaoki et al., 2011, Murayama et al., 2011) or land transportation (Nogami et al., 2011)using tankers for minimal emissions of methane gas during transit. At the receiving terminal, where the MH pellets are regasified, further processing is executed by dehydration of the gas to market specifications. This technology although still not commercialised is considered to be promising due to the prevailing advantages for storage and transportation of stranded natural gas (methane). As previously mentioned, hydrate using methane gas is the focus of this study because the attributed self-preservation has not yet been clearly established for natural gas hydrates.

3.2 Methane gas hydrate production

The high capacity of gas storage in hydrates makes it an attractive technology for transportation or utilization of natural gas. However, the slow formation rate of hydrates is a challenge, especially when considering scale up of hydrate-forming reactor with process commercialization in focus. Other considerations are the large amount of water in hydrate slurry, about 90 %wt, which require processing, economy of process scale up as well as economic viability of the NGH technology chain compared to conventional stranded gas utilization technologies.

There was increased attention on storage and transportation of gas using methane hydrates ignited by the discovery of the self-preservation phenomena, which maintains metastability of hydrates (methane) at about 253 K (Yakushev and Istomin, 1992). As a result, studies on the feasibility of using the hydrate technology for gas utilization commercially have been reported (Rehder et al., 2012). In the early 1990s, Gudmundsson and his co-workers reported experimental studies of natural gas hydrate formation without additives using conventional continuous stirred tank reactor (CSTR). Likewise, stirred tank reactors are widely used in hydrate studies, with results of enhanced formation rates and induction time reduction (Happel et al., 1994). Similarly, based on the same CSTR application, Mitsui Engineering and Shipping developed a hydrate production rig connected with pellet machine (Murayama et al., 2011). The demerits associated with the use of STR such as energy consumption due to stirring (energy cost) are further factored into this study with eventual economic assessment and comparison with gas utilisation technologies.

However, besides CSTR some other reactor configurations have been explored for hydrate formation process based on literature. Hydrate formation investigation using a bubble column reactor was reported (Myre et al., 2011, Hashemi et al., 2009). On the other hand, fixed-bed reactors have been explored for hydrate formation, in which packing materials such as sand, silica gels, and metallic packings, alongside promoters were used to provide gas-liquid mixing and enhance formation rate (Kumar et al., 2015, Zhong et al., 2014). Although absence of mechanical mixing in the reactors suggest less energy inventory, however, whether methane hydrate kinetics are higher compared to CSTR without the aid of additives or promoters seem not clearly substantiated. Likewise, spray reactors have also been investigated in which water spraying into a gas phase for hydrate formation was used (Gnanendran and Amin, 2004).

Takahashi et al. (2003) suggested the use of microbubble technology for hydrate formation process. According to their report, this technology is believed to aid gas dissolution, providing massive gas-liquid interfacial area. However, this apparatus has not be substantiated for hydrate production with follow up studies so far (Takahashi et al., 2003, Ohnari, 2002). Although not

within the focus of this study, another means that have been largely discussed by researchers regarding the challenge of slow kinetics of gas hydrate is the use of promoters (Karaaslan and Parlaktuna, 2000, Veluswamy et al., 2016).

3.2.1 Production concept of gas hydrate in stirred tank reactors

The use of mechanical agitation is an established avenue of improving gas liquid contact for enhanced hydrate formation rate (Vysniauskas and Bishnoi, 1983). Stirred tank reactor operations can be in batch, semi-batch or continuous mode. In the batch mode operation, the gas and water are neither fed nor discharged from the reactor until the operation is over. Usually pressure drop is observed as the hydrate formation progresses. For semi-batch mode operation, the gas stream is continuously fed to the reactor as a result constant pressure is maintained as hydrate formation occurs by replenishing loss of gas in the reactor. For the continuous mode operation, the gas and water streams (reactants) as well as the formed hydrate slurry (product) are continuously fed and discharged respectively, a result, constant pressure and uniform composition are maintained constant in the reactor (Mori, 2015). Steady state process is achieved in continuous stirred tank reactors (CSTR), which are suitable for scale-up and industrial operations. CSTRs besides continuous mode operation, offer good temperature control, low operating cost, and ease of maintenance compared to the other modes of STR. Veluswamy et al. (2018) further pointed out the need for reactor configuration with enhanced gas/liquid contact for hydrate formation kinetics and also the consideration of energy inventory associated with scale-up for commercialization. These considerations are explored further in this study, for instance, the process analysis will explore the energy consumption associated to stirring in the STR to ensure it is within economic feasibility frame.

Although the general assumption in continuous stirred tank reactors (CSTR) is that it provides perfect mixing but in practical terms, mixing is largely a factor of the reactor design (Tatterson, 1991, Paul et al., 2004). CSTR design usually comprises reactor sizing and geometry definition, impeller type, equipment such as sparger, baffles, and heat transfer system. This also applies for the implementation of CSTR for gas hydrate production study for good mixing involving the three phase process (gas, liquid and solid phases) since stirring is largely used in enhancing mass and heat transfer process (Paul et al., 2004, Coker and Kayode, 2001). In addition, using STRs with baffles on the reactor walls further enhances mixing as well as higher gas-liquid interfacial area due to the gas injection. On the contrary, batch reactors are usually without baffles and spargers (Paul et al., 2004).

3.2.1.1: Standard Geometry of Stirred Tank Reactor (STR)

Experimental and modelling studies on mixing in STRs are usually determined using standard geometry design with standard impellers. Standard geometry design is best described as

reference geometry with standard configurations usually considered for most processes to minimize cost and for simplified design (Tatterson, 1991). These standard configurations or dimensions are for reactor diameter, liquid height, impeller diameter, impeller blade width, baffle width, and impeller/tank bottom clearance. The reactor usually contains four baffles spaced out 90 degrees and the standard geometry allows effective agitation and gas dispersion at the upper section of the vessel and below the impeller as well as effective solid solids suspension. Gudmundsson and co-workers also reported experimental studies for formation of methane gas hydrate using CSTR based on standard geometry configuration (Mork and Gudmundsson, 2002, Mork et al., 2001, Gudmundsson, 1996a). This gave an increase in hydrate formation, up to three orders of magnitude higher than that of semi-batch reactors at similar stirring rate and process conditions (Mork et al., 2001).

According to Tatterson (1991), six-blade disk style impeller is mostly used in the standard configuration with gas spargers below the impeller in fully baffled turbulent stirred tank. The impeller geometry is also a primary factor that defines flow pattern in STR as well as whether the reactor have wall baffle or not. Baffles are vertically mounted plate frame placed in the flow, which disrupt and redirect flow as such providing improved mixing. There are several types of baffles but the mostly studied are the wall baffles. This has the ability to promote stability of power drawn by the impeller as well as prevent swirl and vortex development in liquid, thereby improve mixing (Tatterson, 1991, Lu et al., 1997). It also provides additional mechanical support to the reactor. Two impeller types commonly associated with turbulent mixing are axial flow and radial flow impellers (Doran, 2013a). Axial impellers discharge fluid axially (up and down discharge) often used for blend of liquids and solid materials in liquids with limited discharge.

On the contrary, radial flow impellers, which an example is the Rushton turbine, discharges fluid in radial (side-to-side) direction to the reactor wall with trailing vortices at the top and the bottom of the impeller blade (Doran, 2013a). Rushton turbines is associated with high shear rates due to their disc angle of attack and relatively low pumping number which makes them sensitive to viscosity (Tatterson, 1991). In addition, Rushton turbines have good gas handling capacity as such can be operated with relatively high flowrates without impeller flooding (Doran, 2013b, Nienow et al., 1986, Doran, 2013a).

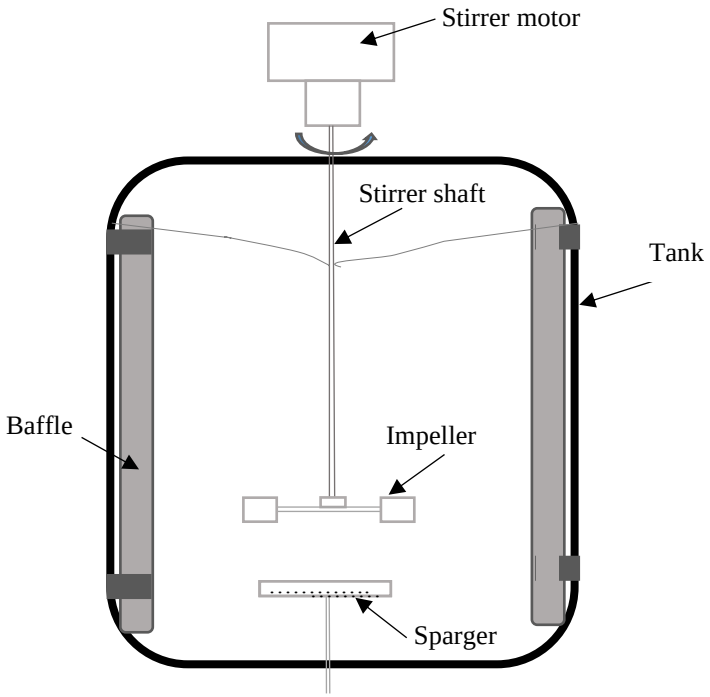

Figure 3.1: Typical stirred tank reactor configuration (Doran, 2013a)

Standard STR for gas-liquid mixing using Rushton turbines have been extensively studied in literature and are found to be excellent for gas dispersion (Nienow, 1996, Tatterson, 1991) as such is considered for this study based on literature for methane hydrate formation. In addition, at turbulent condition and since low concentration (10 wt %) of methane hydrate slurry (hydrate-water slurry) is formed, it can be considered to be homogeneous with viscosity similar to water (Andersson and Gudmundsson, 2000).

3.2.1.2 Power consumption in Stirred reactors

The adjustments of the operating parameters (such as impeller and tank geometry/design, stirring rate, sparger ring design, baffle design and location) of STRs as well as the fluid properties largely dictate performance of a stirred tank. On rotation of the impeller blade, it transits kinetic energy to the surrounding liquid phase in the reactor with the power transferred causing mixing of the fluid. The power dissipation in the fluid induces heat in the fluid with its time-averaged dissipation flux known as power draw or power consumption at steady state condition (Doran, 2013a). Power consumption and pumping capacity depend on the discussed operating parameters and physical properties of the fluid. In a standard STR for mixing the power consumption, P is given as:

$$P = N_p \rho N^3 D_i^5 \qquad 3.1$$

where N_p is the power number, stirring rate is N, impeller diameter, D_i and fluid density, ρ indicate the effect of geometry and fluid flow conditions. Power number is a dimensionless

parameter used for estimating the power consumed due to rotating impeller in a stirred tank. The lower the number indicates better dispersion of gas in the fluid without impeller flooding. Equation 3.1 can be presented in terms of two dimensionless groups: impeller Reynold number $\mathrm{Re} = \frac{\rho N D_i^2}{\mu}$ and Froude number $\mathrm{Fr} = \frac{N^2 D_i}{g}$ as:

$$N_p = K\left(\frac{\rho N D_i^2}{\mu}\right)^a \left(\frac{N^2 D_i}{g}\right)^b \left(\frac{D}{D_i}\right)^c \left(\frac{h}{D_i}\right)^d \left(\frac{W}{D_i}\right)^e \left(\frac{C}{D_i}\right)^f \quad 3.2$$

The other terms are geometric parameters that show the effect of geometry. Standard geometry is assumed, and geometric similarity is established, Equation 3.2 becomes:

$$N_p = K(\mathrm{Re})^a (\mathrm{Fr})^b \quad 3.3$$

The Froude number accounts for vortex formation in a swirling system, as such, assuming insignificant vortex formation around the impeller region with the baffles, so that no effect on power number at turbulent flow conditions due to Froude number (Tatterson, 1991, Bates et al., 1963, Coker and Kayode, 2001) Equation 3.3 reduces to:

$$N_p = K(\mathrm{Re})^a \quad 3.4$$

However, relationship of N_p with Re is different depending on the tank and impeller geometry. Figure 3.2 shows the typical N_p – Re relationship for Rushton turbine impeller.

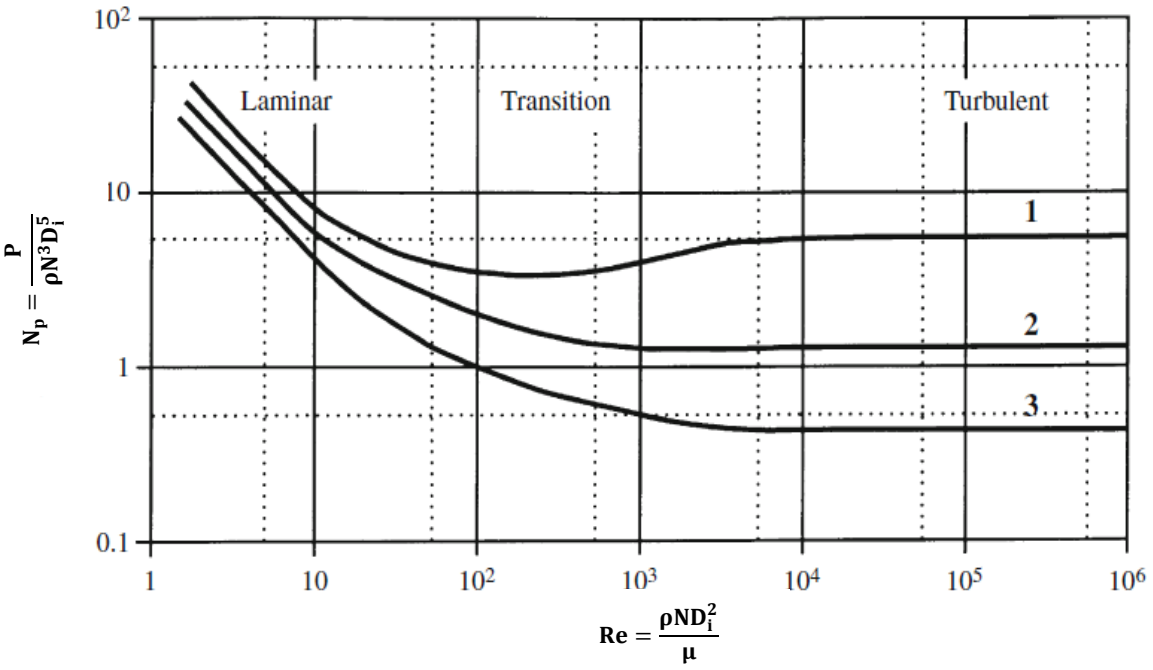

Figure 3.2:Power number and Reynold number correlation for Rushton turbines (Doran, 2013a)

The effect of impeller and tank geometry, baffles as well as location of impeller, stirring rate, fluid properties is shown in Equation 3.2. These parameters are important for determining the power number and power consumption.

3.2.1.3 Gas-liquid mixing in CSTR for methane hydrate production

Gas injection into a STR with water interrupts flow field as such significantly affects reactor performance. Gas dispersion in liquid is known to be highly sensitive of the impeller design. In gas-liquid STRs, different flow patterns can be observed as shown in Figure 3.3Figur. Rushton turbines have been identified to be most convenient for gas dispersion in liquid phase as earlier discussed. Flow patterns associated with gas-liquid dispersion in stirred reactors and important parameters in gas dispersion are discussed in this section.

According to Tatterson (1991), different processes associated with gas dispersion are complicated. However, a normal case, using a Rushton turbine, gas is injected via a sparger, below which rises to the impeller and is dispersed by the impeller (to rise to the top of the reactor or recirculate to the impeller). Two important dimensionless group govern flow: gas flow number ($FI = \frac{Q_g}{ND_i^3}$) and Froude number ($Fr = \frac{N^2 D_i}{g}$). The gas flow number or aeration number is important in defining the flow phenomena occurring in the impeller region and includes the effects of gas injection rate, Q_g, impeller diameter, D_i and the stirring rate, N. The other dimensionless group is Froude number which is the ratio of the flow field to the gravitational forces.

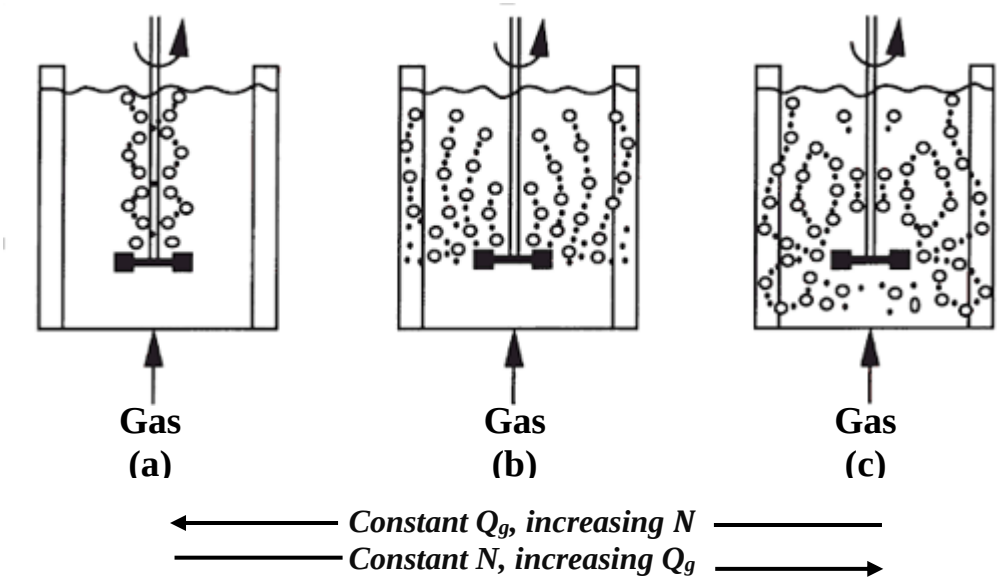

Figure 3.3: Flooding (a) – loading (b) – complete dispersion (c) for Rushton turbine (Doran, 2013a)

Figure 3.3 shows typical flow patterns in gas-liquid reactors, which depends on relative rates of gas flowrate and stirring. At low stirring rate or high gas flowrate, the impeller is overwhelmed by gas indicating impeller flooding. Under this condition, the impeller is unable to disperse gas adequately (low pumping rate of the impeller), as such, gas rise undisturbed near impeller shaft as indicated in Figure 3.3 (a). Flooding transition is the flow regime boundary

between the impeller being flooded and a good gas dispersion condition. At higher stirring rate or lower gas flowrate, the gas is dispersed radially towards the reactor walls as impeller is loaded with gas captured behind the impeller blades with the pumping effect of the impeller dominating as shown in Figure 3.3 (b). Complete dispersion occurs at further increase of stirring rate or decrease of gas flowrate, which sufficiently disperse all the gas entering the reactor as also illustrated in Figure 3.3 (c). This result in a uniform gas dispersion in liquid phase, that is, the bubbles are swept into below impeller region. The gas-liquid interfacial area is high with high contact time as well as the mass transfer. Further increase in power supplied to the reactor produces recirculation flow pattern. Flow pattern demonstrates whether gas-liquid system is impeller controlled or gas controlled which is important for the validity of empirical correlations and scale up relationships (Doran, 2013a).

Therefore, based on Nienow's correlations for predicting operating conditions for Rushton impeller (flooding – loading transition), complete dispersion, and recirculation (Nienow et al., 1986), Flow number FI is given as:

$$FI_F = 30\left(\frac{D_i}{D}\right)^{3.5}Fr \quad \ldots\ldots \quad 3.5 \quad \text{flooding – loading transition}$$

$$FI_{CD} = 0.2\left(\frac{D_i}{D}\right)^{0.5}Fr^{0.5} \quad \ldots\ldots \quad 3.6 \quad \text{complete dispersion}$$

$$FI_R = 13\left(\frac{D_i}{D}\right)^{5}Fr^{2} \quad \ldots\ldots \quad 3.7 \quad \text{complete dispersion} - \text{recirculation}$$

The Equations are reported to work well within reactor diameter of 2.67m, $\frac{D_i}{D}$ ratio from 0.22 – 0.50 and impeller clearance, $\frac{C}{D}$ from $0.25 - 0.40$ which is standard geometry for STR. The impeller power required reduces with presence of gas around the impeller (i.e. at gassed condition) compared with absence of gas in the reactor (ungassed conditions). This is due to gas cavities behind the impeller blades and drags which results in reduced power consumption. Power consumption at gassed condition, P_g are used as parameters for estimating gas-liquid interfacial area, so that the determination of power consumption gas-liquid systems (Tatterson, 1991) is given as:

$$\frac{P_g}{P} = 1 - 12.6FI \quad \text{for } FI < 3.5 \times 10^{-2} \quad 3.8$$

$$\frac{P_g}{P} = 0.62 + 1.85FI \quad \text{for } FI > 3.5 \times 10^{-2} \quad 3.9$$

3.2.2 Scale up

The discussion on scale up is necessary because of the need to evaluate stranded gas utilization using different reactor capacities, which match large and small gas reserve capacities.

The scale up of stirred tank reactor involves specifying the critical parameters which the reactor is sensitive to and examining the resultant effects and process changes due to scale up

(Tatterson, 1991, Mori, 2015). This involves knowledge of the operation conditions relative to the reactor and impeller geometry as well as heat transfer consideration. In addition, suitable procedures for scale up should be ascertained to know the parameters (both for dimensional parameters and dimensionless groups) to be kept constant or not in scale up calculations (Tatterson, 1991, Mori, 2015, Oldshue, 1983). It is important to consider power consumption changes and its effects as well as heat discharge capacity due to increased reactor volume on scale up. This directly reflects on reactor operations and cost estimation, which is one of the objectives in this study.

Since the hydrate formation process is governed by mass and heat transfer, the concept of geometric similarity is considered in this study (Coker, 2007, Rase, 1977, Coker and Kayode, 2001). This approach provides suitable CSTR scale up with equal ratio of power consumption and reactor volume (P/V). Geometric similarity also involves applying the same dimensional ratios at constant P/V on scale up of reactor (Coker, 2007). Constant P/V on scale up of CSTRs indicates equivalent interfacial area per unit volume, which implies maintaining appropriate gas-liquid mixing and similarity of turbulent flow regime of the original reactor (Doran, 2013a, Evangelista et al., 1969). With the geometric similarity during scale up, the rate of heat transfer (heat removal) will be affected, and so must also be considered. As such, the disparity in temperature between the CSTR reactor and the coolant jacket will become significantly increased and so must be factored into the scale up calculation.

3.3 MH hydrate dewatering, pelletization and storage

Methane hydrates produced using CSTR enable the production of gas hydrate slurry with typically 10 % hydrate mass fraction, which implies very large amount of un-converted water in the slurry (Nakai, 2012a). As a result, water removal is required for hydrate formation into methane hydrate pellets ideal for storage and transportation purpose. In addition, slurry processing is a significant consideration of the MHT chain evaluation. As earlier mentioned, methane hydrates can be produced in three forms: slurry, dry powder and pellets forms. The slurry form is often further processed to the dry (powder) and pellet form which is the most stable as the dissociation is minimized due to the inherent self-preservation characterises at 253 K for methane hydrates (Rehder et al., 2012). Additionally, transport of MH as pellets reduces space volume and weight compared to dry and slurry form (Murayama et al., 2011).

From literature, some technologies have been explored for the production of MH pellet from the produced MH slurry. These technologies were reviewed for industrial application of MH slurry processing.

In recent years, the Japanese company Mitsui Engineering & Shipping (MES) and partners have dominated the research. In 2003, MES developed a 25 kg hr^{-1} capacity methane hydrate Process

Development Unit (PDU) to demonstrate a continuous NGH pellet production, dewatering, pelletization, storage, and regasification (Nakai, 2012a). Then, in further development established 10 kg hr^{-1} NGH pellet experimental production plant at Chiba known as Bench Scale Unit (BSU) developed in 2005 using mixed gas stream with dewatering and high-pressure pelletizer demonstrating the continuous hydrate pellet production, and storage (Mimachi et al., 2015, Takahashi et al., 2008). The main process of the NGH pellet plant include MH formation using CSTR; dewatering of un-converted water in MH slurry using roller press; pelletizing using moulding roll; and cooling and depressurization step (drum) to achieve storage conditions (see Figure 3.4). In the dewatering chamber, 40−60 wt % hydrate increase was achieved by mechanical squeezing of the slurry from the reactor, which is fed between two cylindrical rotary drums and compacted in the gap. Then in the pelletizer chamber, the dewatered hydrate was processed into NGH pellet (25 × 20 × 16 mm in size) with further dewatering to 80−90 wt% hydrate by the rotary drums with depression along the circumference. The NGH pellets were stored in the tank in which the tank temperature was reduced to 253 K and then depressurized at the 0.1 MPa/min to atmospheric pressure (Mimachi et al., 2015, Takahashi et al., 2008).

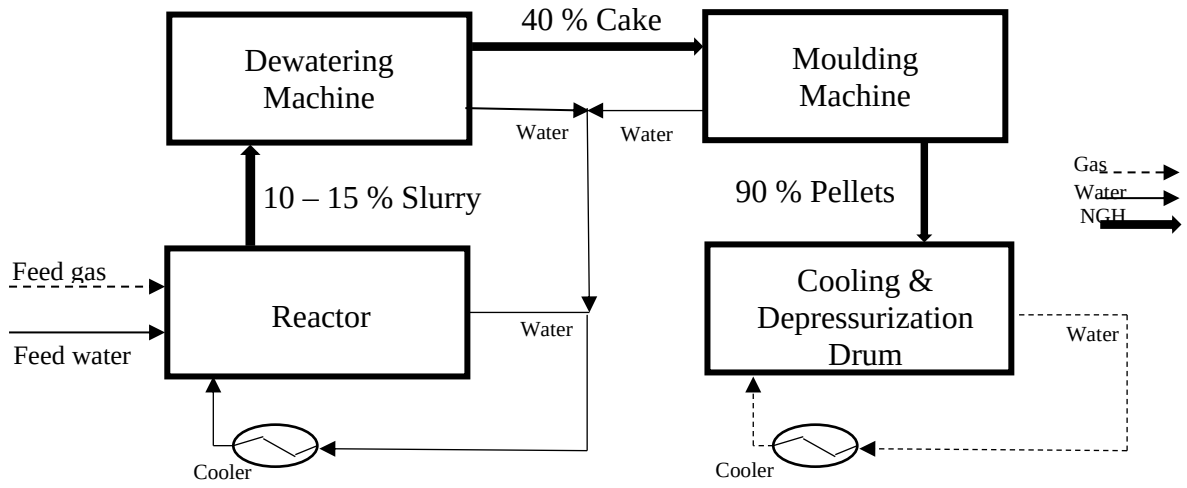

Figure 3.4: Hydrate pellet production scheme of BSU with the four major steps (Mimachi et al., 2015)

Similarly, in 2011 and Murayama and his co-workers of the MES Company, reported a newly designed 10 kg hr^{-1} pilot hydrate pellet technology, which is optimized for improved hydrate pellet transport economics. The dewatering unit called Hydrate Pellet Processing Machine (HPPM) facilitates direct pelletization from the hydrate slurry using a piston-cylinder mechanism. Typically, 10 wt% of hydrate slurry is produced from the CSTR is pumped into the HPPM where it is filtered or dewatered by a cylindrical filter and then the concentrated

hydrate mechanically compressed using piston. By having pelletizing-filtration vessel, not only that a high-pressure vessel is eliminated, the need for transferring the produced slurry between equipment is also avoided in the system. In addition, since all the processes in the NGH particle are performed in the liquid implies that gas bubble entrainment in the pellet in course of the process is minimized (Murayama et al., 2011). The HPPM process for the produced hydrate pellet based on the filtration and compression are outlined in the paper. A significantly NGH higher pellet size (100 × 50 mm) is obtained with the HPPM system compared to other reported NGH pellet studies (Murayama et al., 2011). Thus, so far in literature of hydrate slurry processing to pellets research, this technology seems the most advanced in view of hydrate technology commercialization. For these reasons, the technology is further explored by modelling dewatering and pelletization units, which will form basis for cost estimation and evaluation in this study (see Figure 4.2 in chapter 4).

Equally, Veluswamy et al. (2018) reported 42 kg hr^{-1} (1 Ton/day) capacity NGH pellet production by the Korea Institute of Industrial Teachnology (KITECH). The NGH pellet plan consists of hydrate formation and dewatering, pelletizng, cooling and depressurizing as well as 0.21 m^3/hr capacity hydrate pellet storage and regasification processes as main units. The hydrate formation and dewatering unit is based on a cooling-jacketed double helix gas hydrate reactor with an inner helix blades (Lee et al., 2015). However, sufficient information for modelling was not provided.

A laboratory scale extrusion-type twin-roll continuous pelletizing system (TPCP) for contiuous production of NGH pellet was reported in literature (Lee et al., 2013b). The NGH pelletization process was carried out within an enclosed 253 K freezer to present dissociation of NGH, producing a rectangar-shaped NGH pellet strip (10 × 10 × 11 mm in size) from the extrusion plant. The pressure created by the rotating twin-roll and the overhead feeding force squeezes the supplied hydrate powder form slurry-forming reactor to form pellets (Lee et al., 2013b).

Previously, the BG Group (former British Gas) with the Advantica Technologies in the 1990s had research and development programme on the methane hydrate production process for natural gas transportation and associated gas utilization (Fitzgerald and Taylor, 2001). Some other inventions and studies on gas transport using frozen hydrates and pellets are those of Gudmundsson of the NTNU Trondheim with the Aker Engineering (Gudmundsson, 1994), and the MES company Ltd (Murayama and Uchida, 2010, Watanabe et al., 2012). The Korea Institute of Industrial Teachnology (KITECH) (Lee et al., 2013a), and the German Integrated Submarine Gas Hydrate Resources (SUGAR) (Falenty et al., 2014, Rehder et al., 2012) etc.

The SUGAR study was based on a conceptual MH technology chain design for hydrate pellet production, which adopted a CSTR for the hydrate slurry production (with 90 wt % water

content). The study which recommended a typically 50 % water elimination from the slurry before pelletizing can be carried out, also suggested the use of pressure drum filters to achieve the dewatering (Rehder et al., 2012). Moreover, filtration and pelletization are established engineering processes that can be applied to the hydrate slurry processing. Besides the fact that filtration is a mature dewatering technology widely used industrially, it also provides energy efficient filtration using the rotary drum filter (Shao et al., 2015).

3.4 Methane hydrate pellet regasification

As expected, higher energy is required for the dissociation of hydrate pellets (solid form) compared to that of slurry discussion in Section 2.5.3. However, as has be mentioned that methane hydrate pellets remain in metastable zone at 253 K under atmospheric pressure due to the self-preservation effect, which influences its dissociation rate. Therefore, the self-preservation effect is discussed in Session 3.3.1 below, and then followed by the discussions on hydrate pellet dissociation or regasification and processing of the produced methane gas to pipeline quality by dehydration process in the subsequent sections.

3.4.1: Self-preservation phenomena

Self-preservation effect in gas hydrates can be defined as an anomaly in which hydrates remain stable for prolonged time outside the hydrate stable region. According to Istomin et al. (2006), it is a slow dissociation of gas hydrates when system pressure is below the three-phase equilibrium pressure of a V−I−H system at below 270−271 K and typically 0.1 MPa. Although this anomalous effect of gas hydrate previously has be explored by some researchers (Handa, 1986a, Davidson et al., 1986), the term self-preservation was first reported by Russian researchers (Yakushev and Istomin, 1992) who in the course of laboratory experiments observed virtually halt in hydrate dissociations due to forming of ice film on the surface (at initial dissociation stage). The ice film or microstructure on the surface of methane hydrates, which is referred to as ice shielding is believed to be the basic mechanism of the thermodynamic anomaly that results in incomplete dissociation (Stern et al., 2001b, Yakushev and Istomin, 1992, Davidson et al., 1986, Falenty et al., 2014, Kuhs et al., 2004). However, the underlying mechanism of self-preservation behaviour is still not fully understood (Veluswamy et al., 2018). Self-preservation in methane hydrates according to other laboratory studies, has also be reported to occur when pressure is lowered to 0.1 MPa within temperature range of 241−271 K (Stern et al., 2001a, Zhang and Rogers, 2008, Yakushev and Istomin, 1992). This plays a vital role in hydrate-based gas transportation technology as it allows hydrate pellets transport at atmospheric pressure which is a safer gas storage by remaining in metastable state at 253 K and 0.1 MPa enveloped by ice (Istomin et al., 2006). Typically, during pure methane hydrate dissociation, temperature range of 241−271 K (the anomalous hydrate preservation zone) is

associated with retaining over 90 vol% methane hydrates in at least 10's of hours. Conversely, for a similar methane hydrate sample at temperature ranges 195−240 K and above 272 K dissociated at least 10's seconds (Stern et al., 2001b). Fundamentally, at the anomalous hydrate preservation regime of 241−271 K within which dissociation rate decay rapidly, non-uniform rate of dissociation was observed (Stern et al., 2001b).

The crystal structure of gas hydrates also influences the self-preservation effect. The sI hydrates as already highlighted are identifiable in many literatures. Aside from methane hydrate, self-preservation effects is not yet clearly established for sII crystal structure according to some authors. For instance, Stern et al. (2003) reported an absence of the self-preservation behaviour using two samples of a methane−ethane hydrate mixture (sII hydrates). They observed about 96 % of it dissociated in 3 minutes on depressurizing to atmospheric pressure at 268 k, notwithstanding the established stability of sII hydrates compared to sI hydrates at higher temperatures and lower pressures (Stern et al., 2003).

However, on the contrary, Zhang and Rogers (2008) reported the detection of self-preservation effect in sII hydrates formed with natural gas components: 90 % methane, 6 % ethane and 4 % propane gas mixture in the presence of a sodium dodecyl sulphate (SDS) surfactant at about 268.2 K and 0.1 MPa. In what they called ultrastability of the natural gas hydrate storage lasted up to 256 hours (≈ 11 days) at extended temperature of 270.2 K and 0.1 MPa, with not more than 0.04 % loss of total gas in the hydrate (Zhang and Rogers, 2008). In this case, the ultrastability was attributed mainly to the use of SDS. According to the author, the SDS induced small hydrate particle sizes implying efficient mass transfer, high heat transfer, and minimum hydrate mass surface area exposure characterize the surfactant process which achieved the ultrastability (Stern et al., 2003). Furthermore, in a review paper on solidified natural gas hydrate technology, Veluswamy et al. (2018) also highlighted the option of using thermodynamic promoter at moderate temperature range for sII hydrates with grave potentials for its commercialization.

However, the use of methane hydrates for storage and transportation of natural gas in focus for commercialization is the underlying concentration and therefore, the vital self-preservation properties as well as its influence on the dissociation rate have been explored. The dissociation rate will be further discussion in relation to the methane hydrate regasification unit (NGH process supply chain) discussions in Section 3.3.2.

3.4.2 Methane hydrate pellet regasification and produced methane gas dehydration

As discussed in previous session that due to the anomalous self-preservation effect, pure methane hydrate (definite hydrate stability) can be stored at temperature of 241−271 K at normal pressure (Stern et al., 2001b). Therefore, recovery of the stored methane or NG from

the frozen or hydrate pellet can be achieved with external supply of heat for sustained gas production, as hydrate dissociation is an endothermic reaction. Usually referred to as the regasification of hydrates, it is a key unit of hydrate-based technology chain. However, unlike drastic release of gas associated with conventional gas utilization technologies, controlled release of gas is feasible with supply of heat at appropriate conditions for gas hydrate technology (Veluswamy et al., 2018). It is important to note that not a lot of studies on the dissociation of hydrate pellets in the laboratory reported in literature, as a result pellet dissociation discussion relies on the perspective of gas extraction from hydrate reservoirs.

Thermal stimulation, depressurization, inhibitor injection and replacement of trapped methane molecules in the hydrate structure with CO_2 are common processes that have been proposed for dissociation of methane hydrate pellets (Li et al., 2007, Demirbas, 2010b). The thermal stimulation and the depressurization methods, which in some cases are combined involve gas recovery from applying heat in the reservoir beyond the hydrate formation temperature or decreasing the reservoir pressure beyond the equilibrium pressure respectively. Low waste heat, hot water, or hot brine could be used for thermal stimulation. Whereas for chemical inhibition method, chemical inhibitor such as ethylene glycol or methanol is injected into the reservoir to alter the P-T equilibrium conditions to hydrate thermodynamically unstable zone (Li et al., 2007, Østergaard et al., 2005, Demirbas, 2010a).

Lee et al. (2011) reported a study on methane hydrate dissociation using hot water injection (thermal stimulation) using a pressurized reactor. The total time required for melting of the pellet was determined at varying water flowrate and temperature in the pressurized reactor. It was observed that although it is promising for efficient regasification plant operation, a substantial flowrate of hot water is required for considerable decrease in the dissociation time. In addition, the bubbling gas released from the surface of the pellet induced a secondary flow, leading to greater heat transfer rate as well as reduced dissociation rate. Using the depressurization method Lijun et al. (2012) investigated methane hydrate dissociation based on the time variations of pressure, resistance, temperature, and cumulative gas production. Accordingly, suggested their experimental process of dissociation of MH involves three phases: free gas release phase, rapid hydrate dissociation phase, and slow hydrate dissociation phase. A significantly rapid increase in gas production with temperature and resistance slight decrease on depressurisation was observed for the first phase. For the rapid dissociation phase associated with large gas production rate, it began with significant decrease in temperature and resistance but gradually the temperature recovered due to the heat transfer. While for the third phase which is the slow dissociation rate, as expected slow increase in gas production rate was observed as with little changes. This study however further indicates that gas production rate is significantly

dependent on pressure and temperature of the reservoir agreeing with other studies. On the other hand, (Li et al., 2007) using injection of different concentrations of ethylene glycol solution in an experimental apparatus investigated gas production characteristics from methane hydrate porous sediment. It was observed that the gas production efficiency is affected by both the injection rate and concentration of the inhibitor (ethylene glycol). An increase in production efficiency from 0 – 60 wt % concentration of ethylene glycol injection with 60 wt % depicting the maximum efficiency.

Consideration must also be given to the cost of the inhibitor for this method. As previously stated, from the perspective of gas recovery from hydrate reservoirs is employed to try to define the regasification of hydrate pellet, which will be useful in establishing conjectures for the modelling of the process. However, more focused studies on the dissociation of produced hydrate pellets are necessary.

3.5 Review of economic assessment of natural gas hydrate for transporting natural gas

The global consumption of natural gas as an important low emission fuel is on the increase (EIA, 2018). As such, the commercialization of gas hydrate technology for storage and transportation of natural gas has been an underlying focus of many researchers in recent years (Veluswamy et al., 2018, Mitsui Engneering and Shipping, 2016, Javanmardi et al., 2005, Khalilpour and Karimi, 2009). As outlined earlier, although conventional technologies such as LNG and pipelines exist, adverse limitations or challenges still suffice relating to cost, capacity of reservoirs, market distance, environmental concerns, and safety risk. These are more distinct for low volume capacity reservoirs or locations without access to pipelines.

Feasibility and economic studies of gas hydrates for transportation of natural gas relative to conventional technologies was pioneered by Gudmundsson and Co-workers. Using cost estimate of transporting approximately 11 standard million cubic metres per day (≈ 400 MMscf/d) over about 5500 km based on hydrate technology and LNG process economically compared the two technologies for utilization natural gas. They reported a 25 % higher capital cost for LNG chain compared to the hydrate technology chain (Gudmundsson and Borrehaug, 1996a, Gudmundsson et al., 1995). Similarly, (Bortnowska, 2009) based on their economic analysis of transportation of natural gas (11.32 million m^3/yr. of NG over 6000 km distance) using LNG and NGH process reported about 12 % higher cost for LNG chain compared to the hydrate technology chain. This also agrees with the process simulation and economic analysis study by (Javanmardi et al., 2005), which indicates higher capital expenditure for the LNG chain compared to the NGH chain.

For stranded gas reserves as well as small capacity gas reserves over short distances of up to about 5500 km, NGH and CNG were suggested to be most economically suitable (Bortnowska,

2009). A number of other studies of NGH feasibility and economic estimations also support NGH as being suitable economically for small capacity (Takaoki et al., 2011, Takaoki et al., 2004). Similarly, for CNG studies suggest it as being viable for small capacity (Economides et al., 2005, Wagner and van Wagensveld, 2002), whereas for LNG despite its high cost and complexity, is commonly considered to be the most economical method to transport NG from large capacity reserves (Bortnowska, 2009, Khalilpour and Karimi, 2012).

Furthermore, considering LNG, CNG, GTL, and NGH technologies for transporting NG, (Khalilpour and Karimi, 2009) carried out an evaluation based on literatures which explored the capital cost, operating cost, reserve volume capacity, and market distance of each method. With the comparison of the technologies and conceptual sweet spot plot-based reserve volume capacity and market distance, it was found that in the absence of pipelines, that CNG and NGH are the most promising NG transporting technologies for small volume reserve capacities. However, contrary to Bortnowska (2009), it was suggested that NGH is also suitable for long distances beyond 6000 km (Khalilpour and Karimi, 2009). For Osokogwu et al. (2011) based on their economic comparison study with GTL, GTW, CNG and NGH, suggested CNG to be the most promising NG transporting technology. Although, in terms of capital cost, NGH was reported the least compared to the others. The study applied economic analysis using Capex and Opex as well as profitability indicators including net present value, NPV, internal rate of return, profitability index and payback time (Osokogwu et al., 2011).

Rehder et al. (2012) also investigated NG transportation using a conceptual technoeconomic analysis of MH pellet chain and its comparison with pipeline, CNG and LNG. In contrast to other studies suggested economic non-viability of methane hydrate pellet chain for reserve volume capacity (i.e. production rate) 20, 000 to 800, 000 $Nm^3 h^{-1}$ ($\approx$ 0.1 to 5.0 MTPA) over market distance 200 to 10, 000 km.

However, a previous study by Takaoki et al. (2004) as part of the MES company Ltd program for commercialization of NGH pellet for NG transportation reported economic evaluation of 600 kg per day capacity NGH (methane hydrate) chain and comparison with LNG. It was found that NGH pellet is economically viable and had an advantage over LNG for market distance less than $\approx$ 5500 km. While all the discussed case studies in this section involves sea transportation, other favourable economics for the NGH compared to LNG for NG transportation were also reported by similar evaluations by the MES Ltd (Takaoki et al., 2011, Nakai, 2012a). In addition, the conceptual design of NGH pellet shipping carrier with loading and unloading facilities were also explored with suggested 100,000 deadweight tonnes (DWT) Panamax bulk-carrier with vessel capacity of 160,000 m^3 (Nakata et al., 2008, Takaoki et al., 2004)

The observed contractions relating to economic studies on NGH technology for the utilization of NG suggests a comprehensive process simulation and economic evaluation of NGH chain is further explored as considered in this study. The process simulation will consider the costing and revenues of the process units and material balance relating to the different production capacities of hydrate pellet as presented in Chapter 4 as well as assemble procedure based on detailed chemical engineering costing principles as described in Chapter 5. This will entail two cases of large and small capacity ranges of which will be compared with LNG and CNG respectively.

3.6 Concluding remarks and research objectives

3.6.1 Motivation

In view of commercialization of the hydrate-based utilization of NG, more research efforts are required to effectively reduce the barriers to stranded and associated gas utilisation as well as channel this cheaper energy resource to useful purposes such as power generation, cleaner fuel, and chemicals production. Natural gas is fast becoming a premier fuel resource in the world economy, adequate transportation and infrastructure for processing and moving gas from stranded gas locations to market is a key research consideration (Economides, 2005b, Wood et al., 2008, Khalilpour and Karimi, 2012). It is estimated that up to 60% of the world proven natural gas are considered stranded, and more than half of these stranded gas resources are of small and medium oil and gas reserves (Nexant, 2005, Chabrelie and Rojey, 2000, Mitsui Engneering and Shipping, 2016). The bulk of the number of the stranded gas reserves globally has been reported to be of small capacity of about 0.3 to 28.3 bcm (0.01 to 1 Tcf) (Moulijn et al., 2013, Mitsui Engneering and Shipping, 2016). However, hydrate pellet technology has gained research attention as a method of utilizing stranded gas (Mitsui Engneering and Shipping, 2016, Kang et al., 2016, Rehder et al., 2012, Kanda, 2006, Dawe et al., 2003, Mork et al., 2001, Gudmundsson et al., 1998, Gudmundsson, 1996a). Thus, this chapter focused on the fundamental aspects of the hydrate pellet chain for NG utilization and the rationale for the use of methane hydrate (sI hydrate).

Although, a number of studies have been reported on the use of thermodynamic promoters such as tetrahydrofuran (THF), it is imperative to note environmental implication of use of these promoters at commercial large scale are yet to be established (Veluswamy et al., 2018). In addition, it can be observed that good number of studies in literature explored the methane hydrate (sI) production in conventional CSTR without thermodynamic promoter. Hence, this study limited hydrate-based utilisation of NG (pre-processed to methane) without promoters giving consideration to environmental impact on process commercialization.

Furthermore, it is noted based on literature that produced slurry contain about 90 %wt water content (Rehder et al., 2012) and in addition, the scarcity of research studies relating to processing (dewatering and pelletization) of hydrate slurry suggests more focused studies which is considered in this study.

Further as outlined earlier in Section 3.4.1, self-preservation effect is majorly established for methane hydrates and as such, this study is limited to sI methane hydrate pellets. However, adequate cost estimates and assumptions for gas reserves platforms, abandonment, drilling, and pre-processing facilities are made with consideration of NG composition dynamics at different field locations.

3.6.2 Objectives

The aim of this research project is to evaluate the methane hydrate technology for hydrate pellet chain and utilization of stranded natural gas from small and large capacity reserves. The objectives of the project are:

- to evaluate the conventional methods for utilizing stranded gas and compare with the methane hydrate technology process chain
- To evaluate the methane hydrate pellet technology chain comprising production, transportation, and regasification
- to develop methane hydrate pellet production model with reactor simulation implemented in Aspen HYSYS
- to investigate methane hydrate slurry processing to pellet
- to carry out cost estimations and profitability assessments of methane hydrate technology chain for stranded gas utilization using small reserve capacity range of 0.3 – 25.5 bcm (0.01 – 0.90 Tcf) and large reserve capacity range of 28.3 – 566.0 bcm (1.0 – 20 Tcf) over varied end-users' market distances of 10,000 km, compare with other utilization technologies. The considered transportation distance is based on methane transportation from natural gas-rich Niger-Delta region of Nigeria to Europe and Asia.

Chapter 4 Evaluation Methodology: Methane hydrate pellet production (MHPP) model

4.1 Introduction

In this study, the evaluation of methane hydrate technology (MHT) chain for utilizing stranded gas was explored for natural gas transportation from small and large capacity stranded gas reserves to a demand market by the development of methane hydrate pellet production (MHPP) model. This chapter presents the model development of the MHPP model, its simulation using Aspen HYSYS and investigation approaches. Section 4.2 describes the MHPP model framework comprising the reactor, slurry processing and pellet storage units. The reactor unit development and implementation using Aspen HYSYS as well as the model parameter investigations are described in Section 4.3. In addition, adequate scale up assumptions were carried for the reactor model to match the capacity requirement of 0.3 – 25.5 bcm (0.01 – 0.90 Tcf) as small reserve capacities range and 28.3 – 566.0 bcm (1.0 – 20 Tcf) as large reserve capacities range. Section 4.4 presents the dewatering and pelletization processes and model development. Then, a storage tank was specified for the produced pellet prior to loading onto ship vessel for transportation as shown in Section 4.5. The MHPP model developed in this chapter and its results analysed in chapter 5 will be used together with the presented cost estimations of ship transportation, reservoir exploration, and pre-processing for the economic investigation of MHT chain in chapters 6.

4.2 MHPP model framework and process description

The summary of MHPP model framework is shown in Figure 4.1. This forms part of the technology chain of methane hydrate for the utilization of stranded gas. The MHPP model framework comprises of three main operation units: (i) The hydrate formation unit, which produces hydrate slurry, (ii) The hydrate slurry dewatering and pelletization units, and (iii) The pellet storage unit.

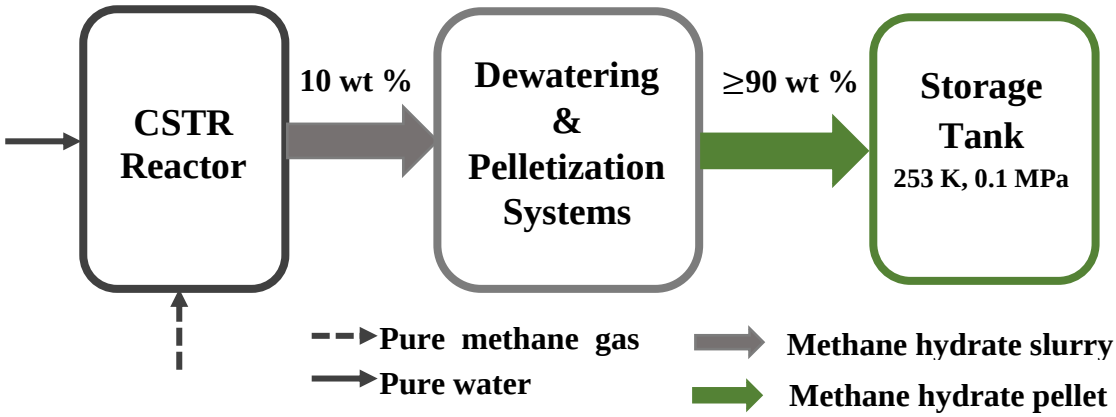

Figure 4.1: Summary framework of the MHPP model

4.3 Reactor unit development and implementation using Aspen HYSYS

4.3.1 Reactor Design

The steady state simulation of a jacketed continuous stirred tank reactor (CSTR) for methane hydrate formation process was implemented using the HYSYS conversion reactor model that was modified to include a methane hydrate formation rate equation and other parameter specifications linked using the HYSYS spreadsheet. Therefore, values of these parameters are inserted into the conversion reactor by the spreadsheet within HYSYS. This was considered in order to factor in the considered parameters and conditions in this study. The reactor design of the base case is based on experimental studies (Mork, 2002, Murayama et al., 2011). As discussed in chapter 3 (Section 3.3), pilot plant scale 10 kg hr^{-1} hydrate pellet production comprised a CSTR and downstream MH slurry processing units as shown in Figure 4.2 (Murayama et al., 2011), which in this study is modelled as MHPP model. In Figure 4.2 below, the reactor has been presented together with the dewatering and pelletization units that are discussed in subsequent sessions.

The sizing of the reactor for the formation of methane hydrate slurry was based on methane gas mixing with water in cooling jacketed CSTR (see Equation 4.1) with steady state operation and assuming a pseudo-first order reaction of methane gas with water.

The formation rate is calculated based on a correlation from experimental data (Mork, 2002).

$$CH_4\,(g) + nH_2O\,(l) \Leftrightarrow CH_4.nH_2O\,(s) \qquad 4.1$$

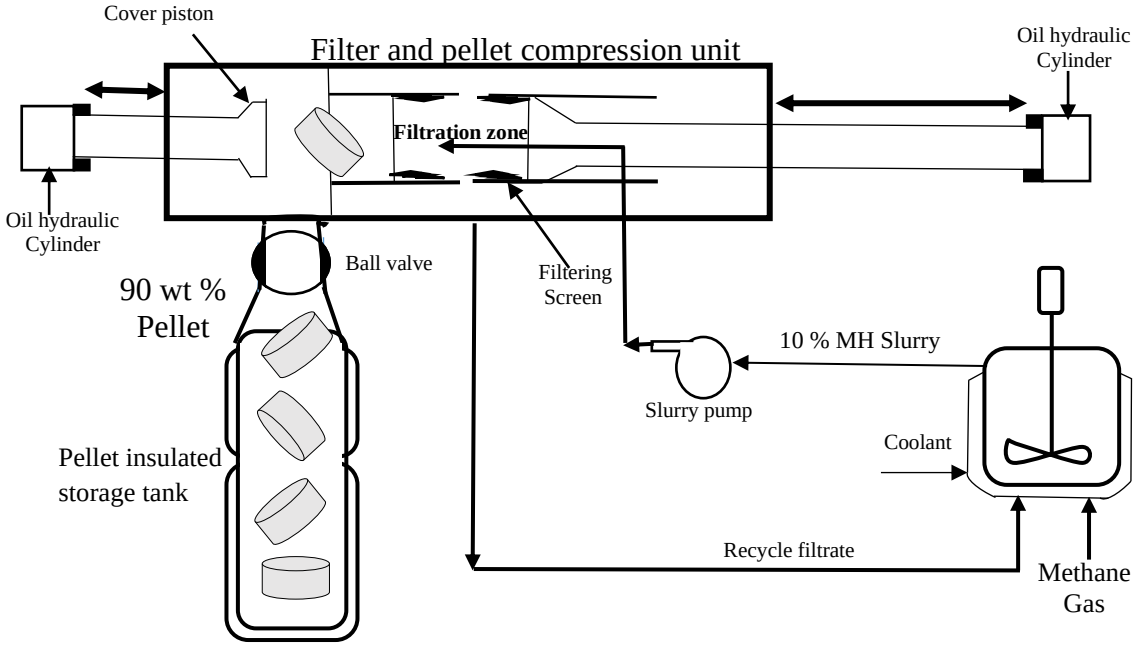

Figure 4.2: Process flow diagram for MH production. Adapted from (Murayama et al., 2011)

The volume, V of the reactor is calculated using mass balance:

$$V = \frac{F_{A_1} X}{-r_A} \qquad 4.2$$

where F_{A_1} is the feed molar flowrate of component A (methane gas), X is the conversion and r_A is the reaction rate, that is, rate of consumption of gas component A to form methane hydrate as shown schematically in Figure 4.2. The consumption rate with respect to the gas phase in the gas-liquid system is based on an adapted correlation from experimental data given in Section 4.3.2. The conversion is defined with respect to the gas consumption rate, that is, the hydrate formation rate proportional to the superficial gas velocity (gas injection rate), which is 44 % based on experimental data (Mork, 2002)

In addition, as discussed in chapter 3, the reactor diameter : impeller diameter ratio was 0.5 and the reactor height : reactor diameter ratio was 2 which are within range of standard geometry stirred tank reactor (Coker, 2007). These values were used to calculate the dimensions from the reactor volume calculated using Equation 4.2.

4.3.2 Application of hydrate formation rate correlation

The formation rate of methane hydrate was simulated using pure methane gas and liquid water in a continuous stirred tank reactor, with correlation based on sequence of laboratory experimental data (Mork, 2002):

$$r = kpv_{sg}^{a} P_g^{\,b} \Delta T^{c} \qquad 4.2$$

where r (m^3s^{-1}) is the hydrate formation rate, k which is 1.43×10^{-4} is the correlation constant, p is the operating pressure, v_{sg} is superficial gas velocity (gas injection rate into the reactor), P_g is the power consumption with gas-liquid mixing in the system while a, b and c are 1.00, 0.146, 0.02 respectively. It is important to know that the difference between the equilibrium temperature (T_{eq}) and operating temperature (T) in the reactor is the subcooling, ΔT (Knox et al., 1961, Ke and Svartaas, 2013).

In this study, using Equation 4.2, methane hydrate formation in a stirred tank reactor was simulated at the process conditions and under the assumptions already discussed in Section 3.1 in chapter 3. These computation components were used to develop a modified correlation rate model that will be implemented for the simulation of MHPP reactor unit as conversion reactor in HYSYS.

Applying the molar density, ρ_m of feed gas stream (methane), equation 4.2 can be given in terms of moles of methane consumed with time as:

$$r = kp\rho_m v_{sg}^{a} {P_g}^{b} \Delta T^{c} \qquad 4.3$$

where the unit of r is hydrate formation rate in mols s^{-}. Gas was injected into the water-filled baffled reactor using a sparger below the impeller. Bubbles rose to the Rushton turbine impeller, which was operated in the completed dispersion-recirculation regime for effective mixing and gas-liquid mass transfer. Nienow's correlation (Equation 3.7) was used to calculate the impeller speed (Oldshue, 1983, Tatterson, 1991). In addition, as discussed in chapter 3, flow number, FI combines with the power consumption prior to and after injecting gas into the gas−liquid reactor with correlations given in Equations 3.8 and 3.9 respectively. Therefore, with the standard power consumption expressed as $P = N_p\rho N^3 D_i^5$ (Equation 3.1) and Froude number as well as considering the dispersion water volume in the system, the modified rate correlation becomes:

$$r = \left(kp\rho_m V_w^{-1} V_{sg}^{a} \left[\left(1 - 163.8N^4 {D_i}^7 D^{-5} g^{-2}\right)\left(N_p\rho N^3 D_i^5\right)\right]^{b} \Delta T^{c}\right) \qquad 4.4$$

$$r = \left(kp\rho_m V_w^{-1} V_{sg}^{a} \left[\left(0.62 + 24.05N^4 {D_i}^7 D^{-5} g^{-2}\right)\left(N_p\rho N^3 D_i^5\right)\right]^{b} \Delta T^{c}\right) \qquad 4.5$$

Equation 4.4 and 4.5 are for gas flow numbers of FI < 0.035 and FI > 0.035 respectively. where r: hydrate formation rate (mol $m^{-3}s^{-1}$), N: stirring rate (s^{-1}), D_i: impeller diameter (m), D: reactor diameter (m), V_{sg}: superficial gas velocity (m s^{-1}), V_w: the dispersion water volume (m^3), ρ_m: molar density ($mol\ m^{-3}$), ρ: mass density (kg m^{-3}), g: acceleration due to gravity, k: empirical correlation constant and ρ_m: molar density of feed stream (mol m^{-3}). An impeller speed of $6.67s^{-1}$ was considered as sufficient speed as suggested by Mork (2002) experimental study. The modified rate model was expressed in terms of key parameters of the reactor design and

operations will be applied in a base case of the modelled 10 kg hr^{-1} MH production as well as the key parameters investigated in an evaluation and sensitivity analysis below. The design calculations presented in sections 4.3.1 – 4.3.2 may be applied with caution, to obtain the CSTR reactor volume at plant operating conditions assuming the modified rate model holds for the specified conditions

4.3.3 Implementation in Aspen HYSYS and key process simulation specification

4.3.3.1 Aspen HYSYS Software

HYSYS software package (version 8.8) was selected for the MHPP reactor simulation of the process. It is an interactive process simulation software widely used in the industry. HYSYS software is a general-purpose process simulation program with capability of simulation of chemical processes, estimating physical properties, and material and energy balances. HYSYS also has capacity to predict hydrate formation equilibrium conditions for hydrates using predictive model (hydrate formation utility with three phase Ng and Robinson (1976) equilibrium model) and the use of cubic equation of state (EOS) generated properties based on fundamental thermodynamic principles (Carroll, 2014).

The fluid package used for the simulation of the reactor is the Peng-Robinson (PR) EOS. Peng-Robinson EOS is robust and can be applied to a wide range of operating conditions. It is generally recommended as a property package for natural gas systems (Davarnejada et al., 2014). Therefore, besides implementing the rate of hydrate formation, achieving the CSTR reactor sizing, and the material and energy balance, the hydrate formation conditions will be explored using the HYSYS predictive reactor model and compared with literature data.

4.3.3.2 Key specifications for the base case MHPP reactor simulation

The pressure of pure methane gas feed stream of 5 MPa was used, which was considered to be an average of the typical pipeline delivery pressures for pre-processing facilities (Mokhatab et al., 2015). The gas stream passed through the compressor and attained the reactor base case operating pressure. A cooler reduced the temperature of the gas after the compressor to the operating temperature as shown in Figure 4.3. A target conversion of 44% (Mork, 2002) of the base component (methane gas) was also considered with the unreacted gas recycled to the reactor. The target conversion was obtained based on experimental data of methane hydrate formation using CSTR (Mork, 2002).

The pure water stream was assumed to be from a source at atmospheric pressure and ambient temperature, which is pumped and cooled to achieve the reactor operating conditions.

The product stream, methane hydrate slurry (sI hydrate), was defined as a hypothetical solid stream in HYSYS with defined properties. The production of MH using a continuous stirred tank reactor was reported to yield a very large amount of un-converted water in the slurry

(Murayama et al., 2011, Nakai, 2012a, Rehder et al., 2012). Therefore, with the HYSYS adjust operator relative to the feed gas flowrate, mass fraction of 0.1 was specified as the solid content of the 10 kg hr^{-1} MH slurry production.

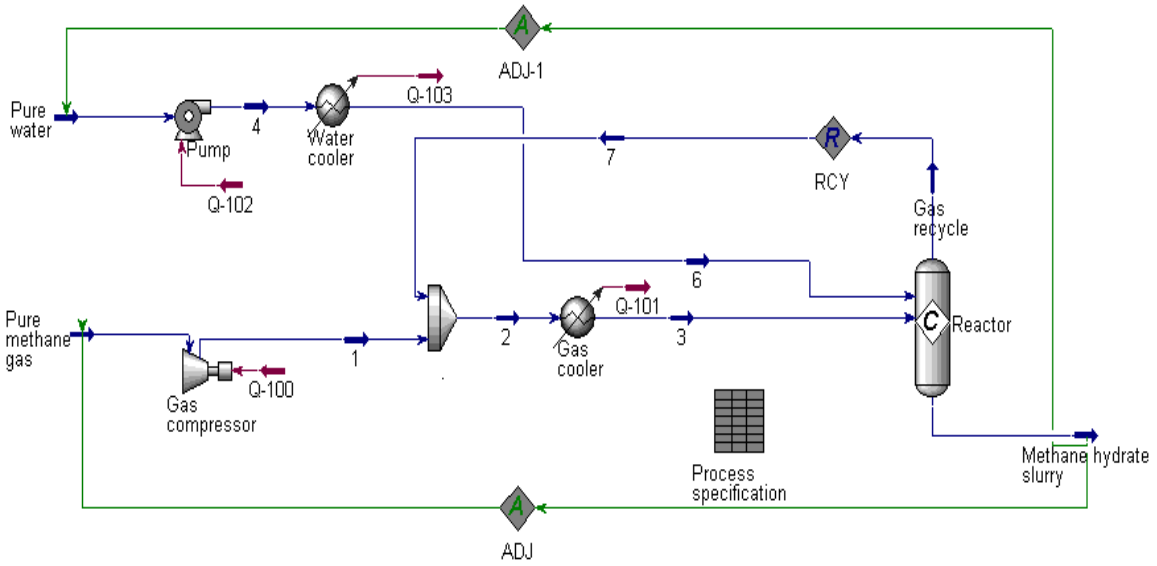

Figure 4.3: HYSYS process flowsheet for methane hydrate process

For the base case simulation of hydrate formation in HYSYS, the enthalpy of methane hydrate formation was determined based on enthalpy of dissociation, ΔH_d, using proposed correlations by (Holder et al., 1988a). This enables calculation of ΔH_d of pure methane hydrate from gas and liquid water at methane hydrate equilibrium pressure according to linear expression [$\Delta H_d = 4.18\ (13500.0 + 4.0T)$] as discussed in Section 2.4 (Holder et al., 1988a). Similarly, the hydration number, n for the base case was obtained using its crystal structure and degree of occupancy of the cavities [$n = 46\ (6\theta_L + 2\theta_S)^{-1}$], where θ_L and θ_S are the fractional occupancy of large and small cavities respectively which was estimated using the CSMhyd software (1998 version) at 285.15 K. It should be noted that the Clausius-Clapeyron equation was applied for determining the enthalpy and hydration number in a broader condition range for the evaluation and sensitivity analysis (see Section 4.3.5). The molecular weight of methane gas hydrate was determined from its crystal structure and the degree of saturation (fraction of cavity filled since hydrates are non-stoichiometric), which is a function of the temperature and pressure, given as (Carroll, 2014):

$$MW = \frac{N_w MW_{H_2O} + \sum_{J=1}^{C} \sum_{i=1}^{N} \theta_{iJ} \nu_i MW_{CH_4}}{N_w + \sum_{J=1}^{C} \sum_{i=1}^{N} \theta_{iJ} \nu_i} \qquad 4.6$$

where N_w is the number of water molecules per unit cell (46 and 136 for sI and sII respectively). MW_{H_2O} and MW_{CH_4} are molecular weights of water and methane gas respectively. θ_{iJ} is the fractional occupancy of cavities of type i by component j (θ_L and θ_S are large and small cavities respectively for sI and sII). N is the number of cavity types in unit cell,

ν_i is the number of type i cavities per water molecule in unit cell (two small, 5^{12} and six large, $5^{12}6^2$ cavities for sI) and c is the number of components which for this case is only methane. Other properties of the methane hydrate were also estimated as follows. The methane hydrate phase density in kg m^{-3} was estimated based on the equation of Holder et al. (1988a) as:

$$\rho_{hyd} = 1000 \frac{N_w MW_{H_2O} + \sum_{J=1}^{C} \sum_{i=1}^{N} \theta_{iJ} \nu_i MW_J}{N_{Ava} v_o} \quad 4.7$$

In addition, using the methane phase density and water density alongside hydrate phase mass fraction, the hydrate-water slurry density was estimated as follows (Meindinyo and Svartaas, 2016):

$$\rho_{slurry} = \alpha_{hyd} . \rho_{hyd} + (1 - \alpha_{hyd}) . \rho_l \quad 4.8$$

For the specific heat of methane hydrate, a linear fit of the correlation of Handa (1986a) was carried out by Waite et al. (2007) between 274.15 – 290.15 K (1−17 ℃). This equation was used to estimate specific heat, c_p (kJ $kg^{-1}K^{-1}$), given by:

$$c_p = [2100 - 7.07\ T\ (℃) + 0.66\ T^2\ (℃) + 0.051\ T^3\ (℃)] / 1000 \quad 4.9$$

It should be noted that the temperature is in degrees Celsius. The specific heat of water at the conditions was specified from HYSYS databank.

4.3.4 Evaluation of the HYSYS base case reactor simulation using energy balance calculations

The mass and energy balances for the methane hydrate production in this study were based on the assumption of perfect mixing conditions in CSTRs. Typically in CSTRs, the conditions in the reactor are equal to the conditions at the outlet. The focus of the mass and energy balance calculation was used to verify and further examine the simulated reactor operation in HYSYS and establish the cooling conditions of the jacketed reactor. The energy balance was based on Fogler (2016) and Mork (2002). Contrary to the Mork (2002) study in which their hydrate forming CSTR experimental results were also verified using energy balance calculation, is that heat of hydrate formation removal from the CSTR reactor with coolant was not considered. However, in this study, the energy balance of the coolant fluid entering and leaving the coolant jacket was included. The heat of hydrate formation in the considered CSTR in this study is removed by the heat exchange with the coolant jacket as shown in Figure 4.4.

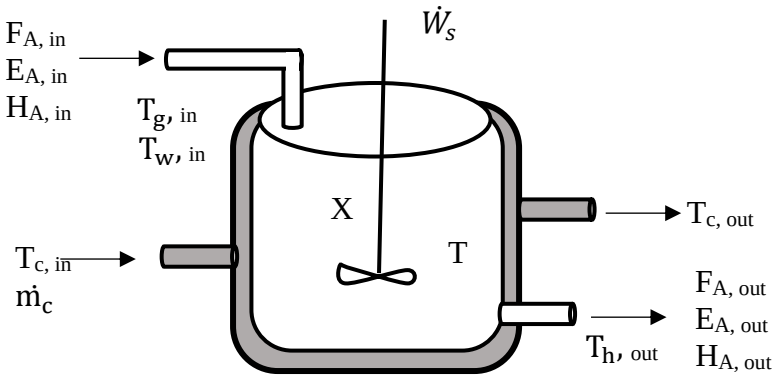

Figure 4.4: CSTR reactor with jacketed cooling showing an open system (Fogler, 2016)

4.3.4.1 Mass balance of methane hydrate process

The mole balance for the number of moles, n for component A with molar flow rates, in ($F_{A,\,in}$) and out ($F_{A,\,out}$) the CSTR reactor of component A with volume V at steady state condition is given as:

$$\frac{dn_A}{dt} = F_{A,\,in} - F_{A,\,out} - r_A V = 0 \qquad 4.10$$

$$V = \frac{F_{A_{in}} - F_{A_{out}}}{-r_A} = \frac{F_{A_{in}} X}{-r_A} \qquad 4.11$$

4.3.4.2 Energy balance of methane hydrate process

An energy balance for an open system over time interval (inlet and outlet the system) was considered suitable for this study with energy, E_A exchanges brought about by components inflow and outflow with molar flowrates, F_A. Therefore, the system over time interval is the sum of the product of the number of moles of each component in the system multiplied by the respective energies given as:

$$\Delta E_{system} = \dot{Q} - \dot{W} + \sum F_{A_{in}} E_{A_{in}} - \sum F_{A_{out}} E_{A_{out}} \qquad 4.12$$

where $\dot{Q}$ is the heat flow to the system and the work term $\dot{W}$ (work by the system) comprises of flow work, shaft work, W_s from stirrer in a CSTR (i.e. power consumption) and other work. E_A is the energy term which is the sum of internal, kinetic and potential energy and any other energies like electric and so on. Mostly in reactor scenarios, kinetic and potential energy are negligible, and the internal energy is combined with the flow work term, so that the enthalpy inlet, H_{A_1} or outlet, H_{A_2} of the system is expressed as sum of internal energy inlet or outlet the system by mass flow plus flow work. The energy balance over time interval becomes:

$$\Delta E_{system} = \dot{Q} - W_s + \sum F_{A_1} H_{A_1} - \sum F_{A_2} H_{A_2} \qquad 4.13$$

The subscripts 1 and 2 indicate inlet and outlet of the system. Considering the gas hydrate formation process with Equation 4.1, comprised of gas, water and hydrate component (with subscripts g, w, and h respectively) where n is the hydration number.

Then, the enthalpies and the molar flow rate of gas, water and hydrate components in the system are described in terms of the inlet and outlet streams as:

$$\sum F_{A_1} H_{A_1} = F_{g_1} H_{g1} + F_{w_1} H_{w1} \quad 4.14$$

$$\sum F_{A_2} H_{A_2} = F_{h_2} H_{h2} + F_{g_2} H_{g_2} + F_{w_2} H_{w_2} \quad 4.15$$

$$F_{g_2} = F_{g_1}(1 - X) \quad 4.16$$

$$F_{w_2} = F_{g_1}\left(\frac{F_{w_1}}{F_{g_1}} - nX\right) \quad 4.17$$

$$F_{h_2} = F_{g_1}\left(\frac{F_{h_1}}{F_{g_1}} - X\right) = F_{g_1} X \quad 4.18$$

Combining the equations and simplified, it becomes:

$$\sum F_{A_1} H_{A_1} - \sum F_{A_2} H_{A_2} = F_{g_1}\left[\left(H_{g1} - H_{g_2}\right) + \frac{F_{w_1}}{F_{g_1}}\left(H_{w1} - H_{w_2}\right)\right] - F_{g_1} X(H_{h2} - nH_{w_2} - H_{g_2}) \quad 4.19$$

$$\sum F_{A_1} H_{A_1} - \sum F_{A_2} H_{A_2} = F_{g_1}\left[\left(H_{g1} - H_{g_2}\right) + \frac{F_{w_1}}{F_{g_1}}\left(H_{w1} - H_{w_2}\right)\right] - \Delta H_r F_{g_1} X \quad 4.20$$

where ΔH_r is the heat of reaction, that is, the heat of formation at the reactor temperature and with assumption of a limited temperature change from inlet to outlet, which implying constant heat capacity so that the energy balance becomes:

$$\Delta E_{system} = \dot{Q} - W_s + F_{g_1}\left[c_{p_g}\left(T - T_{g_1}\right) + \frac{F_{w_1}}{F_{g_1}} c_{p_w}\left(T - T_{w_1}\right)\right] - \Delta H_r F_{g_1} X \quad 4.21$$

Where T is the reactor temperature which is same as temperature of the product hydrate slurry, $T_{h,\,out}$, while T_{g_1} and T_{w_1} are inlet temperatures and c_{p_g} and c_{p_w} are heat capacities of gas and water respectively.

Therefore, reactor temperature of the MHPP HYSYS simulation is compared with that from the Equation 4.21 to verify the simulation. It should be noted that reactor coolant parameters could not be implemented in HYSYS running in steady state mode as with this study. As a result, the MHPP reactor simulation calculation, which includes the reactor coolant parameters (Equations 4.28 and 4.29) below, was carried out in an Excel spreadsheet.

4.3.4.3 E**nergy balance on the coolant fluid inflow and outflow the coolant exchanger jacket**

The energy balance on the coolant fluid entering and leaving the coolant heat exchanger system of a gas hydrate producing jacketed CSTR assuming a quasi-steady state for the coolant is:

$$\underbrace{\dot{m}_c c_{P_c}\left(T_{c_1} - T_R\right)}_{\text{Rate of energy in by flow}} - \underbrace{\dot{m}_c c_{P_c}\left(T_{c_2} - T_R\right)}_{\text{Rate of energy out by flow}} - \underbrace{\dot{Q}}_{\text{Rate of heat transfer to the coolant}} = 0 \quad 4.22$$

where $\dot{m}_c$ is the mass flowrate which enters the reactor at temperature, T_{c_1} and leaves at temperature, T_{c_2} while T_R is the reference temperature and c_{P_c} is the heat capacity of the coolant fluid. Considering a coolant that will handle an exothermic reaction, so that $T > T_{c_2} > T_{c_1}$, then heat transfer between the coolant exchanger jacket and reactor fluid at operating temperature is given as:

$$\dot{Q} = \frac{UA_h(T_{c_1} - T_{c_2})}{\ln[(T - T_{c_1})/(T - T_{c_2})]} \quad 4.23$$

So that the energy balance is simplified as:

$$\dot{Q} = \dot{m}_c c_{P_c}(T_{c_1} - T_{c_2}) = \frac{UA_h(T_{c_1} - T_{c_2})}{\ln[(T - T_{c_1})/(T - T_{c_2})]} \quad 4.24$$

The energy balance is further resolved for the coolant outlet temperature, T_{c_2} as:

$$T_{c_2} = T - (T - T_{c_1})\exp\left(\frac{-UA_h}{\dot{m}_c c_{P_c}}\right) \quad 4.25$$

Substituting for T_{c_2} and simplifying, the heat transferred becomes:

$$\dot{Q} = \dot{m}_c c_{P_c} - (T_{c_1} - T)[1 - \exp\left(\frac{-UA_h}{\dot{m}_c C_{P_c}}\right)] \quad 4.26$$

When large values of $\dot{m}_c$ is considered, the exponent will be small, an expansion in Taylor's series ($e^x = 1 - x + \cdots$) can be carried with the second order terms omitted to get:

$$\dot{Q} = \dot{m}_c c_{P_c} - (T_{c_1} - T)[1 - (\frac{-UA}{\dot{m}_c C_{P_c}})] = UA_h(T_{c_1} - T) \quad 4.27$$

where U is the overall heat transfer coefficient and A_h is the heat transfer area of the reactor and surrounding jacket.

Water with ethylene glycol was considered as the coolant fluid for the jacketed MHPP reactor model. T_{c_1} with limited temperature difference to T_{c_2} which is effective when high enough heat transfer cooling water flowrates was assumed (Fogler, 2016). Therefore, with the coolant heat exchange for the methane gas hydrate forming CSTR, $\dot{Q}$ (Equation 4.27) as derived, when substituted into Equation 4.23 and considered to operate at steady state conditions, the outlet temperature of the reactor can be determined as:

$$T = \frac{F_{g_1} c_{p_g} T_{g_1} + F_{w_1} c_{p_w} T_{w_1} + \Delta H_r F_{g_1} X + W_s - UAT_{c_1}}{F_{g_1} c_{p_g} + F_{w_1} c_{p_w} - UA_h} \quad 4.28$$

However, at known reactor outlet temperature, the overall heat transfer coefficient with the coolant temperature, heat transfer area and the rate of heat removal specified can be estimated using:

$$U = \frac{F_{g_1} c_{p_g} T_{g_1} + F_{w_1} c_{p_w} T_{w_1} + \Delta H_r F_{g_1} X + W_s - F_{g_1} c_{p_g} T - F_{w_1} c_{p_w} T}{A_h(T_{c_1} - T)} \quad 4.29$$

On the other hand, to verify the hydrate formation conditions obtained using the HYSYS predictive model at the reactor operating conditions, CSMhyd was also employed to compare the determined hydrate formation condition from HYSYS simulation.

4.3.5 Evaluation and sensitivity analysis of the parameters used in the simulation

An assessment and sensitivity analysis of major correlations used in the MHPP reactor simulation was carried out to ascertain the influence of the key variables on the simulation results. Sensitivity analysis involves the study of how the variations in the output of a system can be apportioned to the input parameters, in other words, ranks the influence of the principal input parameters on the output of the system (Alam et al., 2016). The one-factor-at-a-time approach of sensitivity analysis was applied.

This investigation is important in order to ascertain the prime controlling parameters of the MHPP reactor simulation relating to a better understanding of the gas hydrate system. These variables have distinct significant effects on the hydrate formation process as applied in the MHPP reactor simulation study. Hence, it is important to evaluate the effects of the variables to determine preeminent conditions for an efficient methane hydrate formation process.

Therefore, with simulation runs the effects of the following variables within defined range: temperature (subcooling), pressure, reactor impeller stirring rate, methane gas supply conditions into the reactor as gas injection rate or superficial gas velocity and the gas-to-water ratio (hydration number) as well as the enthalpy of hydrate formation were examined. The required amount of water in a hydrate formation system is an important variable in gas hydrate formation process and the hydration number varies based on the composition of the guest component and the pressure (Rajnauth et al., 2012).

In addition, sensitivity analysis was used to investigate hydration number with theoretically estimated MH equilibrium conditions using two commercial simulators HYSYS and CSMhyd. For the adapted methane gas consumption rate correlation (Equation 4.4), pressure range of 5.40 – 9.0 MPa and subcooling 276.09 – 281.09 K respectively were used.

The considered range covers the operating P-T conditions of the simulated pilot scale hydrate forming CSTR. In addition, the gas injection rate to the reactor indicated as superficial gas velocity was also investigated within the range of $9.5 \times 10^{-6} - 4.2 \times 10^{-3}$ ms^{-1} and likewise the impeller power consumption to ascertain the effect magnitude on hydrate formation rate over impeller stirring rates, 6.7, 10.0 and 13.3 revolution per seconds.

Similarly, using HYSYS MHPP reactor simulator, at the pressure range 5.40, 7.00, 8.00 and 9.00 MPa, the equilibrium temperature conditions were estimated and applied to calculate enthalpy of dissociation at the equilibrium conditions using Clausius-Clapeyron correlation plot (ΔH_d = -zsR) (Sloan and Fleyfel, 1992, Sloan and Koh, 2008). Then, applying the approach

used by de Forcrand method (Sloan and Koh, 2008), which considers the equilibrium of gas, and n mol of liquid water (or ice) with hydrates either sides of the ice point. So that with the estimated enthalpy values of methane + liquid water at (Lw-H-V) subtracted from that of methane + ice at (I-H-V) equilibrium with outcome of the number of moles of liquid water converted to ice from the two reactions. Then, dividing the difference in enthalpy by the molar enthalpy of fusion of ice, the number of moles of water converted to hydrates is obtained (Sloan and Koh, 2008). Methane hydrate enthalpy ΔH_d = 19.06 KJ mol^{-1} for methane + ice was used (Frost and Deaton, 1946) cited in (Levik, 2000).

Likewise, using the Clausius-Clapeyron correlation plot, the enthalpy of dissociation was also calculated based on temperature range of 280.15 – 286.15 K and equilibrium condition prediction (including fractional cage filling) using CSMhyd. The actual occupancies of methane guest molecules into the large, θ_L and small θ_S cages were considered and using [$n = 46\ (6\theta_L + 2\theta_S)^{-1}$] to determine the hydration number at specified conditions. Fully occupied hydrate cages by methane molecules implies n-ideal value of 5.75. However, gas hydrates are non-stoichiometric implying that not all of the cages are occupied, and fractional cages occupancy is system dependent at specified pressure and temperature conditions. Moreover, hydrate filling or occupancy of guest molecules is largely dependent on pressure and temperature.

Using the two approaches, the guest gas dependent correlation and the Clausius-Clapeyron equation, the effect of hydration number within the considered pressure and temperature conditions of methane hydrates are investigated. In addition, comparison of the HYSYS simulator applied in this study with the CSMhyd used to estimate the equilibrium conditions. Then, the obtained hydration number values and enthalpy of formation are compared with literature data. Results of the evaluations and sensitivity analysis are reported in Section 5.4 of Chapter 5.

4.3.6 Reactor scale up and specification of considered natural gas reserve capacities

4.3.6.1 MHPP Reactor model scale up using base case

The concept of geometric similarity was applied to scale up the reactor. As mentioned earlier, geometric similarity entails using the same dimensional ratios at constant P/V on scale up of reactor. To achieve geometric scale up, a scale ratio, R employed based on scale up number for the standard geometry STR is applied. Let the base reactor volume be denoted with V_1 and the scaled up reactor V_2, so that the ratio of the volumes is given as Coker (2007):

$$\frac{V_2}{V_1} = \frac{D_2^3}{D_1^3} \qquad 4.30$$

Therefore, the scale factor is determined as:

$$R = \left(\frac{V_2}{V_1}\right)^{1/3} \quad 4.31$$

Considering the disparity in heat removal rate with the temperature difference between the reactor and the cooling jacket, given as:

$$R = \left(\frac{V_2}{V_1}\right)^{1/3} * (T - T_{c_1}) \quad 4.32$$

To maintain the basic flow regime in the geometrically similar reactor, dispersion scale up is required (Evangelista et al., 1969). Therefore, with the scale factor defined, the reactor diameter in relation with the impeller speed, N of scaled up reactor is given as:

$$N_2 = N_1 \left(\frac{1}{R}\right)^n \quad 4.33$$

where n is a dynamic scale up factor. The value of 0.667 for n was considered in order to achieve constant energy input per volume $\left(P/V\right)$, which can depict uniform mass transfer coefficient and similarity of turbulent flow regime in both reactors (Evangelista et al., 1969). The value of n is based on theoretical and empirical considerations for six blade Rushton turbine mixing in literature which aligns with this study (Coker, 2007, Oldshue, 1983).

4.3.6.2 Reactor simulation range for the evaluation of small and large stranded gas capacities

The methane hydrate technology chain evaluation was based on the MHPP reactor simulation and scale up using two case scenarios of small reserve capacity range of 0.3 – 25.5 bcm (0.01 – 0.90 Tcf) and large reserve capacity range 28.3 – 566.0 bcm (1.0 – 20 Tcf) reserve capacities. The required number of reactors for utilizing these reserve capacities was estimated using an equation based on the MHPP reactor simulation, which indicates the feed stream flowrate relating to each gas reserve capacity. It is important to note that the reactor scale up studied was constrained to 30 m^3 as an upper limit, which is the maximum volume obtained using reactor diameter of 2.67 m (limit of Nienow's correlation for Rushton impeller used) (Nienow et al., 1986). However, in any scenario, which requires reactor capacity over 30 m^3, multiple reactors were worked out using required reactor volume, V_r equation is given as:

$$V_r = \frac{Q_{fg}X}{\left(kP\rho_m V_w^{-1} V_{sg}^a \left[\left(1-163.8N^4 {D_i}^7 D^{-5} g^{-2}\right)\left(N_p \rho N^3 D_i^5\right)\right]^b \Delta T^c\right)} \quad 4.34$$

The equation is based on the standard reactor design equation presented in Section 4.3.1 where X is conversion, Q_{fg} denotes the feed stream (pure methane gas) flowrate which is dependent on the annual production rate of each reserve (gas field or reservoir).

Table 4.1: Simulation specification for small and large capacity stranded gas utilization

Case	Annual gas production rate (bcm) per 20 years	Methane feed gas flowrate Q_{fg} (mol s^{-1})
Small reserve capacity range scenario		
1	0.3	21.0
2	2.8	211.0
3	11.3	844.0
4	25.5	1899.0
Large reserve capacity range scenario		
5	28.3	2105.9
6	169.9	12593.7
7	339.8	25187.4
8	566.3	41979.0

4.4 Dewatering and pelletization units

As previously highlighted the MH slurry downstream the reactor typically yields 90 wt % water content (Rehder et al., 2012). Therefore, the slurry processing units are significant consideration of the MHT chain as discussed in chapter 3 (Section 3.3). Figure 4.2 shows the MHPP model flow diagram with reactor and downstream processing based on slurry filtration and compression to pellet based on pilot scale hydrate pellet processing machine (HPPM) explored experimentally by the Mitsui Engineering and Shipping CO. Ltd (Murayama et al., 2011). Therefore, for the evaluation of the MH slurry processing in this study, modelling based on the experimental study data was carried out. The principle of filtration and standard filtration correlations in literature were also employed in the analysis of the processing unit (Tarleton and Wakeman, 2007). The large water content in the MH slurry from the reactor suggests perhaps a cost-intensive dewatering and pelletizing to achieve substantial solid concentration of the methane hydrate suitable for pelletizing. Subsequently, cost estimation based on the investigations in this section was also carried out in Chapter 6 of this study as part of the MHT chain economic evaluation of stranded gas utilization. It is important to note that explicit investigations on hydrate slurry processing together with its technoeconomic evaluation are rarely included in hydrate value chain studies in literature (see Section 3.3 of Chapter 3). This is an important consideration for the commercialization of the hydrate-based process.

In the HPPM, as the methane hydrate slurry is fed, system performs filtration and subsequently pelletizing in the same cylindrical container as shown in the pilot rig flow diagram (Figure 4.2). The process operation modelling explored is this section was carried out in three stages of constant rate filtration, constant pressure filtration and compression stages (Sections 4.4.1 – 4.4.2).

4.4.1 Modelling and simulation of MH slurry dewatering unit (constant rate filtration)

The produced MH slurry from the reactor pumped into the cylindrical filtration−compression chamber is dewatered by a cylindrical filtering screen wire installed inside the chamber. So over time the methane hydrate particles or cake deposits on the inner surface of the screen while the filtrate flowing outside of the screen and is recycled to the reactor as shown in Figure 4.2 (Murayama et al., 2011). The slurry pump is a displacement pump and at the end of the compression piston has a poppet valve, which when opened the slurry is fed into the cylindrical filtration−compression chamber.

The pressure of 5.4 MPa from upstream reactor is considered to drive the downstream slurry flow into the filtration−compression chamber as filtration commences, so that the volume of the filtrate flowing per unit time, which is, rate of filtration at constant rate can be determined. However, with progress in the filtration, the thickness of depositing MH cake inside surface of the screen increases. Likewise, resistance to filtrate flow also increases which will result in pressure drop driving force (between inside and outside screen pressure difference) increases maintaining constant filtration rate. The constant rate filtration endpoint is based on detection of pressure drop set value obtained using experimental rig data (Murayama et al., 2011). Figure 4.5 illustrates the constant rate filtration operation of the cylindrical filtration−compression chamber due to the filtration pressure drop with a woven wire screen of resistance of $1.0 \times 10^{10} \mathrm{m}^{-1}$ considered (Holdich, 2002). The area and capacity of the cylindrical filtration−compression chamber based on (Murayama et al., 2011) data was considered, 0.45 m length and diameter of 0.09 m for the chamber specified which was used to obtain the area and volume of a cylinder respectively. The effective filtration area was also calculated with 0.20 m and 0.05 m length and diameter respectively of the cylindrical filtering screen as shown in Figure 4.5.

Using Microsoft Excel, the operation configuration in the constant rate filtration at defined filter dimensions and at progressive pressure drop due to the flow resistance related to the MH cake build-up on the filtering screen was executed (Holdich, 2002, Tarleton and Wakeman, 2007). Using filter dimensions from Murayama et al. (2011) data and calculation with general filtration equation, the filtration operation and methane hydrate cake properties were estimated in the simulation.

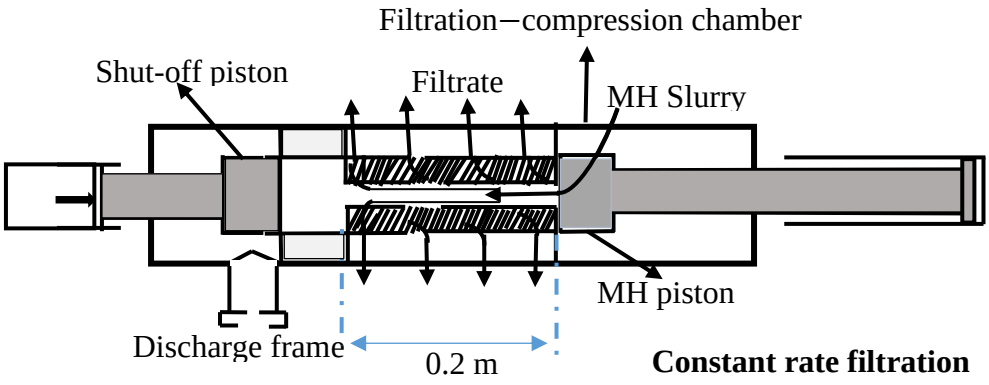

Figure 4.5: Constant rate filtration operation of MHPP model. Adapted from (Murayama et al., 2011)

The general filtration equation usually stated as the reciprocal volume flowrate (q_f) of filtrate was applied to describe the constant filtration rate in the first stage operation (Holdich, 2002, Chopey, 2004, Wakeman and Tarleton, 1994):

$$\frac{dt_f}{dV_f} = \frac{\mu \alpha_{av} c_m}{A_f^2 \Delta P} V_f + \frac{\mu R_m}{A_f \Delta P} \qquad 4.35$$

where V_f is the cumulative filtrate volume, A_f is the effective filter area (filtering screen area), α_{av} is the average filtration resistance and the filtering screen wire resistance (R_m), μ is the filtrate viscosity and c_m is the mean dry cake mass per unit volume filtrate.

Since the simulation target is 30 wt% solid based on experimental data (Murayama et al., 2011), the filtrate rate $q_f\,(m^3 s^{-1})$, from start of methane hydrate slurry filtration $q_{f_{t=0}} = \frac{dV_f}{dt}$ (at $V_f = 0$) was calculated with the slurry feed flowrate and concentration (volume fractions) of feed slurry and cake as:

$$q_f = Q_s \left(1 - \frac{C_f}{C_c}\right) \qquad 4.36$$

Q_s $(m^3 s^{-1})$ is the feed slurry flowrate, C_f and C_c are the concentration by volume fraction of MH slurry and cake respectively. The pressure difference ΔP_m (MPa) over the filter screen (inside/outside) before MH cake deposition was estimated using Equation 4.37 (Holdich, 2002, Tarleton and Wakeman, 2007) as:

$$\Delta P_m = \frac{R_m \mu 10^{-6}}{A_f} q_f \qquad 4.37$$

Then for the MH cake properties, the following equations were applied. The mean dry cake mass per unit volume filtrate which is the effective concentration of solid in the feed slurry, c_m $(kg\,m^{-3})$ was calculated using the slurry solid concentration by mass fraction, s as well as solid density, ρ_s and liquid density, ρ_l (McKetta and Cunningham, 1976, Tarleton and Wakeman, 2007) as.

$$c_m = \left[\frac{\rho.s}{1-m_r.s}\right] \quad 4.38$$

m_r is the ratio of mass wet to dry cake:

$$m_r = 1 + \frac{\rho}{\rho_s}\left(\frac{1-C_c}{C_c}\right) \quad 4.39$$

Since methane hydrate cake is compressible, the compressibility of the MH cake was accounted for by relating the average filtration resistance to the applied or compressive pressure using average specific resistance, α_{av} for methane hydrate solid given by empirical correlation obtained from (Murayama et al., 2011) data given as:

$$\alpha_{av} = 4.0 \times 10^9 \times \Delta P^{0.55} \quad 4.40$$

It is important to note that a similar average hydrate grain size as with the (Murayama et al., 2011) experiment was considered. The MH cake compressed at the incremental pressure drop (inlet/outlet pressure difference) will conform to the increase in the filtration resistance, since the filtration progresses at constant rate with hydrate cake deposition inside the filtering screen with time. However, rearranging the general filtration equation (Equation 4.35) shows the pressure drop and filtrate volume, V_f are the variables since filtrate rate, q_f is constant shown as:

$$\Delta P \times 10^{-6} = \frac{\mu \alpha_{av} c_m}{A_f^2} q_f V_f - \frac{\alpha_{av} R_m}{A_f} q_f \quad 4.41$$

The simulation of the filtration is divided into small increasing pressure increments (20 simulation runs) with the assumption that the cake properties are constant at those increments based on the suggested approach by Holdich (2002). This is because in practice, the effective concentration of solid in the feed slurry, c_m and the hydrate cake resistance,α_{av} changes as the pressure drop increases during constant rate filtration. In addition, the 5.4 MPa (the upstream pressure drive for filtration) subtracted from pressure drop due to the filtering medium resistance (calculated using Equation 4.37) was applied as the pressure drop over the 20 simulation runs in equal increments. So that the filtrate volume is determined using Equation 4.41 for the simulation runs. The solid concentration by volume fraction of the feed slurry and hydrate cake after constant rate filtration are 1.08×10^{-1} and 3.19×10^{-1} respectively, which were also spread into equal increment for the 20 simulation runs.

4.4.2 Modelling and simulation of MH secondary operation and compression

In the secondary filtration operation, hydrate cake build-up progressively with discharge of filtrate volume at constant pressure filtration as a result of the applied piston compressive force as illustrated in Figure 4.6. As the filtration advances, the hydrate cake deposited inside the effective filter area grows which implies the filtration resistance increases which results in decrease in the filtration rate.

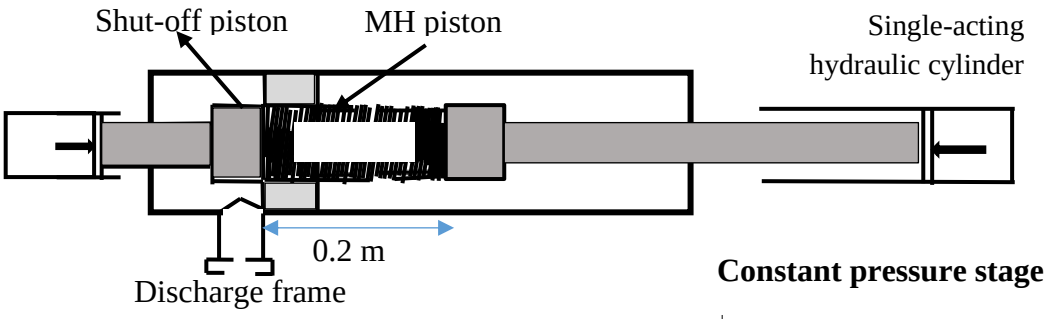

Figure 4.6: Constant pressure filtration operation of the MHPP model Adapted from (Murayama et al., 2011)

The simulation of the secondary filtration at constant pressure was modelled using the filtration equation (Equation 4.34) which was integrated and rearranged as the filtrate volume in terms of a quadratic equation (Holdich, 2002):

$$\left(\frac{\mu\alpha c_m}{2A_f^2\Delta P}\right)V_f{}^2 + \frac{\mu R_m}{A_f\Delta P}V_f - t = 0 \qquad 4.42$$

Using positive root of Equation 4.42, the filtrate volume, V_f was resolved as (Holdich, 2002):

$$V_f = \frac{-\left(\frac{\mu R_m}{A_f\Delta P}\right)+\left[\left(\frac{\mu R_m}{A_f\Delta P}\right)^2+4\left(\frac{\mu\alpha c_m}{2A_f^2\Delta P}\right)t\right]^{0.5}}{\left(\frac{\mu\alpha c_m}{A_f^2\Delta P}\right)} \qquad 4.43$$

Figure 4.6 above shows the constant pressure filtration operations from the experimental rig. The simulation was also divided into small increasing time (10 increments), which gives filtrate volume at the 10 output intervals with assumption that the cake properties are constant at those increments using Holdich (2002) simulation approach. However, due to fact that the details of the hydraulic cylinder operation, position displacement and speed associated with the compression pressure was not available so as to work out time, a time range of 3600 seconds was assumed.

The simulation is implemented to further concentrate the 30 wt% MH cake to a set point of 90 wt % by pressure compression of the piston with pressure which was reported as 9 MPa. Then for the pelletization, additional application compression by further advancing the piston was applied as Figure 4.7. The maximum compression pressure of the HPPM rig was considered which results in gradual decrease of the effective filter capacity with the cake compressed to the pellet length of 0.05 m.

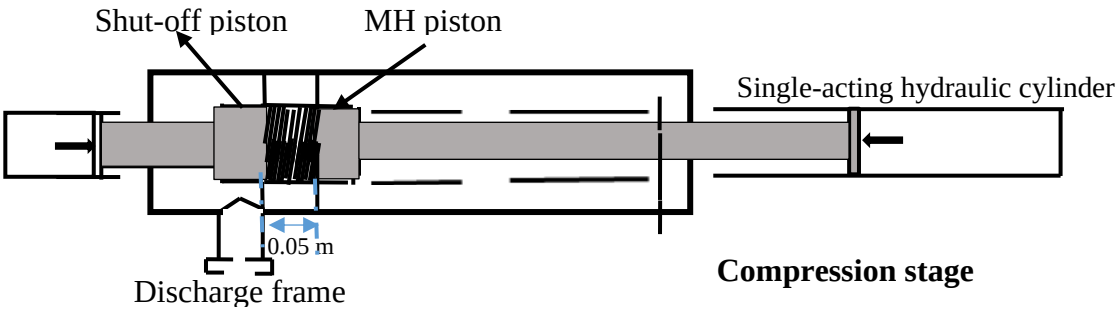

Figure 4.7: Compression operation of the MHPP model Adapted from (Murayama et al., 2011)

The produced pellet was initially held in between the caps of the two hydraulic cylinders (see Figure 4.7). The applied compression pressure from the piston was considered as 15 MPa (compression pressure for the rig) according to Murayama et al. (2011) data, since the piston travel speed is kept constant by the hydraulic system. It is important to note that hydraulic pumps that can easily be switched automatically (for low and high pressures) based on the compression and travel speed was applied for the experimental rig. The left-side cylinder is a shutoff cylinder used for discharge of the formed pellet into the storage tank at 253 K and atmospheric pressure.

The difference in the capacity of the effective filter zone was used to estimate the operating energy for the constant pressure filtration and compression stages using mechanical energy ($P\Delta V$). In this study, cost estimation of the two single-acting hydraulic cylinders or rams together with the sized units and other equipment (see Figure 4.2) will be carried out in chapter 6 as part of the MHT chain evaluation. Furthermore, the economic sensitivity of the processing unit in MHT chain, as lacking in most evaluation studies reported in literature was established.

4.5 Specification of MHPP storage unit at 253 K

In order to specify the storage vessel for the pilot-scale methane hydrate production, an estimate of an insulated storage vessel with suitable capacity was made. Assumptions were made using the size of the methane hydrate pellet in consideration (0.10 × 0.05 m considered) (Murayama et al., 2011) and density to work out the capacities relative to the production rates of each considered scenario. So, for the base case scenario, the 10 kg hr^{-1} MH production rate was used to estimate the storage capacity assuming for five days since the reactor run continuous mode. In addition, according to literature active cooling is considered not essential for storage if the hydrate pellet is cooled to the storage temperature of 253 K and atmospheric pressure, meaning that insulation of storage vessel is sufficient (Gudmundsson et al., 2000, Levik, 2000). Therefore, this might indicate economic merit of gas hydrate storage and transport technology, which will be further discussed with the economic evaluation in Chapter 6.

4.6 Concluding remarks

In this chapter, the methodology for the simulation of evaluation of methane hydrate for the utilization of stranded gas was presented based on the MHPP model framework comprising CSTR reactor, dewatering, and pelletization unit as well as storage unit models. Using a pilot scale methane hydrate pellet production (MHPP) as a base case, the reactor simulation which detailed reactor sizing, investigation of process parameters and sensitivity analysis as well as mass and energy balance verifying calculations was implemented in HYSYS software with a proposed modified methane hydrate formation rate model.

Established data and correlations from literature together with viable justifications and assumptions were employed for calculating and specifying the system thermodynamic model, hydrate system properties and the hydration number at temperature and pressure conditions. Likewise, methane hydrate slurry processing comprising the dewatering and pelletization simulations were also carried out using data and correlations from literature.

Finally, the MHPP insulated storage at 253 K was also specified. The simulation results and discussions are presented in Chapter 5, which will be applied together with the other units of MHT chain process simulation for the process chain economic evaluation in Chapter 7.

Chapter 5 Simulation results and discussion of the methane hydrate pellet production (MHPP) model

5.1 Introduction

The simulation results, analysis, and discussions of the methane hydrate pellet production model of Chapter 4 are reported in this chapter. This comprises of the following:

- Base case simulation conditions and results are presented in Section 5.2.
- Section 5.3 and 5.4 present the analysis of the MHPP HYSYS simulation condition results and the results evaluation of the sensitivity analysis and a comparison of the reactor unit simulation compared to the calculated energy balance.
- Section 5.5 presents the simulation results and discussion of the dewatering and pelletization processes.
- Section 5.6 shows and discusses the reactor unit simulation results and scale up assumptions used to define capacities of 0.3 – 25.5 bcm (0.01 – 0.90 Tcf) as small reserve capacities range and 28.3 – 566.0 bcm (1.0 – 20 Tcf) as large reserve capacities range.

5.2 HYSYS simulation results and discussions of the MHPP reactor unit

5.2.1 Base case reactor design and simulation results

The methane hydrate pellet production (MHPP) simulation comprised of the reactor unit (cooling jacketed continuous stirred tank reactor, CSTR) for the production of methane hydrate slurry, which fed the downstream dewatering and pellet processing units. The simulation results of the HYSYS conversion reactor using the methane gas consumption rate equation are presented in this section. These results are based on MHPP simulation procedure discussed in Sections 4.3.1 – 4.3.3. Table 5.1 below outlines the obtained reactor design geometry, operating parameters and formation rate as well as the inlet feed streams flowrates and pressure-temperature conditions of the reactor.

As indicated in Table 5.1, with inlet feed flowrate 5.15×10^{-3} mol s^{-1} and 1.53×10^{-1} mol s^{-1} for methane gas and water respectively based on an assumed conversion of 44% in a reactor volume of 9.16×10^{-3} m^3 yielded 10 kg hr^{-1} methane hydrate production. The estimated methane consumption rate per water dispersion volume to produce methane hydrate slurry was 2.48×10^{-1} mol m^3s^{-1}. The methane consumption rate is 22 % less than reported methane consumption rate from 9.16×10^{-3} m^3 CSTR study at 7.0 MPa and 279.15 K conditions (Mork et al., 2001).

Table 5.1: Parameters and values in the base case of MHPP reactor unit in HYSYS

Parameters	**Values**
Reactor Diameter (m)	1.80×10^{-1}
Impeller Diameter (m)	9.00×10^{-2}
Reactor Height (m)	3.60×10^{-1}
Reactor Volume (m^3)	9.16×10^{-3}
Impeller speed (s^{-1})	6.67
Superficial gas velocity (ms^{-1})	7.77×10^{-5}
Reynold number (-)	4.07×10^{4}
Power number (-)	5.00
Gas flow number FI (-)	6.76×10^{-2}
Froude number (-)	4.08×10^{-1}
Viscosity (Pa s)	1.23×10^{-3}
Power consumption, P (W)	8.03
Formation rate per dispersion (mol $s^{-1}m^{-3}$)	2.48×10^{-1}
Conversion (%)	44.09
Pressure, p (MPa)	5.40
Subcooling, ΔT (K)	276.09

The estimated methane consumption rate per water dispersion volume to produce methane hydrate slurry was 2.48×10^{-1} mol s^{-1} m^3. The methane consumption rate is 22 % less than reported methane consumption rate from 9.16×10^{-3} m^3 CSTR study at 7.0 MPa and 279.15 K conditions (Mork et al., 2001). Although the same stirring rate with this study was used in the experimental study, the discrepancy may be as a result of difference in the pressure and temperature conditions that are 5.4 MPa and 285.15 K respectively. The applied temperature and pressure values were approximate average (as base case HYSYS simulation) of the range later considered in the sensitivity analysis covering the conditions in the referenced study. The superficial gas velocity was obtained as the volumetric feed gas flowrate over the cross-sectional area of the reactor, which depicts the methane gas bubbling rate into the reactor. The dependence of the formation rate on the superficial gas velocity as well as power consumption and subcooling, within defined value range are discussed and compared with literature in Section 5.4.

Moreover, from Table 5.1, at the estimated reactor geometry the gas flow number of 6.76×10^{-2} which being above 3.50×10^{-2} shows the reactor operate without impeller flooding based on the Nienow's correlation (see Equation 3.9 in Section 3.2.1), which suggests optimum dispersion of methane gas in the liquid bulk (Doran, 2013a, Coker and Kayode, 2001). This also agrees with the fact that using Ruston turbine impellers (considered in this study) are effective for gas dispersion (Tatterson, 1991). Rushton turbine impellers usually chosen because of their robust gas-handling capacity, operated with relatively high gas flowrates without impeller flooding (Doran, 2013a). It is typical to characterize gas-liquid dispersion using dimensionless parameters of gas flow number and Froude number in which gas supply rate and gravitational acceleration are related to the impeller characteristics (Tatterson, 1991).
As further observed from Table 5.1, the Reynold number of 10^4, is typical of mass transfer processes in stirred vessels in turbulent flow regime and corresponds to a power number of 5 (Coker and Kayode, 2001). The hydrate-water slurry viscosity of 1.23×10^{-3} Pa.s was estimated using equation proposed by Meindinyo and Svartaas (2016). This suggests a low viscosity for the methane hydrate slurry with 10 wt% concentration and may be comparable to a non-Newtonian fluid as attributed by (Andersson and Gudmundsson, 2000) study of gas hydrates. Subcooling 276.09 K near ice point or 10 K below the expected equilibrium temperature is often considered to form gas hydrates (Holder et al., 1988a). Subcooling is computed as the difference between the hydrate equilibrium temperature and average system temperature (Mali et al., 2017).

5.2.2 Hydrate equilibrium estimation for methane gas using HYSYS (version 8.8)

The hydrate equilibrium temperature for methane hydrate at 5.40 MPa was calculated at 288.09 K using the conversion reactor on HYSYS (version 8.8) as shown below in the methane hydrate equilibrium curve prediction of pressure 3 – 10 MPa as shown in Figure 5.1. This range covers all the explored pressure range for methane hydrate process in this study, which is indicated to be in hydrate formation zone.

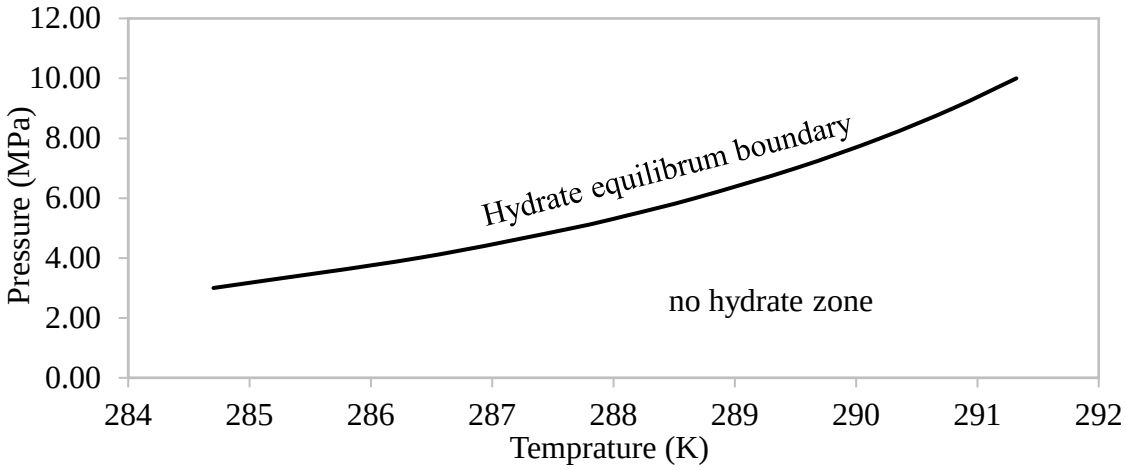

Figure 5.1: Methane hydrate equilibrium curve using HYSYS (version 8.8)

The predicted properties for methane hydrate slurry specified in the hydrate formation simulation are presented in Table 5.2 below. As earlier mentioned, the methane hydrate product stream was implemented as hypothetical solid in HYSYS with these properties using the discussed correlations. According to Carroll (2014), the prediction of hydrate properties depends on the type of the hydrate, the guest-gas molecule engaged in the hydrate and the fraction of cavity of the hydrate cage occupied (degree of saturation). The degree of saturation is a function of the temperature and pressure conditions. Therefore, the CSMhyd was employed in order to determine the fractional occupancy of methane gas molecule considering that hydrates are nonstoichiometric and since HYSYS do not have such capability.

Table 5.2: HYSYS simulation properties specification for methane hydrate at 285.15 K

Parameters	**Values**
Molecular weight (g mol^{-1})	17.71
Phase density ρ_{hyd} (kg m^{-3})	915.30
Hydrate-water slurry density ρ_{slurry} (kg m^{-3})	991.54
Enthalpy of formation (kJ mol^{-1})	−51.61
Hydration number	5.92
Fractional cage occupancy θ_s, θ_L	0.927, 0.985 respectively

As can be observed from Table 5.2, it is understandable that the molecular weight of the methane hydrate is 17.71 g mol^{-1} at fractional cage occupancy for small and large cavities 0.927 and 0.985 respectively for sI (methane) hydrates because hydrates composed mostly of water

which standard MW is 18.015 g mol^{-1}. In addition, the fractional occupancy indicates non-filling of the methane hydrate cages, as such agrees with obtained hydration number higher than ideal value of 5.75 (Sloan, 1998). The value of methane hydrate formation enthalpy of −51.61 kJ mol^{-1} using the correlation by Holder et al. (1988a) is an underestimated compared to the reported calorimetric measurements −54.19 kJ mol^{-1} (Handa, 1986c). However, the evaluation and sensitivity analysis in Section 5.4.6 further discusses the enthalpy of formation and hydration number parameters relating to literature at different saturation values and pressure and temperature range.

The reported values in Table 5.1 depict functionality of the MHPP reactor simulation implementation in HYSYS as further results are presented in sections below. In this study the reported base case reactor simulation will be considered as the bench scale for the scaling up assumptions to different reactor volume scenario as discussed in Section 5.6.2.

5.3 Analysis and evaluation of the HYSYS base case reactor simulation using energy balance calculations

5.3.1 The simulation results of MHPP reactor model design with cooling characteristics

The HYSYS simulation results of MHPP base case reactor was evaluated using the energy balance development of Equations 4.10 – 4.29 in Chapter 4. Preliminary MHPP simulation runs on HYSYS hypothetically without cooling characteristics (coolant temperature, overall heat transfer coefficient, and surface area) were executed which indicated a temperature of 298.15 K. Then, the value was employed in calculating the coolant characteristics to adjust the outlet reactor temperature. It was assumed that the enthalpy of methane hydrate formation could be efficiently dissipated in water phase with large heat capacity. The actual simulation which included the reactor characteristics with results as reported in Tables 5.2 − 5.4 was then executed. As discussed earlier in Chapter 4, the reason is due to the inability to implement the reactor coolant characteristics in HYSYS steady state mode on which the simulation is defined. However, using the Equation 4.21 (see Section 4.3.4) established to check the accuracy of simulation was used in the initial hypothetical simulation run in HYSYS without the consideration of the coolant characteristics. So, with the energy balance (Equation 4.28), the flowrates of methane gas and water as well as specific heat capacities and heat of formation as shown in Table 5.3 below, the reactor outlet temperature was obtained as 294.17 K (See Appendix A1), which is close to the temperature of 298.99 K obtained from the preliminary simulation run using HYSYS. This could be used to imply the accuracy of the MHPP HYSYS reactor simulation and indicates that the outlet temperature is determined by the flowrates and specific heat capacities of gas and water as well as the heat of formation and the shaft work (power consumption). The energy balance also correlates of the enthalpy of methane hydrate

formation to the conversion and molar feed gas rate (injection rate), which is higher than power consumed due to the impeller. As such, an increase in methane gas consumption rate by increase in superficial velocity would result in a proportional increase in the total energy production in the system. The value discrepancy could be attributed to approximation error. It is also important to highlight that normally the hydrate formation process would not proceed beyond the temperature of the hydrate equilibrium temperature, which is 288.09 K at 5.4 MPa for methane (HYSYS version 8.8).

Table 5.3: The MHPP reactor model design with coolant

Parameters	**Values**
Inlet gas molar flowrate (mol s^{-1})	5.15×10^{-3}
Inlet water molar flowrate (mol s^{-1})	1.53×10^{-1}
Specific heat capacity of gas (kJ $mol^{-1}K$)	4.28×10^{-2}
Specific heat capacity of water (kJ $mol^{-1}K$)	7.77×10^{-2}
Enthalpy of formation (kJ mol^{-1})	-51.662
Shaft work (W)	8.03

Then, to consider the rate of heat removal, $\dot{Q}$ via the cooling jacket, cooling characteristics were included in the MHPP reactor simulation. Based on the energy balance calculation (using Equation 4.29 – heat transfer equation across reactor surface for the hydrate system) (Fogler, 2016, Sinnott and Towler, 2009a), the overall heat transfer coefficient was estimated as 215 $Wm^{-2}K^{-1}$. The rate of heat removal was factored in the jacketed reactor model with reactor surface area, A_h of 2.54×10^{-1} m^2 and water coolant at specified coolant temperature of 283.15 K. Reactor outlet temperature of 285.15 K assuming the reactor ran isothermally by having heat exchange with assumption of large enough flowrate of the coolant water (Fogler, 2016). The overall heat transfer coefficient obtained agrees and is within the suggested range of overall heat transfer coefficient for jacketed vessels using water by Sinnott and Towler (2009a).

Table 5.4: Cooling characteristics of the MHPP jacketed reactor simulation

Parameters	**Values**
Coolant temperature T_{c_1} (K)	283.2
Overall heat transfer coefficient U ($Wm^2.K$)	215
Heat transfer area A_h (m^2)	0.254
Reactor temperature (K)	285.2

5.4 Results and discussion of the key process parameters for MHPP

Critical evaluation of the developed MHPP reactor model using simulation runs was used to analyse the effect of the model parameters; reactor methane gas injection rate (superficial velocity), pressure, subcooling, stirring rate on the methane formation rate. The methane hydrate formation rate (methane gas consumption rate) correlation Equation 4.5:

$\left[r = \left(kp\rho_m V_w^{-1} V_{sg}^a \left[\left(0.62 + 24.05N^4 {D_i}^7 D^{-5} g^{-2}\right)\left(N_p \rho N^3 D_i^5\right)\right]^b \Delta T^c\right)\right]$ adapted from (Mork, 2002) study, was investigated using the listed correlation parameters.

5.4.1 Simulation conditions for the critical evaluation of the MHPP reactor model

The range of simulation conditions are as shown in Table 5.5 below.

Table 5.5: Simulation conditions of the critical evaluation of the MHPP reactor model

Parameters	**Values**
Superficial gas velocity (ms^{-1})	$5.56 \times 10^{-6} – 4.17 \times 10^{-3}$
Gas injection rate (m^3s^{-1})	$1.42 \times 10^{-7} – 6.93 \times 10^{-4}$
Stirring rate (s^{-1})	6.67 – 13.33
Subcooling (K)	276.09 – 281.09
Pressure (MPa)	5.40 – 9.03

5.4.2 Effects of superficial gas velocity and methane gas injection rate on methane gas consumption rate using MHPP simulation

The effects of superficial gas velocity on the methane gas consumption rate (or methane hydrate formation rate) in the MHPP reactor at the simulation condition 5.40 MPa pressure, stirring rate of 6.67 s^{-1} and subcooling of 276.09 K are shown in Figures 5.2. The superficial gas velocity range of between 5.56×10^{-6} to 4.17×10^{-3} ms^{-1} was investigated leading to methane consumption rate of between 1.77×10^{-2} (6.24×10^{-8} m^3s^{-1}) to 1.33×10^{1} (4.68×10^{-4} m^3s^{-1})

mole per seconds per dispersion volume (mol m^3s^{-1}). As with all the analysis, each data point was an MHPP reactor simulation run on HYSYS.

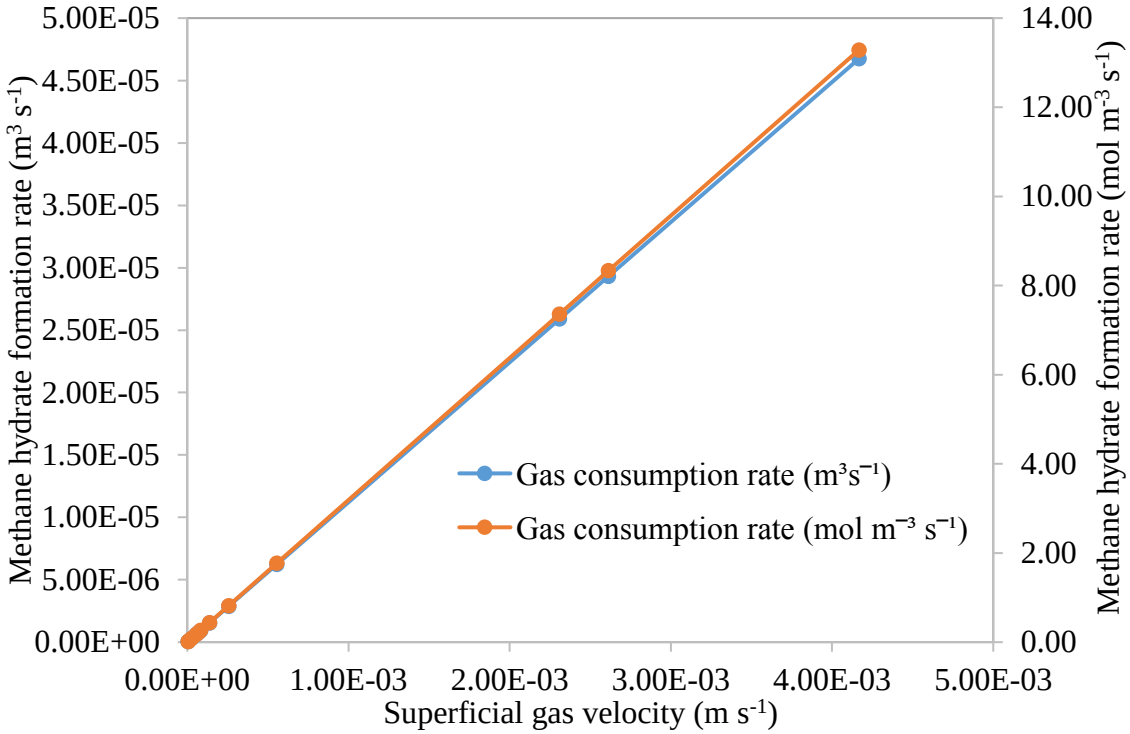

Figure 5.2: Methane gas consumption rate against superficial gas velocity at 5.4 MPa, stirring rate of 6.7 s^{-1}, and 276.09 K

The linear correlation in Figures 5.2 indicates that the methane consumption rate increases proportionally with the superficial gas velocity. The coefficient of determination for the both is unity, which indicates good correlation of the superficial gas velocity and injection rate to the methane consumption rate. The obtained simulation result follows the same trend with the earlier discussed results of experimental study in section 2.5.2 and therefore, agrees with the outcome of the implemented MHPP reactor simulation in HYSYS.

The superficial gas velocity was defined as the gas supply volumetric rate to the reactor over the reactor cross sectional area. The obtained results further show that with the increase in the gas injection rate (superficial gas velocity), implying higher gas supply rate into the continuous stirred reactor, which increases the gas-liquid dispersion. Additionally, with increasing gas velocity, gas-liquid interfacial area increases with decrease in the mean diameter of the bubbles, which improves gas-liquid mass transfer in the stirred reactor (Gelves-Zambrano et al., 2016). Furthermore, as discussed in the energy balance evaluation in Section 5.3, increasing the methane consumption rate with the increment in superficial gas velocity also implies that the total energy generation in the reactor increases proportionally.

5.4.3 Effects of stirring rate and methane gas injection rate on gas consumption rate using MHPP simulation

The effects of methane gas injection rate and stirring rate of the Rushton impeller relating to the methane consumption rate was also investigated. Using the MHPP reactor simulation condition of 5.40 MPa pressure, subcooling of 276.09 K and same gas injection rate of between $1.42 \times 10^{-7} - 1.06 \times 10^{-6}\ m^3\ s^{-1}$. As shown in Figure 5.3, methane consumption rate of between $1.02 \times 10^{-7}\ m^3 s^1 - 4.67 \times 10^{--5}\ m^3\ s^{-1}$ was obtained for impeller stirring rates of 6.7 s^{-1}, 10.0 s^{-1} and 13.3 s^{-1}. The simulation result, which is consistent with several studies (Vysniauskas and Bishnoi, 1983, Natarajan et al., 1994, Kashchiev and Firoozabadi, 2002, Mork, 2002) shows the rate of methane consumption increases with the stirring rate. In these studies, increment in stirring rate at different system conditions resulted in increase in gas consumption rate. (Mork, 2002) highlighted, that the rate increases due to stirring rate is not significant compare to the effect of superficial gas velocity (gas injection rate). However, a significant increase was observed as shown in Figure 5.2. During stirring more of methane gas molecules are brought in contact with liquid bulk and together with increased amount of dissolved gas increases the rate of methane consumption rate.

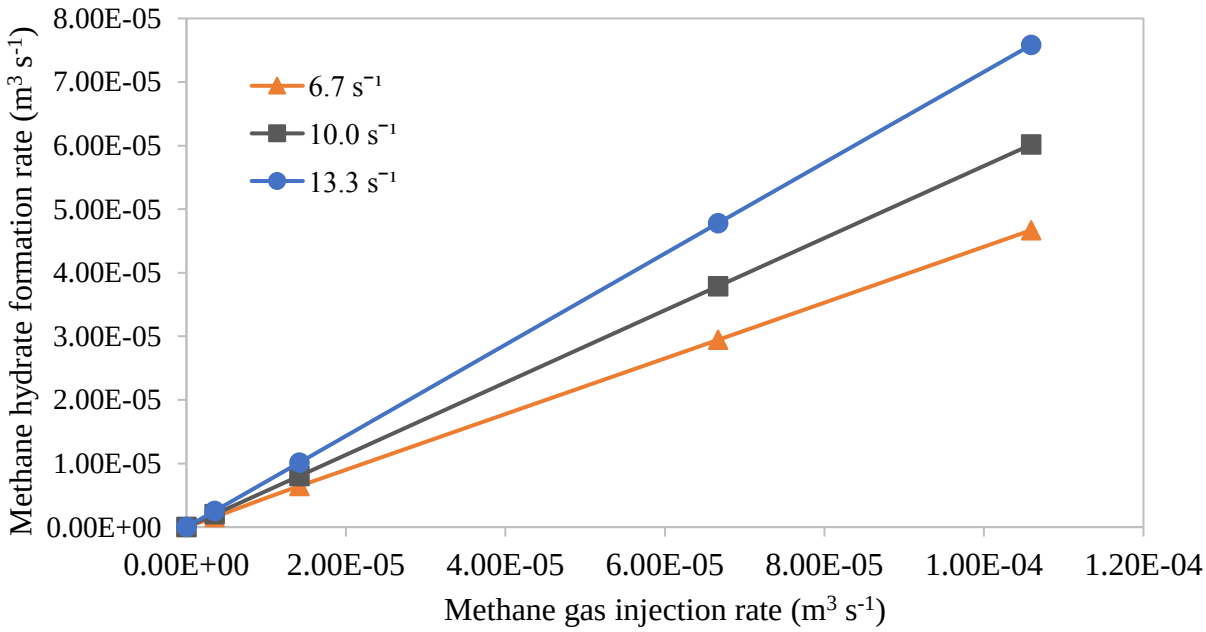

Figure 5.3: Methane consumption rate against gas injection rate at stirring rate 6.7−13.3 s^{-1}, pressure 5.4 MPa, and 276.09 K subcooling

Vysniauskas and Bishnoi (1983) reported substantial increase in the gas consumption rate with increase in stirring rate. They visually observed in their experiments, that at least 6.7 s^{-1} was required to remove the hydrate crystal from the gas-liquid interface. In this study using MHPP

simulation, the Nienow's correlations for recirculation flow pattern in Equation 3.7 (Nienow et al., 1986) was factored into the derivation of the proposed gas consumption rate correlation. Therefore, the hydrodynamic effects of superficial gas velocity and power consumption to the gas consumption rate can be considered significant (Meindinyo and Svartaas, 2016). Ke and Svartaas (2013) in their study also highlighted the need for using appropriate stirring rate because of its significant effects on nucleation and growth of hydrate formation as well as the effect of cooling due the reprisal effect of stirring rate. For this study, standard geometry stirred reactor theory together with established experimental data was considered. Similar increment in gas consumption rate of about 78 % was also observed between 6.7 s^{-1} to 10.0 s^{-1} and 10.0 s^{-1} to 13.3 s^{-1} due to similar gas injection rate of 1.06×10^{-4} m^3s^{-1} (4.16×10^{-3} ms^{-1} superficial gas velocity) and hydrodynamic conditions in the reactor. The simulations indicated that, as gas was continuously bubbled into the reactor with single Rushton turbine impeller, better gas-liquid dispersion with assumption of completely dispersed or gas recirculation regime with impeller at 6.7 s^{-1} to 13.3 s^{-1} stirring rates.

5.4.4 Effects of subcooling and methane gas injection rate on methane gas consumption rate using MHPP simulation

The gas consumption rate as a function of gas injection rate over the considered range for subcooling of 276.09 – 281.09 K is plotted in Figure 5.4. The simulation result is based on MHPP reactor simulation in HYSYS as shown in Figure 5.4. A slight increase in the rate of gas consumption with increasing subcooling was observed, which is consistent with the experimental study by (Mork, 2002). However, an unclear pattern is observed at the midpoints and higher injection rate where at subcooling of 276.65 K seemed to cause higher gas consumption. The subcooling was computed in the model as the difference between the hydrate equilibrium temperature and the reactor temperature.

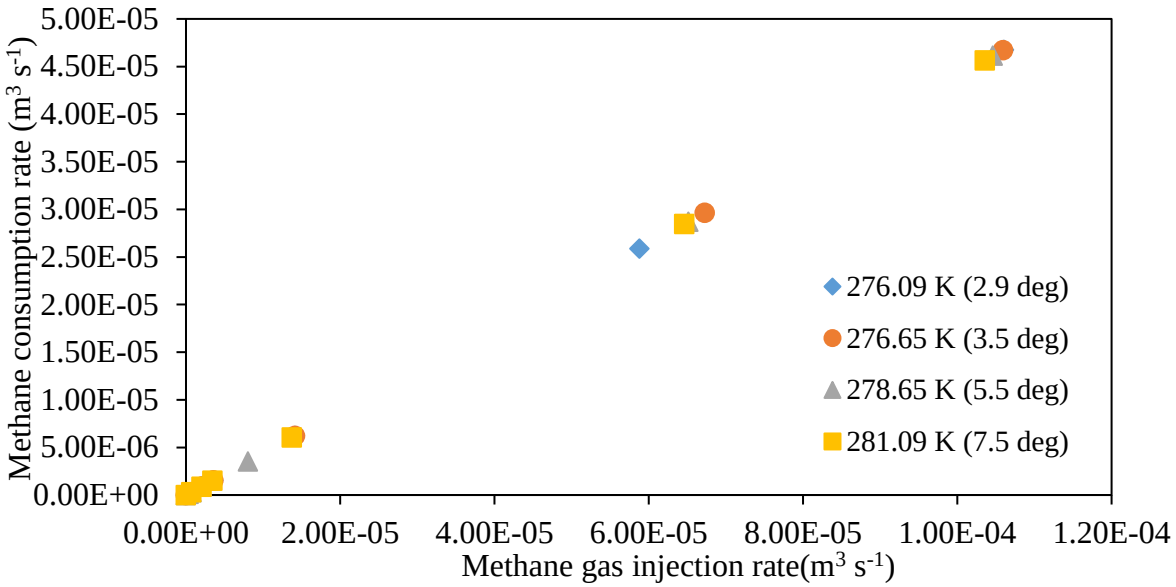

Figure 5.4: Methane consumption rate against methane gas injection rate at subcooling 276.09 K (2.94 ℃) – 281.09 K (7.5 ℃), 5.4 MPa pressure, and 6.7 s^{-1} stirring rate

The equilibrium temperature of methane hydrate formation at 5.4 MPa was estimated with HYSYS (version 8.8) as 288.09 K. It is not certain if the inconsistency in the simulation result was as a result of the HYSYS prediction, however, the equilibrium temperature predictions at pressure conditions are compared with the CSMhyd software in Section 5.4.5. Some studies attribute significant effect of subcooling on gas hydrate formation coupled into hydrate nucleation and growth correlations (Vysniauskas and Bishnoi, 1983, Ke and Svartaas, 2013, Arjmandi et al., 2005). Arjmandi et al. (2005) in their study attributed subcooling at given pressure conditions as solely the driving force for pure components hydrate forming systems. Using subcooling as driving force is also considered to offer a simple option in modelling the nucleation and growth of hydrate forming systems (Meindinyo and Svartaas, 2016). However, in contrast to these studies but in agreement with Mork (2002), the obtained simulation result from this study suggests an increase in subcooling do not have a very significant effect on gas consumption at given pressure.

5.4.5 Effects of water – gas ratio (hydration number) and enthalpy of methane hydrate formation (dissociation) using MHPP simulation

As shown in Figure 5.5, the slope of the logarithm of the hydrate dissociation pressure plotted against inverse of temperature gave a negative slope, s, which multiplied by the compressibility factor and universal gas constant to obtain the methane hydrate enthalpy of dissociation. This is consistent with the fact that dissociation enthalpy remains constant over close temperature range (Sloan and Fleyfel, 1992).

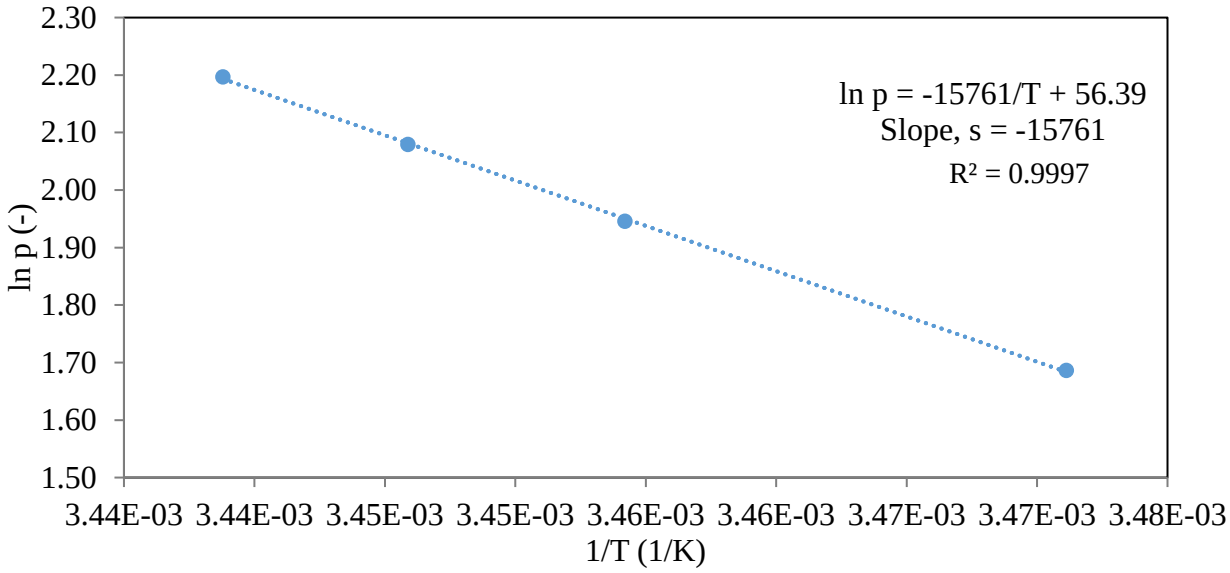

Figure 5.5: Clausius-Clapeyron plot of logarithm of pressure against inverse of temperature for methane hydrate equilibrium from 5.40 – 9.0 MPa. Hydrate equilibrium data obtained from HYSYS

The result of the predicted equilibrium temperature conditions at the considered pressure range based on the HYSYS simulator is as shown in Table 5.6, which increases with increase in system pressure. Using the Clausius-Clapeyron equation with the equilibrium temperature obtained from HYSYS, the dissociation enthalpy 98.230 kJ mol^{-1} was obtained which seem overestimated considerably compared that of the correlation by (Holder et al., 1988a) (Table 5.2). Similarly, the hydration number estimated using the de Forerand approach (Sloan and Koh, 2008) as shown in Table 5.6 also seems largely overestimated compared to the value of 6 reported by (Handa, 1986a, Handa, 1986c).

Table 5.6: Methane hydrate enthalpy of formation ΔH_f and hydration number at pressure range 5.40 – 9.0 MPa and 285.15 K using Clausius-Clapeyron method and HYSYS estimated equilibrium temperatures

Pressure (MPa)	Temperature (K) (HYSYS prediction)	Methane hydrate enthalpy ΔH_f (kJ mol^{-1}) using Clausius-Clapeyron equation	Hydration number using de Forerand approach
5.40	288.09	98.230	13.18
7.00	289.50		
8.00	290.20		
9.00	290.80		

The values obtained using Clausius-Clapeyron equation is inconsistent with those of calorimetric measurements in literature (Handa, 1986a). However, higher pressures were considered in this study against the calorimetric measurements, which were at standard conditions. Sloan and Fleyfel (1992) compared dissociation enthalpies of sI and sII hydrates including methane hydrates obtained from measurements and Clausius-Clapeyron equation, with the conclusion that Clausius-Clapeyron method provides acceptable accuracy. However, due to the observed large discrepancies from the using HYSYS predictions, CSMhyd simulator was also applied for calculating the methane hydrate dissociation enthalpy and hydration number using Clausius-Clapeyron equation.

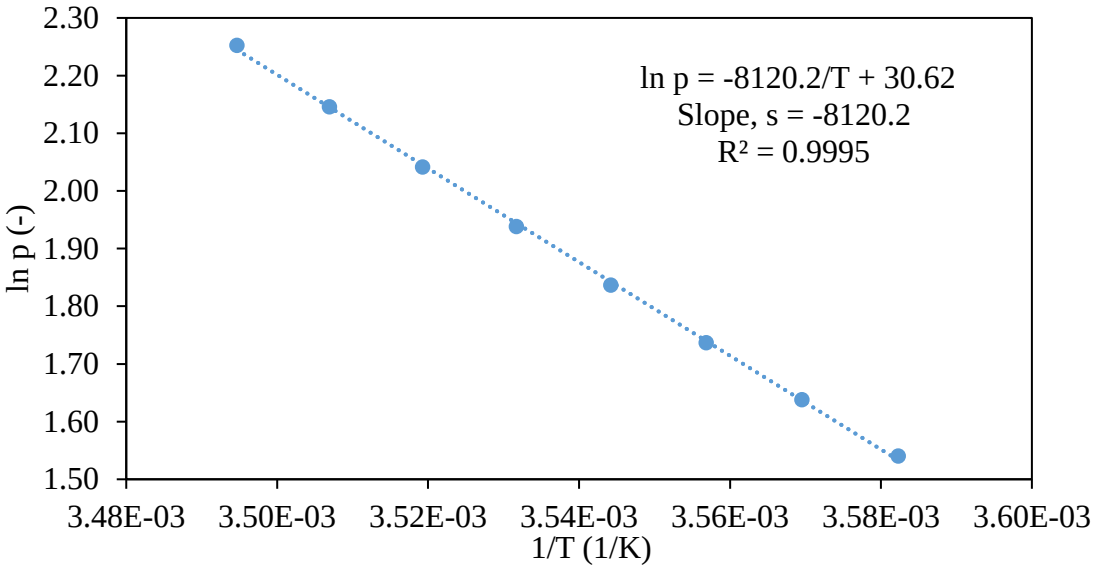

Figure 5.6: Clausius-Clapeyron plot of logarithm of pressure against inverse of temperature for methane hydrate equilibrium from 5.40 – 9.0 MPa. Hydrate equilibrium data obtained from CSMhyd

Figure 5.6 shows the Clausius-Clapeyron correlation linear plot of logarithm of dissociation pressure of methane gas hydrate against inverse of temperature. The enthalpy of dissociation for methane hydrate obtained using the Clausius-Clapeyron equation based on the range pressure and equilibrium temperature conditions was −53.945 kJ mol^{-1} at temperature 279.15 – 286.15 K and corresponding estimated equilibrium pressure data 3.18 – 10.60 MPa (CSMhyd). The enthalpy of formation as applied in this calculation is based on enthalpy of dissociation. The obtained enthalpy value is closer to the literature data as shown in Table 5.7. Furthermore, using guest gas dependent correlation [$n = 46\ (6\theta_L + 2\theta_S)^{-1}$] (Sloan and Koh, 2008) and values of methane hydrate fractional cage occupancy of 9.20×10^{-1} – 9.85×10^{-1}

respectively obtained with the CSMhyd simulator, at 285.15 K the hydration number was estimated as 5.92.

The value obtained agrees with literature data as shown in Table 5.7 below, which were based on the Clausius-Clapeyron equation aside from (Handa, 1986a) obtained by calorimetric method. This also depicts the accuracy of the CSMhyd over HYSYS for prediction of hydrate equilibrium conditions. This might be related to complexities and adjustments made in the HYSYS simulation to suit the gas hydrate process.

Table 5.7: Enthalpy of dissociation and hydration number measurements

ΔH_d (kJ mol^{-1})	Hydration number	Reference
54.19	6.0	(Handa, 1986a)
54.36	7.0	Robert et al (1941) cited in (Levik, 2000)
67.83	6.3	de Roo (1983) cited in (Levik, 2000)
51.61	5.92	This study
53.95	5.93	
98.23	13.18	

5.4.6 Result of the sensitivity analysis

The results presented (see Figures 5.7 – 5.10) cover the gas consumption rate output in mol m^{-3}s^{-1} for analysis carried out on each input parameter. The parameters considered one by one are the superficial gas velocity, stirring rate, subcooling and pressure. The range of operating conditions in the reactor as defined in Section 5.4.1 was split and assumed for each parameter as the minimum, average and maximum values respectively as shown in Table 5.8 below. This demonstrates the sensitivity analysis of the MHPP reactor model based on the considered parameters and operating conditions.

In the analysis on parameters carried out using Matlab, the parameter in focus is varied from its minimum threshold to its maximum threshold while the other parameters are kept constant. Three sets of analysis are carried out by considering the constant parameters at their minimum, average and maximum values. The aim is to find the sensitivity of gas consumption rate to changes in the input parameters in order to study the contribution of each parameter to output performance.

Table 5.8: Parameter for the sensitivity analysis of the MHPP reactor model

	Superficial gas velocity (ms^{-1})	**Stirring rate (s^{-1})**	**Subcooling (K)**	**Pressure (MPa)**
Min. value	5.56×10^{-6}	6.70	276.09	5.40
	3.84×10^{-4}	7.30	276.54	5.73
	7.63×10^{-4}	7.90	277.00	6.06
	1.14×10^{-3}	8.50	277.45	6.39
	1.52×10^{-3}	9.10	277.91	6.72
	1.90×10^{-3}	9.70	278.36	7.05
	2.28×10^{-3}	10.30	278.82	7.38
	2.66×10^{-3}	10.90	279.27	7.71
	3.03×10^{-3}	11.50	279.73	8.04
	3.41×10^{-3}	12.10	280.18	8.37
	3.79×10^{-3}	12.70	280.64	8.70
Max. value	4.17×10^{-3}	13.30	281.09	9.03
Ave. value	2.09×10^{-4}	10.00	278.59	7.22

Figure 5.7 shows perfect straight lines through the origin for the three cases considered when superficial gas velocity is varied for the range 5.56×10^{-6} to 4.17×10^{-3} s^{-1}. This confirms a direct and linear relationship between superficial gas velocity and gas consumption rate as the rate of change of the output is constant.

This confirms a direct and linear relationship between superficial gas velocity and gas consumption rate as the rate of change of the output is constant. In addition, the gas consumption rate increases as the constant parameters increase, since the highest values occurred for the maximum constant parameters. The percentage difference between the results obtained for the minimum constant parameters and the maximum constant parameters is 383 % increase for the lowest superficial velocity ($0.018-0.087$ mol $m^{-3}s^{-1}$) and 389 % for the highest superficial velocity ($13.31-65.04$ mol $m^{-3}s^{-1}$).

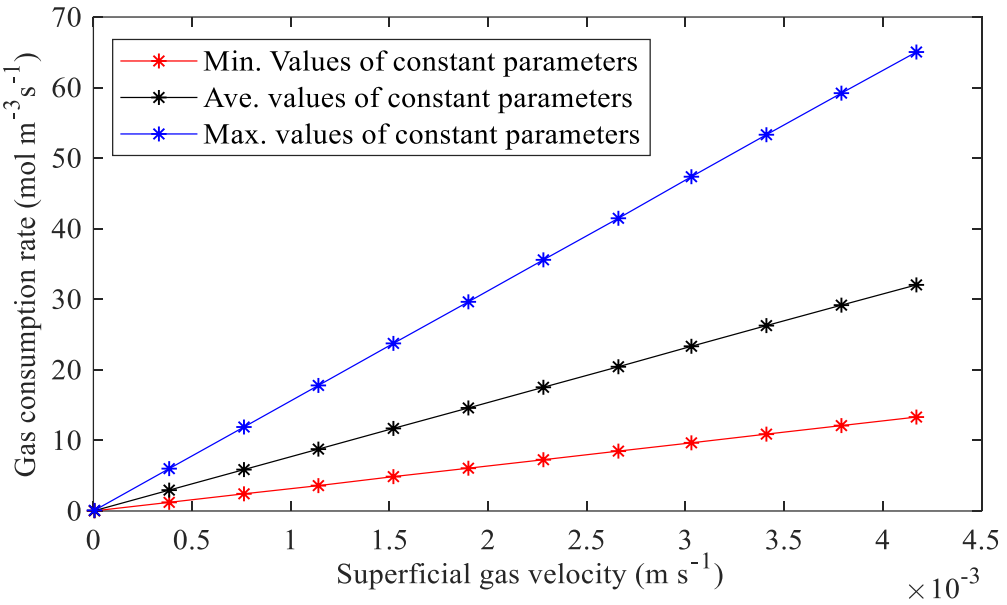

Figure 5.7: Sensitivity analysis - effect of superficial gas velocity on the methane gas consumption rate

In Figure 5.8 below the stirring rate range for the reactor model operation considered is 6.7 s^{-1} to 13.3 s^{-1} to explore the effect of stirring rate on the methane gas consumption rate in the sensitivity analysis carried out. In this case, the output plot is not perfectly linear, though there is an increase in gas consumption rate with increasing values of the stirring rate and the plots also do not pass through the origin. The increasing trend from the minimum, to average and to maximum values is similar to that of the superficial gas velocity. Figure 5.8 shows percentage increase at the maximum values giving 201% for both the least and highest values of the stirring rate. This is depicted in the table showing gas consumption rate of 6.674 mol $m^{-3}s^{-1}$ (for minimum values of other constant parameters) and 20.120 mol $m^{-3}s^{-1}$ (for maximum values of other constant parameters) at the lowest stirring rate of 6.7 s^{-1}.

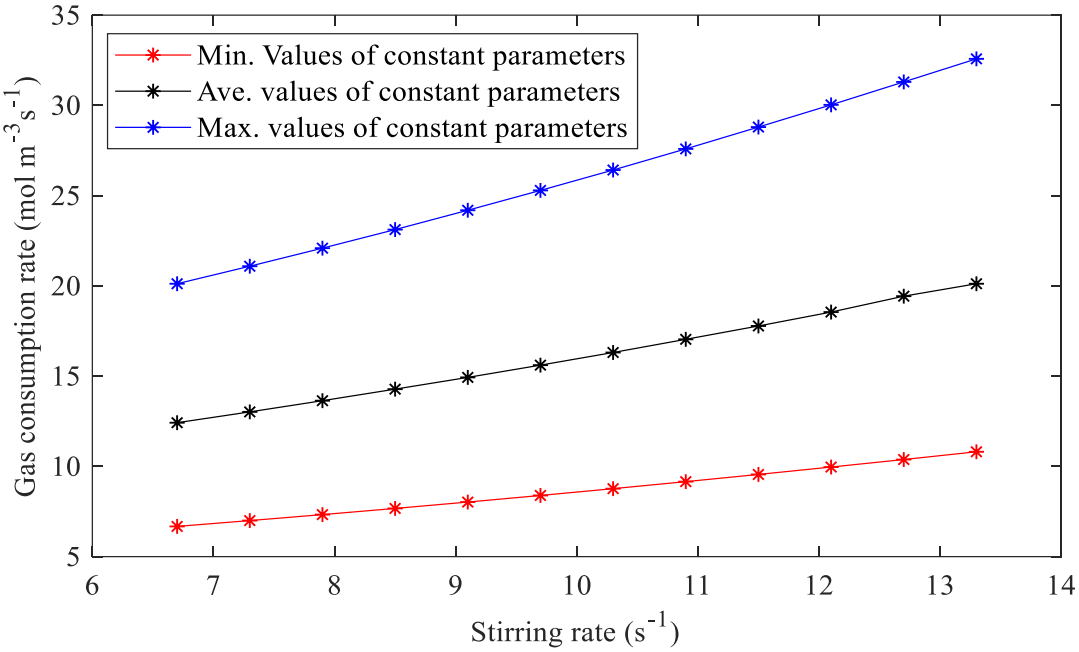

Figure 5.8: Sensitivity analysis - effect of stirring rate on the methane gas consumption rate

Similarly, gas consumption rate obtained for the highest stirring rate of 13.30 s^{-1} is obtained as 10.810 mol $m^{-3}s^{-1}$ (for minimum values of other constant parameters) and 32.58 mol $m^{-3}s^{-1}$ (for maximum values of other constant parameters).

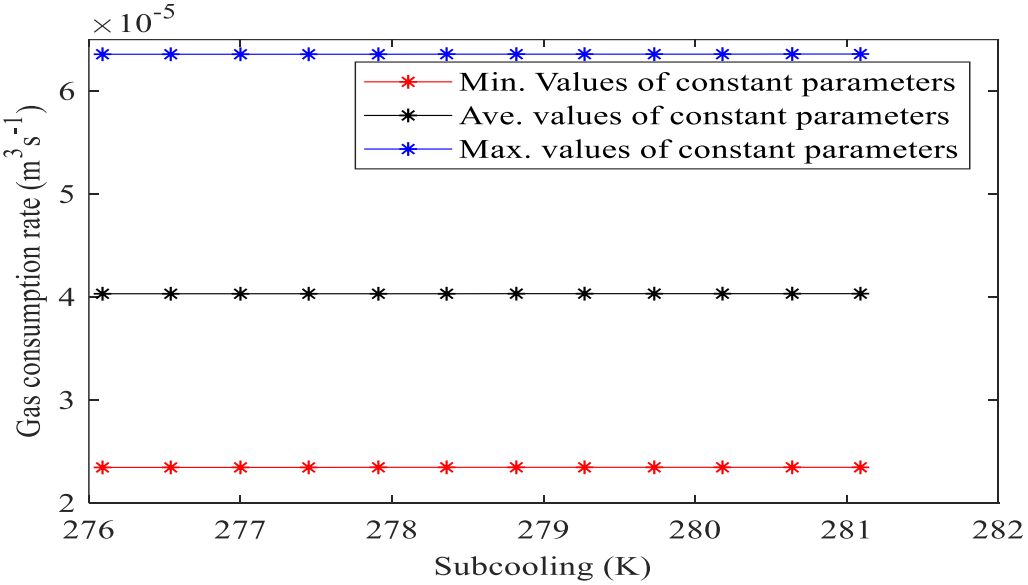

Figure 5.9: Sensitivity analysis - effect of subcooling on the methane gas consumption

For the subcooling as shown in the above Figure 5.9 indicate that over the range of the considered values (276.09 K - 281.09 K), gas consumption rates remain mostly the same.

However, comparing the results over the minimum and maximum values of the constant parameters a percentage increase of 388 % was obtained for all cases, equivalent to (6.707 mol $m^{-3}s^{-1}$ as minimum and 6.707 mol $m^{-3}s^{-1}$ as maximum). The percentage increment is similar to the case in the analysis based on superficial gas velocity.

For the results on pressure, the output also increases with increasing input as Figure 5.10 shows, for the range $(5.40 - 9.03$ MPa). The sensitivity analysis reveals 62% increase in gas consumption rate from the minimum to maximum constant values of the other parameters, for the least value of pressure (5.40 MPa) which in the case of the highest value (9.03 MPa), the percentage increase also was 62%.

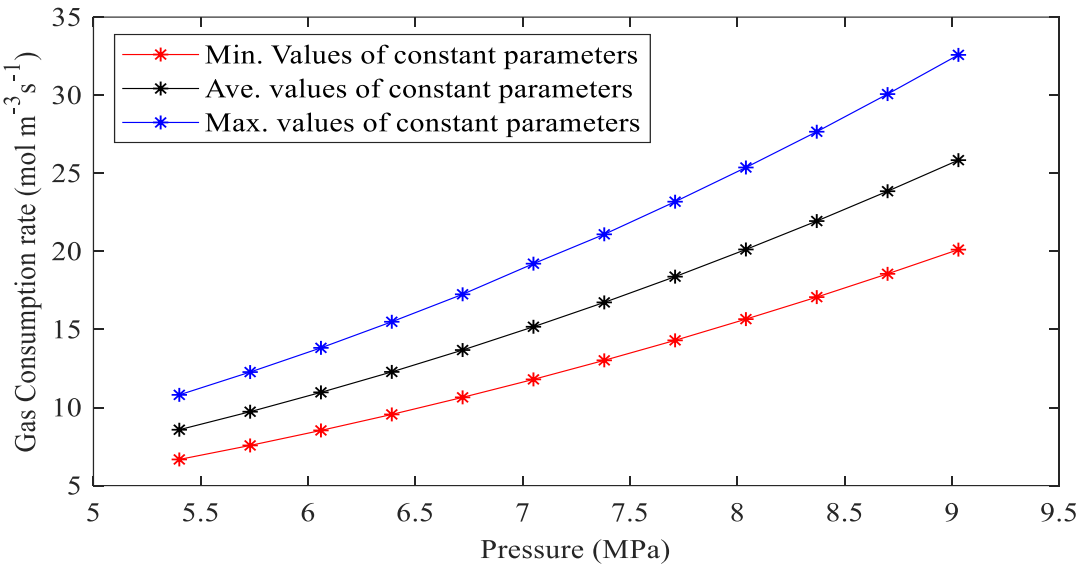

Figure 5.10: Sensitivity analysis - effect of pressure on the methane gas consumption

As shown in Table 5.9 below, the percentage increase across stirring rate and pressure for their least and highest values are similar across the minimum and maximum values of other parameters which is slightly different in the case of superficial gas velocity. This depicts that the former two parameters give more predictable and controlled results than the latter. Table 5.9 also shows entire sensitivity results which reveals that the superficial velocity has highest effect on the gas consumption rate with values 65.04 mol $m^{-3}s^{-1}$ compared to 32.58, 32.77 and 32.58 mol $m^{-3}s^{-1}$ respectively for pressure, stirring and subcooling with range of 51.73 (for the highest value of focus parameter).

Having realized the one-factor-at-a-time sensitivity analysis for each parameter separately, entire ranges of possible values for both superficial gas velocity and stirring rate parameters are

plotted against each other as shown in Figure 5.11. The 3D plot shows how the gas consumption rate varies when the effects of both superficial gas velocity and stirring rate are considered. This is an extension of the analysis earlier presented for each parameter separately and indicates that a much higher variation of gas consumption rate when viewed from the axis of superficial gas velocity compared to that of stirring rate. This is in agreement with the results of (Mork, 2002) and these analyses are carried out in respect of enhancement of methane gas consumption rate for the commercial application of technology for the utilization stranded gas.

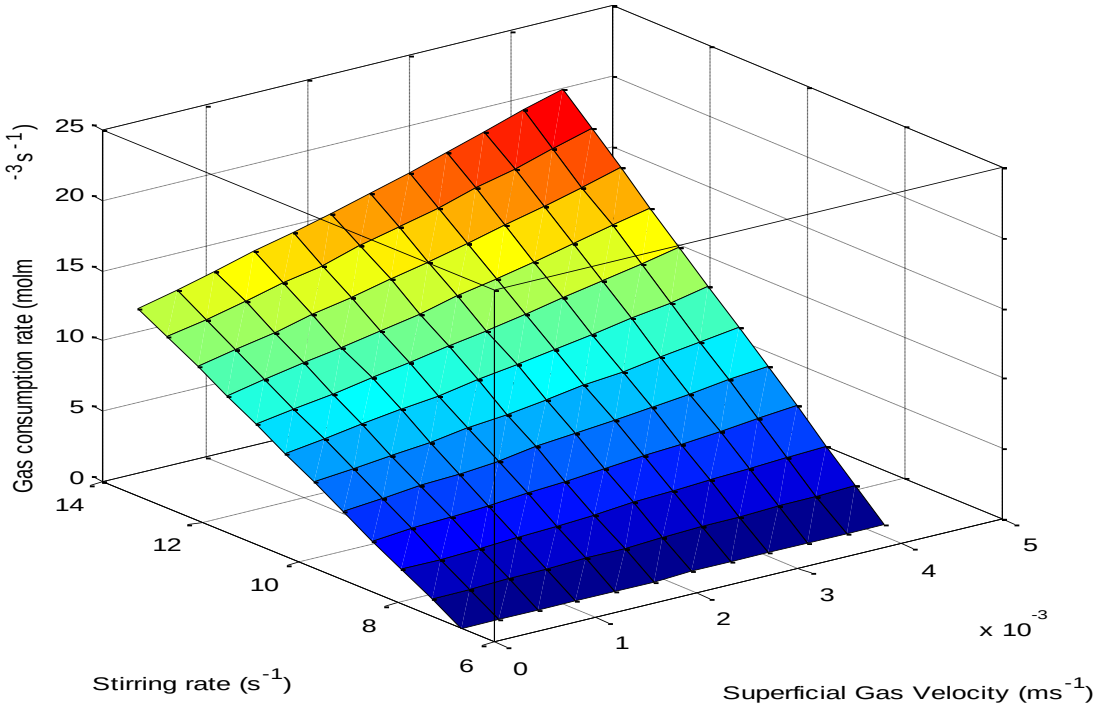

Figure 5.11: 3D plot of the effects of both superficial gas velocity and stirring rate on gas consumption rate

Table 5.9: Summary of the sensitivity analysis of the gas consumption rate correlation of MHPP reactor model

Focus parameter	**Least value of focus parameter**				**Highest value of focus parameter**				**% Difference between highest value and overall highest**
	Minimum Gas consumption rate ($mol\ m^{-3}s^{-1}$)	**Maximum Gas consumption rate ($mol\ m^{-3}s^{-1}$)**	**Range**	**% Difference**	**Minimum Gas consumption rate ($mol\ m^{-3}s^{-1}$)**	**Maximum Gas consumption rate ($mol\ m^{-3}s^{-1}$)**	**Range**	**% Difference**	
Superficial Gas Velocity	0.018	0.087	0.069	**383**	13.310	**65.040**	**51.730**	**389**	0
Stirring rate	6.674	20.120	13.446	201	10.810	**32.580**	21.770	201	**100**
Subcooling	6.707	32.770	**26.063**	**389**	6.707	**32.770**	26.063	**389**	98
Pressure	6.674	10.810	4.136	62	20.110	**32.580**	12.470	62	**100**

The highlighted values in are values emphasized in the discussion

5.5 Result and discussion of the dewatering and pelletizing simulations

5.5.1 MHPP base case hydrate pellet processing machine (HPPM) simulation results

The base case simulation results of dewatering and pelletizing unit of the MHPP model based on the modelling calculations presented in Sections 4.4.1 – 4.4.2 are reported in this section. The simulation considered that the rate of discharge of filtrate from the 9.80×10^{-2} m^2 effective filtration area of the filter-compression chamber depends on the design parameters and operation, methane hydrate concentration and its compressibility. Therefore, the obtained filtrate rate of 1.86×10^{-6} m^3s^{-1} as expected is less than the supply feed slurry rate from upstream MHPP HYSYS reactor model 2.80×10^{-6} m^3s^{-1} due to the fact that hydrate solids and liquids are retained in the hydrate cake which vary with time (Murayama et al., 2011). In constant rate filtration, the filtration pressure difference over the hydrate cake on the surface of cylindrical screen which is assumed to be driven with the upstream reactor pressure of 5.4 MPa maintain a constant filtration rate of 1.86×10^{-6} m^3s^{-1}. The filtration rate was obtained using mass balance of the feed slurry flowrate 2.80×10^{-6} m^3s^{-1} and the solid volume fractions of feed and the hydrate cake 1.08×10^{-1} and 3.19×10^{-1} respectively.

The filter design, operational parameters, and the slurry and methane hydrate cake properties are presented in Table 5.10. As explained in Chapter 4, the hydrate pellet processing machine is a combined dewatering and pelletizing unit which the simulation approach involved rate constant filtration, constant pressure filtration and compression (dewatered MH cake to pellet) operational stages. The constant rate filtration simulation based on 10 wt % methane hydrate slurry supply to the filter-compression chamber of HPPM pilot plant. The endpoint of the constant rate filtration simulation which agrees with the (Murayama et al., 2011) data is 30 wt% solid concentration and 70 wt% water with maximum pressure difference of 5.4 MPa (inside/outside filter pressure difference).

Table 5.10: Design parameters, slurry and cake properties and operational conditions for the constant rate filtration, constant pressure, and compression simulation

Parameters	**Constant rate filtration**	**Constant pressure filtration**
Filter Design Characteristics		
Filtration-compression chamber capacity (m^3)	6.92×10^{-3}	6.92×10^{-3}
Filtering screen capacity (m^3)	2.26×10^{-3}	2.26×10^{-3}
Filtering screen Area (m^2)	9.80×10^{-2}	9.80×10^{-2}
Operating Conditions		
Filter screen pressure drop, ΔP_m (MPa)	2.32×10^{-4}	2.32×10^{-4}
Pressure drop ΔP (MPa)	5.39	9.00
Feed Slurry flowrate, Q_s (m^3s^{-1})	2.80×10^{-6}	–
Filtrate volume flowrate, q_f (m^3s^{-1})	1.86×10^{-6}	$5.69 \times10^{-6} – 1.81 \times 10^{-6}$
Energy (J)	1.22×10^{4}	2.03×10^{4}
Particle and fluid properties		
Feed solid concentration, s (wt %)	10.00	30.00
Feed solid volume concentration, C_f (vol %)	10.81	31.85
Solid concentration in the cake, s_c (wt %)	30.00 Constant filtration rate endpoint	90.00 Constant pressure filtration endpoint
Liquid fraction in the cake, s_c (wt %)	70.00	10.00
Density of solid, ρ_s ($kg\ m^{-3}$)	917.30	917.30
Density of filtrate, ρ ($kg\ m^{-3}$)	1000.00	1000.00
Viscosity of filtrate, μ (Pa s)	1.23×10^{-3}	1.23×10^{-3}
Cake properties		
Average dry cake/filter volume, c_m ($kg\ m^{-3}$)	151.50	448.55
Average cake Resistance, α_{av} ($m\ kg^{-1}$)	1.01×10^{10}	1.34×10^{10}
Cake compressibility, a	0.55	0.55

Methane hydrate average filtration ratio resistance empirical equation $\alpha_{av} = \alpha_o \Delta P^a$. *Ave. resistance* α_0 *is* 4×10^9

Figure 5.12 shows the estimate of the filtrate volume obtained from the simulation runs using Equation 4. 40 (Holdich, 2002). The graph relates linearly the pressure difference increment between the inside and outside of the filtering screen with the discharge filtrate volume during constant rate filtration with the assumption that the cake properties are constant at the pressure increments. This implies that as the hydrate cake grow on the surface of the screen (filtration resistance), the increasing pressure drop driving force sustains constant filtration rate under the assumption. The value of 2.32×10^{-4} MPa in Figure 5.12 obtained represents that the pressure drop due to filtering screen resistance between the inside and outside. This corresponds to zero filtrate volume indicating start of the filtration and 15.01 m^3 represent the cumulative filtrate volume at end of the rate constant filtration, which yielded 30 wt % solid concentration.

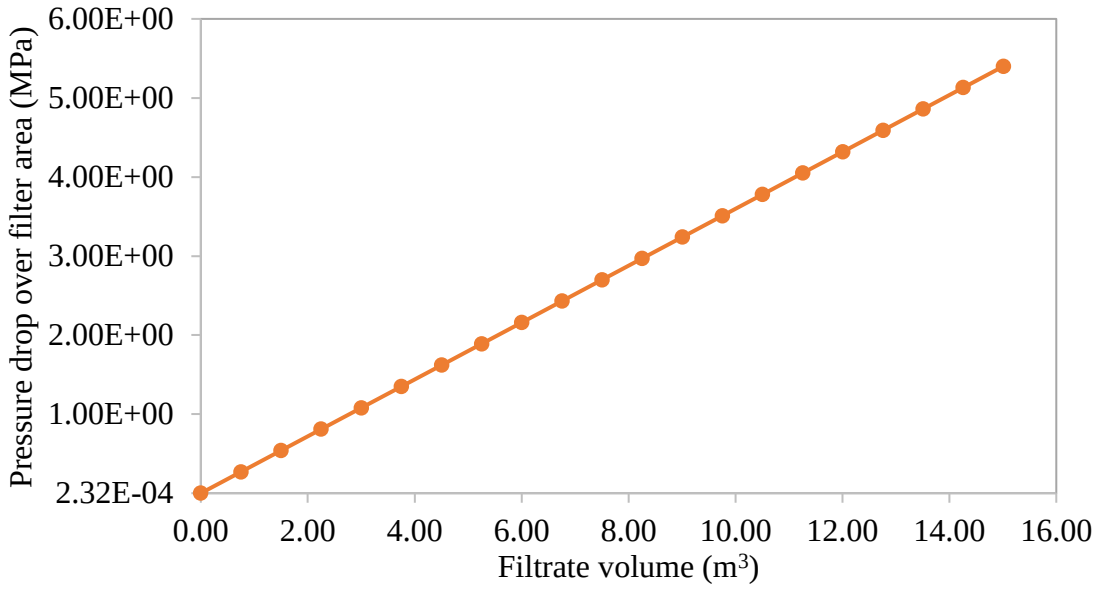

Figure 5.12: Simulation of pressure drop increment with filtrate volume at constant rate filtration

To increase the solid concentration of the hydrate in the cylindrical screen, following the 30 wt % from constant rate filtration, compression pressure by compression piston is applied. Compression pressure of 9 MPa as agrees with the Murayama et al. (2011) data resulted in 90 wt% concentration of the hydrate cake. As shown in Table 5.10,with the sceondary filtration using compression pressure of 9 MPa, the soild concentration increased with increase in specific cake resistance of over 75 % (1.34×10^{10} m^{-1}) compared to that of the rate constant filtration. This was obtained using correlation of average filtration ratio resistance in methane hydrate (Murayama et al., 2011). As expected, less filtrate volume flowrate compared to the constant rate filtration was obtained (see Figure 5.13), increasing with the time between 5.69×10^{-6} to 1.81×10^{-6} m^3s^{-1} in the simulation over 3600 seconds. This results in higher cumulative filtrate discharge with increasing time.

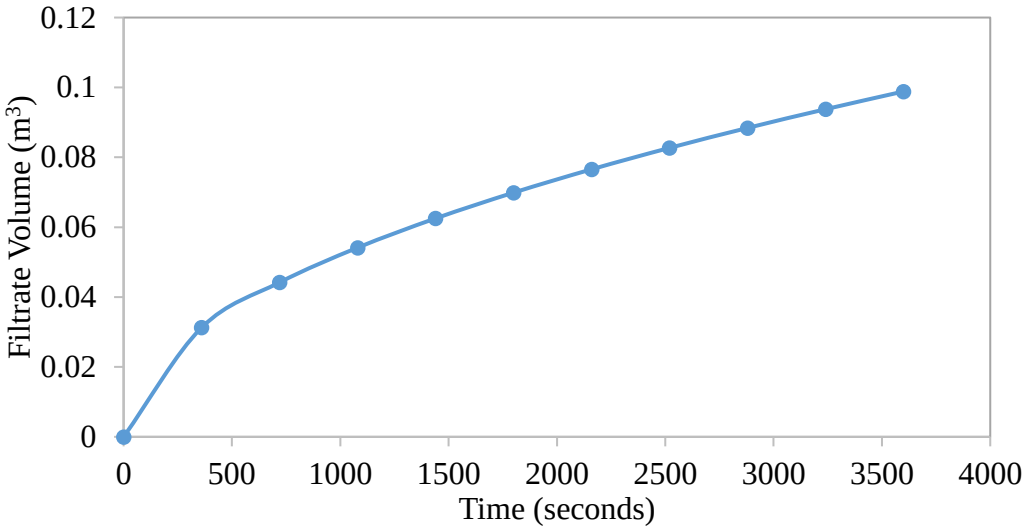

Figure 5.13: Filtrate volume discharge per time at constant pressure filtration

In addition, the increase of the dry cake per filter volume from 151.5 kg m^{-3} to 448.6 kg m^{-3} with the application of mechanical force (see Table 5.10), depicts an effectively dewatered hydrate cake at endpoint of constant pressure filtration. Furthermore, the filtrate volume simulation at constant pressure filtration simulation was limited to an hour filtration based on the simulation assumption. The energy input of 2.03×10^4 J was estimated for the constant pressure filtration of the hydrate cake using compression piston with compression pressure of 9 MPa.

The final stage operation was further applying further compression pressure up to 15 MPa using the reference experimental data (Murayama et al., 2011) whilst assuming constant piston speed for its supply from the hydraulic cylinder which resulted in compression of the methane hydrate cake in the cylindrical screen to pellet. The pellet size of 0.05 m and 0.10 m in length and diameter respectively as considered agrees with the experimental data (Murayama et al., 2011). The energy input of 8.48×10^3 J was estimated for the pelletization of the dewatered hydrate cake to 0.05 m thickness using compression piston with compression pressure of 15 MPa. The effective filter capacity, 5.65×10^4 m^3 was lower compared to 2.26×10^3 m^3 for constant pressure filtration because of reduction of the filtering screen to 0.05 m length.

5.6 Simulation result of scale-up case scenarios of MHPP reactor simulation

5.6.1 Stranded gas utilization simulation specifications

The reactor design size obtained based on the methane hydrate pellet production simulation and the assumption that data from the base case reactor scale can be used for large reactors were employed in specifying methane hydrate technology chain investigation. Using two case scenarios as scope of the investigation of small reserve capacity range of 0.3 – 25.5 bcm (0.01

– 0.90 Tcf) and large reserve capacity range 28.3 – 566.0 bcm (1.0 – 20 Tcf) reserve capacities. Table 5.11 shows the reactor volume and number of reactors required with hydrate formation rate per dispersion volume of 2.48×10^{-1} mol $m^{-3}s^{-1}$ and appropriate feed gas supply rate with a reference case scenario reactor capacity of 30 m^3 (indicated as Ref.) as explained in Section 4.3.8. This is the summary of range of reactor capacities relative to the specified gas reservoirs capacities used in the reactor and equipment costing in chapter 6.

As shown in Table 5.11, in a scenario of approximately 6 bcm capacity stranded gas reservoir over 20 years project operation at annual production rate of 0.3 bcm, two methane hydrate forming CSTR reactors of 7.3 m^3 and 30 m^3 were obtained by 4.10 mol s^{-1} and 16.86 mol s^{-1} feed gas flowrates respectively.

Table 5.11: Simulation specification for small and large capacity stranded gas utilization

Case Scenario	**Annual gas production rate (bcm) over 20 years**	**feed gas flowrate Q_{fg} (mol s^{-1})**	**Reactor volume capacity V_r (m^3)**	**Number of Reactors**
Small reserve capacity range scenario				
Ref.	0.2	16.9	30.0	-
1	0.3	21.0	37.3	2
2	2.8	211.0	374.4	12
3	11.3	844.0	1497.4	49
4	25.5	1899.0	3369.2	112
Large reserve capacity range scenario				
5	28.3	2105.9	3736.3	124
6	169.9	12593.7	22343.7	744
7	339.8	25187.4	44687.3	1489
8	566.3	41979.0	74478.9	2482

The reactor design and parameters were worked out using the MHPP simulation with hydrate formation rate per dispersion volume of 2.48×10^{-1} mol $m^{-3}s^{-1}$ and conversion of 44 %. Further details of the 30 m^3 methane hydrate-forming reactor are presented in Table 5.12 below. The same applies for scenarios 1 – 8, which the number of reactors is just a value factor to multiply the costed reference reactor.

MHPP simulation as with base case reactor was carried in HYSYS which was employed with costing the reference reactors as well as estimated power input for other equipment such as the pump, gas compressor and coolers (see Table 5.12). In addition, this data was also employed in

the economic comparison with conventional technologies such as liquefied natural gas (LNG) and compressed natural gas (CNG). A strong interest in the industrialization of hydrate process for stranded gas utilization is due to the small gas fields, which as earlier stated accounts for about 70 % of the number of natural gas reserves globally. Therefore, the defined scale capacity scenario is of essence especially producing energy to end users who require affordable scale for small businesses, of which it is clearly uneconomical for conventional technologies requiring large capacities (Mitsui Engneering and Shipping, 2016).

Likewise, for large scale stranded gas capacities. Although, a couple of economic evaluations for conventional technologies used for large scale reserves exist in literature, this evaluation was specific to the stated case scenarios to draw a technoeconomic comparison with MHT chain in order to assign its feasibility in this study (refer to Chapter 6). Nevertheless, other considerations aside from economic reasons that may reduce the opportunities for a proven gas transportation technology to be utilized relate to safety, environmental impact such as gas emissions on transportation, which was qualitatively investigated in Chapter 1 (Sections 1.4-1.5). In this regard, MHT chain appear promising option and further due its inherent self-preservation mechanism that suggest ensures minimal discharge on transportation as methane hydrate at sub-zero condition (Gudmundsson and Borrehaug, 1996b, Gudmundsson, 1996a).

5.6.2 MHPP reactor model scale-up simulation case results

The reactor scale-up model assumptions were based on the MHPP base case for large reactor capacities used industrially. The rationale for including the scale-up is to introduce reference process capacities in this study, which is similar to industrial process capacities for the MHT chain evaluation of stranded gas utilization. Therefore, the summary of the parameters of MHPP reactor of 9.16×10^{-3} m^3 scaled up to the reference reactor volumes at 44 % conversion and formation rate per dispersion of 2.48×10^{-1} as shown in Table 5.10 below.

As can be observed, the reactor design dimensions, feed gas flowrate, and operational parameters increase with the increasing volume capacities. An exception is the stirring rate, which decreases relative to the increasing impeller diameters and reactor dimensions to maintain the geometric scale-up assumptions. In addition, the constant power consumption per unit volume (P/V) is also observed indicating that assumed optimum mixing as well as equal mass transfer rate is the large volume reactors with the base case reactor (Coker and Kayode, 2001). The traditional scale up approach of constant power consumption per unit volume for stirred reactors with geometric similarities (Oldshue, 1983) as applied are shown in Table 5.10, so that similar turbulent mixing is expected with the impeller speed reducing to 1.10 from 6.67 revolution per sec (s^{-1}). Gas flow number decrease from 6.76×10^{-2} to 1.12×10^{-2} maintains non-impeller flooding with a constant gas consumption rate in the reactors.

The power consumption in agitated systems required to maintain a given stirring rate is usually less when loaded with a dispersion of gas in liquid compared with when operating with water alone (Smith, 2011). This aligns with the obtained results relating the gassed power P_g with ungassed power consumed, P in the reactors using the P_g/P, which decreases with the decreasing stirring rate relative to the geometric scale up assumptions.

The geometric similarity from 9.16×10^{-3} to 30.00 m^3 volume capacities was achieved with the highest scale up factor of 14.85. In addition, four order of magnitude increase of the power consumption was obtained which is expected for the industrial-scale production of methane hydrate stirred reactors. This agrees with Mori (2015) values, however he suggested that the sharp increase in power consumption imply industrial scale hydrate production using stirred reactor is uneconomical. The economic investigation in the chapter will further review their assertion for viability for stranded gas utilization for a known capacity. Furthermore, in Table 5.12 the estimated duty for all the other equipment of the MHPP model such as gas compressor, pumps, and coolers (see Figure 4.3 in Section 4.3.3) as shown in the HYSYS model are also presented. These data are required for the MHT chain process economic evaluation and costing carried out in Chapter 6. Recall as earlier discussed in Section 4.3.3 of Chapter 4 that the gas and water stream were passed through these units to achieve the required pressure and temperature conditions of the feed stream in the MHPP reactor.

Table 5.12: MHPP reactor HYSYS model scale-up simulation result

Reactor parameters	**Values**	**Scale up**							
Reactor capacity V (m^3)	9.16×10^{-3}	5.80×10^{-1}	6.30×10^{-1}	7.30	9.20	16.30	23.70	27.40	30.00
Reactor Diameter (m)	1.80×10^{-1}	7.17×10^{-1}	7.37×10^{-1}	1.67	1.80	2.18	2.47	2.59	2.67
Impeller Diameter(m)	9.00×10^{-2}	3.59×10^{-1}	3.69×10^{-1}	8.34×10^{-1}	9.01×10^{-1}	1.09	1.24	1.30	1.34
Reactor Height (m)	3.60×10^{-1}	1.44	1.48	3.34	3.61	4.36	4.94	5.19	5.35
Feed gas flowrate Q_{fg} (mol s^{-1})	5.15×10^{-3}	3.26×10^{-1}	3.54×10^{-1}	4.10	5.17	9.16	13.32	15.40	16.86
Impeller Speed (s^{-1})	6.67	2.65	2.61	1.51	1.44	1.26	1.16	1.13	1.10
Reynold number (-)	4.03×10^{4}	2.55×10^{5}	2.64×10^{5}	7.85×10^{5}	8.70×10^{5}	1.12×10^{6}	1.32×10^{6}	1.41×10^{6}	1.47×10^{6}
Gas flow number (-)	6.76×10^{-2}	2.69×10^{-2}	2.64×10^{-2}	1.53×10^{-2}	1.46×10^{-2}	1.28×10^{-2}	1.18×10^{-2}	1.14×10^{-2}	1.12×10^{-2}
Power number N_p (-)	5.00	5.00	5.00	5.00	5.00	5.00	5.00	5.00	5.00
Power consumed P (W)	8.03	5.09×10^{2}	5.52×10^{2}	6.40×10^{3}	8.07×10^{3}	1.43×10^{4}	2.08×10^{4}	2.40×10^{4}	2.63×10^{4}
Gassed power consumed P_g (W)	5.98	3.41×10^{2}	3.70×10^{2}	4.15×10^{3}	5.22×10^{3}	9.20×10^{3}	1.33×10^{4}	1.54×10^{4}	1.69×10^{4}
Constant P/V (-)	8.77×10^{2}	8.77×10^{2}	8.77×10^{2}	8.77×10^{2}	8.77×10^{2}	8.77×10^{2}	8.77×10^{2}	8.77×10^{2}	8.77×10^{2}
P_g/P (-)	7.45×10^{-1}	6.70×10^{-1}	6.69×10^{-1}	6.48×10^{-1}	6.47×10^{-1}	6.44×10^{-1}	6.42×10^{-1}	6.41×10^{-1}	6.407×10^{-1}
Production rate (kg h^{-1})	1.0×10^{1}	2.11×10^{1}	2.75×10^{1}	4.48×10^{1}	5.11×10^{1}	7.01×10^{1}	8.11×10^{1}	9.35×10^{1}	9.75×10^{1}
Duty of other equipment from simulation									
Gas compressor [Q-100] (KW)	2.81×10^{-2}	2.05	5.07	8.29	9.47	12.98	15.99	17.32	18.22
Gas cooler [Q-101] (KW)	1.90×10^{-1}	1.38×10^{1}	3.44×10^{1}	5.61×10^{1}	6.39×10^{1}	8.77×10^{1}	1.08×10^{2}	1.17×10^{2}	1.22×10^{2}
Pump [Q-102]	8.71×10^{-1}	6.35×10^{1}	1.57×10^{2}	2.57×10^{2}	2.93×10^{2}	4.01×10^{2}	4.95×10^{2}	5.36×10^{2}	5.58×10^{2}
Water cooler [Q-103]	8.65	6.30×10^{2}	1.56×10^{3}	2.55×10^{3}	2.91×10^{3}	3.99×10^{3}	4.91×10^{3}	5.32×10^{3}	5.55×10^{3}

5.7 MHPP storage unit

The volume capacity of MHPP storage unit estimate using the cylindrical shaped MH pellets (0.05 × 0.1 m) with density of 917.30 kg m^{-3} and the production rates assuming five days production are shown in Table 5.13 below for the different production scale up assumptions. The cylindrical shaped MH pellets (0.05 × 0.1 m). In the base case scenario, for a single pellet, mass of 0.36 kg is estimated which at 10 kg hr^{-1} production rate will yield 28 pellets. This in volumetric production rate will be 0.01 m^3 hr^{-1} and for the assumed five days production was computed as 1.30 m^3 per [5 days]. Table 5.13 values are based on the scenarios defined in Table 5.12. An insulated tank is assumed with methane hydrate pellets stored at atmospheric pressure.

Table 5.13: Methane hydrate pellet storage vessel capacity

Case Scenarios	Production rate (kg hr^{-1})	Storage vessel volume (m^3)
Base case MHPP model	10.00	1.30
Scenario 1	1.42×10^2	3.73×10^1
Scenario 2	1.19×10^3	3.74×10^2
Scenario 3	4.87×10^3	1.50×10^3
Scenario 4	1.10×10^4	3.37×10^3
Scenario 5	1.21×10^4	3.74×10^3
Scenario 6	7.26×10^4	2.23×10^4
Scenario 7	1.45×10^5	4.47×10^4
Scenario 8	2.42×10^5	7.45×10^4

5.8 Concluding remarks

The results of the MH pellet production (MHPP) simulation have been presented using a pilot-scale system data in literature. MHPP reactor simulations were implemented successfully from HYSYS software. The MHPP model demonstrates design of a standard geometry continuous stirred tank reactor simulation using pure methane gas and water and a correlation of methane gas consumption rate based on a pilot scale experimental data. At various conditions using the MHPP simulation of 10 – 97.5 kg hr^{-1} production scale of methane gas hydrate pellets in 9.16 × 10^{-3} – 30 m^3 and suitable pellet storage estimates which were used to evaluate large capacity reactors for the methane hydrate production in different commercial scale scenarios. In addition, the MHPP reactor simulation included coolant characteristics of a typical jacketed vessel and energy balance calculations for producing hydrate-producing CSTR.

Sensitivity analysis of the developed MHPP reactor model reveals that the superficial velocity has significant effect on the gas consumption rate, double the effect compared to that of either stirring rate, pressure or subcooling. Further evaluation of the parameters of the MHPP reactor simulations indicated the following:

- The superficial gas velocity (or gas injection rate into the reactor) increased proportionally with the methane gas consumption rate
- Methane gas consumption rate increased significantly with increase in the stirring rate
- Methane gas consumption rate increased slightly with increase in subcooling
- The dissociation enthalpy of methane hydrate and hydration number was overestimated using equilibrium conditions obtained from HYSYS compared to literature.

Furthermore, for the dewatering unit, the hydrate pellet processing machine with combined dewatering and pelletizing unit was simulated using three operational stages of constant rate filtration, constant pressure filtration, and compression. The filter-compression chamber design, operational parameters, as well as the slurry and methane hydrate cake properties were reported for the processing of 10 wt % methane hydrate slurry to 90 wt % methane hydrate pellet HPPM pilot plant scale.

Chapter 6 The transportation and regasification Units and Economic Evaluation of Methane Hydrate Technology Chain

The methane hydrate technology chain cost estimate is reported in this chapter. This comprises the following sections:

- The MH pellet transportation framework based on ship bulk-carriers and assumptions are presented in Section 6.1.
- Section 6.2 presents the regasification framework of methane hydrate pellet.
- Sections 6.3 and 6.4 present the costing and economic estimation framework of the methane hydrate technology (MHT) chain comprising production, transportation, and regasification units and the MHT chain estimated economic performance.
- Section 6.5 presents the comparison investigation of MHT with other conventional technologies, liquefied natural gas (LNG) and compressed natural gas (CNG) for the utilization of stranded natural gas.

6.1 Methane hydrate pellet transportation unit

Transportation unit is the mid-stream operation, which requires safe operation with minimal emissions of methane gas on transit. The transportation of natural gas as solid (pellet) and the self-preservation phenomenon is massive advantage in terms of safety compared to other technologies. Methane hydrate transportation can be onshore, offshore, and land. Land transport of gas hydrate pellet has been demonstrated by MES Ltd with an established pilot plant (Nogami et al., 2011). Conceptual studies exist in literature on offshore/ocean transport with highlight of self-preservation effect merit of gas hydrate pellets (Gudmundsson and Borrehaug, 1996b, Gudmundsson, 1996a, Gudmundsson, 1996b), which is considered an advantage for safer transport. It is important to establish the transportation cost for the MHT chain, not just, because it is a unit of the chain but also provides data to compare with transportation cost of other technologies. Therefore, detailed costing of the MHT offshore/sea transportation was executed following the developed computation equations of the required number of ship bulker-carrier trips as well as round trip transport time (Khalilpour and Karimi, 2012) associated with the MH production capacity and market distance (Sections 6.3.1.2 and 6.3.2.2).

6.2 Methane hydrate regasification unit

The methane hydrate pellets transported via bulk-carrier ship to the receiving terminal require regasification for the methane gas recovery. The gas is further processed in a dehydration unit to typical pipeline quality as sales natural gas. In addition, water recovered from the

regasification unit was also considered as a source of revenue if sold as process water (see Section 6.3.3). Some literature studies on regasification methods were presented in Section 3.4.2. However, the challenge in employing the experimental studies in setting up a simulation was the ability to scale up to suit the considered reserve capacities utilization in this study. Therefore, assumptions were based on literature, which also were used in the cost estimation of the unit discussed in sections 6.3.1.3 and 6.3.2.3.

The summary of the framework of the regasification of methane hydrate pellet considered in this study is as shown in Figure 6.1. The two main operations considered are the pellet regasification vessel and the gas dehydration to ≤ 84 ppm (4 lb water/MMscf of gas) which is the typical pipeline specification.

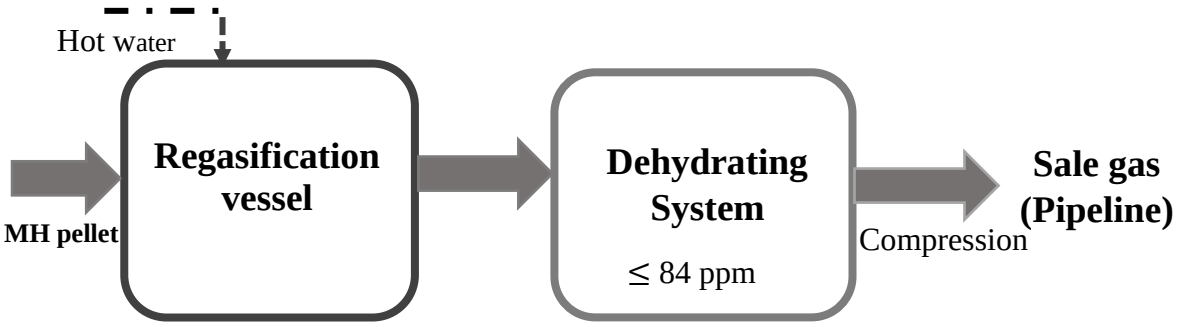

Figure 6.1: Summary framework of methane hydrate regasification

Based on literature the following assumptions were made as depicted in the framework (Gudmundsson and Borrehaug, 1996b, Kanda, 2006, Takaoki et al., 2004, Rehder et al., 2012, Lee et al., 2011). Heated water from a water tank is pumped or injected into the regasification vessel. The dissociation of gas hydrates is an endothermic process and so requires a supply of heat. Although the depressurization method was considered most economical, compared to the thermal stimulation as external source of energy is not required but it has low gas recovery rate due to slow reaction for hydrate dissociation. Thermal stimulation on the other hand is considered most energy efficient if viewed thermodynamically since the heat required to dissociate hydrates is just about 10 % the heat value of the produced natural gas (Lee et al., 2010).

The main process equipment defined for the unit are regasification vessel, water pump, water tank, dehydrating system (glycol dehydrating plant) and a gas compressor. Large diameter pipe of the regasification vessel is assumed and the gas compression from the dehydrating plant (to 8.0 MPa) to sales gas pipeline network. The dehydrating plant was simulated in HYSYS with pre-installed wet gas stream from mixture of pure methane gas with water stream as shown in

Figure 6.2. The water was assumed recycled to the hot water tank. An assumption of 130.80 m^3s^{-1} (400 MMscf/d) of gas recovery from the regasification vessel as a base case was used, requiring about 10,600 kg s^{-1} (water mass) of 293 K water for the 12 cargo volume vessels making up total cargo volume of 460000 m^3 (Gudmundsson and Borrehaug, 1996b).

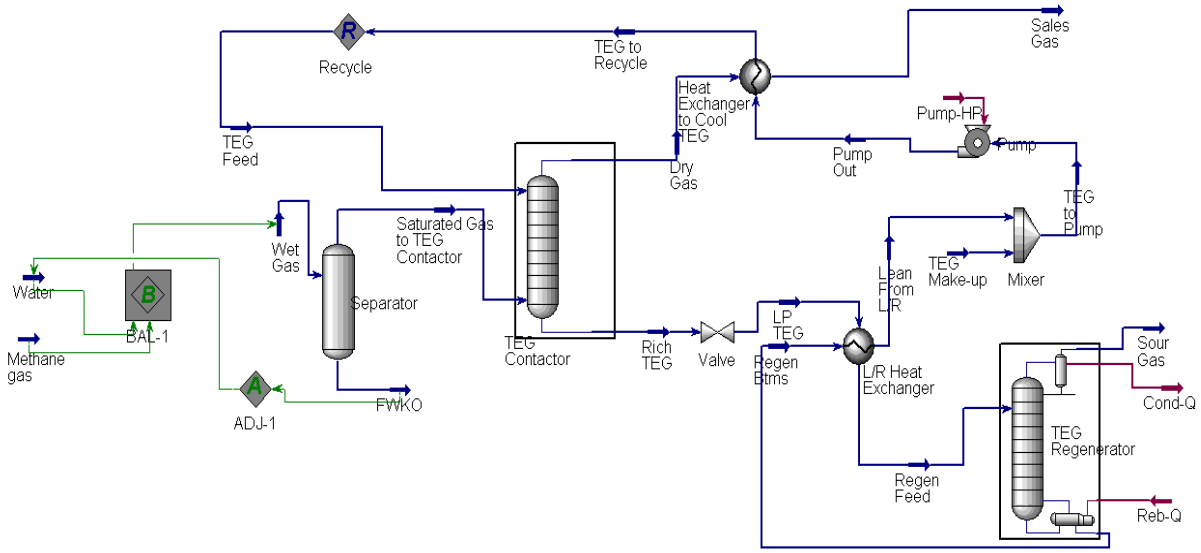

Figure 6.2: Implemented glycol dehydrating unit in HYSYS after MH regasification

6.3 Economic estimation of methane hydrate technology (MHT) Chain

For a project or technology to be justified for execution, its economic performance must be evaluated. More so, an attractive project especially for commercialization needs an established economic viability compared with alternatives. Most chemical engineering design projects are evaluated to work out economic performance from which the costs and revenues estimates are made (Sinnott and Towler, 2009b). Before a technology or project can be sold to a management for investment or progress with commercialization considered, its profitability must be demonstrated. Owing to the primitive developmental stage of the MHT commercially as was previously discussed in Chapters 2 and 3, the economic analysis of the MHT chain was explored in this study.

As earlier mentioned, the MHT chain comprises of three units, namely MH pellet production, transportation and regasification of methane hydrate pellets. In this study, cost estimates for these units were established using economic evaluation framework of components of the total capital investments and annual operating costs as defined in Figure 6.3 (Section 6.3.1). For the production unit, outcome of the MHPP simulations discussed in Chapters 4 and 5 were considered. The transportation assumptions as well as framework of the methane regasification unit including the gas dehydration presented in Sections 6.1 – 6.3 were also considered for the

cost estimates of transportation and regasification units respectively. Standard units used in the oil and gas industries such as trillion cubic feet (Tcf), thousand cubic feet (Mcf) and million British thermal unit (MMBtu) are used for capacities and energy of natural gas respectively.

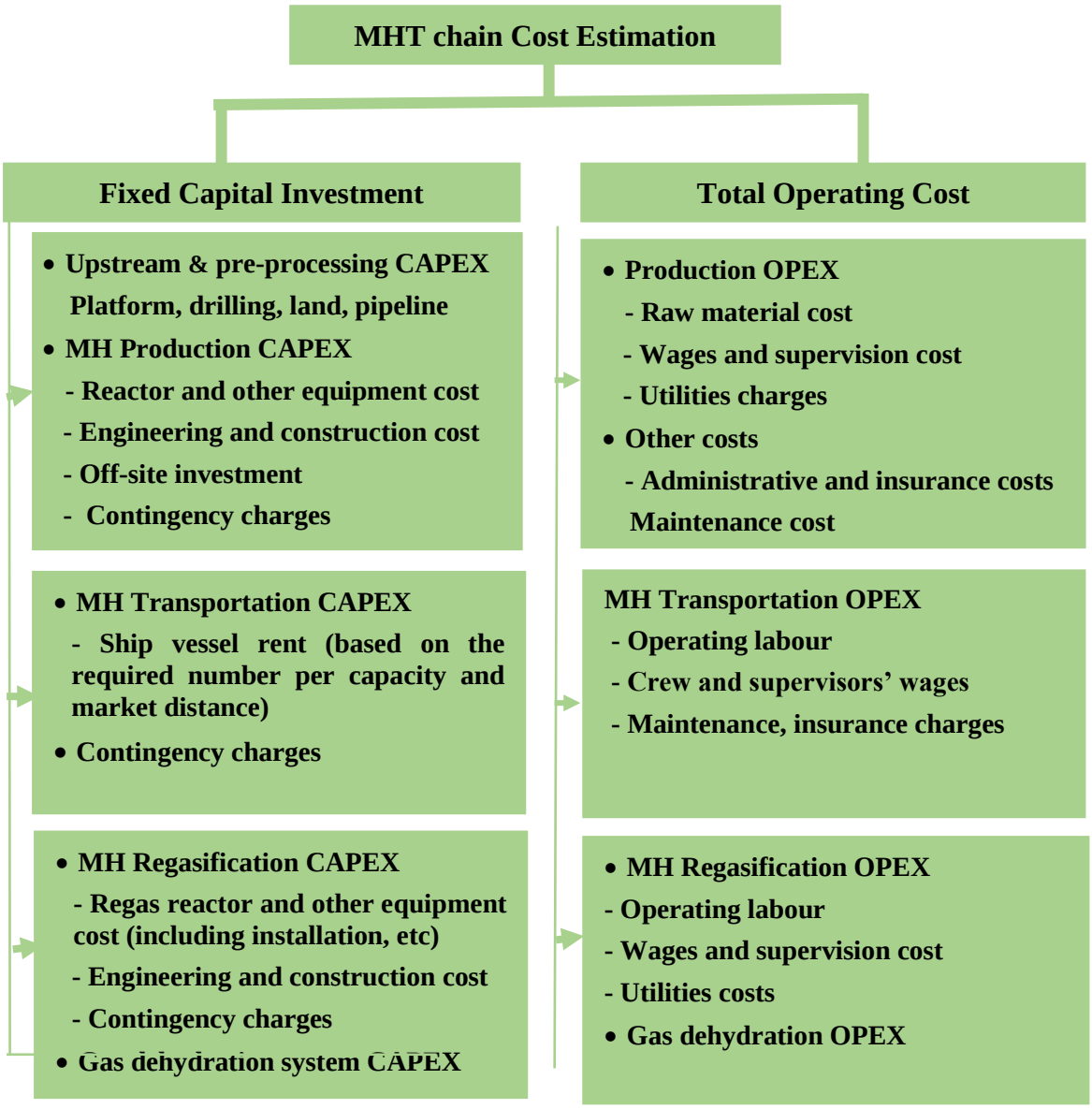

Figure 6.3: Summary of MHT estimate cost components

Then, to establish the feasibility of MHT chain, net present value (NPV) which is an established and commonly used method of profitability assessment (Peter and Timmershaus, 1991), was employed for the MHT chain economic evaluation, and similarly employed for comparison with other established technologies for utilization of stranded gas.

All net incomes and cash flows in the economic life of a project are calculated using the net present value (Peter and Timmershaus, 1991). In other words, it is the sum of the present values of the future cash flows. A positive NPV shows a net gain relative to the cash flow while a net

loss is indicated by a negative NPV reflecting non-profitability, thus, the project is rejected. It is common practice to use the NPV model in comparing project alternatives, in which the project with the highest NPV gets the highest preference for investment.

NPV is defined mathematically as:

$$\mathrm{NPV} = -\mathrm{CF_n} + \sum_{n=M+1}^{n=t} \frac{\mathrm{CF_n}}{(1+i)^n} \qquad 6.1$$

where CF_n is cash flow in years, i is the interest rate, t is the life span of project and M is the construction time.

The cost and revenue parameters are required in any economic evaluating tool. For a plant, cost parameters usually comprise the total capital investment cost and total annual operating cost throughout the project life span, while the revenues are profit generated after tax, from all cash inflows of the project as computed in Sections 6.3.1 – 6.3.3. In this evaluation study, the cost of equipment units, raw materials and utilities associated with the MHT chain project were obtained from published literature and manufacturer's or vendor's catalogue. The associated capacities of the units and amount of raw materials and utilities were defined using MHPP simulations as discussed in Chapters 4 and 5 as well as the transportation and regasification simulations in Chapters 6. The project cost was updated to the capacities and execution year using either sixth-tenth rule (Equation 6.2) or cost correlations (Equation 6.3) (Sinnott and Towler, 2009b)), and the Chemical Engineering Plant Cost Index (CEPCI) in Equation 6.4 respectively.

Sixth-tenth rule (Peter and Timmershaus, 1991):

$$\mathrm{E_n} = \mathrm{E_o}\left(\mathrm{C_n}/\mathrm{C_o}\right)^e \qquad 6.2$$

Where E_n is equipment cost to be estimated, E_o is equipment cost known, C_n equipment capacity to be estimated, C_o is equipment capacity known and the exponent, e (0.6 usually used).

Cost correlations obtained from Sinnott and Towler (2009b) based on cost index, Jan. 2007 (CEPCI=509.7)

$$\mathrm{C_n} = \mathrm{a} + \mathrm{b}\mathrm{E_n}^{\mathrm{N}} \qquad 6.3$$

where a and b are cost constants, and N is the exponent for equipment types.

The Chemical Engineering Cost Index:

$$\mathrm{C_n} = \mathrm{C_o}\left(\mathrm{CEPCI_n}/\mathrm{CEPCI_o}\right) \qquad 6.4$$

where $CEPCI_n$ is current time index and $CEPCI_o$ is the original equipment cost index.

6.3.1 Total capital investment estimation for MHT chain

Methane hydrate technology (MHT) chain involves the production of MH (MH pellets for this study) for the utilization of methane gas from stranded locations. To produce MH and deliver as methane gas requires interdependent steps. These include exploration of gas (upstream), associated pre-processing, and MH hydrate slurry processing grouped under MH production, the transportation (mid-stream), and then regasification and gas dehydration (at the receiving terminal) grouped under regasification unit. Therefore, the capital cost (CAPEX) and operating cost (OPEX) for the project must include the costs associated with all the units of the MHT chain. The sums of the CAPEXs for the units are thus the amount of the total capital investment cost. Similarly, the sum of the OPEXs for the units was estimated as total operating cost. Land-based MH production basis within or near the gas exploration field was assumed.

6.3.1.1 MH pellets production CAPEX estimate

The CAPEX estimate is the purchase cost of the major equipment of the production unit of MHT chain. The case scenarios based on the capacity specification outcome of the MHPP simulation (see section 5.6 of Chapter 5) comprising the reactor, coolers, pump, compressor and storage vessel were employed for the cost estimate. Sinnott and Towler (2009b) cost correlation using historical data based on a US Gulf Coast basis, January 2007 with CEPCI index of 509.7 was employed for all the equipment except for the cost of hydraulic ram (for the HPPM processing system), which was obtained from vendors (FLOWFIT®). All the equipment items are index-corrected to the considered year using the CEPCI (Nov. 2017) index of 573.2 (see Equation 6.4). In addition, the production CAPEX estimation also includes costs such as piping, equipment construction, instrumentation, and control, electricals, structures, and plant lagging, which were factored in using the widely used Lang factor. The various Lang factors as well as typical indirect cost factors are obtained from Chemical Engineering design by Coulson and Richardson Volume 6 (see Table 6.1). The Inside battery limits (ISBL) investment comprised the costs of equipment purchase itself and the modifications to be made on the infrastructures and equipment including installations such as piping, instrumentations etc, known as offsite or OSBL investments. The upstream capital cost of USD 2.5 billion was assumed across board including facilities including wells, platform, pre-processing, and pipeline (Osokogwu et al., 2011).

The total capital investment for the MHT chain becomes the CAPEX of production, transportation, and regasification units. For the other fixed capital cost components; off-sites, engineering & construction cost, and contingency, typical factors for solid-liquid systems presented by Sinnott and Towler (2009b) were employed. Usually some extra capital as a

percentage of the fixed capital investment (FCI), the working capital is allowed for plant start-up and running of the plant prior to earning income. Working capital was considered as 15 % of the FCI. Thus, the total capital investment is then calculated as the sum of the fixed capital investment and the working capital.

Standard method of depreciation called the Modified Accelerated Cost Recovery System (MACRS) was employed for depreciation associated with project CAPEX. So, 10 years property depreciation usually used for assets used in petroleum refining and oil and gas transportation equipment was employed (Khalilpour and Karimi, 2012)

Table 6.1: Typical factors for CAPEX estimation (Sinnott and Towler, 2009b)

Installation factor f_p for piping	0.6
Installation factor f_{er} for equipment erection	0.5
Installation factor f_e for electrical work	0.2
Installation factor f_i for instrumentation and process control	0.3
Installation factor f_c for civil engineering work	0.3
Installation factor f_s for structures and buildings	0.2
Installation factor f_l for lagging, insulation or paint	0.1
ISBL plant cost (with summation of correction factors)	
Offsite Design and Engineering Contingency	40% ISBL 25% ISBL 10% ISBL
MHPP Production Fixed Capital Investment (FCI)	
Working Capital	15% FCI
MHPP Production Total Capital Investment (TCI)	

As is common practice capital cost estimates of chemical process plants are usually based on the major equipment items required for the process while the other costs are worked out as factors of the equipment cost (Sinnott and Towler, 2009b). Equipment materials are also taken into consideration with correction factors depending on the material of the estimated equipment.

6.3.1.2 Estimate of MH pellet transportation CAPEX

Usually the carrier ship has loading and unloading facilities installed (Moore and Greiner, 2017). Transportation of MH pellets has been mentioned in literature using train (Taheri et al., 2014), on land (Nogami et al., 2011, Nakai, 2012b) and using ship (Gudmundsson and Graff,

2003, Kanda, 2006). However, ship (sea transport) is most workable considering offshore reserves as well as due to the capacity and considering that it is transported under relatively less stringent pressure conditions (Shin et al., 2016), thus, it is considered in this study.

Therefore, a 100,000 deadweight tonnes (DWT) Panamax bulk-carrier with vessel capacity of 160,000 m^3 suggested by Takaoki et al. (2004) was considered assuming land-based MH production plant, a harbour to another harbour (receiving terminal) ship transport concept, similar to the scenario presented by the MES Ltd (Nakai, 2012b, Kanda, 2006). Since ships are usually charted, average charter rate of $10,298/day for 2017 was obtained from the 2017 Review of Marine Transport by United Nations Conference on Trade and Development (UNCTAD) (Hoffmann, 2017).

However, for a given reservoir (reserve) capacity and transport market distance, the round-trip transport time for one ship delivery was estimated using equation adapted from Khalilpour and Karimi (2012):

Round−trip transport time for the one ship delivery, T_r

$$\mathrm{T_r} = \frac{2\mathrm{d}}{\mathrm{s_o}} + \mathrm{V_M}\left(\frac{1}{\mathrm{L_r}} + \frac{1}{\mathrm{D_r}}\right) \qquad 6.5$$

where d is one-way trip distance from the plant to the receiving terminal (km), s_o is average speed (km hr^{-1}), V_M is ship vessel capacity (m^3), L_r: loading rate at the plant, and D_r is unloading rate at the receiving terminal or port. Then, with the estimated round-trip transport time for one ship delivery, the number of ship bulk-carriers required was calculated using equation derived based on Khalilpour and Karimi (2012):

Number of ship bulk-carriers required, N_c

$$\mathrm{N_c} = \frac{\mathrm{P_C} * \mathrm{T_r}}{\mathrm{V_M}} \qquad 6.6$$

where P_c is production capacity in bcm per year (Tcf per year).

The transportation CAPEX was then obtained by multiplying the number of bulk-carriers required by the bulk-carrier charter rate.

6.3.1.3 MH pellets Regasification CAPEX Estimate

The CAPEX estimate is the purchase cost of the major equipment in the regasification unit of MHT chain. Like with the production unit estimate, the cost of the main equipment of the units was carried out based on Sinnott and Towler (2009b) and cost correlation using historical data based on a US Gulf Coast basis, January 2007 with CEPCI index of 509.7 was employed for all the equipment. For the glycol dehydration plant, HYSYS cost data was used on based the simulation of the dehydration system on HYSYS. All the equipment items are index-corrected to the considered year using the CEPCI (Nov. 2017) index of 573.2 (see Equation 6.4). The

base case of 400 MMscf/d was used for the cost estimation relative to the different methane hydrate production capacities employed with the consideration of gas content of pure methane gas hydrate 170 m^3/ m^3 assumed, which is less than completely filled hydrate structure.

The main process equipment defined were for the unit are, regasification vessel, water pump, water tank, a gas compressor estimated based on data from Gudmundsson and Borrehaug (1996b) while the glycol dehydrating plant included pump, heat exchanger, glycol contactor and regenerator. The dehydrating plant was simulated in HYSYS with pre-installed wet gas stream from mixture pure methane gas with water stream and then processed gas stream to sales gas pipeline network compressed to 8.0 MPa since gas pipelines typically operate at pressure ranges 7.0 – 10.0 MPa (Mokhatab et al., 2015).

6.3.2 MHT total operating cost estimation

Similarly, for the estimation of total annual operating cost of the MHT chain using the components of production, transportation, and regasification (including the gas dehydration system) units were used. The cost estimates were worked out as the units running costs as shown in Figure 6.3 above.

The total operating cost was calculated as the sum of the OPEX for production, transportation, and regasification units:

$$\text{Total OPEX} = (1 + \varphi)^n * [OP_P + OP_T + OP_R] \quad 6.7$$

where OP_P is the production OPEX including the raw material cost (USD per year), OP_T is the transportation OPEX (USD per year), OP_R is the regasification unit OPEX (USD per year), φ is operating cost escalation rate assumed as 3 % and n represents time in year.

The raw materials for MHT in this study are methane gas (feed gas) and water. The feed gas prices vary considerably due to uncertainties in gas demand and gas contracts, as such varies for different regions due to production costs and transportation distances. In addition, global political considerations and whether it is associated or non-associated gas reserves. However, since this evaluation is based on 2017 data, an assumption of gas price estimate was used based on the Henry Hub natural gas spot price average for 2017 (USD 3.00 per MMBtu) (EIA, 2017). There have been drops of the natural gas spot price up to USD 2.22 per MMBtu in August of 2019 (EIA, 2017). The feed gas prices factors in the running costs to operate and maintain gas facilities including facilities and equipment used in gas exploration (Khalilpour and Karimi, 2012, Gaddis et al., 1992). It is important to note that the same feed gas price was considered to ensure uniformity with comparison for alternative stranded gas utilization technologies such as LNG and CNG. Water was estimated as treated pure water for industrial use. A 353.15 cubic feet pure water tanker is supplied at USD 99.4 in 2017 (source: Waterpit Nigeria Limited, Port

Harcourt, Nigeria). Operating labour was roughly estimated using the rule of thumb presented by (Peter and Timmershaus, 1991). For the operating labour and employee for the production including the MH processing unit to pellet and for the regasification unit were assumed generically as 10 employees for 100 kg hr^{-1} with the continuous system operation. Whereas that of transportation unit are built into the ship operating cost discussed in Section 6.3.2.2 below. The labour cost covers number of employees including managers, operator technicians, engineers, and unskilled workers based on the minimum rates and laws in Nigeria.

6.3.2.1 MH pellet production system operating cost estimate

The OPEX of major plant equipment and utilities were defined using the MHPP model whose development was described in Chapters 4 and 5. The production maintenance cost as well as administrative and insurance were defined as 2 % and 0.7 % of the CAPEX respectively (Sinnott and Towler, 2009b). The unit electricity cost (C_e) was assumed to be USD 0.068 per KWh for 2017 (EIA, 2017). The consideration of mechanical power consumption of the hydrate pellet-processing machine (HPPM) was used for the internal filter capacities of the operational stages of constant pressure filtration and compression (Murayama et al., 2011). So that with the estimated power consumption and the unit electricity cost, the running cost was obtained.

6.3.2.2 MH pellets transportation OPEX estimate

The transportation OPEX for each round-trip transport time (one ship delivery) is multiply by the number of ship bulk-carriers (see Equation 6.6) based on the considered reservoir capacity and market distance. The OPEX consisting of the ship bulk-carrier operating cost was estimated using derived equation based on Khalilpour and Karimi (2012):

Transportation OPEX, OP_T

$$\mathrm{OP_T} = \mathrm{T_{r_M}} * \mathrm{voc} * \mathrm{N_c} \qquad 6.8$$

Where voc is vessel or ship bulk-carrier operating cost (USD/year)

100,000 DWT Panamax bulk-carrier suggested by Takaoki et al. (2004) was considered using speed of 31.48 km hr^{-1} with daily rate operating cost obtained based on Moore Stephens' OPCost 2017 as USD 5678 for 8−15 years old (Moore and Greiner, 2017). The voc daily rate covers the crew wages, lubricants, repairs and maintenance, insurance and other administrative charges.

6.3.2.3 MH pellets regasification unit OPEX estimate

The operating cost estimation of the regasification unit was carried using the utilities of the major components of the unit; regasification vessel, water pump, water tank, dehydrating system (glycol dehydrating plant) and a gas compressor. The utility of the equipment were

based on 400 MMscfd capacity regasification data from Gudmundsson and Borrehaug (1996b). Heat pump system with duty 2.42×10^5 KW and steam turbine 2.03×10^5 KW, plus 2.40×10^4 KW and 1.00×10^5 KW (from steam condenser and compressor after-coolers respectively) for water heating, as well as 1.00×10^5 KW compressor duty used for produced gas compression from atmospheric pressure to 8.0 MPa. For the dehydrating system, costing was obtained from the simulation in HYSYS. Water cost was estimated using price of the raw water as USD 2 per 264 m^3 gallon of water (Sinnott and Towler, 2009b).

6.3.3 Revenue estimation

The income earned from a main product and/or by-product of a project is the revenue of that project. This is usually estimated with respect to the production rate specified. The profit or net-income is however, the income left over after all revenues, gains and losses, expenses, and taxes have been accounted for fully.

The revenue in this study is the sales gas from the regasification unit, which have gone through the dehydration unit to remove water vapour from the saturated gas to pipeline quality. The sales gas was estimated based on average of year 2017 NBP (Natural Balancing Point) price USD 6.86 per MMBtu (55.47 p/therm), since Europe end-users market is a main consideration (Ofgem, 2019). The water from the regas unit was also considered a revenue. The rough estimate of the sale price of the raw was made as USD 2 per 264 m^3 gallon of water (Sinnott and Towler, 2009b).

6.4 Economic evaluation of methane hydrate technology (MHT) chain: case scenarios for natural gas utilization

The case scenarios of different capacities and market distances of stranded gas utilization were used to investigate the MHT economic viability for utilization of stranded natural gas from offshore regions in Nigeria to Europe and Asia covering transportation of 10 000 km. Therefore, using the described MHT chain cost estimation development as discussed in the previous section for considered case scenarios to ascertain the economic influence of stranded gas utilization based on MHT was carried out. The estimation results of the production, transportation, and regasification units are therefore presented in this subsection. Furthermore, alternative technologies for stranded natural gas utilization were explored and compared with the obtained result data form MHT chain in Section 6.5.

In this study, eight case scenarios were considered; small and mid-scale commercial reservoir capacities of 0.3 – 25.5 bcm (0.01 – 0.90 Tcf) while the others comprised larger reservoir

capacities of 28.3 – 566.0 bcm (1.0 – 20 Tcf) assuming 20 years project life and over 10,000 km market distance.

6.4.1 Estimation results of MHT production and regasification CAPEX and OPEX based on the small capacity reserve scenarios

The cost estimation of the four scenarios of small capacity stranded gas is shown in Table 6.2, which presents the results of the CAPEX and OPEX estimations for the production and regasification units using the procedure discussed in previous section. The cost estimates as shown in Table 6.2 increase with increase of the reserve capacity, which shows it as a fundamental factor of for the viability of the MHT chain for the utilization of stranded gas. The data will be used to compute the feasibility of the technology using NPV model.

Table 6.2: MHT production and regasification CAPEX and OPEX of small capacity scenarios

Reserve Capacity	**Scenario 1 (0.3 bcm)**	**Scenario 2 (2.8 bcm)**	**Scenario 3 (11.3 bcm)**	**Scenario 4 (25.5 bcm)**
Production CAPEX (USD)	2.51×10^9	2.61×10^9	2.92×10^9	3.47×10^9
Regasification CAPEX (USD)	2.37×10^7	2.21×10^8	8.90×10^8	2.01×10^9
Production OPEX (USD/yr.)	5.06×10^7	4.89×10^8	1.97×10^9	4.45×10^9
Regasification OPEX (USD/yr.)	2.92×10^7	2.75×10^8	1.16×10^9	2.87×10^9

6.4.2 Estimated cost of MHT transportation CAPEX and OPEX for the small capacity reserve scenarios technology over 10,000 km

The result of the methane hydrate pellet transportation CAPEX and OPEX using the derived equations (see Equations 6.5−6.6 and 6.8. in Section 6.3.1) for the transport of 0.3, 2.8, 11.3 and 25.5 bcm per year of stranded natural gas over 10,000 km are shown in Figure 6.4 below. Both the transportation CAPEX and OPEX indicated as Figure 6.4 a and b respectively increased proportional with increased reserve capacity over the 10,000 km market distance.

As can be observed, maximum CAPEX and OPEX of USD 1.79×10^8 and USD 1.01×10^8 respectively were obtained for transport of 25.5 bcm per year natural gas over 10,000 km showing just about 56 % difference between CAPEX and OPEX. This depicts relatively low capital expenditure for MHT transport CAPEX, which suggests it could be viable solution for stranded gas problem.

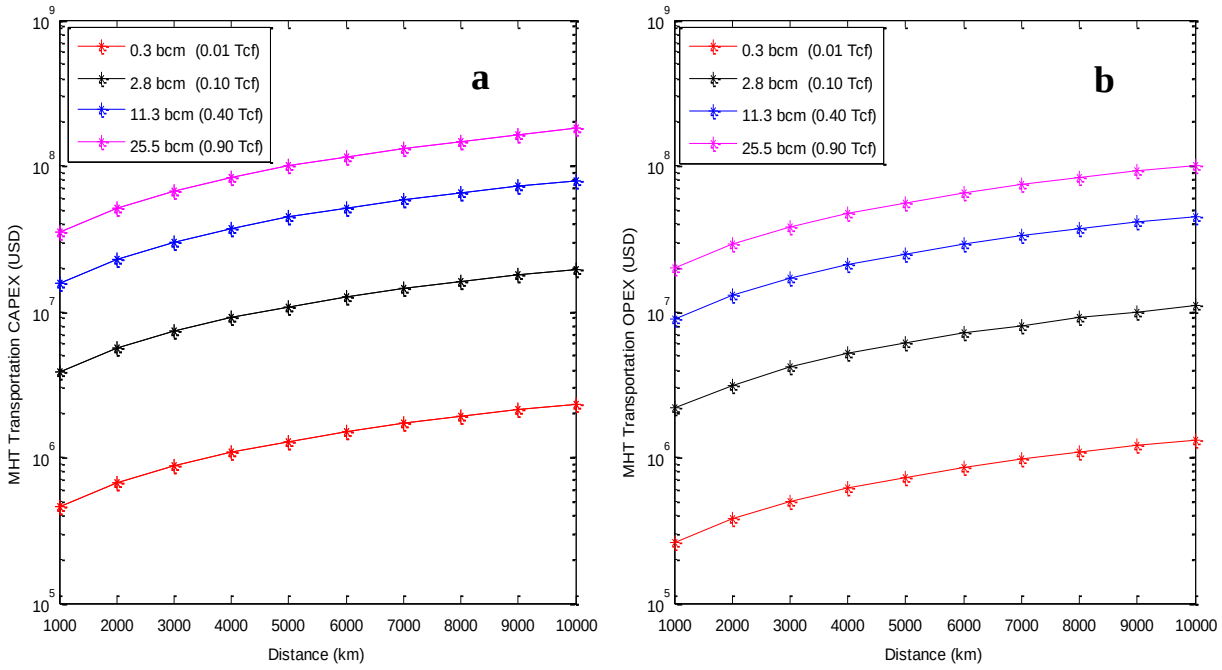

Figure 6.4: MHT transportation (a) CAPEX and (b) OPEX

In addition, about 77 % increase is observed due to reserve volume capacity 0.3 to 25.5 bcm while just about 5 % increase due to distance (1000 to 10000 km) implying a far higher cost sensitivity to gas reserve capacity compared to market distance. This shows that contrary to alternative technologies such as CNG, with transport distance as major factor for its feasibility (Economides et al., 2005) as discussed in Chapter 1, the reserve volume capacity seems be a prime factor compared to transport distance for the MHT.

Table 6.3 below shows the transport CAPEX and OPEX details for 25.5 bcm gas capacity over 10000 km market distance. Therefore, transportation of methane hydrate pellet equivalent to 25.5 bcm gas capacity over 1000 km market distance with maximum cargo of 160,000 m^3 capacity bulk-carrier ship will require 10 of it with each making round-trip deliveries in 5.9 days.

Table 6.3: Transportation CAPEX and OPEX with the bulk-carrier details for the transport of 25.5 bcm/yr of natural gas

Distance (km)	Round trip transport time for one Bulk-carrier ship delivery Tr (days)	No of Bulk-carrier Ns	Transport OPEX (USD per year)	Transport CAPEX (USD per year)
1000	5.85	10	1.99×10^7	3.53×10^7
2000	8.49	14	2.90×10^7	5.12×10^7
3000	11.14	19	3.80×10^7	6.72×10^7
4000	13.79	23	4.70×10^7	8.32×10^7
5000	16.43	27	5.60×10^7	9.91×10^7
6000	19.08	32	6.51×10^7	1.15×10^8
7000	21.73	36	7.41×10^7	1.31×10^8
8000	24.37	41	8.31×10^7	1.47×10^8
9000	27.02	45	9.22×10^7	1.63×10^8
10000	29.67	49	1.01×10^8	1.79×10^8

The outlined specifications of the bulk-carrier ship in Table 6.4 is based on design of the Mitsui Engineering & Shipping Co., Ltd Japan (Nakata et al., 2008, Takaoki et al., 2004). Established Panamax cargo ship within similar capacity was assumed in order to estimate the vessel operating cost (Moore and Greiner, 2017). The bulk-carrier, which is usually hired, was also assumed to have installed loading and offloading facilities.

Table 6.4: Cost estimation details for Transportation CAPEX and OPEX

Bulk-carrier ship capacity and operational details	Value
Loading and unloading rate (m^3 hr^{-1})	4167.00
Bulk-carrier speed (km hr^{-1})	31.48
Panamax Bulk-carrier Capacity (275 m Length, 46 m Breadth, 25.5 m Depth) (10000 DWT) (m^3)	160000
Bulk-carrier operating cost, voc (USD/day) for panamax 8 - 15 years old	5678
Bulk-carrier charter cost (USD/day) 2017 index price (Charter for 12 months T&C)	10298

6.4.3 Summary of economic analysis of MHT chain based on small capacity stranded gas

As mentioned earlier the main source of revenue in this project is sales gas from the regasification unit, dehydrated and compressed to typical pipeline quality and conditions. In addition to the comparison of CAPEX and OPEX discussed in previous session, feasibility study using profitability indicator of the MHT was calculated based on the computed net present value (NPV) scenarios. Figure 6.5 shows a log plot of the MHT net present value of the four reserve capacity scenarios over 10000 km end-users' market. The log plot is presented in two compartments indicating positive and negative NPV above and below respectively. Figure 6.5 also reveals that 2.8 – 25.5 bcm over 10,000 km with positive values are feasible project based on the conditions of this study. As expected, the NPV over the 10,000 km market distance decreased for all scenarios, however, very mildly indicating less sensitivity of transport cost. The bulk-carrier ship concept by the MES Ltd (Nakata et al., 2008, Takaoki et al., 2004) and that by Aker Engineering Oslo (collaboration with Norwegian University of Science and Technology) (Gudmundsson and Borrehaug, 1996b) suggest atmospheric pressure and 253 K conditions for the pellets or solid hydrate in the bulk-carrier shipping. This offer less complicated and cost MHT transport compared to LNG and CNG technologies with stringent conditions.

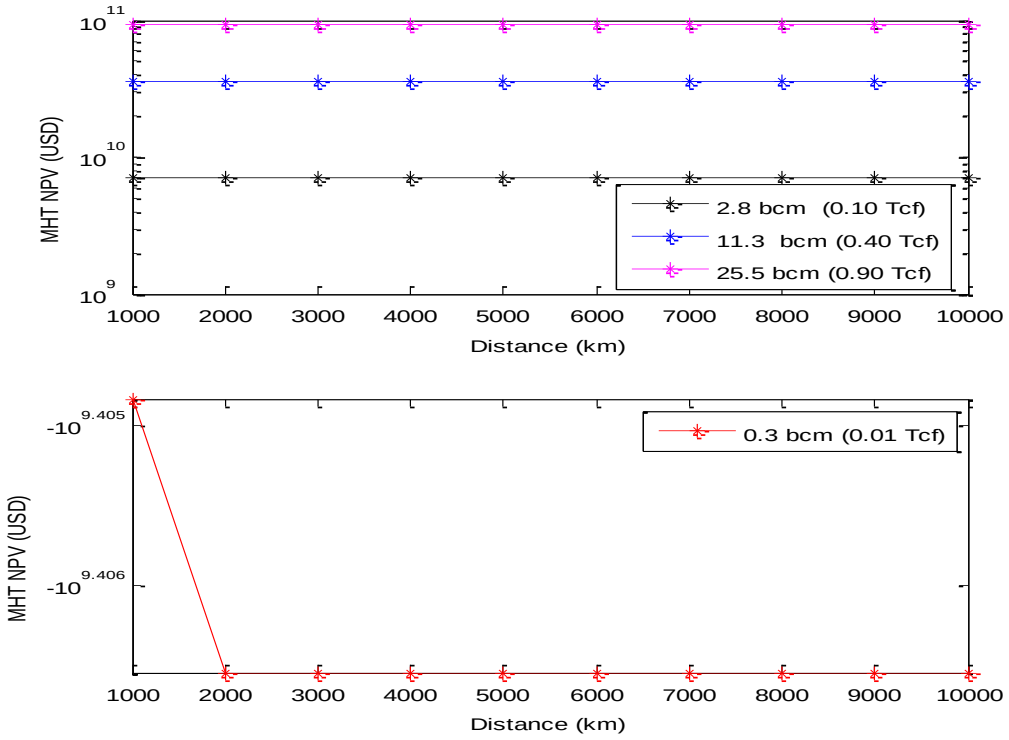

Figure 6.5: MHT NPV for utilization of small-scale capacity reserve over 10,000 km distance

The scenario one having the least reserve volume capacity of 0.3 bcm is indicated not to be profitable with negative NPV. As earlier observed, the decrease in NPV, (-2.5410×10^9 to -2.5468×10^9) between distance of 1000 – 2000 km which is quite minimal was capture as shown in the Figure 6.5. This further suggests relatively less sensitivity to transportation unit cost to the production and regasification cost.

However, it is important to mention that wellhead gas cost and sales gas price variabilities play a core economic role as observed by Khalilpour and Karimi (2012) but this is not with the focus of this study. The point to make here is that the MHT technology could be largely driven by reserve volume capacity rather than market distance for the small-scale stranded natural gas utilization.

6.4.5 Summary of economic analysis of MHT chain based on large capacity stranded gas

The same approach applied for small capacity reserve was employed in the cost estimation and of the major equipment of the MHT chain, which comprised the MH pellet production, sea transportation, and regasification of the produced pellet to sales gas quality after processing.

In the same view the feasibility of MHT for the four-capacity scenarios were examined using the CAPEX and OPEX in addition to profitability indicator NPV presented in Figure 6.6.

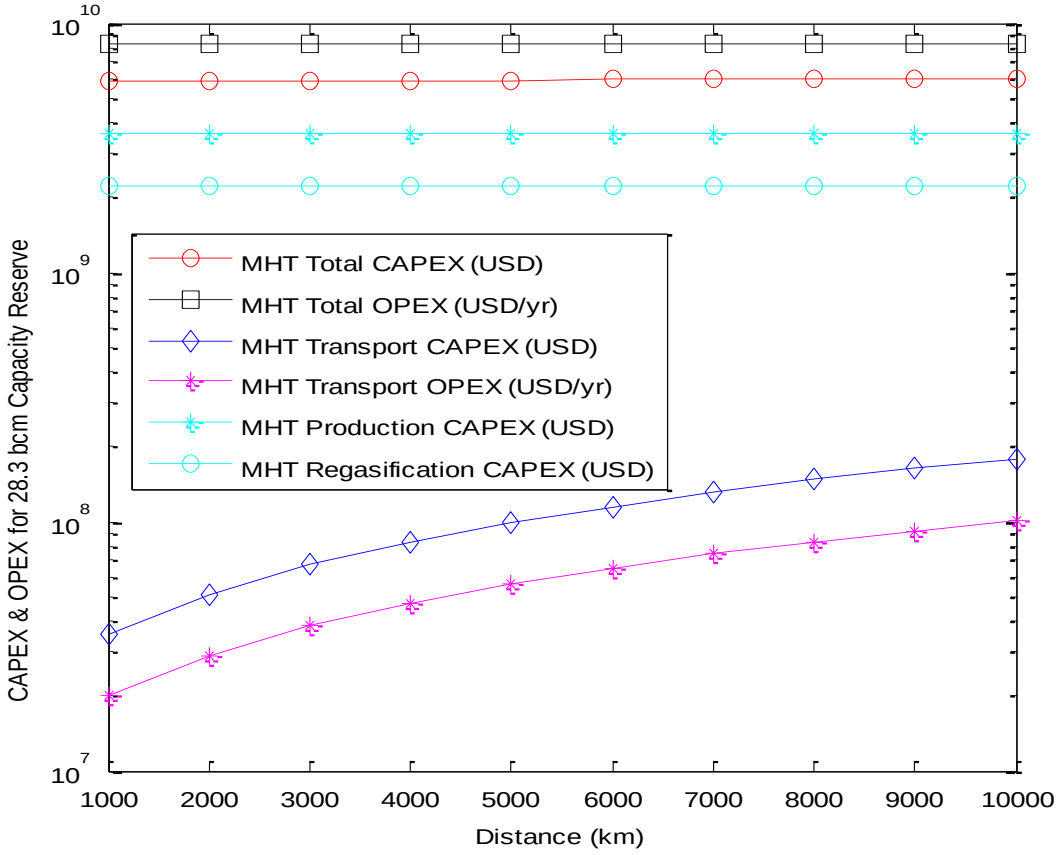

Figure 6.6: CAPEX and OPEX for 28.3 bcm (1.0 Tcf) stranded gas (large capacity reserve)

In Figure 6.6, using the 28.3 bcm (1.0 Tcf) capacity reserve, the total CAPEX and OPEX of the MHT chain are presented as well as that of transport CAPEX and OPEX. The transport CAPEX and OPEX increased with increase in the distance to just about 20 %, which explains the distribution of the total CAPEX and OPEX over the 10,000 km as shown in Figure 6.6. The transport cost inference of the total CAPEX and OPEX shows that production and regasification each contribute more to MHT chain than that of transportation unit cost. The MHT production plant is considered to be capital intensive (Rehder et al., 2012) and even higher due to the pellet processing in addition, for the regasification unit due to the attached dehydration system. This is consistent with the study by Kang et al. (2016) for the production CAPEX but disagree with low transport cost effect to the MHT chain. The MHT total OPEX was also observed to be higher than the CAPEX, which is considered to have been overestimated and could be attributed to the water cost and operating labour estimate and assumptions.

Similarly for the large gas scenario of stranded gas utilization, the same costing protocol as discussed in Section 6.3 was applied, in addition to the profitability indicator to determine the feasibility of the MHT technology for reserve capacities over 10,000 km distance. Figure 6.7 depicts positive NPV for the reserve capacity 28.3 – 566.0 bcm per year, which shows it, is economically feasibility of using MHT for large capacity stranded gas with the conditions of our study.

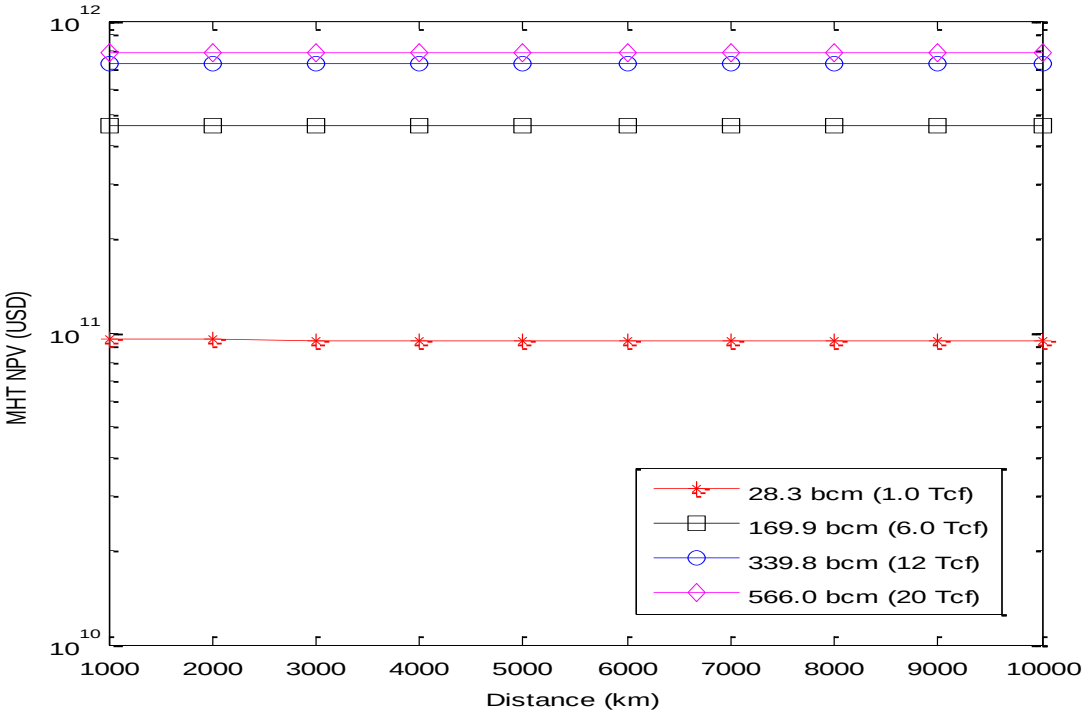

Figure 6.7: MHT NPV for large capacity reserve scenarios

The observed difference between the NPV of the scenarios closing up significantly (with 566.0 and 339.8 bcm closest) not clear but may be attributed to the higher profitability margin of MHT with reserve capacities.

Based on this study results, all the large volume stranded gas capacity reserves (28.3 – 566.0 bcm per year) indicate a positive NPV which implies that MHT is feasible technology for transportation of stranded gas over 10,000 km market distance.

6.5 Economic comparison of stranded gas utilization technologies for large and small-scale capacities: MHT, LNG and CNG case as well as MHT and CNG case

A further investigation on applying the MHT chain for utilizing stranded gas, economic analysis, and comparison with some conventional alternatives was carried out in this study. The obtained cost data for MHT based on the eight considered scenarios were used in this analysis. Among technologies for stranded gas utilization discussed in Chapter 2, LNG and CNG were considered as established options (considering pipeline inaccessible cases), which are significantly influenced by market distance and reservoir capacities (Wood et al., 2008). These were employed for the large-scale capacity scenarios. However, for the small-scale capacity reserves, just the CNG technology was compared. This is because LNG requires large capacities and long-term contracts while CNG technology is largely considered to possess potentials for small capacities stranded gas utilization over small to medium market distances (Davies and Stenning, 2015). About $80-90\%$ of total investment is on the shipping containment, infrastructure and operations, thus, it is highly sensitive to market distance and gas capacity (World Bank, 2015).

Table 6.5 indicates assumptions for the evaluation relating to the production output for the units and sea transportation parameters. We assumed for MHT pellet production that 90 wt % pellets are realized based modelling study of the pilot scale pellet production (Murayama et al., 2011). While for the regasification 99 % gas recovery was assumed (Veluswamy et al., 2018). Production output for LNG and CNG units were based by (Khalilpour and Karimi, 2012).

Table 6.5: Process parameters and considerations for the comparison study

Parameters	MHT pellet	LNG	CNG
Production Output	Production: 0.90 Regasification: 0.99 (Murayama et al., 2011)	Liquefaction: 0.85 Regasification: 0.99 (Khalilpour and Karimi, 2012)	Compression: 0.97 Decompression: 0.99 Khalilpour and Karimi, 2012)
Bulk-carrier speed (km hr^{-1})	31.48 (Takaoki et al., 2004)	33.34 (Songhurst, 2017)	35.19 (Kang et al., 2016)
Loading and unloading ($m^3\,hr^{-1}$)	4.17×10^3 (Kang et al., 2016)	6.67×10^3 (Rogers, 2018)	1.45×10^6 and 4.01×10^5 (Hines, 2011)

Some authors have reported the high significant influence of reserve gas capacities and distance to market parameters to the utilization of stranded gas as an important criterion for selecting adequate method or technology for gas utilization. LNG in Chapter 2 was discussed as relating to high process cost with niche for large-scale natural gas utilization. This is because of the large energy density output associated with liquefying gas to a factor of 600 in volume. Khalilpour and Karimi (2012) in their study developed economic sweet spots for three technologies (LNG, CNG and GTL) using the reservoir capacities and distance to market, highlighting the technoeconomic significance and preference for each of the options in large capacity reserves. Kang et al. (2016) considered small-scale gas capacities for their conceptual economic feasibility study using CAPEX comparison of natural gas hydrate and small-sized LNG over 1500, and 3500 NM market distances. For the GTL technology, although with high energy density and versatile products as well as influenced by field capacity and market distance, are benchmarked on crude oil price for its economic viability (Wood et al., 2012). While, for gas-to-wire (GTW) technology, usually from land-based supply are limited to locations with field proximity for its economic viability.

Therefore, based on the highlighted views in these literatures, economic comparison analysis for MHT and CNG were considered for the small reserve capacity scenarios (scenarios 1 – 4) while MHT, LNG, and CNG were employed for the large reserve capacity (scenarios 5 – 8). The profit evaluation using NPV model was also used as defined in Section 6.3 and cost estimates were carried out using literature while the computations were carried out in HYSYS, Microsoft Excel, and MATLAB.

6.5.1 Comparison of small reserve stranded gas utilization scenario for MHT and CNG

The economic comparison was carried out with the same reserve capacities as well as the same upstream cost as with computed MHT chain NPV in previous section of this chapter.

CNG supply chain comprises of three units, namely compression, transportation, and decompression. CNG ship of 9.91×10^9 m^3 CNG Coselle® technology was considered with estimated at USD 2.56×10^8. The capital and operating costs of compression and decompression units were estimated based on Khalilpour and Karimi (2012) data which was updated to the considered year 2017 and applied relative volumes to the considered reserve capacities (0.3 – 25.2 bcm per year).

Figure 6.8 shows comparison using a log plot of NPV for MHT and CNG which is presented in two boxes indicating positive and negative NPV above and below respectively.

The scenarios $2-4$ comprising of 2.8 to 25.5 bcm reserve capacities with the MHT show positive NPV over the 10000 km market distance. This implies that offers MHT offers a feasible technology for the utilization of stranded natural gas for the considered market distances. The observed advantage for MHT over 10,000 km market distance could be attributed to the earlier highlighted low sensitivity of MHT to transportation cost. However, CNG seems the best alternative for small reserves less than 0.3 bcm (0.01 Tcf) as also shown in Figure 6.8. In addition, positive NPV for 0.3 to 2.8 bcm reserve capacities (scenarios 1 and 2) for CNG over small market distance of 2000 km, as indicated in the findings also show its economic viability.

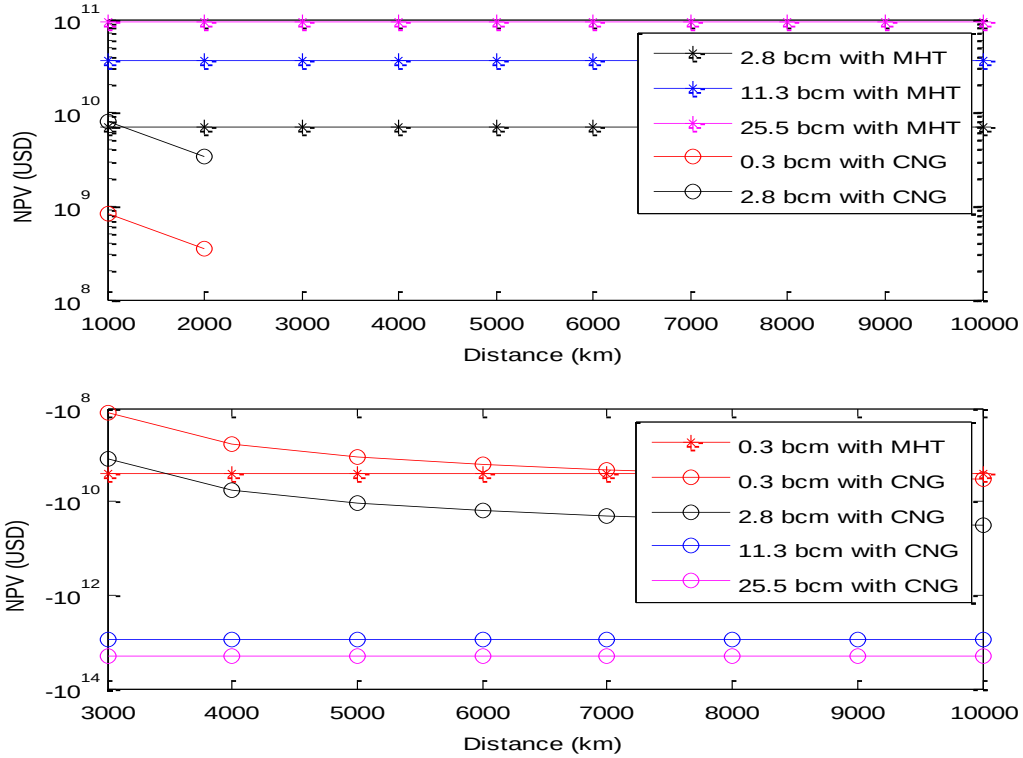

Figure 6.8: Comparison of the NPV of MHT and CNG for 0.3 – 25.6 bcm (0.01-0.9 Tcf) reserve capacities (Small-capacity reserve scenarios)

The obtained results shown in Figure 6.8 align with the findings consistent with (Khalilpour and Karimi, 2012, Economides et al., 2006, Wood et al., 2008) for small capacity reserves over 2000 km distance. Though, for Khalilpour and Karimi (2012), their results based on evaluation of larger reserves (beyond 28.3 bcm), which indicated viability over 2000 km and higher market distances for CNG. This further necessitated the inclusion of CNG in the large capacity scenarios comparison study discussed in next subsection. The obtained CNG result could be attributed to the earlier highlighted point that the CNG ships account for over 85 % of total investment of CNG project (Wood et al., 2008), which implies it is highly sensitive to market distance.

Therefore, according to our findings MHT share the feasibility prospect with CNG for utilizing reserves capacities up to 2.8 bcm. Beyond which the NPV of CNG decreased consistently with market distance and do not seem a viable technology for stranded gas utilization.

6.5.2 Comparison of the large reserve capacity scenarios using MHT, LNG and CNG

LNG and CNG as alternative technologies to MHT for large capacities stranded gas utilization were considered. Similar to the small-scale scenarios, the goal of the comparison was to ascertain the most feasible among the three technologies for utilizing stranded gas at the considered commercial reserve capacities of 28.3 – 566.0 bcm (1.0 – 20 Tcf) over 10,000 km market distance. This will provide useful data for the furtherance of the MHT technology application to commercial utilization of stranded natural gas.

The traditional land-based LNG technology was employed to maintain uniformity with the comparison with MHT and CNG in this study. The LNG technology supply chain comprises of three units, namely liquefaction, transportation, and regasification. For the liquefaction unit, according to the 2017 Oxford Institute for Energy Studies Review study, for 3 MTPA production with 180,000 m^3 storage tank for traditional onshore LNG facility amount to USD 7.50×10^8 (Songhurst, 2017). The cost estimate was updated to the considered year, 2017 and relative volumes to the reserve capacities. The regasification CAPEX was also obtained based on Khalilpour and Karimi (2012). For the transportation, charter rate of 63,000 per day was estimated using Rogers (2018) for short term contracts with 20 years project life. Operating cost for the vessel which includes the crew labour, utilities, and maintenance, etc., was estimated as USD 9,091 per day, Suezmax 8-15 years old (Moore and Greiner, 2017).

For CNG, similar cost estimate as with the previous section using Khalilpour and Karimi (2012) and updated to 2017 and relative volumes to the reserve capacities.

Figure 6.9 shows comparison of NPV for MHT, LNG, and CNG. This is a log plot presented in two boxes indicating all positive MHT NPV values above and below show the NPV for the

CNG and LNG. The scenarios 5 – 8 (28.3 – 556.0 bcm) reserve capacities with the MHT are all to the power of 11 (with 556.0 bcm reserve capacity the highest) show positive NPV throughout the entire market distance range of 10,000 km.

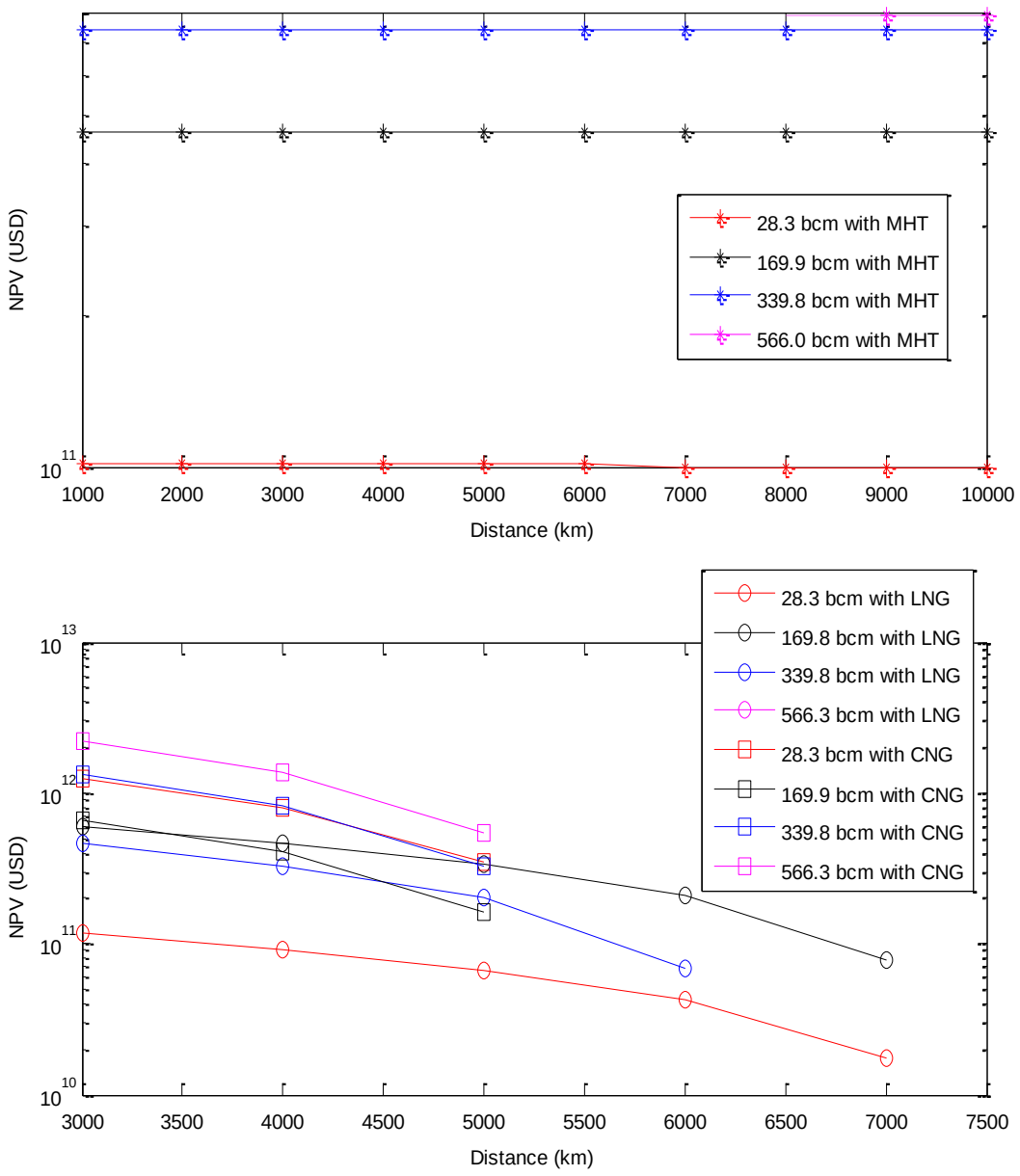

Figure 6.9: Comparison of the NPV of MHT, LNG and CNG for 28.3 – 566.0 bcm (scenario 5–8)) reserve capacities

Figure 6.9 shows that below 5000 km, CNG possess positive NPV for reserve capacities 28.3 – 566 bcm (scenarios 5–8) and can be said to be feasible for the reserve capacities and market distance below 5000 km. As seen also in Figure 6.9, for reserve capacities 28.3 – 169.8 bcm

(scenario 5−6), LNG show positive NPV below 7000 km market distance and for 339.8 bcm (scenario 7) possess positive NPV below 6000 km distance. Whereas, for 566 bcm (scenario 8) show a negative NPV that indicate the LNG seem not feasible for reserve capacity greater than 339.8 bcm.

Therefore, it can be observed from the comparison study that stranded natural gas reserve capacity and market distance have significant influence on the economic viability of the MHT. This further indicates the comparison of the profitability index for the LNG, CNG, and MHT options for transporting large capacity stranded gas resources using NPV. LNG and CNG seems to show advantage over MHT for the utilization of large-scale stranded gas for 28.3 – 339.8 bcm reserve capacities below 7000 km and 5000 km market distance respectively but above 7000 km, MHT seems the best option. In addition, for 566.0 bcm reserve capacity (scenario 8) CNG show advantage over LNG below 5000 km whereas MHT seems the best option above 5000 km market distances. The advantages of MHT over LNG and CNG at stated market distances could be attributed to the lower cost and conditions of MHT ship bulk carriers.

6.6 Concluding remarks

Economic evaluation of the methane hydrate technology for the utilization of stranded gas from small capacity and large capacity reserves was explored using the MHT chain, which comprised of production, transportation, and regasification units.

Net present value was used as a profitability index to analyse the viability of MHT for 0.3−25.5 and 28.3 – 566.0 bcm per year reserve capacities (scenario 1-4 and 5-8 respectively) through 10,000 km market distance, considered as distance from Nigeria offshore to Europe and further to Asia.

The findings of the economic evaluation revealed that MHT possesses best economic viability for utilizing stranded gas for 2.8 – 25.5 bcm per year reserve capacities but do not seem viable for reserve capacities below that for 10,000 km market distance. CNG was observed to be best alternative for small market distance of 2000 km for 0.3 – 2.8 bcm per year reserve capacities. Furthermore, although MHT show feasibility for the utilization of stranded gas for 28.3 – 566.0 bcm reserve capacities for entire 10,000 km market distances, the findings of this study indicate LNG and CNG to have advantages over MHT below 7000 km and 5000 km respectively. As a result, LNG and CNG seem to be the best options for utilizing stranded gas of 28.3 – 339.8 bcm reserve capacities from Nigerian region to Europe (less than 7000 km and 5000 km respectively). Above 339.8 bcm reserve capacities and for longer distance over 5000 km from Nigeria to Asian continent, MHT seems the best option.

Chapter 7 Conclusions and recommendations for future work

This is the final chapter of this thesis, which highlights the major conclusions, findings, and future work recommendations for the utilization of stranded natural gas using methane hydrate technology (MHT) chain under the perspectives of this study.

7.1 Comprehensive conclusion

This thesis evaluates the utilization of stranded natural gas from small and large capacity reserves with the MH pellet technology chain using process simulation and economic investigations of the main MHT units covering production, transportation, and regasification.

The critical role of natural gas utilization as low carbon dioxide emission fuel for global energy demand plus the prospects of methane hydrate technology were observed in the qualitative evaluation and comparison of six typical technologies for stranded NG utilization with focus on developmental stages, process complexity, volume capacity and storage, economic feasibility and environmental and safety merits. Among the six technologies compared, LNG, CNG, GTL, GTW, and pipeline, methane hydrate technology was underlined as primly promising. However, limitations of the developmental stage of MHT in terms of research and commercialization were identified as well as the need to establish its feasibility especially regarding stranded small capacity natural gas reserves utilization.

For the evaluation of the MHT production unit, a methane hydrate pellet production (MHPP) model was developed comprised of reactor and pellet processing system and pellet storage using a pilot-scale system data from the literature. The MHPP reactor model was applied in Aspen HYSYS (version 8.8) showing design implementation of 9.16×10^{-3} m^3 MH slurry production in jacketed continuous stirred tank reactor as a base case simulation using pure methane gas (sI hydrate) and pure water with an empirical methane gas consumption rate equation at 5.4 MPa and 285.15 K. The purpose realised was to obtain data and MH production operation simulation adequate for reactor scale up assumptions. With the MHPP reactor simulation, specifications of 2.4 – 4033.7 kg s^{-1} methane gas hydrate pellets production were achieved for stranded natural gas utilization for 0.3 – 25.5 and 28.3 – 566.0 bcm per year reserve production used to evaluate small and large-scale capacities reserve range respectively. Additionally, the pellet storage vessels were estimated as 3.73×10^{1} – 7.45×10^{4} m^3 for the methane hydrate production in the considered commercial scale scenarios.

It was shown that superficial gas velocity (or gas injection rate into the reactor), stirring rate and pressure in the MHPP reactor increased the methane gas consumption rate while just a slight increase was observed with the subcooling. However, the dissociation enthalpy of

methane hydrate and hydration number were overestimated using equilibrium temperature conditions obtained from HYSYS compared to that in literature. In addition, the sensitivity analysis of the parameters of the MHPP simulation reactor model further confirms that the superficial gas velocity has a significant effect on the gas consumption rate, about double the effect compared to that of either stirring rate or pressure.

Modelling of an optimized dewatering and pelletizing system was based on a piston-cylinder mechanism as the hydrate pellet-processing system model, with implemented constant rate filtration, constant pressure filtration and compression operational stages using pilot scale system data. The result reveals a 90 wt % methane hydrate pellet obtained from processing of 10 wt% methane hydrate slurry.

The transportation unit equations were developed based on consideration of sea transport with computation equations of the required number of ship bulker-carrier trips as well as round trip transport time associated with the MH production capacity and market distance. On which basis, the detailed costing of the MHT offshore/sea transportation was executed.

For the regasification unit, which includes the hydrate solid dissociation, gas dehydration, and compression to sales gas condition, a regasification framework was presented based on literature for the main equipment and utilities required for gas production or recovery from methane hydrate pellet.

Therefore, MHT chain detailed cost estimation protocol and data were presented based on the MHPP, sea transportation, and regasification units for 0.3 - 566.0 bcm per year reserve capacity reserves for the utilization of stranded natural gas from Nigerian Niger-Delta offshore region to Europe and further Asia (10,000 km).

In addition, the economic evaluation revealed that MHT shows best economic viability for utilizing stranded gas for 2.8 – 25.5 bcm per year reserve capacities but do not seem viable for reserve capacities below those reserve capacities for 10,000 km market distance. CNG was observed to be best alternative for small market distance of 2000 km for 0.3 – 2.8 bcm per year reserve capacity. Furthermore, MHT showed feasibility for the utilization of stranded gas for 28.3 – 566.0 bcm reserve capacity for entire 10,000 km market distance but LNG and CNG showed clear advantage over MHT below 7000 km and 5000 km respectively. As a result, LNG and CNG seem to be the best options for utilizing stranded gas of 28.3 – 339.8 bcm reserve capacities from Nigerian region to Europe (less than 7000 km and 5000 km respectively). Above 339.8 bcm reserve capacities and for longer distance over 5000 km from Nigeria to Asian continent as specified in this study, MHT seems the best option.

7.2 Future research recommendations

One key challenge for the industrial development of gas hydrate technology is the low rate of gas hydrate formation. Several experimental studies have been reported which use promoters to increase the rate of formation. Therefore, large-scale studies on gas hydrate formation with promoters such as tetrahydrofuran (THF) are recommended to try to understand the associated environmental implications of their use at commercial scale.

For better research clarity and progress in commercializing the application of gas hydrate technology as stranded natural gas utilization technology, future studies are recommended into the natural gas self-preservation phenomenon using mixed mixtures of gas component such as C_{1+} hydrocarbons. Self-preservation of hydrates is not yet clearly established in literature for sII hydrates, which are a key aspect of hydrate-based gas transportation technology as it sustains hydrate pellets at atmospheric pressure and temperature of 253 K as well as offers safety advantages compared to other natural gas utilization options. However, without this, a high cost pre-processing could be required, which might render MHT non-feasible depending on the reserve capacity and transport distance. This study considered the use of methane gas, pre-processed to pure methane gas for the utilization of natural gas. Further study is recommended with access to requisite data of different gas reserves, which can be used to define the pre-processing explicitly considering that natural gas reserves have different NG compositions. An observed limitation this study was the assumption of a unified upstream capital cost across board all the scenarios and technologies with it considered to include facilities including wells, platform, pre-processing, and pipeline. This assumption was made because it was not possible to obtain sensitive commercial data for specified reserve capacity volumes and as such, the recommended future study is considered an adequate furtherance in this research study.

Furthermore, in this study, land-based MHT plant was considered in uniformity with the conventional LNG and CNG technologies used for comparison. However, the author recommends that future research be carried out, exploring the feasibility of gas hydrate technology on a floating ship vessel for the utilization of stranded gas. This if considered might be useful in ascertaining the overall economic advantage especially for offshore small-scale reserve capacities.

Another aspect that is out of scope of this study that is recommended for future study is to incorporate a stochastic model that will factor in gas price variability in the economic evaluation of gas hydrate. Since several other volatile commercial variables such as regional and local gas prices, petroleum products prices (which compete for market), and regional risk factors which may significantly affect the decision of technologies for the utilization stranded gas.

It was intended in this study to compare the MHT evaluation for stranded gas utilization with the intensified gas to liquid technology (GTL), but this was constrained by difficulties in obtaining sensitive commercial company data. Therefore, it is recommended that future study be carried out to evaluate and compare MHT chain with intensified GTL to ascertain the preferred option for stranded gas utilization particularly for small-scale reserves considering the advantage of varied products and higher energy density of GTL fuel.

In this research, an optimized pilot scale gas hydrate filtration and pelletization processing system developed by Mitsui Engineering & Shipping, Japan was identified and used as basis for the modelling of the methane hydrate slurry processing. However, future study is recommended towards commercial scale capacity of the system and scale-up protocol for the hydrate slurry processing pellet machine. In this study, due to insufficient operational data of the pellet machine in literature, scale-up could not be carried out and led to the application of multiple pilot scale model units in estimating the cost. Future study on the design and operation of the large cylindrical chamber and the filtration zone as well as the compression operation based on the piston mechanism is therefore recommended. As noted, the scale up studies in addition will be useful in obtaining data for further clarity of the gas hydrate slurry processing costing for better comparison of MHT with other alternative technologies for the utilization of stranded natural gas.

The regasification unit of the methane gas hydrate is also recommended for research exploration at commercial scale. Experimental studies using thermal stimulation method is recommended to study the effects of water temperature, flow rate, and gas recovery rate relative to specified regasification vessel capacity and the pellets properties.

The result from the small-scale reserve study showed sweet spot for CNG that indicate feasibility for only scenarios 1 and 2 (0.3 and 2.8 bcm reserve capacity) within 2000 km which agrees with literature. However, some contractions exist relating to reserve capacities beyond 2.8 bcm for which MHT NPV indicate as the best option. Therefore, further evaluations for MHT and CNG are recommended covering lower reserve capacities and extended range of reserve capacities and market distance. This forms part of the current studies of the author for a paper publication.

Reference

ALAM, M., ABEDI, V., BASSAGANYA-RIERA, J., WENDELSDORF, K., BISSET, K., DENG, X., EUBANK, S., HONTECILLAS, R., HOOPS, S. & MARATHE, M. 2016. Chapter 6 - Agent-Based Modeling and High Performance Computing. *In:* BASSAGANYA-RIERA, J. (ed.) *Computational Immunology*. Academic Press.

ANDERSSON, V. & GUDMUNDSSON, J. S. 1999. Flow Experiments on Concentrated Hydrate Slurries. Society of Petroleum Engineers.

ANDERSSON, V. & GUDMUNDSSON, J. S. 2000. Flow properties of hydrate-in-water slurries. *Annals of the New York Academy of Sciences.*

ANGAYS, P., GUILHEM, J. C. & ARJONA, J. Monetization of associated gases from offshore oil fields by electrical power generation. PCIC Europe (PCIC EUROPE), 2013 Conference Record, 28-30 May 2013 2013. 1-9.

ANOSIKE, B. N. 2013. Production History Variation Based Probabilistic Simulation Analysis of Gas-to-Wire Monetisation of Associated Natural Gas. Accessed from: http://www.palisade.com/downloads/UserConf/EU13/London/2013PalisadeLondonConf_NBAnosike_CranfieldUniversity.pdf (June 2014).

ARJMANDI, M., TOHIDI, B., DANESH, A. & TODD, A. C. 2005. Is subcooling the right driving force for testing low-dosage hydrate inhibitors? *Chemical Engineering Science,* 60**,** 1313-1321.

ATTANASI, E. D. & FREEMAN, P. 2012. Role of Stranded Gas From Central Asia, Russia, Southeast Asia, and Australia in Meeting Asia. *SPE Hydrocarbon Economics and Evaluation Symposium.* Calgary, Alberta, Canada: Society of Petroleum Engineers.

AZARINEZHAD, R., VALKO, I., CHAPOY, A. & TOHIDI, B. 2008. Can Gas Hydrates Provide a Solution to Gas Utilisation Challenges in Russian Oil Fields? *SPE Russian Oil and Gas Technical Conference and Exhibition.* Moscow, Russia: Society of Petroleum Engineers.

BABU, P., LINGA, P., KUMAR, R. & ENGLEZOS, P. 2015. A review of the hydrate based gas separation (HBGS) process for carbon dioxide pre-combustion capture. *Energy,* 85**,** 261-279.

BALLARD, A. L. & SLOAN, E. D. 2002. The Next Generation of Hydrate Prediction: An Overview. *Journal of Supramolecular Chemistry,* 2**,** 385-392.

BALLARD, A. L. & SLOAN, E. D. 2004. The next generation of hydrate prediction: Part III. Gibbs energy minimization formalism. *Fluid Phase Equilibria,* 218**,** 15-31.

BATES, R. L., FONDY, P. L. & CORPSTEIN, R. R. 1963. Examination of Some Geometric Parameters of Impeller Power. *Industrial & Engineering Chemistry Process Design and Development,* 2**,** 310-314.

BBOSA, B., OZBAYOGLU, E. & VOLK, M. 2018. Experimental investigation of hydrate formation, plugging and flow properties using a high-pressure viscometer with helical impeller. *Journal of Petroleum Exploration and Production Technology*.

BERGERON, S., BELTRÁN, J. G. & SERVIO, P. 2010. Reaction rate constant of methane clathrate formation. *Fuel,* 89**,** 294-301.

BISHNOI, P. R., GUPTA, A. K., ENGLEZOS, P. & KALOGERAKIS, N. 1989. Multiphase equilibrium flash calculations for systems containing gas hydrates. *Fluid Phase Equilibria,* 53**,** 97-104.

BISHNOI, P. R. & NATARAJAN, V. 1996. Formation and decomposition of gas hydrates. *Fluid Phase Equilibria,* 117**,** 168-177.

BORTNOWSKA, M. 2009. Development of New Technologies for Shipping Natural Gas by Sea Accessed from: https://www.degruyter.com/downloadpdf/j/pomr.2009.16.issue-3/v10012-008-0036-2/v10012-008-0036-2.pdf (Dec., 2018): Polish Maritime Research.

BP 2018a. BP Energy Outlook 2018. Accessed from: https://www.bp.com/en/global/corporate/energy-economics/statistical-review-of-world-energy/natural-gas.html (October,2018): BP p.l.c.

BP 2018b. Natural gas - BP Statistical Review of World Energy 2018. 67th edition ed. Accessed from:https://www.bp.com/content/dam/bp/en/corporate/pdf/energy-economics/statistical-review/bp-stats-review-2018-natural-gas.pdf (October,2018): BP.

CADY, G. H. 1983a. Composition of clathrate gas hydrates of hydrogen sulfide, xenon, sulfur dioxide, chlorine, chloromethane, bromomethane, difluorochloromethane, difluorodichloromethane, and propane. *The Journal of Physical Chemistry,* 87**,** 4437-4441.

CADY, G. H. 1983b. Composition of gas hydrates. New answers to an old problem. *Journal of Chemical Education,* 60**,** 915.

CALL, R., CARBON, E. & DELGADO, J. 2008. Technology Evaluation Methodology For Stranded Gas Monetization Options. World Petroleum Congress.

CARROLL, J. 2014. Natural Gas Hydrates - A Guide for Engineers (3rd Edition). Gulf Professional Publishing: Elsevier Inc.

CHABRELIE, M. & ROJEY, A. 2000. Prospects for Exploiting Stranded Gas Reserves. *GasTech* Houston USA: Accessed from: http://www.ivt.ntnu.no/ept/fag/tep4215/innhold/LNG%20Conferences/2000/Data/Papers/Chabrelie.pdf (November, 2014).

CHANDRA, V. 2006a. 1.1 Introduction. *Fundamentals of Natural Gas - An International Perspective.* PennWell.

CHANDRA, V. 2006b. Introduction. *Fundamentals of Natural Gas - An International Perspective.* PennWell.

CHONG, Z. R., YANG, S. H. B., BABU, P., LINGA, P. & LI, X.-S. 2016. Review of natural gas hydrates as an energy resource: Prospects and challenges. *Applied Energy,* 162**,** 1633-1652.

CHOPEY, N. P. 2004. *Handbook of chemical engineering calculations,* New York, New York : McGraw-Hill.

CIA 2017. Natural Gas - Proven Reserves *In:* US, C. I. A. (ed.). Accessed from: https://www.cia.gov/library/publications/the-world-factbook/rankorder/2253rank.html (September, 2018): THE WORLD FACTBOOK.

COKER, A. K. 2007. Mixing of Liquids. *Ludwig's Applied Process Design for Chemical and Petrochemical Plants, Volume 1 (4th Edition).* Elsevier.

COKER, A. K. & KAYODE, C. A. 2001. Chapter Seven - Fluid Mixing in Reactors. *Modeling of Chemical Kinetics and Reactor Design.* Woburn: Gulf Professional Publishing.

D. SLOAN, E. 1990. *Natural Gas Hydrate Phase Equilibria and Kinetics : Understanding the State-Of-The-Art,* Oil & Gas Science and Technology-revue De L Institut Francais Du Petrole.

DAVARNEJADA, R., AZIZIA, J. & AZIZIB, J. 2014. Prediction of Gas Hydrate Formation using HYSYS Software. *International Journal of Engineering,* 27**,** 1325-1330.

DAVIDSON, D. W., DESANDO, M. A., GOUGH, S. R., HANDA, Y. P., RATCLIFFE, C. I., RIPMEESTER, J. A. & TSE, J. S. Some Physical and Thermophysical Properties of Clathrate Hydrates. *In:* ATWOOD, J. L. & DAVIES, J. E. D., eds. Inclusion Phenomena in Inorganic, Organic, and Organometallic Hosts, 1987// 1987 Dordrecht. Springer Netherlands, 219-223.

DAVIDSON, D. W., GARG, S. K., GOUGH, S. R., HANDA, Y. P., RATCLIFFE, C. I., RIPMEESTER, J. A., TSE, J. S. & LAWSON, W. F. 1986. Laboratory analysis of a naturally occurring gas hydrate from sediment of the Gulf of Mexico. *Geochimica et Cosmochimica Acta,* 50**,** 619-623.

DAVIES, S. & STENNING, D. A contemporary examination of stranded gas and monetization strategies with floating CNG. Proceedings of the Annual Offshore Technology Conference, 2015. 4206-4218.

DAWE, R. A., THOMAS, S. & KROMAH, M. 2003. Hydrate Technology for Transporting Natural Gas. *Engineering Journal of the University of Qatar,* 16**,** pp.11-18.

DEMIRBAS, A. 2010a. Methane hydrates as potential energy resource: Part 2 – Methane production processes from gas hydrates. *Energy Conversion and Management,* 51**,** 1562-1571.

DEMIRBAS, A. 2010b. Processes for Methane Production from Gas Hydrates. *Methane Gas Hydrate.* London: Springer London.

DICKSON, W., OGOLO, F. & DELBIANCO, A. 2015. Project Options to Monetize Stranded Gas. *Offshore Mediterranean Conference and Exhibition.* Ravenna, Italy: Offshore Mediterranean Conference.

DOE, U. S. 2017. Understanding Natural Gas and LNG Options. Accessed from: https://www.energy.gov/sites/prod/files/2017/09/f36/Understanding%20Natural%20Gas%20and%20Lng%20Options_general%20no%20appendix.pdf (October, 2018): United State Department of Energy.

DORAN, P. M. 2013a. Chapter 8 - Mixing. *In:* DORAN, P. M. (ed.) *Bioprocess Engineering Principles (Second Edition).* London: Academic Press.

DORAN, P. M. 2013b. *Chapter 8: Mixing*.

DRY, M. E. 1996. Practical and theoretical aspect of the catalytic Fischer-Tropsch process. *Applied Catalysis A: General,* 138**,** pp 319 - 344.

DUAN, Z., LI, D., CHEN, Y. & SUN, R. 2011. The influence of temperature, pressure, salinity and capillary force on the formation of methane hydrate. *Geoscience Frontiers,* 2**,** 125-135.

DURHAM, W. B., STERN, L. A. & KIRBY, S. H. 2003. Ductile flow of methane hydrate *Canadian Journal of Physics,* 81**,** 373-380.

ECONOMIDES, M. J. 2005a. The Economics of Gas to Liquids Compared to Liquefied Natural Gas. *World Energy,* 8.

ECONOMIDES, M. J. 2005b. The Economics of Gas to Liquids Compared to Liquid Natural Gas. *World Energy*.

ECONOMIDES, M. J., KAI, S. & SUBERO, G. Compressed natural gas (CNG): An alternative to liquid natural gas (LNG). 2005 SPE Asia Pacific Oil and Gas Conference and Exhibition - Proceedings, 2005 Jakarta. 9-15.

ECONOMIDES, M. J., SUN, K. & SUBERO, G. 2006. Compressed natural gas (CNG): an alternative to liquefied natural gas (LNG). *SPE* SPE Asia Pacific Oil and Gas Conference Jakarta 2005: SPE Production & Operations

EIA. 2016. *Nigeria* [Online]. Accessed from https://www.eia.gov/beta/international/analysis.php?iso=NGA (Feb, 2019): U.S. Energy Information Administration. [Accessed Feb. 2019].

EIA 2017. NATURAL GAS. Accessed from: https://www.eia.gov/outlooks/steo/report/natgas.php (Aug., 2019): US Energy Information Administration.

EIA 2018. Annual energy outlook 2018: with projections to 2050. *In:* (2018), U. S. D. O. E. (ed.). Accessed from: https://www.eia.gov/outlooks/aeo/pdf/AEO2018.pdf (October, 2018): Energy information administration.

EKEJIUBA, A. I. 2017. Real- Time Monetization of the Flared Associated Stranded Natural Gas in Nigeria: Quantitative Analysis and Qualitative Values. *The International Journal Of Science & Technoledge* 5**,** 89-103.

ENGLEZOS, P. 1993. Clathrate hydrates. *Industrial & Engineering Chemistry Research,* 32**,** 1251-1274.

ENGLEZOS, P., KALOGERAKIS, N. & BISHNOI, P. R. 1990. Formation and decomposition of gas hydrates of natural gas components. *Journal of inclusion phenomena and molecular recognition in chemistry,* 8**,** 89-101.

ENGLEZOS, P., KALOGERAKIS, N., DHOLABHAI, P. D. & BISHNOI, P. R. 1987a. Kinetics of Formation of Methane and Ethane Gas Hydrates. *Chem. Eng. Sci.,* 42**,** 2647-2658.

ENGLEZOS, P., KALOGERAKIS, N., DHOLABHAI, P. D. & BISHNOI, P. R. 1987b. Kinetics of gas hydrate formation from mixtures of methane and ethane. *Chemical Engineering Science,* 42**,** 2659-2666.

ESLAMIMANESH, A., MOHAMMADI, A. H., RICHON, D., NAIDOO, P. & RAMJUGERNATH, D. 2012. Application of gas hydrate formation in separation processes: A review of experimental studies. *The Journal of Chemical Thermodynamics,* 46**,** 62-71.

EVANGELISTA, J. J., KATZ, S. & SHINNAR, R. 1969. Scale-up criteria for stirred tank reactors. *AIChE Journal,* 15**,** 843-853.

FALENTY, A., KUHS, W. F., GLOCKZIN, M. & REHDER, G. 2014. "self-preservation" of CH4 hydrates for gas transport technology: Pressure-temperature dependence and ice microstructures. *Energy and Fuels,* 28**,** 6275-6283.

FARIAS, F. R. C., SILVA, F. R. C., CARTAXO, S. J. M., FERNANDES, F. A. N. & SALES, F. G. 2007. Effect of Operating Conditions on Fischer-Tropsch Liquid Products. *Latin American Applied Research,* 37**,** 283-287.

FITZGERALD, A. & TAYLOR, M. 2001. Offshore Gas-To-Solids Technology. Society of Petroleum Engineers.

FOGLER, S. H. 2016. *Elements of chemical Reaction Engineering* United States of America, Pearson Education Inc.

FREER, E. M., SAMI SELIM, M. & DENDY SLOAN, E. 2001. Methane hydrate film growth kinetics. *Fluid Phase Equilibria,* 185**,** 65-75.

GADDIS, D., BROCK, H. & BOYNTON, C. 1992. PROS, CONS OF TECHNIQUES USED TO CALCULATE OIL, GAS FINDING COSTS. *Oil & Gas Journal.* Accessed from: https://www.ogj.com/articles/print/volume-90/issue-22/in-this-issue/exploration/pros-cons-of-techniques-used-to-calculate-oil-gas-finding-costs.html (March, 2018): Oil & Gas Journal.

GELVES-ZAMBRANO, G. R., LÓPEZ, L. C. & PEÑUELA, M. 2016. Improving of gas-liquid mass transfer in a Stirred Tank Bioreactor: A CFD Approach *International Journal of Applied Engineering Research,* 11**,** pp 6097-6108

GNANENDRAN, N. & AMIN, R. 2004. Modelling hydrate formation kinetics of a hydrate promoter–water–natural gas system in a semi-batch spray reactor. *Chemical Engineering Science,* 59**,** 3849-3863.

GOEL, N. 2006. In situ methane hydrate dissociation with carbon dioxide sequestration: Current knowledge and issues. *Journal of Petroleum Science and Engineering,* 51**,** 169-184.

GUDMUNDSSON, J. & BORREHAUG, A. 1996a. *Natural gas hydrate - An alternative to liquefied natural gas?*

GUDMUNDSSON, J. S. 1994. *Method for production of gas hydrates for transportation and storage*. United States patent application.

GUDMUNDSSON, J. S. 1996a. Method for production of gas hydrates for transportation and storage. Google Patents.

GUDMUNDSSON, J. S. 1996b. Natural Gas Hydrate an Alternative to Liquified Natural Gas. Accessed from: http://www.ipt.ntnu.no/~ngh/library/paper2.html (March, 2016): Norwegian University of Science and Technology Trondheim, Norway.

GUDMUNDSSON, J. S., ANDERSSON, V., DURGUT, I., LEVIK, O. I. & MORK, M. NGH on FPSO - slurry process and cost estimate. 1999 Houston, TX, USA. Soc Pet Eng (SPE), PI/.

GUDMUNDSSON, J. S., ANDERSSON, V., LEVIK, O. I. & PARLAKTUNA, M. Hydrate concept for capturing associated gas. Proceedings of the European Petroleum Conference, 1998. 247-253.

GUDMUNDSSON, J. S. & BORREHAUG, A. 1996b. Frozen Hydrate for Transport of natural gas. *2nd International Conference on Natural Gas Hydrates.* Toulouse, France: Accessed from: www.ipt.ntnu.no/~ngh/paper4/paper4.html (Feb. 2014).

GUDMUNDSSON, J. S. & GRAFF, O. F. 2003. HYDRATE NON-PIPELINE TECHNOLOGY FOR TRANSPORT OF NATURAL GAS Accessed from: http://members.igu.org/html/wgc2003/WGC_pdffiles/10056_1046347297_14776_1.pdf (Sept, 2016): Norwegian University of Science and Technology

GUDMUNDSSON, J. S., HVEDING, F. & BØRREHAUG, A. 1995. Transport Or Natural Gas As Frozen Hydrate. *The Fifth International Offshore and Polar Engineering Conference.* The Hague, The Netherlands: International Society of Offshore and Polar Engineers.

GUDMUNDSSON, J. S., PARLAKTUNA, M., LEVIK, O. I. & ANDERSSON, V. 2000. Laboratory for Continuous Production of Natural Gas Hydrates. *Annals of the New York Academy of Sciences,* 912**,** 851-858.

GUPTA, A., DEC, S. F., KOH, C. A. & SLOAN, E. D. 2007. NMR Investigation of Methane Hydrate Dissociation. *The Journal of Physical Chemistry C,* 111**,** 2341-2346.

GUPTA, A. K., RAJ BISHNOI, P. & KALOGERAKIS, N. 1991. A method for the simultaneous phase equilibria and stability calculations for multiphase reacting and non-reacting systems. *Fluid Phase Equilibria,* 63**,** 65-89.

H. VAN DER WAALS, J. & C. PLATTEEUW, J. 1959. Clathrate Solutions.

HAMMERSCHMIDT, E. G. 1934. Formation of Gas Hydrates in Natural Gas Transmission Lines. *Industrial & Engineering Chemistry,* 26**,** 851-855.

HANDA, Y. P. 1986a. Calorimetric determinations of the compositions, enthalpies of dissociation, and heat capacities in the range 85 to 270 K for clathrate hydrates of xenon and krypton. *The Journal of Chemical Thermodynamics,* 18**,** 891-902.

HANDA, Y. P. 1986b. Calorimetric Studies of Laboratory Synthesized and Naturally Occurring GasCalorimetric Studies of Laboratory Synthesized and Naturally Occurring Gas. *AIChE Annual Meeting* Miami Beach: AIChE.

HANDA, Y. P. 1986c. Compositions, enthalpies of dissociation, and heat capacities in the range 85 to 270 K for clathrate hydrates of methane, ethane, and propane, and enthalpy of dissociation of isobutane hydrate, as determined by a heat-flow calorimeter. *The Journal of Chemical Thermodynamics,* 18**,** 915-921.

HAPPEL, J., HNATOW, M. A. & MEYER, H. 1994. The Study of Separation of Nitrogen from Methane by Hydrate Formation Using a Novel Apparatus. *Annals of the New York Academy of Sciences* 715**,** 412–424.

HASAN, M. M. F., ZHENG, A. M. & KARIMI, I. A. 2009. Minimizing boil-off losses in liquefied natural gas transportation. *Industrial and Engineering Chemistry Research,* 48**,** 9571-9580.

HASHEMI, S., MACCHI, A. & SERVIO, P. 2009. Dynamic Simulation of Gas Hydrate Formation in a Three-Phase Slurry Reactor. *Industrial & Engineering Chemistry Research,* 48**,** 6983-6991.

HERRI, J. M., PIC, J. S., GRUY, F. & COURNIL, M. 1999. Methane hydrate crystallization mechanism from in-situ particle sizing. *AIChE Journal,* 45**,** 590-602.

HINES, L. 2011. CNG Developer Sea NG Costs Out Offshore Solution. Accessed from: http://www.coselle.com/resources/news/cng-developer-sea-ng-costs-out-offshore-solution (July 2014): SEA NG.

HOFFMANN, J. 2017. The Review of Marine Transport *In:* DEVELOPMENT, U. N. C. O. T. A. (ed.). Accessed from: http://unctad.org/en/PublicationsLibrary/rmt2017_en.pdf (Feb., 2018): UNITED NATIONS PUBLICATION, GENEVA.

HOLDER, G. D., ZETTS, S. P. & PRADHAN, N. 1988a. Phase behavior in systems containing clathrate hydrates: A review. *Reviews in Chemical Engineering,* 5**,** 1-70.

HOLDER, G. D., ZETTS, S. P. & PRADHAN, N. 1988b. Phase behavior in systems containing clathrate hydrates: A review. *Reviews in Chemical Engineering,* 5**,** 199-204.

HOLDICH, R. G. 2002. Fundamentals of Particle Technology. Accessed from: http://particles.org.uk/particle_technology_book/particle_book.htm (July 2017): Midland Information Technology and Publishing, UK.

IGU 2018. 2018 World LNG Report. *27th World Conference Edition* Accessed from: https://www.igu.org/sites/default/files/node-document-field_file/IGU_LNG_2018_0.pdf (October, 2018): Internation Gas Union.

INSTITUTIONAL ANALYST INC 2018. Stranded Gas. Learn This Term. Accessed from: http://alternativeenergystockreview.ning.com/profiles/blogs/stranded-gas-learn-this-term (October, 2018): Institutional Analyst Inc.

ISTOMIN, V. A., YAKUSHEV, V. S. & MAKHONINA, N. A. 2006. The self-preservation phenomenon of gas hydrates. *Digest "Gas Industry of Russia"* Digest "Gas Industry of Russia"

JADHAWAR, P., YANG, J., JADHAWAR, J. & TOHIDI, B. Preliminary experimental investigationon replacing methane in hydrate structure with carbon dioxide in porous media 5th International Conference on Gas Hydrates, 2005 Trondheim, Norway.

JAVANMARDI, J., NASRIFAR, K., MOSHFEGHIAN, M. & NAJIBI, H. 2005. Natural Gas Transportation, NGH Or LNG. World Petroleum Congress.

JEZARD, A. 2017. Fossil fuels will still dominate energy in 20 years despite green power rising. Accessed from: https://www.weforum.org/agenda/2017/10/fossil-fuels-will-dominate-energy-in-2040/ (October, 2018): World Economic Forum.

KAMATH, V. A. & HOLDER, G. D. 1987. Dissociation heat transfer characteristics of methane hydrates. *AIChE Journal,* 33**,** 347-350.

KAMATH, V. A., HOLDER, G. D. & ANGERT, P. F. 1984. Three phase interfacial heat transfer during the dissociation of propane hydrates. *Chemical Engineering Science,* 39**,** 1435-1442.

KANDA, H. Economic study on natural gas transportation with natural gas hydrate (NGH) pellets. International Gas Union World Gas Conference Papers, 2006. 1990-2000.

KANG, H. J., YANG, Y., KI, M. S., SHIN, M. S., CHOI, J., CHA, J. H. & LEE, D. 2016. A concept study for cost effective NGH mid-stream supply chain establishing strategies. *Ocean Engineering,* 113**,** 162-173.

KANG, K. C., LINGA, P., PARK, K. N., CHOI, S. J. & LEE, J. D. 2014. Seawater desalination by gas hydrate process and removal characteristics of dissolved ions (Na+, K+, Mg 2+, Ca 2+, B 3+, Cl–, SO 4 2−). *Desalination,* 353**,** 90.

KARAASLAN, U. & PARLAKTUNA, M. 2000. Surfactants as Hydrate Promoters? *Energy Fuels,* 14**,** 1107.

KASHCHIEV, D. & FIROOZABADI, A. 2002. Driving force for crystallization of gas hydrates. *Journal of Crystal Growth,* 241**,** 220-230.

KE, W. & SVARTAAS, T. 2013. Effects of Stirring and Cooling on Methane Hydrate Formation in a High Pressure Isochoric Cell. *Materials Science and Engineering B,* 3**,** 436-444.

KE, W., SVARTAAS, T. M. & CHEN, D. 2019. A review of gas hydrate nucleation theories and growth models. *Journal of Natural Gas Science and Engineering,* 61**,** 169-196.

KESZEI, E. 2012. *Chemical Thermodynamics: An Introduction,* Springer-Verlag Berlin Heidelberg Springer

KHALILPOUR, R. & KARIMI, A. I. 2009. Evaluation of LNG, CNG, GTL and NGH for Monetization of Stranded Associated Gas with the Incentive of Carbon Credit. *International Petroleum Technology Conference.* Doha, Qatar: International Petroleum Technology Conference.

KHALILPOUR, R. & KARIMI, I. A. 2010. Evaluation of LNG, CNG, GTL, and NGHs for monetization of stranded gas. *JPT, Journal of Petroleum Technology,* 62**,** 61-62.

KHALILPOUR, R. & KARIMI, I. A. 2012. Evaluation of utilization alternatives for stranded natural gas. *Energy,* 40**,** 317-328.

KHAN, M. N., WARRIER, P., PETERS, C. J. & KOH, C. A. 2016. Review of vapor-liquid equilibria of gas hydrate formers and phase equilibria of hydrates. *Journal of Natural Gas Science and Engineering,* 35**,** 1388-1404.

KHAN, M. N., WARRIER, P., PETERS, C. J. & KOH, C. A. 2018. Advancements in hydrate phase equilibria and modeling of gas hydrates systems. *Fluid Phase Equilibria,* 463**,** 48-61.

KIDNAY, A. J., PARRISH, W. R. & MCCARTNEY, D. G. 2011. *Fundamentals of Natural Gas Processing,* United States of America, CRC Press Taylor & Francis Group.

KIM, H. C., BISHNOI, P. R., HEIDEMANN, R. A. & RIZVI, S. S. H. 1987. Kinetics of methane hydrate decomposition. *Chemical Engineering Science,* 42**,** 1645-1653.

KING, A., HENLEY, B. & HAWKINS, E. 2017. What is a pre-industrial climate and why does it matter? *The Conversation.* Accessed from: https://theconversation.com/what-is-a-pre-industrial-climate-and-why-does-it-matter-78601 (October, 2018): The Conversation.

KNOX, W. G., HESS, M., JONES, G. E. & SMITH, H. B., CHEM. ENG. PROG. 57 (2) () 1961. The hydrate process. *Chemical engineering progress,* 57**,** 66–71.

KOH, C. A. 2002. Towards a fundamental understanding of natural gas hydrates. *Chem. Soc. Rev.,* 31**,** 167.

KOH, C. A., SLOAN, E. D., SUM, A. K. & WU, D., T. 2011. Fundamentals and Applications of Gas Hydrates. *Annual Review of Chemical and Biomolecular Engineering,* 2**,** 237-257.

KOJIMA, M. 1999. Commercialization of Marginal Gas Fields. *Energy Issues* [Online].

KOORTZEN, J. G., BAINS, S., KOCHER, L. L., BAXTER, I. K. & MORGAN, R. A. 2013. Modular Gas-to-Liquid: Converting a Liability into Economic Value. *Industrial & Engineering Chemistry Research,* 53**,** 1720-1726.

KUHS, W. F., GENOV, G., STAYKOVA, D. K. & HANSEN, T. 2004. Ice perfection and onset of anomalous preservation of gas hydrates. *Physical Chemistry Chemical Physics,* 6**,** 4917-4920.

KUMAR, A., SAKPAL, T., LINGA, P. & KUMAR, R. 2015. Enhanced carbon dioxide hydrate formation kinetics in a fixed bed reactor filled with metallic packing. *Chemical Engineering Science,* 122**,** 78-85.

LEE HUEN, YOUNGJUNE PARK, MINJUN CHA, JONG-HO CHA, KYUCHUL SHIN, KEUN-PIL PARK, DAE-GEE HUH, HO-YOUNG LEE, SE-JOON KIM & LEE, J. SWAPPING CARBON DIOXIDE FOR COMPLEX GAS HYDRATE STRUCTURES. 6th International Conference on Gas Hydrates (ICGH), 2008

Vancouver, British Columbia, CANADA. Proceedings of the 6th International Conference on Gas Hydrates (ICGH.
LEE, J., PARK, S. & SUNG, W. 2010. An experimental study on the productivity of dissociated gas from gas hydrate by depressurization scheme. *Energy Conversion and Management,* 51**,** 2510-2515.
LEE, J. D., JAE KIM, H., RYUL KIM, S., YEON HONG, S., OK PARK, H., KEUN HA, M., KU JEON, S., AHN, H. & KWAN WOO, T. 2013a. *Apparatus and method for continuously producing and pelletizing gas hydrates using dual cylinder*.
LEE, J. D., WOO LEE, J., NAM PARK, K. & HA KIM, J. 2015. *Double helix type gas hydrate reactor*.
LEE, S.-H., YONG-SEOK YOON & SEONG., K.-J. 2011. Experimental Study on the Dissociation Characteristics of Methane Hydrate Pellet by Hot Water Injection. *Transactions of the Korean Society of Mechanical Engineers B,* 35**,** 1177-1184.
LEE, Y.-H., KOH, B.-H., KIM, H. S. & SONG, M. H. 2013b. Compressive Strength Properties of Natural Gas Hydrate Pellet by Continuous Extrusion from a Twin-Roll System. *Advances in Materials Science and Engineering,* 2013**,** 6.
LEVIK, O. I. 2000. *Thermophysical and Compositional Properties of Natural Gas Hydrate.* PhD, Norwegian University of Science and Technology.
LI, G., LI, X.-S., TANG, L.-G. & ZHANG, Y. 2007. Experimental Investigation of Production Behavior of Methane Hydrate under Ethylene Glycol Injection in Unconsolidated Sediment. *Energy & Fuels,* 21**,** 3388-3393.
LIGHT, H. 2017. Why natural gas is the future - not coal.
LIJUN, X., XIAOSEN, L., YI, W. & CHUNGANG, X. 2012. Experimental Study on Methane Hydrate Dissociation by Depressurization in Porous Sediments
Energies 5**,** 518-530
LIN, W., CHEN, G. J., SUN, C. Y., GUO, X. Q., WU, Z. K., LIANG, M. Y., CHEN, L. T. & YANG, L. Y. 2004. Effect of surfactant on the formation and dissociation kinetic behavior of methane hydrate. *Chemical Engineering Science,* 59**,** 4449-4455.
LINGA, P., KUMAR, R. & ENGLEZOS, P. 2007. The clathrate hydrate process for post and pre combustion capture of carbon dioxide. *J. Hazard. Mater.,* 149**,** 629.
LINGA, P., KUMAR, R., LEE, J. D., RIPMEESTER, J. & ENGLEZOS, P. 2010. A new apparatus to enhance the rate of gas hydrate formation: Application to capture of carbon dioxide. *International Journal of Greenhouse Gas Control,* 4**,** 630-637.
LU, W.-M., WU, H.-Z. & JU, M.-Y. 1997. Effects of baffle design on the liquid mixing in an aerated stirred tank with standard Rushton turbine impellers. *Chemical Engineering Science,* 52**,** 3843-3851.
MALI, G. A., CHAPOY, A. & TOHIDI, B. 2017. Investigation into the Effect of Subcooling on the Kinetics of Hydrate Formation. *The Journal of Chemical Thermodynamics*.
MASOUDI, R. & TOHIDI, B. 2005. Gas Hydrate Production Technology for Natural Gas Storage and Transportation and CO2 Sequestration. *SPE Middle East Oil and Gas Show and Conference.* Kingdom of Bahrain: Society of Petroleum Engineers.
MCKETTA, J. J. & CUNNINGHAM, W. A. 1976. *Encyclopedia of chemical processing and design,* New York, New York : M. Dekker.
MEINDINYO, R.-E. & SVARTAAS, T. 2016. Gas Hydrate Growth Kinetics: A Parametric Study. *Energies,* 9**,** 29.
MIMACHI, H., TAKAHASHI, M., TAKEYA, S., GOTOH, Y., YONEYAMA, A., HYODO, K., TAKEDA, T. & MURAYAMA, T. 2015. Effect of Long-Term Storage and Thermal History on the Gas Content of Natural Gas Hydrate Pellets under Ambient Pressure. *Energy & Fuels,* 29**,** 4827-4834.

MITSUI ENGNEERING AND SHIPPING 2016. Developement of Small and Medium Unmonetized Gas Fields Accessed from: http://www.mes.co.jp/english/mes_technology/ngh.html (June, 2016): Mitsui Engneering and Shipping Ltd.

MOKHATAB, S., PEO, W. A. & SPEIGHT, J. G. 2008. *Handbook of Natural Gas Transmission and Processing*.

MOKHATAB, S. & POE, W. 2012. *Handbook of Natural Gas Transmission and Processing*.

MOKHATAB, S., POE, W. A. & MAK, J. Y. 2015. *Handbook of Natural Gas Transmission and Processing*, Oxford, UK, Elsevier Inc.

MOORE, S. & GREINER, R. 2017. Shipping operating cost: future and current trends. Accessed from: http://www.propellerclub.gr/files/Richard_Greiner.pdf (March, 2018): Moore Stephens.

MORADPOUR, H., CHAPOY, A. & TOHIDI, B. 2011. Controlling Hydrate Slurry Transportability by Optimizing Anti-Agglomerant Usage in High Water Cut Systems. *OTC Brasil.* Rio de Janeiro, Brazil: Offshore Technology Conference.

MORI, Y. 2015. On the Scale-up of Gas-Hydrate-Forming Reactors: The Case of Gas-Dispersion-Type Reactors. *Energies,* 8**,** 1317.

MORK, M. 2002. *Formation Rate of Natural Gas Hydrate.* PhD, Norwegian University of Science and Technology.

MORK, M. & GUDMUNDSSON, J. S. 2002. Hydrate Formation Rate in a Continuous Stirred Tank Reactor: Experimental Results and Bubble-to-Crystal Model. *4th International Conference on Gas Hydrates.* Yokohama.

MORK, M., GUDMUNDSSON, J. S. & PARLAKTUNA, M. Hydrate formation rate in a continuous stirred tank reactor. International Gas Research Conference Proceedings, 2001.

MOULIJN, J. A., MAKKEE, M. & AVAN-DIEPEN, A. E. 2013. *Chemical Process Technology*, John Wiley & Sons, Ltd. West Sussex, United Kingdom

MURAYAMA, T., IWABUCHI, M. I. & TAKAHASHI, M. Effect of guest gas on pelletizing performance of natural gas hydrate pellets. 7th International Conference on Gas Hydrates, 2011 Edinburgh, Scotland, UK. ICGH.

MURAYAMA, T. & UCHIDA, K. 2010. *Process and Apparatus for producing Gas Hydrates* United States patent application.

MYRE, D., MACCHI, A. & SERVIO, P. 2011. Synthesis of CO2 hydrates in a slurry bubble column. *7th International Conference on Gas Hydrates* Edinburgh, United Kingdom

NAKAI, S. Development of Natural Gas Hydrate (NGH) Supply Chain. 25th World Gas Conference, 2012a Kuala Lumpur. Accessed from: http://members.igu.org/@@search?SearchableText=Development+of+Natural+Gas+Hydrate+%28NGH%29+Supply+Chain (Sept., 2017): International Gas Union, 1-23.

NAKAI, S. 2012b. Development of Natural Gas Hydrates (NGH) Supply Chain. *World Gas Conference.* Kuala Lumpur: Mitsui Engineering & Shipbuilding Co., Ltd.

NAKATA, T., HIRAI, K. & TAKAOKI, T. 2008. Study of natural gas hydrate (NGH) carriers. *6th Gas Hydrates International Conference [ICGH] (Vancouver, British Columbia, 7/6-10/2008) Proceedings*.

NATARAJAN, V., BISHNOI, P. R. & KALOGERAKIS, N. 1994. Induction phenomena in gas hydrate nucleation. *Chemical Engineering Science,* 49**,** 2075-2087.

NAVAB, E. K., KHOSHNOODI, M. & ALI FANAEI, M. 2008. Hydrate Kinetics: The Main Problem in the Gas Hydrate Industrialization. *5th International Chemial Engineering Congress and Exhibition.* Kish Island, Iran: Accessed from: https://profdoc.um.ac.ir/articles/a/1007056.pdf (Nov, 2018).

NEXANT 2005. Stranded Gas Utilization: Methane Refineries of the Future. Accessed from: http://thinking.nexant.com/sites/default/files/report/field_attachment_prospectus/200101/MC-StrandGas-pros-02-15-02.pdf (June 2014).

NG, H.-J. & ROBINSON, D. B. 1976. The Measurement and Prediction of Hydrate Formation in Liquid Hydrocarbon-Water Systems. *Industrial & Engineering Chemistry Fundamentals,* 15**,** 293-298.

NIENOW, A., KONNO, M. & BUJALSKI, W. 1986. *Studies on three-phase mixing: A review and recent results,* CHEM. ENGNG. RES. & DES. (ICHEME).

NIENOW, A. W. 1996. Gas-liquid mixing studies : A comparison of rushton turbines with some modern impellers. *Chemical Engineering Research and Design,* 74**,** 417-423.

NNPC. 2010. *Nigerian Gas Company Limited* [Online]. Nigerian National Petrolum Corporation http://www.nnpcgroup.com/NNPCBusiness/Subsidiaries/NGC.aspx. [Accessed 5th March 2014].

NNPC. 2016. *Nigerian Oil and Gas Production* [Online]. Accessed from: http://nnpcgroup.com/NNPCBusiness/UpstreamVentures/OilProduction.aspx (08June, 2017): Nigerian National Petroleum Corporation. [Accessed 08 June 2017].

NOGAMI, T., WATANABE, S. & NAKAI, S. 2011. World's First Demonstration Project of Natural Gas Hydrate (NGH) Land. International Petroleum Technology Conference.

NOUS, D., VERHAEGHE, H., DAMME, V. L. & DEBLAUWE, B. 2010. The LNG Terminal of Zeebrugge: Future Development. *PIANC MMX Congress.* Liverpool UK: Accessed from: http://www.dma.dk/themes/LNGinfrastructureproject/Documents/Infrastructure/Paper_LNGZeebrugge_Version5.pdf June 2014.

OFGEM. 2019. *Gas prices: Day-ahead contracts – monthly average (GB)* [Online]. Accessed from: https://www.ofgem.gov.uk/data-portal/gas-prices-day-ahead-contracts-monthly-average-gb (Feb, 2017): Ofgem. [Accessed].

OHNARI, H. 2002. *Swirling Fine-Bubble Generator*

OIL AND GAS AUTHORITY 2018. Gas to Wire report: UK SNS and EIS. Accessed from: https://www.ogauthority.co.uk/news-publications/publications/2018/gas-to-wire-report-uk-sns-and-eis/ (Dec., 2018): Oil and Gas Authority, UK.

OLDSHUE, J. Y. 1983. *Fluid Mixing Technology*, New York, McGraw-Hill Publications Co.

OSOKOGWU, U., ADEMUJIMI, M. & AJIENKA, J. A. 2011. Economic Analysis of GTP, GTL, CNG, NGH for Offshore Gas Development in Nigeria. Society of Petroleum Engineers.

ØSTERGAARD, K. K., MASOUDI, R., TOHIDI, B., DANESH, A. & TODD, A. C. 2005. A general correlation for predicting the suppression of hydrate dissociation temperature in the presence of thermodynamic inhibitors. *Journal of Petroleum Science and Engineering,* 48**,** 70-80.

PALLIPURATH, M. I. 2008. Gas Transport as Hydrate. *International Petroleum Technology Conference.* Kuala Lumpur, Malaysia: International Petroleum Technology Conference.

PAUL, E. L., ATIEMO-OBENG, V. A. & KRESTA, S. M. 2004. *Handbook on Industrial Mixing,* New Jersey, John Wiley & Sons, INC.

PETER, M. S. & TIMMERSHAUS, K. D. 1991. *Chemical Design and Economics for Chemical Engineers,* United States, McGraw-Hill.

PRASAD, P. S. R. & CHARI, V. D. 2015. Preservation of methane gas in the form of hydrates: Use of mixed hydrates. *Journal of Natural Gas Science and Engineering,* 25**,** 10-14.

RAJNAUTH, J. & BARRUFET, M. Monetizing gas - Focusing on developments in gas hydrate as a mode of gas transportation. 70th European Association of Geoscientists and

Engineers Conference and Exhibition 2008: Leveraging Technology. Incorporating SPE EUROPEC 2008, 2008. 892-899.
RAJNAUTH, J. & BARRUFET, M. 2012. Monetizing Gas: Focusing on Developments in Gas Hydrate as a Mode of Transportation. *Energy Science and Technology CSCanada,* 4**,** 61-68.
RAJNAUTH, J., BARRUFET, M. & FALCONE, G. 2012. Hydrate Formation: Considering the Effects of Pressure, Temperature, Composition and Water. *Energy Science and Technology,* 4**,** 60-69.
RASE, H. F. 1977. *Chemical Reactor Design For Process Plants*, United States of America, John Wiley and Sons Inc.
REHDER, G., ECKL, R., ELFGEN, M., FALENTY, A., HAMANN, R., KÄHLER, N., KUHS, W. F., OSTERKAMP, H. & WINDMEIER, C. 2012. Methane hydrate pellet transport using the self-preservation effect: A techno-economic analysis. *Energies,* 5**,** 2499-2523.
RIPMEESTER, J. A., TSE, J. S., RATCLIFFE, C. I. & POWELL, B. M. 1987. A new clathrate hydrate structure. *Nature,* 325**,** 135-136.
RITCHIE, H. & ROSER, M. 2018. Fossil Fuels. Accessed from: http://ourworldindata.org/fossil-fuel (October, 2018): Our World in Data.
ROGERS, H. 2018. The LNG Shipping Forecast: costs rebounding, outlook uncertain. Accessed from: https://www.oxfordenergy.org/wpcms/wp-content/uploads/2018/02/The-LNG-Shipping-Forecast-costs-rebounding-outlook-uncertain-Insight-27.pdf (Feb., 2018).
SAAVEDRA, C. G. & FALES, R. P. 2012. Alternative Methods of Handling Produced Gas. Retrieved from http://pennwell.websds.net/2012/dot/papers/T3S1O2-paper.pdf (20/02/2014): Deep Offshore Technology International. Granherne, Inc.
SARSFIELD-HALL, R. & GARETH, D. 2010. Gas: At the Centre of a Low Carbon Future *A review for Oil & Gas UK.* Accessed from: http://oilandgasuk.co.uk/wp-content/uploads/2015/04/EC022.pdf (August, 2016): Oil & Gas UK.
SHAH, P. & DURR, C. 2009. *Petroleum Engineering Handbook - Monetizing Stranded Gas*, 2009, KBR (Kelly Brown & Root, LLC).
SHAO, P., DARCOVICH, K., MCCRACKEN, T., ORDORICA-GARCIA, G., REITH, M. & O'LEARY, S. 2015. Algae-dewatering using rotary drum vacuum filters: Process modeling, simulation and techno-economics. *Chemical Engineering Journal,* 268**,** 67-75.
SHIN, S., LEE, Y., SONG, K., NA, J., PARK, S., LEE, Y., LEE, C.-J. & HAN, C. 2016. Design and economic analysis of natural gas hydrate regasification process combined with LNG receiving terminal. *Chemical Engineering Research and Design,* 112**,** 64-77.
SINNOTT, R. K. & TOWLER, G. 2009a. 12. Heat-Transfer Equipment. *Chemical Engineering Design (5th Edition).* Elsevier.
SINNOTT, R. K. & TOWLER, G. 2009b. Costing and Project Evaluation. *Chemical Engineering Design - SI Edition (5th Edition).* Elsevier.
SKOVBORG, P. & RASMUSSEN, P. 1994. A mass transport limited model for the growth of methane and ethane gas hydrates. *Chemical Engineering Science,* 49**,** 1131-1143.
SLOAN, D. & KOH, C. 2008. *Clathrate Hydrates of Natural Gases,* London, Boca Raton, Fla. ; London : CRC
SLOAN, E. D. 1998. Gas Hydrates: Review of Physical/Chemical Properties. *Energy & Fuels,* 12**,** 191-196.
SLOAN, E. D. & FLEYFEL, F. 1992. Hydrate dissociation enthalpy and guest size. *Fluid Phase Equilibria,* 76**,** 123-140.
SMEDLEY, M. 2018. GLOBAL GAS FLARING DOWN 5% IN 2017: WORLD BANK. Accessed from: https://www.naturalgasworld.com/global-gas-flaring-down-5-in-2017-

world-bank-62843#snews (October, 2018): Global Gas Flaring Reduction (GGFR) initiative.
SMITH, C. E. 2008. Natural gas pipeline profits surge; oil flat. Accessed from: http://www.ogj.com/articles/print/volume-106/issue-33/transportation/natural-gas-pipeline-profits-surge-oil-flat.html (July 2014): Oil&Gas Journal.
SMITH, J. M. 2011. Agitated Vessel Mass Transfer. 02/2011 ed. http://www.thermopedia.com/content/548/: Thermopedia.
SONGHURST, B. 2017. The Outlook for Floating Storage and Regasification Units (FSRUs) Accessed from: https://www.oxfordenergy.org/wpcms/wp-content/uploads/2017/07/The-Outlook-for-Floating-Storage-and-Regasification-Units-FSRUs-NG-123.pdf (Jan., 2018): Oxford Institute for Energy Studies.
SPATH, P. L. & DAYTON, D. C. 2003. Preliminary Screening —Technical and Economic Assessment of Synthesis Gas to Fuels and Chemicals with Emphasis on the Potential for Biomass-Derived Syngas. National Renewable Energy Laboratory.
SPE. 2013. *Monetizing Stranded Gases* [Online]. Society of Petroluem Engineers SPE International Accessed from: http://petrowiki.spe.org/PEH%3AMonetizing_Stranded_Gas (29/11/2013). [Accessed 29/11/2013 2013].
SPE INTERNATIONAL. 2013. *Monetizing Stranded Gases* [Online]. Society of Petroluem Engineers SPE International Accessed from: http://petrowiki.spe.org/PEH%3AMonetizing_Stranded_Gas (29/11/2013). [Accessed 29/11/2013 2013].
STERN, L. A., CIRCONE, S., KIRBY, S. H. & DURHAM, W. B. 2001a. Anomalous Preservation of Pure Methane Hydrate at 1 atm. *The Journal of Physical Chemistry B,* 105**,** 1756-1762.
STERN, L. A., CIRCONE, S., KIRBY, S. H. & DURHAM, W. B. 2001b. Preservation of Methane Hydrate at 1 Atm. *Energy & Fuels,* 15**,** 499-501.
STERN, L. A., CIRCONE, S., KIRBY, S. H. & DURHAM, W. B. 2003. Temperature, pressure, and compositional effects on anomalous or "self" preservation of gas hydrates. *Canadian Journal of Physics,* 81**,** 271-283.
TAHERI, Z., SHABANI, M. R., NAZARI, K. & MEHDIZAHEH, A. 2014. Natural gas transportation and storage by hydrate technology: Iran case study. *Journal of Natural Gas Science and Engineering,* 21**,** 846-849.
TAKAHASHI, M., KAWAMURA, T., YAMAMOTO, Y., OHNARI, H., HIMURO, S. & SHAKUTSUI, H. 2003. Effect of Shrinking Microbubble on Gas Hydrate Formation. *The Journal of Physical Chemistry B,* 107**,** 2171-2173.
TAKAHASHI, M., MORIYA, H., KATOH, Y. & IWASAKI, T. 2008. *Development of natural gas hydrate (NGH) pellet production system by bench scale unit for transportation and storage of NGH pellet*.
TAKAOKI, T., HIRAI, K. & M, K. 2004. Natural Gas Transportation in the Form of Hydrate Pellets. *Design and Operation of Gas Carriers.* The Royal Institution of Naval Architects.
TAKAOKI, T., NOGAMI, T., WATANABE, S. & NAKAI, S. 2011. Natural Gas Hydrate (NGH) Technology for Monetizing Small to Medium Gas Fields and Its Development Status. World Petroleum Congress.
TAMSILIAN, Y., EBRAHIMI, A. N. & RAMAZANI S.A, A. 2013. Formation and Economic Study on Hydrate Technology with NGH Pellets. *Journal of Dispersion Science and Technology,* 34**,** 259-267.

TARLETON, E. S. & WAKEMAN, R. J. 2007. Solid/Liquid Separation - Equipment Selection and Process Design. Accessed from: https://goo.gl/NjMCgY (06 August 2017): Elsevier.

TATTERSON, G. B. 1991. *Fluid Mixing and Gas Dispersion in Agitated Tanks*, Gary Benjamin Tatterson.

TOHIDI, B., BURGASS, R. W., DANESH, A., ØSTERGAARD, K. K. & TODD, A. C. 2000. Improving the Accuracy of Gas Hydrate Dissociation Point Measurements. *Annals of the New York Academy of Sciences,* 912**,** 924-931.

TOHIDI KALORAZI, B., DANESH, A., OSTERGAARD, K. & A., T. 1996. Kinetics of structure-H hydrate formation, experimental data and modelling. *2nd International Conference on Gas Hydrates.* Toulouse, France.

TOWLER, B. F. & MOKHATAB, S. 2005. Quickly estimate hydrate formation conditions in natural gases. *Hydrocarbon Processing,* 84**,** 61-62.

ULLERICH, J. W., SELIM, M. S. & SLOAN, E. D. 1987. Theory and measurement of hydrate dissociation. *AIChE Journal,* 33**,** 747-752.

V. STACKELBERG, M. & MÜLLER, H. R. 1954. Solid gas hydrates II † . Structure and Spatial Chemistry. *Journal of Electrochemistry, reports of the Bunsen Society for Physical Chemistry banner,* 58**,** 25-39.

VELUSWAMY, H. P., KUMAR, A., SEO, Y., LEE, J. D. & LINGA, P. 2018. A review of solidified natural gas (SNG) technology for gas storage via clathrate hydrates. *Applied Energy,* 216**,** 262-285.

VELUSWAMY, H. P., KUMAR, R. & LINGA, P. 2014. Hydrogen storage in clathrate hydrates: current state of the art and future directions. *Appl. Energy,* 122**,** 132.

VELUSWAMY, H. P., WONG, A. J. H., BABU, P., KUMAR, R., KULPRATHIPANJA, S., RANGSUNVIGIT, P. & LINGA, P. 2016. Rapid methane hydrate formation to develop a cost effective large scale energy storage system. *Chemical Engineering Journal,* 290**,** 161-173.

VITUCCI, J. 2010. *Natural Gas Processing and Handling* [Online]. Accessed from: http://www.spe.org/jpt/print/archives/2010/04/16NGPFocus.pdf Society of Petroleum Engineers [Accessed 20th Feb. 2014].

VLASOV, V. A. 2013. Formation and dissociation of gas hydrate in terms of chemical kinetics. *Reaction Kinetics, Mechanisms and Catalysis,* 110**,** 5-13.

VYSNIAUSKAS, A. & BISHNOI, P. R. 1983. A kinetic study of methane hydrate formation. *Chemical Engineering Science,* 38**,** 1061-1072.

WAGNER, J. V. & VAN WAGENSVELD, S. 2002. Marine Transportation of Compressed Natural Gas A Viable Alternative to Pipeline or LNG. Society of Petroleum Engineers.

WAITE, W. F., STERN, L. A., KIRBY, S. H., WINTERS, W. J. & MASON, D. H. 2007. Simultaneous determination of thermal conductivity, thermal diffusivity and specific heat in sI methane hydrate. *Geophysical Journal International,* 169**,** 767-774.

WAKEMAN, R. J. & TARLETON, E. S. 1994. A framework methodology for the simulation and sizing of diaphragm filter presses. *Minerals Engineering,* 7**,** 1411-1425.

WANG, X. & ECONOMIDES, M. 2009. *Advanced Natural Gas Engineering*, Houston, Texas., Gulf Publishing Company.

WATANABE, K., SUGANOYA, K., YOSHIDA, T., OGAWA, K., NANBARA, S. & IMAI, S. 2012. *Gas Hydrate Compression Molding Machine*. United States patent application.

WHITE, N. & MORGAN, J. 2012. Rules of Thumb For Screening LNG Developments. Accessed from: https://www.engineersaustralia.org.au/sites/default/files/shado/Divisions/Western%20Australia%20Division/Groups/Oil_Gas/lng_technical_presentation_ieaustralia_oil_an

d_gas_division_perth_october_2012.pdf (Dec, 2016): The Institution of Engineers Austalia.
WOOD, D. A., MOKHATAB, S. & ECONOMIDES, M. J. Technology Options for Securing Markets for Remote Gas. Proc 87th annual convention, GPA, 2008.
WOOD, D. A., NWAOHA, C. & TOWLER, B. F. 2012. Gas-to-liquids (GTL): A review of an industry offering several routes for monetizing natural gas. *Journal of Natural Gas Science and Engineering,* 9**,** 196-208.
WORLD BANK 2015. CNG for commercialization of small volumes of associated gas. Accessed from: http://documents.worldbank.org/curated/en/727861474994769719/pdf/104200-V1-WP-CNG-commericalization-PUBLIC-Executive-summary-REPLACEMENT.pdf (October, 2018): Global Gas Flaring Reduction Partnership - World Bank Group
WORLD BANK REPORT 2018. New Satellite Data Reveals Progress: Global Gas Flaring Declined in 2017. Accessed from: http://www.worldbank.org/en/news/press-release/2018/07/17/new-satellite-data-reveals-progress-global-gas-flaring-declined-in-2017 (October, 2018): World Bank Group.
YAKUSHEV, V. S. & ISTOMIN, V. A. 1992. Gas-Hydrates Self-Preservation Effect *In:* T.HONDOH, E. B. N. M. A. (ed.). Physics and Chemistry of Ice: Hokkaido University Press, Sapporo.
YE, Y. 2013. Chapter 1 - Natural Gas Hydrates: Experimental Techniques and Their Applications. *In:* YE, Y. & LIU, C. (eds.) *Natural Gas Hydrates: Experimental Techniques and Their Applications.* Berlin, Heidelberg: Springer Berlin Heidelberg.
YIN, Z., KHURANA, M., TAN, H. K. & LINGA, P. 2018. A review of gas hydrate growth kinetic models. *Chemical Engineering Journal,* 342**,** 9-29.
ZAKARIA, M. S., OSMAN, K. & ABDULLAH, H. 2013. Greenhouse Gas Reduction by Utilization of Cold LNG Boil-off Gas. *Procedia Engineering,* 53**,** 645-649.
ZHANG, G. & ROGERS, R. E. 2008. Ultra-stability of gas hydrates at 1atm and 268.2K. *Chemical Engineering Science,* 63**,** 2066-2074.
ZHONG, D.-L., HE, S.-Y., SUN, D.-J. & YANG, C. 2014. Comparison of Methane Hydrate Formation in Stirred Reactor and Porous Media in the Presence of SDS. *Energy Procedia,* 61**,** 1573-1576.

Appendix A1: MHPP base case reactor simulation in HYSYS

Spreadsheet: Process specification

	A	B	C	D
1	Reactor Simulation Specifications	Values	Specification Description	
2	Vessel Diameter D	0.1800 m		
3	Vessel Hieght H	0.3600 m		
4	Vessel Pressure p	5.400 MPa		
5	Vessel Temperature T	285.1 K		
6	Subcooling	276.1 K		
7	Vessel Volume V	9.161e-003 m3		
8	Impeller Diameter Di	*9.000e-002 m*		
9	Cross sectional Area	*2.545e-002*	Pi*(B2/2)^2	
10	Impeller Speed N (s-1)	6.667		
11	Superficial gas velocity Vsg (ms-1)	*7.772e-005 m3/s*	B22/B9	
12	Power consumption P (W)	*8.009*	B16*B23*(B10^3)*(B8^5)	
13	Gassed Power Consumption Pg (W)	*5.966*	B12*(0.62+(1.85*B17)) for B17 > 0.035	
14	Pg/P	*0.7450*	B13/B12	
15	Reynold number	*4.019e+004*	B23*B10*(B8^2)/B19	
16	Power Number Np	5.000		
17	Gas flow number Fl	*6.756e-002*	13*((B8/B2)^5)*(B18^2)	
18	Froude number, Fr	*0.4078*	B10*(B8^2)/B32	
19	Viscosity (Pa.s)	1.230e-003 kg/s-m		
20	Molar density of methane gas	2.605 kgmole/m3	Note: kgmole = kmole	
21	Methane feed flowrate	5.152e-006 kgmole/s		
22	Methane feed vol. flowrate	1.978e-006 m3/s		
23	Density (kgm-3)	*915.4 kg/m3*	1000*(((46*18)+(0.927*2*16)+(0.985*6*16))/((6.02*10^23)*(12^3)*(10^-24)))	
24	Gas consumption rate (m3/s)	*8.716e-007*	B34*(B4*10)*(B11^B35)*(B13^B36)*((B6)^B37)	
25	Hydrate formation rate (kgmole/s)	*2.270e-006*	B24*B20	
26	Vessel water volume	9.161e-003 m3		
27	Gas consumption rate per water volume (kgmole/s.m3)	*2.478e-004*	B25/B26*1000	
28	Conversion	*44.07*	B7*B25/B22	
29	Slurry solid mass fraction	0.1013		
30	Methane Hydrate (kg/s)	2.796e-003 kg/s	*10.07*	kg/hr
31				
32	Gravitational force (m/s2)	9.810		
33	Compressibility factor z [-]	0.8973		
34	empirical model rate constant k	1.430e-004		
35	a [-]	1.000		
36	b [-]	0.1460		
37	c [-]	2.000e-002		
38	specific heat capacity of methane gas cpg	4.277e-002 kJ/gmole-K		
39	specific heat capacity of water cpw	7.768e-002 kJ/gmole-K		

Figure A 1.1: HYSYS spreadsheet of MHPP base case reactor simulation

Figure A 1.1 shows the MHPP base case simulation computation on HYSYS as discussed in Sections 4.3 and 5.2.1 of Chapters 4 and 5 respectively. The HYSYS spreadsheet indicates the reactor simulation parameters specifications, obtained values, and description of the simulation parameters.

Figure A 1.2 shows energy balance calculation of the base case MHPP reactor simulation on Excel spreadsheet. This is attached to show the discussed values in Sections 4.3.4 and 5.3.1 of Chapters 4 and 5 respectively. The overall heat transfer coefficient as indicated in Figure A 1.2 was obtained using Equation 4.29 of Chapter 4.

Analysis and evaluation of the HYSYS base case reactor simulation using energy balance calculations					
Inlet Methane gas flowrate F_{g1} (mol/s)	0.005153				
Inlet Water flowrate F_{w1} (mol/s)	0.153200				
Inlet methane gas Temperaturte T_{g1} (K)	285.15				
Inlet water Temerature Tw1 (K)	285.15				
specific heat capacity of gas cp_g (KJ/gmolK)	0.04277				
specific heat capacity of water cp_w (KJ/molK)	0.07768				
Enthalpy of formation (kJ/mol)	-51.61				
Shaft work P (kJ/s)	0.00803				
Conversion	0.44				
Temperature of reactor, T	294.16	without coolant			
Heat Transfer Area (m^2)	0.25	surface area			
Overall heat transfer coefficient W/m2.K	214.72	Calculated based on equation 4.29 (page 85 of Chapter 4)			
Reactor Inlet Temperature (K)	285.15				
Reactor Outlet Temperature (K)	285.15				
Coolant Fluid Inlet Temperature T_{c1} (K)	283.15				

Figure A 1.2: Energy balance calculation of base case MHPP reactor simulation on Excel spreadsheet

Appendix A2: Production CAPEX and OPEX of MHT chain for 0.3 bcm/yr capacity reserves

Table A 2.1: Production CAPEX of MHT chain for 0.3 bcm/yr capacity reserves

Production CAPEX (USD)	Scenario 1 (0.3 bcm/yr)
Upstream with pre-processing (USD)	2.50×10^9
Direct purchase cost	
Jacketed reactor vessel (stainless steel) (USD) with volume 37.30 m^3 (30.00 and 7.30 m^3)	7.52×10^5
Gas compressor [Q-100] (USD)	5.30×10^5
Gas cooler [Q-101] (USD)	6.32×10^4
Pump [Q-102] (USD)	1.42×10^5
Water cooler [Q-103] (USD)	1.95×10^5
MH pellet machine (USD)	2.40×10^4
MH pellet storage vessel (USD)	2.55×10^4
Indirect cost	
ISBL plant cost (with summation of correction factors)	4.70×10^6
Offsite	1.88×10^6
Design and Engineering	1.18×10^6
Contingency	4.70×10^5
MHPP Production Fixed Capital Investment (FCI)	1.24×10^7
Working Capital	1.86×10^6
MHPP Production Total Capital Investment (TCI)	1.43×10^7
MHPP Production Capital plus upstream Capital (Total)	2.51×10^9

CEPCI (November 2017)

Appendix 2 is added to show data and illustrate calculation of the transportation and regasification units and economic evaluation of methane hydrate technology chain in chapter 6.

Table A 2.2: Production OPEX of MHT chain for 0.3 bcm/yr capacity reserves

Production OPEX (USD/yr)	
Raw material: Pure methane gas (USD/yr) Pure water (USD/yr)	 3.00×10^7 1.39×10^7
Cost of equipment utilities (USD/yr)	
Gas compressor [Q-100]	1.58×10^4
Gas cooler [Q-101]	1.06×10^5
Pump [Q-102]	1.53×10^5
Water cooler [Q-103]	4.83×10^6
MH pellet machine	7.08×10^5
Operating labour cost (USD/yr.)	2.08×10^5
Maintenance cost (USD/yr.)	2.48×10^5
Administrative and insurance (USD/yr.)	8.69×10^4
Total production OPEX (USD/yr.)	5.06×10^7

CEPCI (November 2017)

Table A 2.3: HYSYS cost estimate of dehydrating system 130.80 m^3s^{-1} (400 MMScfd) capacity

Name	**Installed Equipment Cost [USD]**
Pump	8.03×10^4
TEG Regenerator	2.05×10^5
L/R Heat Exchanger	6.55×10^4
Separator	3.10×10^5
TEG Contactor	5.70×10^5
Summary	
Total Capital Cost [USD]	4.92×10^6
Total Operating Cost [USD/Year]	1.15×10^6

Table A 2.4: Regasification CAPEX and OPEX of 4.13 bcm/yr. (400 MMScfd) capacity

Regasification CAPEX	Values
Direct purchase cost	
Regasification Vessel (12 vessels equal 460,000 m^3)	1.45×10^7
Water tank (1.25×10^7 m^3)	1.47×10^8
Gas compressor (1.00×10^5 KW)	1.48×10^7
Heat Pump system (5.69×10^5 KW)	3.38×10^6
Glycol dehydrating plant	4.92×10^6
ISBL plant cost	1.84×10^8
Offsite (0.40 * ISBL)	7.37×10^7
Design and Engineering (0.25 * ISBL)	4.60×10^7
Contingency (0.10 * ISBL)	1.84×10^7
MHPP Regasification Fixed Capital Investment (FCI)	3.22×10^8
Working Capital (0.15 * FCI)	4.83×10^7
MHPP Regasification Total Capital Investment (TCI)	3.70×10^8
Regasification OPEX	Values
Utilities	
Gas compressor	5.97×10^7
Heat Pump system	3.39×10^8
Water cost	9.50×10^6
OPEX of dehydrating system	1.15×10^6
Operating labour cost	2.08×10^5
Maintenance cost	4.74×10^5
Administrative and insurance	1.66×10^5
MHPP Production TOC (Total)	4.08×10^8

			MHPP_ 37.3m3_0.3bcmyr							
						Estimation of Equipment Cost				
			empirical constant			factoring in cost escalation due to inflation over time				
MH Production Equpiment Type	Unit	Size, S	a	b	n	Purchased cost (USD) Jan. 2007	CE index Jan. 2007	CE Index (Nov 2017) (USD)	Purchase Cost USD based on 2017	
Upstream including pre-processing										2.50E+09
ISBL direct cost estimate										
Reactor (304 stainless steel - Jacketed, agitated)	Volume m3	30	53000	28000	0.8	478456.37	509.70	573.2	5.38E+05	
CAPEX	Volume m3	7.3	53000	28000	0.8	190346.10	509.70	573.2	2.14E+05	
Pump Q-102	pump for 30m3 reactor KW	558	-950	1770	0.6	77746.20	509.70	573.2	8.74E+04	
CAPEX	pump for 7.3m3 reactor KW	257	-950	1770	0.6	48473.46	509.70	573.2	5.45E+04	
Utilities										
Cost of electricity Dec 2017	USD/KWh	0.068	USD/KWh	595.68	USD/Kwyr					
	pump for 30m3 reactor USD/yr	3.32E+05								
	pump for 7.3m3 reactor USD/yr	1.53E+05								
Gas Compressor (Q-100) - power-driven	compressor for 30 m3 (KW)	18.22	220000	2300	0.75	240283.32	509.70	573.2	2.70E+05	
CAPEX	compressor for 7.3 m3 (KW)	8.29	220000	2300	0.75	231236.83	509.70	573.2	2.60E+05	
Utilities	compressor for 30 m3 (USD/yr)	1.09E+04								
	compressor for 7.3 m3 (USD/yr)	4.94E+03								
Gas Cooler (Q-101)	Gas Cooler for 30 m3 reactor (m2)	56.81	24000	46	1.2	29862.29	509.70	573.2	3.36E+04	
CAPEX	Gas Cooler for 7.3 m3 reactor (m2)	26.1	24000	46	1.2	26305.29	509.70	573.2	2.96E+04	
	Gas Cooler for 30 m3 reactor (USD/yr)	72732.53								
Utilities	Gas Cooler for 7.3 m3 reactor (USD/yr)	33417.65	122.10	KW						
			56.1	KW						
Water Cooler (Q-103)	Water Cooler for 30 m3 reactor (m2)	553.79	24000	46	1.2	114109.79	509.70	573.2	1.28E+05	
	Water Cooler for 7.3 m3 reactor (m2)	254.52	24000	46	1.2	59450.64	509.70	573.2	6.69E+04	
Utilities	Water Cooler for 30 m3 reactor (USD/yr)	3309002.40	5555	KW						
	Water Cooler for 7.3 m3 reactor (USD/yr)	1518984.00	2550	KW						
MH pellet storage vessel	m3	37.3	5000	1400	0.7	22632.919	509.70	573.20	2.55E+04	

Figure A 2.1: Break down of CAPEX and OPEX cost estimate for 0.3 bcm/yr. reserve capacity (screenshot 1)

Two Cylindrical Hydraulic Ram at USD 414.42 each	m	0.3							2.40E+04	for 29 pieces					
Utilities															
Constant rate filtration operation	KJ	12.2					12.20	KWh	7.27E+03						
Constant presure opresion	KJ	20.3					20.30	KWh	1.21E+04						
Compresion operation	KJ	8.48					8.48	KWh	5.05E+03						
									7.08E+05	USD/yr					
	Factor values														
correction factor for carbon steel to 304 stainless steel	1.3														
Installation factor fp for piping	0.6														
Installation factor fer for equipment erection	0.5														
Installation factor fl for electrical work	0.2														
Installation factor fi for instrumentation and process co	0.3														
Installation factor fc for Civil engineering work	0.3														
Installation factor fs for structures and buildings	0.2														
Installation factor fl for lagging, insulation or paint	0.1														
	3.5										Reactor Stainless Steel	1.56E+06			
											Equipment with Carbon steel	3.14E+06			
ISBL cost												4.70E+06			
OSBL (Offsite)	0.4											1.88E+06			
Design and Engineering (D&E)	0.25											1.18E+06			
Contingency (X)	0.1											4.70E+05			
Total capital cost (USD)												1.24E+07	FCI		
Working Capital (USD)	0.15											1.86E+06	working capital		
Total Production Investment Required (USD)												2.51E+09	TCI Production		

Figure A 2.2: Break down of CAPEX and OPEX cost estimate for 0.3 bcm/yr. reserve capacity (screenshot 2)

MH Production Equipment Type	Unit	Size, S	a	b	n	Purchased cost (USD) Jan. 2007	CE index Jan. 2007	CE Index (Nov 2017) (USD)	Purchase Cost USD based on 2017			Total purchase cost (USD	
Production operating cost													
Variable Cost of Production		Raw material + Utilities + Miscellaneous Materials											
Raw Material cost		Raw material	Feed gas (ft3/yr)	Feed gas (MCF/yr)		Unit cost USD/MCF		Total cost (USD/yr)					
		Methane	1.00E+10	1.00E+07		3.00E+00		3.00E+07					
				(MCF/yr)	USD/ft3	USD/MCF		Total cost (USD/yr)					
		Water		5.90E+07	2.36E-04	2.36E-01		1.39E+07					
								4.39E+07					
Total Utility cost (USD/yr)												5.01E+07	USD/yr
Operating labor	10 employees with positions	10	Ave. salary/hour/year (USD10/hr)	2.08E+05							Labor	2.08E+05	USD/yr
Maintainance cost (2% of Total Capital Investment)												2.48E+05	USD/yr
Adiminstrative and Insurance	0.7% of TCI											8.69E+04	USD/yr
MH Production Total Operating cost estimate	with operating cost escalation rate	0.03									Total OPEX productior	5.06E+07	USD/yr
Regasification CAPEX													
Regasification Vessel (12 vessels for 400MMscf/d)	m2	4.60E+05	5000	1400	0.7	1.29E+07	509.7	573.2				1.45E+07	
Water tank	m2	1.25E+07	5000	1400	0.7	1.30E+08	509.7	573.2				1.47E+08	
Compressor	KW	1.00E+05	220000	2300	0.75	1.32E+07	509.7	573.2				1.48E+07	
Pump	KW	2.42E+05	-950	1770	0.6	3.01E+06	509.7	573.2				3.38E+06	
Dehydrating plant (130.8 kg/s equivalent for one train of 400MMscfd)												4.92E+06	
ISBL cost												1.84E+08	
	Factor values												
Offsite	0.40							0.4	7.37E+07				
Design and Engineering (D&E)	0.25							0.25	4.60E+07				
Contingency (X)	0.10							0.1	1.84E+07	FCI of Regas			
Total capital cost (USD)									3.22E+08				
Working Capital (USD)	0.15							0.15	2.76E+06				
Total Regasification Investment Required (USD)									2.37E+07	TCI of Regas			
Regasification OPEX													
Water cost for 38000 m3/hr (1.254*10^9 m3/yr) at USD2/264 m3 gallon of water												9.50E+06	
Water heating using 39MW, 203 MW, 203MW, 24MW, 100MW	569	5.69E+05	KW									3.39E+08	
Compressor	100MW	1.00E+05	KW									5.96E+07	
Dehydrating plant (130.8 kg/s equivalent for I train of 400MMscfd)												1.51E+05	
Total Utility cost (USD/yr)												3.99E+08	
Operating labor	10 employees with positions	10	Ave. salary/hour/year (USD10/hr)		2.08E+05							2.08E+05	
Maintainance cost (2% of Total Capital Investment)												4.74E+05	
Adiminstrative and Insurance (0.7% of TCI)												1.66E+05	
MH Regasification Total Operating cost (4.13*0.073 bcm/yr)	based on 4.13 bcm/yr (one train of 400 MMScfd capacity)										Total OPEX Regas	2.92E+07	

Figure A 2.3: Break down of CAPEX and OPEX cost estimate for 0.3 bcm/yr. reserve capacity (screenshot 3)

Table A 2.5: NPV computation for 0.3 bcm per year reserve capacity over 20-year project life for transport distance 1000 – 10,000 km

Year	CAPEX (USD)	OPEX (USD/yr)	Revenue SR (USD/yr)	Depreciation(USD/yr)	Tax paid (USD/yr)	EBTI (USD/yr)	Cash flow (USD)	Present worth index	NPV (USD)	Sales price (USD/MMBtu)
For 1000 km										
0	2.54E+09	0	0	0	0	0	0	0	0	0
1		8.24E+07	1.49E+08	2.54E+08	5.21E+07	-1.88E+08	1.43E+07	1.15	1.24E+07	6.86
2		8.49E+07	1.49E+08	4.57E+08	5.21E+07	-3.93E+08	1.18E+07	1.32	8.91E+06	6.86
3		8.75E+07	1.49E+08	3.66E+08	5.21E+07	-3.04E+08	9.24E+06	1.52	6.08E+06	6.86
4		9.01E+07	1.49E+08	2.92E+08	5.21E+07	-2.34E+08	6.62E+06	1.75	3.78E+06	6.86
5		9.28E+07	1.49E+08	2.34E+08	5.21E+07	-1.78E+08	3.92E+06	2.01	1.95E+06	6.86
6		9.56E+07	1.49E+08	1.87E+08	5.21E+07	-1.34E+08	1.13E+06	2.31	4.90E+05	6.86
7		9.84E+07	1.49E+08	1.66E+08	5.21E+07	-1.16E+08	-1.73E+06	2.66	-6.52E+05	6.86
8		1.01E+08	1.49E+08	1.66E+08	5.21E+07	-1.19E+08	-4.69E+06	3.06	-1.53E+06	6.86
9		1.04E+08	1.49E+08	1.67E+08	5.21E+07	-1.22E+08	-7.73E+06	3.52	-2.20E+06	6.86
10		1.08E+08	1.49E+08	1.66E+08	5.21E+07	-1.25E+08	-1.09E+07	4.05	-2.68E+06	6.86
11		1.11E+08	1.49E+08	8.33E+07	5.21E+07	-4.53E+07	-1.41E+07	4.65	-3.03E+06	6.86
12		1.14E+08	1.49E+08		5.21E+07	3.47E+07	-1.74E+07	5.35	-3.25E+06	6.86
13		1.18E+08	1.49E+08		5.21E+07	3.12E+07	-2.08E+07	6.15	-3.39E+06	6.86
14		1.21E+08	1.49E+08		5.21E+07	2.77E+07	-2.44E+07	7.08	-3.44E+06	6.86
15		1.25E+08	1.49E+08		5.21E+07	2.41E+07	-2.80E+07	8.14	-3.44E+06	6.86
16		1.28E+08	1.49E+08		5.21E+07	2.03E+07	-3.17E+07	9.36	-3.39E+06	6.86
17		1.32E+08	1.49E+08		5.21E+07	1.65E+07	-3.56E+07	1.08	-3.31E+06	6.86
18		1.36E+08	1.49E+08		5.21E+07	1.25E+07	-3.96E+07	1.24	-3.20E+06	6.86
19		1.40E+08	1.49E+08		5.21E+07	8.43E+06	-4.36E+07	1.42	-3.07E+06	6.86
20		1.45E+08	1.49E+08		5.21E+07	4.22E+06	-4.79E+07	1.64	-2.92E+06	6.86
									-2544338172	

For 2000 km										
0	2.54E+09	0	0	0	0	0	0	0	0	0
1		8.26E+07	1.49E+08	2.54E+08	5.21E+07	-1.88E+08	1.41E+07	1.15	1.23E+07	6.86
2		8.50E+07	1.49E+08	4.57E+08	5.21E+07	-3.93E+08	1.17E+07	1.32	8.82E+06	6.86
3		8.76E+07	1.49E+08	3.66E+08	5.21E+07	-3.04E+08	9.11E+06	1.52	5.99E+06	6.86
4		9.02E+07	1.49E+08	2.92E+08	5.21E+07	-2.34E+08	6.49E+06	1.75	3.71E+06	6.86
5		9.29E+07	1.49E+08	2.34E+08	5.21E+07	-1.78E+08	3.78E+06	2.01	1.88E+06	6.86
6		9.57E+07	1.49E+08	1.87E+08	5.21E+07	-1.34E+08	9.93E+05	2.31	4.29E+05	6.86
7		9.86E+07	1.49E+08	1.66E+08	5.21E+07	-1.16E+08	-1.88E+06	2.66	-7.06E+05	6.86
8		1.02E+08	1.49E+08	1.66E+08	5.21E+07	-1.19E+08	-4.84E+06	3.06	-1.58E+06	6.86
9		1.05E+08	1.49E+08	1.67E+08	5.21E+07	-1.22E+08	-7.88E+06	3.52	-2.24E+06	6.86
10		1.08E+08	1.49E+08	1.66E+08	5.21E+07	-1.25E+08	-1.10E+07	4.05	-2.72E+06	6.86
11		1.11E+08	1.49E+08	8.33E+07	5.21E+07	-4.55E+07	-1.42E+07	4.65	-3.06E+06	6.86
12		1.14E+08	1.49E+08		5.21E+07	3.45E+07	-1.76E+07	5.35	-3.29E+06	6.86
13		1.18E+08	1.49E+08		5.21E+07	3.11E+07	-2.10E+07	6.15	-3.41E+06	6.86
14		1.21E+08	1.49E+08		5.21E+07	2.75E+07	-2.45E+07	7.08	-3.47E+06	6.86
15		1.25E+08	1.49E+08		5.21E+07	2.39E+07	-2.82E+07	8.14	-3.46E+06	6.86
16		1.29E+08	1.49E+08		5.21E+07	2.01E+07	-3.19E+07	9.36	-3.41E+06	6.86
17		1.32E+08	1.49E+08		5.21E+07	1.63E+07	-3.58E+07	1.08	-3.32E+06	6.86
18		1.36E+08	1.49E+08		5.21E+07	1.23E+07	-3.98E+07	1.24	-3.21E+06	6.86
19		1.41E+08	1.49E+08		5.21E+07	8.22E+06	-4.38E+07	1.42	-3.08E+06	6.86
20		1.45E+08	1.49E+08		5.21E+07	4.00E+06	-4.81E+07	1.64	-2.94E+06	6.86
									-254543939	

For 3000 km										
0	2.54E+09	0	0	0	0	0	0	0	0	0
1		8.27E+07	1.49E+08	2.54E+08	5.21E+07	-1.88E+08	1.40E+07	1.15	1.22E+07	6.86
2		8.52E+07	1.49E+08	4.57E+08	5.21E+07	-3.93E+08	1.15E+07	1.32	8.73E+06	6.86
3		8.77E+07	1.49E+08	3.66E+08	5.21E+07	-3.05E+08	8.99E+06	1.52	5.91E+06	6.86
4		9.03E+07	1.49E+08	2.92E+08	5.21E+07	-2.34E+08	6.36E+06	1.75	3.63E+06	6.86
5		9.31E+07	1.49E+08	2.34E+08	5.21E+07	-1.78E+08	3.65E+06	2.01	1.81E+06	6.86
6		9.58E+07	1.49E+08	1.87E+08	5.21E+07	-1.34E+08	8.54E+05	2.31	3.69E+05	6.86
7		9.87E+07	1.49E+08	1.66E+08	5.21E+07	-1.16E+08	-2.02E+06	2.66	-7.60E+05	6.86
8		1.02E+08	1.49E+08	1.66E+08	5.21E+07	-1.19E+08	-4.98E+06	3.06	-1.63E+06	6.86
9		1.05E+08	1.49E+08	1.67E+08	5.21E+07	-1.23E+08	-8.03E+06	3.52	-2.28E+06	6.86
10		1.08E+08	1.49E+08	1.66E+08	5.21E+07	-1.25E+08	-1.12E+07	4.05	-2.76E+06	6.86
11		1.11E+08	1.49E+08	8.33E+07	5.21E+07	-4.56E+07	-1.44E+07	4.65	-3.10E+06	6.86
12		1.14E+08	1.49E+08		5.21E+07	3.43E+07	-1.77E+07	5.35	-3.32E+06	6.86
13		1.18E+08	1.49E+08		5.21E+07	3.09E+07	-2.12E+07	6.15	-3.44E+06	6.86
14		1.21E+08	1.49E+08		5.21E+07	2.74E+07	-2.47E+07	7.08	-3.49E+06	6.86
15		1.25E+08	1.49E+08		5.21E+07	2.37E+07	-2.84E+07	8.14	-3.48E+06	6.86
16		1.29E+08	1.49E+08		5.21E+07	2.00E+07	-3.21E+07	9.36	-3.43E+06	6.86
17		1.33E+08	1.49E+08		5.21E+07	1.61E+07	-3.60E+07	1.08	-3.34E+06	6.86
18		1.37E+08	1.49E+08		5.21E+07	1.21E+07	-4.00E+07	1.24	-3.23E+06	6.86
19		1.41E+08	1.49E+08		5.21E+07	8.02E+06	-4.41E+07	1.42	-3.10E+06	6.86
20		1.45E+08	1.49E+08		5.21E+07	3.79E+06	-4.83E+07	1.64	-2.95E+06	6.86
									-2546540619	

For 4000 km										
0	2.54E+09	0	0	0	0	0	0	0	0	0
1		8.28E+07	1.49E+08	2.54E+08	5.21E+07	-1.88E+08	1.39E+07	1.15	1.21E+07	6.86
2		8.53E+07	1.49E+08	4.57E+08	5.21E+07	-3.94E+08	1.14E+07	1.32	8.63E+06	6.86
3		8.78E+07	1.49E+08	3.66E+08	5.21E+07	-3.05E+08	8.86E+06	1.52	5.82E+06	6.86
4		9.05E+07	1.49E+08	2.93E+08	5.21E+07	-2.34E+08	6.22E+06	1.75	3.56E+06	6.86
5		9.32E+07	1.49E+08	2.34E+08	5.21E+07	-1.79E+08	3.51E+06	2.01	1.74E+06	6.86
6		9.60E+07	1.49E+08	1.87E+08	5.21E+07	-1.34E+08	7.14E+05	2.31	3.09E+05	6.86
7		9.89E+07	1.49E+08	1.66E+08	5.21E+07	-1.16E+08	-2.17E+06	2.66	-8.14E+05	6.86
8		1.02E+08	1.49E+08	1.66E+08	5.21E+07	-1.19E+08	-5.13E+06	3.06	-1.68E+06	6.86
9		1.05E+08	1.49E+08	1.67E+08	5.21E+07	-1.23E+08	-8.19E+06	3.52	-2.33E+06	6.86
10		1.08E+08	1.49E+08	1.66E+08	5.21E+07	-1.26E+08	-1.13E+07	4.05	-2.80E+06	6.86
11		1.11E+08	1.49E+08	8.33E+07	5.21E+07	-4.58E+07	-1.46E+07	4.65	-3.13E+06	6.86
12		1.15E+08	1.49E+08		5.21E+07	3.42E+07	-1.79E+07	5.35	-3.35E+06	6.86
13		1.18E+08	1.49E+08		5.21E+07	3.07E+07	-2.14E+07	6.15	-3.47E+06	6.86
14		1.22E+08	1.49E+08		5.21E+07	2.72E+07	-2.49E+07	7.08	-3.52E+06	6.86
15		1.25E+08	1.49E+08		5.21E+07	2.35E+07	-2.85E+07	8.14	-3.51E+06	6.86
16		1.29E+08	1.49E+08		5.21E+07	1.98E+07	-3.23E+07	9.36	-3.45E+06	6.86
17		1.33E+08	1.49E+08		5.21E+07	1.59E+07	-3.62E+07	1.08	-3.36E+06	6.86
18		1.37E+08	1.49E+08		5.21E+07	1.19E+07	-4.02E+07	1.24	-3.24E+06	6.86
19		1.41E+08	1.49E+08		5.21E+07	7.81E+06	-4.43E+07	1.42	-3.11E+06	6.86
20		1.45E+08	1.49E+08		5.21E+07	3.58E+06	-4.85E+07	1.64	-2.96E+06	6.86
									-2547641843	

For 5000 km										
0	2.54E+09	0	0	0	0	0	0	0	0	0
1		8.29E+07	1.49E+08	2.54E+08	5.21E+07	-1.88E+08	1.38E+07	1.15	1.20E+07	6.86
2		8.54E+07	1.49E+08	4.57E+08	5.21E+07	-3.94E+08	1.13E+07	1.32	8.54E+06	6.86
3		8.80E+07	1.49E+08	3.66E+08	5.21E+07	-3.05E+08	8.73E+06	1.52	5.74E+06	6.86
4		9.06E+07	1.49E+08	2.93E+08	5.21E+07	-2.34E+08	6.09E+06	1.75	3.48E+06	6.86
5		9.33E+07	1.49E+08	2.34E+08	5.21E+07	-1.79E+08	3.37E+06	2.01	1.68E+06	6.86
6		9.61E+07	1.49E+08	1.87E+08	5.21E+07	-1.35E+08	5.74E+05	2.31	2.48E+05	6.86
7		9.90E+07	1.49E+08	1.66E+08	5.21E+07	-1.17E+08	-2.31E+06	2.66	-8.68E+05	6.86
8		1.02E+08	1.49E+08	1.66E+08	5.21E+07	-1.20E+08	-5.28E+06	3.06	-1.73E+06	6.86
9		1.05E+08	1.49E+08	1.67E+08	5.21E+07	-1.23E+08	-8.34E+06	3.52	-2.37E+06	6.86
10		1.08E+08	1.49E+08	1.66E+08	5.21E+07	-1.26E+08	-1.15E+07	4.05	-2.84E+06	6.86
11		1.11E+08	1.49E+08	8.33E+07	5.21E+07	-4.60E+07	-1.47E+07	4.65	-3.17E+06	6.86
12		1.15E+08	1.49E+08		5.21E+07	3.40E+07	-1.81E+07	5.35	-3.38E+06	6.86
13		1.18E+08	1.49E+08		5.21E+07	3.05E+07	-2.15E+07	6.15	-3.50E+06	6.86
14		1.22E+08	1.49E+08		5.21E+07	2.70E+07	-2.51E+07	7.08	-3.54E+06	6.86
15		1.25E+08	1.49E+08		5.21E+07	2.33E+07	-2.87E+07	8.14	-3.53E+06	6.86
16		1.29E+08	1.49E+08		5.21E+07	1.96E+07	-3.25E+07	9.36	-3.47E+06	6.86
17		1.33E+08	1.49E+08		5.21E+07	1.57E+07	-3.64E+07	1.08	-3.38E+06	6.86
18		1.37E+08	1.49E+08		5.21E+07	1.17E+07	-4.04E+07	1.24	-3.26E+06	6.86
19		1.41E+08	1.49E+08		5.21E+07	7.60E+06	-4.45E+07	1.42	-3.12E+06	6.86
20		1.45E+08	1.49E+08		5.21E+07	3.37E+06	-4.87E+07	1.64	-2.98E+06	6.86
									-2548743066	

For 6000 km										
0	2.54E+09	0	0	0	0	0	0	0	0	0
1		8.30E+07	1.49E+08	2.54E+08	5.21E+07	-1.88E+08	1.37E+07	1.15	1.19E+07	6.86
2		8.55E+07	1.49E+08	4.57E+08	5.21E+07	-3.94E+08	1.12E+07	1.32	8.45E+06	6.86
3		8.81E+07	1.49E+08	3.66E+08	5.21E+07	-3.05E+08	8.60E+06	1.52	5.66E+06	6.86
4		9.07E+07	1.49E+08	2.93E+08	5.21E+07	-2.35E+08	5.96E+06	1.75	3.41E+06	6.86
5		9.35E+07	1.49E+08	2.34E+08	5.21E+07	-1.79E+08	3.24E+06	2.01	1.61E+06	6.86
6		9.63E+07	1.49E+08	1.87E+08	5.21E+07	-1.35E+08	4.34E+05	2.31	1.88E+05	6.86
7		9.92E+07	1.49E+08	1.66E+08	5.21E+07	-1.17E+08	-2.45E+06	2.66	-9.22E+05	6.86
8		1.02E+08	1.49E+08	1.66E+08	5.21E+07	-1.20E+08	-5.43E+06	3.06	-1.77E+06	6.86
9		1.05E+08	1.49E+08	1.67E+08	5.21E+07	-1.23E+08	-8.49E+06	3.52	-2.41E+06	6.86
10		1.08E+08	1.49E+08	1.66E+08	5.21E+07	-1.26E+08	-1.16E+07	4.05	-2.88E+06	6.86
11		1.12E+08	1.49E+08	8.33E+07	5.21E+07	-4.61E+07	-1.49E+07	4.65	-3.20E+06	6.86
12		1.15E+08	1.49E+08		5.21E+07	3.38E+07	-1.82E+07	5.35	-3.41E+06	6.86
13		1.18E+08	1.49E+08		5.21E+07	3.04E+07	-2.17E+07	6.15	-3.53E+06	6.86
14		1.22E+08	1.49E+08		5.21E+07	2.68E+07	-2.52E+07	7.08	-3.57E+06	6.86
15		1.26E+08	1.49E+08		5.21E+07	2.32E+07	-2.89E+07	8.14	-3.55E+06	6.86
16		1.29E+08	1.49E+08		5.21E+07	1.94E+07	-3.27E+07	9.36	-3.49E+06	6.86
17		1.33E+08	1.49E+08		5.21E+07	1.55E+07	-3.66E+07	1.08	-3.40E+06	6.86
18		1.37E+08	1.49E+08		5.21E+07	1.15E+07	-4.06E+07	1.24	-3.28E+06	6.86
19		1.41E+08	1.49E+08		5.21E+07	7.40E+06	-4.47E+07	1.42	-3.14E+06	6.86
20		1.46E+08	1.49E+08		5.21E+07	3.16E+06	-4.89E+07	1.64	-2.99E+06	6.86
									-2549844290	

For 7000 km										
0	2.54E+09	0	0	0	0	0	0	0	0	0
1		8.32E+07	1.49E+08	2.54E+08	5.21E+07	-1.88E+08	1.35E+07	1.15	1.18E+07	6.86
2		8.57E+07	1.49E+08	4.57E+08	5.21E+07	-3.94E+08	1.10E+07	1.32	8.35E+06	6.86
3		8.82E+07	1.49E+08	3.66E+08	5.21E+07	-3.05E+08	8.47E+06	1.52	5.57E+06	6.86
4		9.09E+07	1.49E+08	2.93E+08	5.21E+07	-2.35E+08	5.83E+06	1.75	3.33E+06	6.86
5		9.36E+07	1.49E+08	2.34E+08	5.21E+07	-1.79E+08	3.10E+06	2.01	1.54E+06	6.86
6		9.64E+07	1.49E+08	1.87E+08	5.21E+07	-1.35E+08	2.94E+05	2.31	1.27E+05	6.86
7		9.93E+07	1.49E+08	1.66E+08	5.21E+07	-1.17E+08	-2.60E+06	2.66	-9.77E+05	6.86
8		1.02E+08	1.49E+08	1.66E+08	5.21E+07	-1.20E+08	-5.58E+06	3.06	-1.82E+06	6.86
9		1.05E+08	1.49E+08	1.67E+08	5.21E+07	-1.23E+08	-8.64E+06	3.52	-2.46E+06	6.86
10		1.09E+08	1.49E+08	1.66E+08	5.21E+07	-1.26E+08	-1.18E+07	4.05	-2.92E+06	6.86
11		1.12E+08	1.49E+08	8.33E+07	5.21E+07	-4.63E+07	-1.51E+07	4.65	-3.24E+06	6.86
12		1.15E+08	1.49E+08		5.21E+07	3.37E+07	-1.84E+07	5.35	-3.44E+06	6.86
13		1.19E+08	1.49E+08		5.21E+07	3.02E+07	-2.19E+07	6.15	-3.55E+06	6.86
14		1.22E+08	1.49E+08		5.21E+07	2.66E+07	-2.54E+07	7.08	-3.59E+06	6.86
15		1.26E+08	1.49E+08		5.21E+07	2.30E+07	-2.91E+07	8.14	-3.57E+06	6.86
16		1.30E+08	1.49E+08		5.21E+07	1.92E+07	-3.29E+07	9.36	-3.51E+06	6.86
17		1.33E+08	1.49E+08		5.21E+07	1.53E+07	-3.67E+07	1.08	-3.41E+06	6.86
18		1.37E+08	1.49E+08		5.21E+07	1.13E+07	-4.08E+07	1.24	-3.29E+06	6.86
19		1.42E+08	1.49E+08		5.21E+07	7.19E+06	-4.49E+07	1.42	-3.15E+06	6.86
20		1.46E+08	1.49E+08		5.21E+07	2.95E+06	-4.91E+07	1.64	-3.00E+06	6.86
									-2550945513	

For 8000 km										
0	2.54E+09	0	0	0	0	0	0	0	0	0
1		8.33E+07	1.49E+08	2.54E+08	5.21E+07	-1.89E+08	1.34E+07	1.15	1.17E+07	6.86
2		8.58E+07	1.49E+08	4.57E+08	5.21E+07	-3.94E+08	1.09E+07	1.32	8.26E+06	6.86
3		8.83E+07	1.49E+08	3.66E+08	5.21E+07	-3.05E+08	8.35E+06	1.52	5.49E+06	6.86
4		9.10E+07	1.49E+08	2.93E+08	5.21E+07	-2.35E+08	5.70E+06	1.75	3.26E+06	6.86
5		9.37E+07	1.49E+08	2.34E+08	5.21E+07	-1.79E+08	2.97E+06	2.01	1.47E+06	6.86
6		9.65E+07	1.49E+08	1.87E+08	5.21E+07	-1.35E+08	1.54E+05	2.31	6.68E+04	6.86
7		9.94E+07	1.49E+08	1.66E+08	5.21E+07	-1.17E+08	-2.74E+06	2.66	-1.03E+06	6.86
8		1.02E+08	1.49E+08	1.66E+08	5.21E+07	-1.20E+08	-5.72E+06	3.06	-1.87E+06	6.86
9		1.05E+08	1.49E+08	1.67E+08	5.21E+07	-1.23E+08	-8.80E+06	3.52	-2.50E+06	6.86
10		1.09E+08	1.49E+08	1.66E+08	5.21E+07	-1.26E+08	-1.20E+07	4.05	-2.96E+06	6.86
11		1.12E+08	1.49E+08	8.33E+07	5.21E+07	-4.65E+07	-1.52E+07	4.65	-3.27E+06	6.86
12		1.15E+08	1.49E+08		5.21E+07	3.35E+07	-1.86E+07	5.35	-3.47E+06	6.86
13		1.19E+08	1.49E+08		5.21E+07	3.00E+07	-2.20E+07	6.15	-3.58E+06	6.86
14		1.22E+08	1.49E+08		5.21E+07	2.65E+07	-2.56E+07	7.08	-3.62E+06	6.86
15		1.26E+08	1.49E+08		5.21E+07	2.28E+07	-2.93E+07	8.14	-3.60E+06	6.86
16		1.30E+08	1.49E+08		5.21E+07	1.90E+07	-3.30E+07	9.36	-3.53E+06	6.86
17		1.34E+08	1.49E+08		5.21E+07	1.51E+07	-3.69E+07	1.08	-3.43E+06	6.86
18		1.38E+08	1.49E+08		5.21E+07	1.11E+07	-4.09E+07	1.24	-3.31E+06	6.86
19		1.42E+08	1.49E+08		5.21E+07	6.99E+06	-4.51E+07	1.42	-3.17E+06	6.86
20		1.46E+08	1.49E+08		5.21E+07	2.74E+06	-4.93E+07	1.64	-3.01E+06	6.86
									-2552046737	

For 9000 km										
0	2.54E+09	0	0	0	0	0	0	0	0	0
1		8.34E+07	1.49E+08	2.54E+08	5.21E+07	-1.89E+08	1.33E+07	1.15	1.16E+07	6.86
2		8.59E+07	1.49E+08	4.57E+08	5.21E+07	-3.94E+08	1.08E+07	1.32	8.16E+06	6.86
3		8.85E+07	1.49E+08	3.66E+08	5.21E+07	-3.05E+08	8.22E+06	1.52	5.40E+06	6.86
4		9.11E+07	1.49E+08	2.93E+08	5.21E+07	-2.35E+08	5.56E+06	1.75	3.18E+06	6.86
5		9.39E+07	1.49E+08	2.34E+08	5.21E+07	-1.79E+08	2.83E+06	2.01	1.41E+06	6.86
6		9.67E+07	1.49E+08	1.87E+08	5.21E+07	-1.35E+08	1.47E+04	2.31	6.34E+03	6.86
7		9.96E+07	1.49E+08	1.66E+08	5.21E+07	-1.17E+08	-2.89E+06	2.66	-1.08E+06	6.86
8		1.03E+08	1.49E+08	1.66E+08	5.21E+07	-1.20E+08	-5.87E+06	3.06	-1.92E+06	6.86
9		1.06E+08	1.49E+08	1.67E+08	5.21E+07	-1.24E+08	-8.95E+06	3.52	-2.54E+06	6.86
10		1.09E+08	1.49E+08	1.66E+08	5.21E+07	-1.26E+08	-1.21E+07	4.05	-3.00E+06	6.86
11		1.12E+08	1.49E+08	8.33E+07	5.21E+07	-4.66E+07	-1.54E+07	4.65	-3.31E+06	6.86
12		1.15E+08	1.49E+08		5.21E+07	3.33E+07	-1.87E+07	5.35	-3.50E+06	6.86
13		1.19E+08	1.49E+08		5.21E+07	2.99E+07	-2.22E+07	6.15	-3.61E+06	6.86
14		1.22E+08	1.49E+08		5.21E+07	2.63E+07	-2.58E+07	7.08	-3.64E+06	6.86
15		1.26E+08	1.49E+08		5.21E+07	2.26E+07	-2.95E+07	8.14	-3.62E+06	6.86
16		1.30E+08	1.49E+08		5.21E+07	1.88E+07	-3.32E+07	9.36	-3.55E+06	6.86
17		1.34E+08	1.49E+08		5.21E+07	1.49E+07	-3.71E+07	1.08	-3.45E+06	6.86
18		1.38E+08	1.49E+08		5.21E+07	1.09E+07	-4.11E+07	1.24	-3.33E+06	6.86
19		1.42E+08	1.49E+08		5.21E+07	6.78E+06	-4.53E+07	1.42	-3.18E+06	6.86
20		1.46E+08	1.49E+08		5.21E+07	2.52E+06	-4.95E+07	1.64	-3.03E+06	6.86
									-2553147961	

For 10,000 km										
0	2.54E+09	0	0	0	0	0	0	0	0	0
1		8.35E+07	1.49E+08	2.54E+08	5.21E+07	-1.89E+08	1.32E+07	1.15	1.15E+07	6.86
2		8.60E+07	1.49E+08	4.57E+08	5.21E+07	-3.95E+08	1.07E+07	1.32	8.07E+06	6.86
3		8.86E+07	1.49E+08	3.66E+08	5.21E+07	-3.06E+08	8.09E+06	1.52	5.32E+06	6.86
4		9.13E+07	1.49E+08	2.93E+08	5.21E+07	-2.35E+08	5.43E+06	1.75	3.11E+06	6.86
5		9.40E+07	1.49E+08	2.34E+08	5.21E+07	-1.79E+08	2.69E+06	2.01	1.34E+06	6.86
6		9.68E+07	1.49E+08	1.87E+08	5.21E+07	-1.35E+08	-1.25E+05	2.31	-5.41E+04	6.86
7		9.97E+07	1.49E+08	1.66E+08	5.21E+07	-1.17E+08	-3.03E+06	2.66	-1.14E+06	6.86
8		1.03E+08	1.49E+08	1.66E+08	5.21E+07	-1.20E+08	-6.02E+06	3.06	-1.97E+06	6.86
9		1.06E+08	1.49E+08	1.67E+08	5.21E+07	-1.24E+08	-9.10E+06	3.52	-2.59E+06	6.86
10		1.09E+08	1.49E+08	1.66E+08	5.21E+07	-1.27E+08	-1.23E+07	4.05	-3.03E+06	6.86
11		1.12E+08	1.49E+08	8.33E+07	5.21E+07	-4.68E+07	-1.55E+07	4.65	-3.34E+06	6.86
12		1.16E+08	1.49E+08		5.21E+07	3.32E+07	-1.89E+07	5.35	-3.54E+06	6.86
13		1.19E+08	1.49E+08		5.21E+07	2.97E+07	-2.24E+07	6.15	-3.64E+06	6.86
14		1.23E+08	1.49E+08		5.21E+07	2.61E+07	-2.60E+07	7.08	-3.67E+06	6.86
15		1.26E+08	1.49E+08		5.21E+07	2.24E+07	-2.96E+07	8.14	-3.64E+06	6.86
16		1.30E+08	1.49E+08		5.21E+07	1.86E+07	-3.34E+07	9.36	-3.57E+06	6.86
17		1.34E+08	1.49E+08		5.21E+07	1.47E+07	-3.73E+07	1.08	-3.47E+06	6.86
18		1.38E+08	1.49E+08		5.21E+07	1.07E+07	-4.13E+07	1.24	-3.34E+06	6.86
19		1.42E+08	1.49E+08		5.21E+07	6.58E+06	-4.55E+07	1.42	-3.20E+06	6.86
20		1.46E+08	1.49E+08		5.21E+07	2.31E+06	-4.98E+07	1.64	-3.04E+06	6.86
									-2554249185	